

Characterisation of the mitotic Kinesin 13-1

in *Trypanosoma brucei*

DISSERTATION

zur Erlangung des akademischen Grades

Doktor der Naturwissenschaften (Dr. rer. nat.)

im Promotionsprogramm „Molekulare Biowissenschaften“

der Bayreuther Graduiertenschule für Mathematik und Naturwissenschaften (BayNAT)

vorgelegt von

Anna Riemer

geboren in Bamberg

Bayreuth 2017

Die vorliegende Arbeit wurde in der Zeit von Februar 2012 bis Juli 2016 in Bayreuth am Lehrstuhl Genetik unter Betreuung von Herrn Professor Dr. Klaus Ersfeld angefertigt.

Vollständiger Abdruck der von der Bayreuther Graduiertenschule für Mathematik und Naturwissenschaften (BayNAT) der Universität Bayreuth genehmigten Dissertation zur Erlangung des akademischen Grades einer Doktorin der Naturwissenschaften (Dr. rer. nat.).

Dissertation eingereicht am: 28.09.2017

Zulassung durch das Leitungsgremium: 28.09.2017

Wissenschaftliches Kolloquium: 08.03.2018

Amtierender Direktor: Prof. Dr. Dirk Schüler

Prüfungsausschuss:

Prof. Dr. Klaus Ersfeld (Gutachter)
Prof. Dr. Stefan Geimer (Gutachter)
Prof. Dr. Gerrit Begemann (Vorsitz)
Prof. Dr. Stefan Heidmann

Meinen Eltern und Großeltern

Table of contents

1.	Introduction.....	1
1.1.	<i>Trypanosoma brucei</i> spp. and trypanosomiasis.....	1
1.1.1.	<i>T. brucei</i> life cycle.....	3
1.1.2.	<i>T. brucei</i> cell architecture.....	4
1.1.3.	Chromosome segregation in <i>T. brucei</i>	6
1.1.4.	<i>T. brucei</i> cell cycle	7
1.2.	Microtubules	9
1.3.	Kinesins	12
1.3.1.	Kinesin architecture	12
1.3.2.	Kinesin-13 movement and microtubule depolymerisation.....	14
1.3.3.	Kinesin-13 family.....	19
1.3.4.	Kinesin-13 family in <i>T. brucei</i>	20
1.3.5.	Mitotic kinesins as anti-cancer drug targets.....	22
1.4.	Regulation of Kinesin-13	23
1.4.1.	Aurora kinase	23
1.4.2.	<i>T. brucei</i> Aurora kinase	25
1.5.	Nuclear protein import and export	26
1.6.	Aims of the thesis.....	27
2.	Results.....	30
2.1.	Attempt to establish a procedure for a <i>TbKif13-1</i> high-throughput inhibitor screen.....	30
2.1.1.	Heterologous <i>in vivo</i> assay.....	30
2.1.2.	<i>In vitro T. brucei</i> cytoskeleton assay	33
2.2.	Functional dissection of <i>TbKif13-1</i> domains	34
2.2.1.	Localisation of <i>TbKif13-1</i> deletion constructs in <i>T. brucei</i>	35
2.2.2.	Proteasome-dependent degradation of <i>TbKif13-1</i>	43
2.2.3.	Effect of <i>TbKif13-1</i> deletion constructs on cell cycle progression.....	47
2.2.4.	<i>TbKif13-1</i> domains necessary for microtubule binding and depolymerisation	55
2.2.5.	Essential amino acids for depolymerisation and ATPase activity within the motor domain of <i>TbKif13-1</i>	59
2.3.	<i>TbAuk1</i> and <i>TbKif13-1</i>	61
3.	Discussion.....	65
3.1.	Attempt to establish a procedure for a <i>TbKif13-1</i> high-throughput inhibitor screen.....	65
3.2.	Functional characterisation of <i>TbKif13-1</i>.....	68
3.2.1.	<i>TbKif13-1</i> nuclear import and export sequences regulate its subcellular localisation	69
3.2.2.	Cell cycle-specific and proteasome-dependent degradation of <i>TbKif13-1</i>	70
3.2.3.	Ectopic expression of the <i>TbKif13-1</i> neck-motor domain has a dominant-negative effect on cell cycle progression.....	74

Table of contents

3.2.4.	<i>TbKif13-1</i> neck-motor domain and C-terminus are necessary for <i>in vitro</i> microtubule binding and depolymerisation	78
3.2.5.	Conserved decoupled mechanism of microtubule depolymerisation and ATP hydrolysis in <i>TbKif13-1</i>	80
3.3.	<i>TbAuk1</i> and <i>TbKif13-1</i>	82
4.	Material and methods.....	85
4.1.	Materials	85
4.1.1.	Hard- and software	85
4.1.2.	Chemicals, reagents and kits.....	85
4.1.3.	Antibodies	86
4.1.4.	DNA oligonucleotides.....	86
4.1.5.	Plasmids	89
4.2.	Microbiological techniques	92
4.2.1.	<i>E. coli</i> strains and media	92
4.2.2.	Cultivation of <i>E. coli</i>	92
4.2.3.	Transformation of plasmid DNA into chemical competent <i>E. coli</i>	92
4.2.4.	Recombinant protein expression in <i>E. coli</i>	93
4.3.	Molecular biological methods	93
4.3.1.	Isolation of plasmid DNA from <i>E. coli</i> XL1-blue	93
4.3.2.	Determination of DNA concentration.....	94
4.3.3.	Restriction hydrolysis of DNA	94
4.3.4.	Polymerase chain reaction.....	94
4.3.5.	Mutagenesis of multiple cloning sites in plasmid DNA.....	95
4.3.6.	Site-specific mutagenesis of plasmid DNA.....	95
4.3.7.	Separation of DNA fragments by agarose gelelectrophoresis.....	96
4.3.8.	Isolation of DNA from agarose gels	96
4.3.9.	Ligation.....	96
4.3.10.	Linearisation of plasmid DNA for transformation of <i>T. brucei</i>	97
4.4.	Protein biochemical methods.....	97
4.4.1.	Denaturing sodium dodecyl sulfate polyacrylamid gelelectrophoresis (SDS-PAGE)	97
4.4.2.	Methanol-chloroform precipitation of protein samples	99
4.4.3.	Determination of protein concentration in solution	99
4.4.4.	Westernblot (Immunoblot).....	100
4.4.5.	Coomassie staining and destaining.....	101
4.4.6.	Silver staining	101
4.4.7.	Autoradiography	101
4.4.8.	Ni ²⁺ -NTA affinity purification of His ₆ tagged proteins	102
4.4.9.	Tubulin sedimentation assay	104
4.4.10.	Malachite green assay	105
4.4.11.	Immunoprecipitation	106
4.4.12.	³³ P kinase assays	107
4.4.13.	Immunofluorescence	108
4.4.14.	<i>In vitro</i> degradation of <i>T. brucei</i> cytoskeletons	110
4.5.	Cell biological methods	111
4.5.1.	<i>T. brucei</i> cell lines and cultivation	111

Table of contents

4.5.2.	Mammalian cell lines and cultivation	111
4.5.3.	Transformation of <i>T. brucei</i>	112
4.5.4.	Transfection of mammalian cells	113
4.5.5.	Subcloning of <i>T. brucei</i>	114
4.5.6.	Storage of <i>T. brucei</i> and mammalian cells	115
4.5.7.	Ectopic expression in <i>T. brucei</i> and mammalian cells	115
4.5.8.	Growth curves	115
4.5.9.	Flow cytometry analysis	115
4.5.10.	Proteasome degradation assay	116
5.	Abbreviations	117
6.	References	119
7.	Supplementary figures	149
8.	Danksagung	173
	(Eidesstattliche) Versicherung und Erklärungen	174

Summary

Trypanosoma brucei is a unicellular, unflagellated parasite causing sub-Saharan African trypanosomiasis, commonly known as sleeping sickness. In the effort to eradicate this disease, finding new drugs that are without severe side effects for patients and easy to administer, is a challenging task. This thesis assesses the mitotic kinesin *TbKif13-1* as potential drug target. Attempts were made to establish the prerequisites for an *in vivo* and an *in vitro* *TbKif13-1* high-throughput inhibitor screen with automated image analysis. The basis for both assays was the *TbKif13-1* mediated microtubule depolymerisation and its prevention by an appropriate inhibitor. In the *in vivo* assay, the substrate was the interphase microtubule cytoskeleton of HeLa cells. The prerequisite for this assay is a stable HeLa cell line exhibiting a depolymerised microtubule cytoskeleton after inducible overexpression of ^{eGFP}*TbKif13-1* S143A. The mutation prevents its inhibition by phosphorylation. The basic idea worked well in transiently transfected HeLa cells. However, generated stable cell lines did not show microtubule cytoskeleton depolymerisation after ^{eGFP}*TbKif13-1* S143A overexpression. In the *in vitro* assay, the depolymerisation substrate for recombinantly purified ^{His6}*TbKif13-1* were *T. brucei* cytoskeletons. The assay worked well on microscopy slides. However, it did not work in the prerequisite format, 384-well plates.

In this thesis functional characterisation of *TbKif13-1* domains occurred, using *TbKif13-1* deletion constructs for *T. brucei* *in vivo* and *in vitro* assays. Immunofluorescence studies indicated that the intranuclear *TbKif13-1* localisation depends on a balance of several NLS and NES, with the strongest NLS in the C-terminus. *TbKif13-1* was proteasome-dependent degraded and was not found in G1 cells. Degradation signals were supposed within its N- and C-terminus. Full-length *TbKif13-1* bound in mitotic cytoskeleton samples in a shape resembling the mitotic spindle. *In vitro* it bound to and depolymerised taxol-stabilised microtubules in an ATP-dependent manner. The neck-motor domain in conjunction with the C-terminus was found to be its minimal functional construct for *in vitro* microtubule binding and depolymerisation. The decoupled mechanism of depolymerisation and ATPase activity is conserved in *TbKif13-1*. Ectopic expression of full-length *TbKif13-1* led to reduced growth, zoid formation and defects in spindle formation. This dominant-negative phenotype was strongest after ectopic expression of the neck-motor domain. An expected inhibitory regulation of *TbKif13-1*'s depolymerisation activity by *TbAuk1* mediated phosphorylation could not be confirmed.

Zusammenfassung

Trypanosoma brucei ist ein einzelliger Parasit, der eine Flagelle besitzt. Er verursacht südlich der Sahara die afrikanische Trypanosomiasis, die allgemein als Schlafkrankheit bekannt ist. Eine anspruchsvolle Aufgabe beim Bekämpfen dieser Krankheit ist es, neue Medikamente zu finden, die ohne schwerwiegende Nebenwirkungen für den Patienten sowie einfach zu verabreichen sind. Diese Arbeit betrachtet das mitotische Kinesin *TbKif13-1* als ein potentielles Angriffsziel für Medikamente. Es wurde versucht, die Voraussetzungen für eine *in vivo* und eine *in vitro* Suche nach einem *TbKif13-1* Inhibitor im Hochdurchsatz mit automatisierter Bildanalyse zu schaffen. Die Grundlage beider Analysemethoden war die durch *TbKif13-1* vermittelte Depolymerisation von Mikrotubuli und deren Verhinderung durch einen passenden Inhibitor. Im *in vivo* Versuchsaufbau diente das Mikrotubulizytoskelett von HeLa Zellen in Interphase als Substrat. Die Voraussetzung für diesen Versuch war eine stabile HeLa Zelllinie, die nach der induzierten Überexpression von ^{eGFP}*TbKif13-1* S143A ein depolymerisiertes Zytoskelett aufweist. Die eingebrachte Mutation verhinderte dabei seine Inhibition durch Phosphorylierung. Die Grundidee funktionierte in transient transfizierten HeLa Zellen. Allerdings zeigten die erzeugten stabilen Zelllinien keine Depolymerisation des Mikrotubulizytoskeletts nach ^{eGFP}*TbKif13-1* S143A Überexpression. Im *in vitro* Versuchsaufbau dienten *T. brucei* Zytoskelette als Depolymerisationssubstrat für rekombinant aufgereinigtes ^{His6}*TbKif13-1*. Dieser Versuch funktionierte gut auf Objektträgern. Jedoch funktionierte er nicht auf den vorausgesetzten 384-well Platten. In dieser Arbeit wurden *TbKif13-1* Domänen funktionell charakterisiert, indem *TbKif13-1* Deletionskonstrukte in *in vivo* und in *in vitro* Versuche eingesetzt wurden. Immunfluoreszenz-Studien zeigten, dass die intranukleäre *TbKif13-1* Lokalisation von einem Gleichgewicht verschiedener NLS und NES abhängt, mit der stärksten NLS im C-Terminus. *TbKif13-1* wurde Proteasom-abhängig abgebaut und war in G1 Zellen nicht zu finden. Abbausignale wurden im N- und C-Terminus vermutet. *TbKif13-1*, in seiner vollen Länge, band in mitotischen Zytoskelettproben in einer Form, die an die mitotische Spindel erinnert. *In vitro* band es an Taxol stabilisierte Mikrotubuli und depolymerisierte diese ATP abhängig. Die *neck-motor* Domäne in Verbindung mit dem C-Terminus erwies sich als das minimal funktionelle Konstrukt für das Binden an und das Depolymerisieren von Mikrotubuli *in vitro*. Der entkoppelte Mechanismus von Depolymerisation und ATPase Aktivität ist in *TbKif13-1* konserviert. Die ektopische Expression des *TbKif13-1* in seiner vollen Länge führte zu

Zusammenfassung

reduziertem Wachstum, der Ausbildung von Zoiden und Defekten in der Ausbildung der Spindel. Dieser dominant-negative Phänotyp war am stärksten nach der ektopischen Expression der *neck-motor* Domäne ausgeprägt. Eine erwartete inhibierende Regulation der Depolymerisationsaktivität von *TbKif13-1* durch eine *TbAuk1*-vermittelte Phosphorylierung konnte nicht bestätigt werden.

1. Introduction

1.1. *Trypanosoma brucei* spp. and trypanosomiasis

Trypanosoma brucei is a unicellular, unflagellated parasite. It is the agent of sub-Saharan human African trypanosomiasis, commonly known as sleeping sickness. It is transmitted to humans by the bite of the tsetse fly (*Glossina* spp.). The tsetse fly is the vector, which receives the parasite itself from the mammalian host, when taking a blood meal on infected human or wild or domestic animal harbouring human pathogenic parasites. Since trypanosomiasis is a vector-borne disease, its occurrence is restricted to areas where the tsetse fly is prevalent.

Human African trypanosomiasis takes two known forms. They are grouped by causative agent, the *T. brucei* sub-species (Checchi et al., 2008; Odiit et al., 1997). *T. b. gambiense* is most common in western and Central Africa. To date it accounts for the larger part of reported cases of sleeping sickness. It causes a chronic infection and a slow progressing form. *T. b. rhodesiense* is found in eastern and southern Africa and is responsible to a smaller amount of reported cases of sleeping sickness. It induces an acute infection and a faster progressing form.

The Latin American form of human trypanosomiasis (Chagas disease) is caused by *T. cruzi*. It is transmitted by a different vector, the triatomine bugs. Transmission occurs via their faeces or urine.

The course of disease in human African trypanosomiasis includes a first haemo-lymphatic stage. In this stage, trypanosomes propagate in lymph, blood, skin, subcutaneous tissues, and interstitial spaces of organs (Capewell et al., 2016). In a mouse model, visceral adipose tissue also constitutes a trypanosome reservoir (Trindade et al., 2016). In the haemo-lymphatic stage, patients suffer from bouts of fever, joint pains and headaches. After crossing the blood-brain barrier, parasites are found within the central nervous system. In this second neurological stage, typical symptoms are sensory disturbances, poor coordination, changed behaviour, confusion and a disturbed sleeping cycle. Unless treatment is provided, trypanosomiasis almost invariably is a fatal disease progressing to death.

Introduction

Trypanosomes will successfully proliferate in the mammalian bloodstream by antigenic variation of a variant surface glycoprotein (VSG) coat and thus evade the human immune system. Humans and higher primates are innately immune to African *T. b. brucei*, the causative agent of animal African trypanosomiasis, nagana, in cattle. This disease reduces meat and milk availability in affected rural areas. The immunity of humans and higher primates is a result of trypanosome lytic factors (TLFs). TLF1 is a high density lipoprotein binding apolipoprotein L-I (apoL-I) and haptoglobin-related protein (Hpr). TLF2 is lipid-poor and contains apoL-I, IgM (immunoglobulin M) and Hpr (Raper et al., 1999). TLF uptake in *T. b. brucei* and *T. b. rhodesiense* occurs, in addition to unknown mechanisms, via the haptoglobin-haemoglobin receptor (*TbHpHbR*). There are about 300 copies within the flagellar pocket that basically serve the parasite for haem uptake (Bullard et al., 2012; Vanhollebeke et al., 2008). In blood plasma, haem is bound to the carrier protein haptoglobin. This complex is recognised by *TbHpHbR*. Association of haemoglobin to TLF Hpr also facilitates *TbHpHbR* binding of the complex (Drain et al., 2001; Vanhollebeke et al., 2008; Widener et al., 2007).

The exact mechanism for apoL-I induced Trypanosomes' lysis still remains unclear. There is strong evidence that upon endocytotic uptake, apoL-I is localised to acidic endosomes, integrates into their membrane, increases permeability for ions, and subsequent osmotic swelling results in cell death (Pérez-Morga et al., 2005; Vanhollebeke et al., 2007). *T. b. rhodesiense* prevents this by expressing a truncated VSG, the SRA (serum resistance-associated) protein, which binds to apoL-I within endosomes (De Greef and Hamers, 1994; Stephens and Hajduk, 2011; Vanhamme et al., 2003; Xong et al., 1998). *T. b. gambiense* group 1 escapes TLF mediated lysis by several mechanisms. mRNA levels of *TbgHpHbR* are decreased and binding efficacy of TLF to *TbgHpHbR* is reduced due to a single nucleotide polymorphism (DeJesus et al., 2013; Higgins et al., 2013; Kieft et al., 2010). Moreover, a specific truncated VSG, *TbgGP* (*T. brucei gambiense* glycoprotein), stiffens membranes after binding to lipids, thus preventing apoL-I toxicity (Berberof et al., 2001; Capewell et al., 2013; Uzureau et al., 2013).

Drugs are available for treatment of trypanosomiasis. Unfortunately, all of these drugs result in a variety of undesirable side effects. As first stage therapy, pentamidine is used to fight *T. b. gambiense* and suramin to fight *T. b. rhodesiense* infections. Treatment of second stage disease requires drugs that are able to cross the blood-brain barrier. Melarsoprol, a compound containing arsen, can be administered to patients of both infection forms. Yet,

melarsoprol risks high relapse rates, treatment failure, and a mortality rate of about 5% is documented (Balasegaram et al., 2009; Legros et al., 1999; Matovu et al., 2001; Mumba Ngoyi et al., 2010; Pépin et al., 1994; Robays et al., 2008). For *T. b. gambiense* infection, treatment with eflornithine is preferred to melarsoprol because it lowers the risk of death (Chappius et al., 2005). Easier in patient application, with reduced treatment time and frequency, and with reduced therapeutic costs compared to sole eflornithine treatment, is a combination of eflornithine and nifurtimox (Checchi et al., 2007; Priotto et al., 2009). The combination of drugs also is an attempt to counteract increasing drug resistance, which emphasises the need for new drugs against trypanosomiasis.

Finding new drugs that are safe for patients and that are easy to administer remains a challenging task.

1.1.1. *T. brucei* life cycle

The life cycle of *T. brucei* involves two hosts, the insect vector and the mammalian host. The insect vector is the tsetse fly (*Glossina* spp.). It transmits *T. brucei* between mammalian hosts by biting. Upon uptake of stumpy form trypanosomes from the mammalian host, they differentiate into proliferating procyclic trypomastigotes within the tsetse fly midgut. The VSG coat is replaced by a coat of procyclin and energy generation is changed from the bloodstream glycolysis to mitochondrion-based respiration. Midgut trypanosomes then migrate to the proventriculus, where they generate epimastigotes by asymmetric division. After arrival in the tsetse fly's salivary glands, epimastigotes attach via their flagellum to the epithelial cells (Tetley and Vickerman, 1985). This proliferative form generates the non-proliferative metacyclic form, which again possesses a VSG coat in adaptation to the subsequent transmission to a new mammalian host (Rotureau et al., 2012). Within the mammalian bloodstream, trypanosomes proliferate as long slender forms, which establish and maintain an extracellular bloodstream infection. After penetrating the blood vessel endothelium, trypanosomes populate extravascular tissues like the central nervous system. With an increasing number of bloodstream trypanosomes, they change to non-proliferating stumpy forms pre-adapted to transmission by the tsetse fly (MacGregor et al., 2011; Vassella et al., 1997).

1.1.2. *T. brucei* cell architecture

T. brucei has an elongated cell shape defined by a polarised microtubule cytoskeleton. Microtubules of this subpellicular cytoskeleton are arranged with their plus ends posterior and their minus ends anterior, extending in a left-handed helical path (Figure 1 (A); Robinson et al., 1995).

Within this microtubule cell corset the single-copy organelles, i.e. flagellar pocket, flagellum, Golgi, nucleus, kinetoplast and mitochondrion, are located between the posterior end and the centre of the cell (Figure 1 (A)). The most posterior is the flagellar pocket. It is the only site of endo- and exocytosis (Engstler et al., 2004). The flagellar pocket neck is encircled by the flagellar pocket collar.

At the base of the flagellar pocket, the basal body is located. The single flagellum emerges from it. The trypanosomal flagellum contains in addition to the canonical nine-plus-two architecture of the axoneme, an insoluble, paracrystalline filament (Figure 1 (B)). This paraflagellar rod (PFR) runs in parallel to the axoneme and is necessary for flagellar movement (Bastin et al., 1998; Deflorin et al., 1994; Fuge, 1969; Schlaeppi et al., 1989; Vickerman, 1962). The flagellum is required for cell movement, cell division, cell size, infectivity, and potentially, sensory perception (Broadhead et al., 2006; Engstler et al., 2007; Kohl et al., 2003; Oberholzer et al., 2007). It runs in a left-handed helical pattern along the entire cell and the flagellar attachment zone (FAZ). The flagellum runs to the anterior tip until the flagellum's distal tip leaves the cell (Woods et al., 1989).

The FAZ is tightly bound to the cytoskeleton. It consists of an electron-dense filament and a specialised microtubule quartet (MtQ) with reversed polarity, which is connected to the endoplasmatic reticulum (Figure 1 (B); Lacomble et al., 2012; Robinson et al., 1995; Vickerman, 1969). The FAZ is linked to the flagellar pocket collar via the bilobe structure. The function of the bilobe structure is not clear. However, it seems to be involved in Golgi apparatus duplication (Esson et al., 2012; He et al., 2005).

Introduction

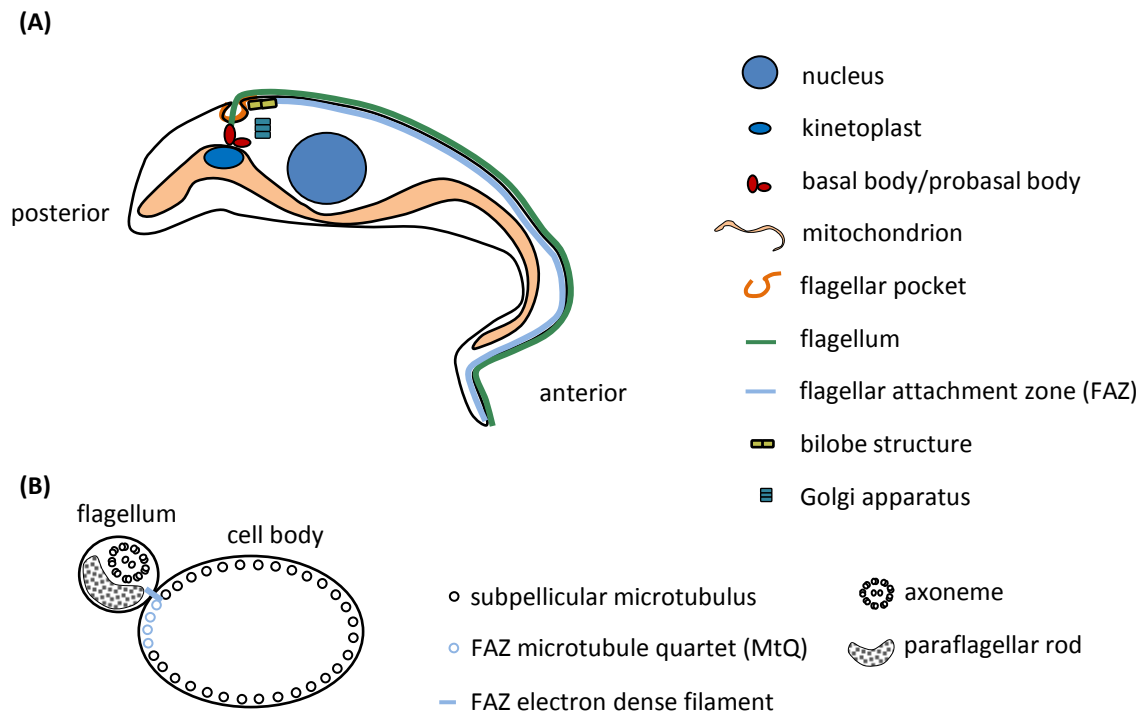


Figure 1: Model of the *T. brucei* cell structure. (A) *T. brucei* has an elongated shape. The single-copy organelles are located between the posterior end and the centre of the cell. The single mitochondrion contains the kinetoplast and extends along the length of the cell. Several cell components like the flagellar pocket collar, the endoplasmic reticulum, lysosomes and endosomes are not depicted. Figure (A) is modified and adapted from Zhou et al., 2014. **(B)** Illustrated cross section of *T. brucei*, showing the cell body with its subpellicular microtubule corset and the FAZ consisting of a specialised microtubule quartet (MtQ) with reversed polarity, and an electron dense filament. The flagellum is depicted with its axoneme containing the classical nine-plus-two architecture, and the paraflagellar rod.

The basal body and its orthogonally positioned immature probasal body are both linked to the mitochondrial kinetoplast by a tripartite attachment complex (TAC; Ogbadoyi et al., 2003; Robinson and Gull, 1991). The mitochondrial genome is located within the disc-like structured kinetoplast. It consists of topologically interlocked circular DNA, the maxi- and minicircles. The 25 - 50 maxicircles (about 20 kb in size) encode mitochondrial proteins and ribosomal RNA. The thousands of minicircles (each about 1 kb in size) encode guide RNA, necessary for posttranscriptional editing of pre-mRNA from maxicircles. The single mitochondrion is unusual among eukaryotes, since it extends along the length of the cell.

The Trypanosome nucleus contains different kinds of chromosomes. The eleven pairs of megabase chromosomes (between 1 and 6 Mbp in size) carry all actively transcribed genes. VSGs are encoded not only on megabase chromosomes, but also on the three to five intermediate chromosomes (200 - 500 kbp in size). The about 100 minichromosomes (30 –

50 kbp in size) code for silent VSGs. They are transcriptionally silent, but increase the number of VSGs. Silent VSGs become active upon duplicative transposition to active VSG expression sites on megabase chromosomes (Morrison et al., 2005; Robinson et al., 1999; Van der Ploeg et al., 1984a; Van der Ploeg et al., 1984b).

1.1.3. Chromosome segregation in *T. brucei*

Trypanosomes undergo closed mitosis. The mitotic spindle microtubules originate from opposing poles within the nuclear envelope. These do not exhibit obvious centriolar structures, but contain a ring-like structure (Ogbadoyi et al., 2000). γ -tubulin, a component of microtubule nucleating MTOCs (microtubule organising centres), colocalises with these poles (Scott et al., 1997). There is evidence that not all *T. brucei* chromosomes are segregated microtubule-dependent, since the number of chromosomes exceeds that of observed mitotic spindle microtubules (Vickerman, 1994; Vickerman and Preston, 1970).

Trypanosomes lack the centromere-specific histone H3 variant CENP-A (centromere protein), which determines the site for kinetochore assembly in vertebrates. Also conventional kinetochore proteins are missing in Trypanosomes. Recently, kinetoplastid specific kinetochore proteins, and a distantly related protein of the outer kinetochore proteins Ndc80 (nuclear division cycle) and Nuf2 (nuclear filament-containing protein) were identified (Akiyoshi and Gull, 2014; D'Archivio and Wickstead, 2017; Nerusheva and Akiyoshi, 2016).

Megabase chromosomes contain centromere sequences and electron microscopy studies suggest kinetochore like structures, into which spindle microtubules terminate (Obado et al., 2007; Ogbadoyi et al., 2000). These data and fluorescence *in situ* hybridisation observations indicate a classical kinetochore-spindle association and segregation for megabase chromosomes during mitosis (Ersfeld and Gull, 1997). For intermediate and minichromosomes, no centromeric sequences were detected (Obado et al., 2007; Wickstead et al., 2004). Segregation of minichromosomes is spindle-dependent, but differs from that of megabase chromosomes (Ersfeld and Gull, 1997). Minichromosomes congress at the metaphase plate before occupying a polar position within the spindle during segregation (Ersfeld and Gull, 1997). A possible model for their segregation is the 'lateral stacking model', proposing a lateral attachment to spindle microtubules, possibly by repeat or telomeric sequences (Gull et al., 1998).

1.1.4. *T. brucei* cell cycle

Like in other eukaryotes, the cell cycle of Trypanosomes is divided into G1-, S-, G2- and M-phase. The cell cycle phases of the kinetoplast and the nucleus are shifted to one another (Figure 2 (A); Sherwin and Gull, 1989; Woodward and Gull, 1990).

During G1-phase, trypanosomes contain one flagellum, one kinetoplast, and one nucleus. This phase is termed 1K1N (Figure 2 (B)). The first marker of the G1-S transition is the formation of a new FAZ microtubule quartet besides the basal and pro-basal body (Lacomble et al., 2010). Upon cell cycle progression, it is linked with its proximal end to the new basal body and with its distal end to the old FAZ (Absalon et al., 2007; Kohl et al., 1999; Lacomble et al., 2010). Furthermore at G1-S transition, the probasal body matures and elongates, thereby forming a new flagellum, which invades the existing flagellar pocket (Lacomble et al., 2010). Within the shared flagellar pocket, the distal tip of the new elongating flagellum is connected to the old flagellum. It remains connected during cell duplication in procyclics via the flagella connector, a cytoskeletal structure probably providing positional guidance to the new flagellum (Briggs et al., 2004; Lacomble et al., 2010; Moreira-Leite et al., 2001).

S-phases of the kinetoplast and the nucleus start almost completely simultaneous and can be determined by an extending kinetoplast, a stage termed 1-2K1N (Woodward and Gull, 1990). During kinetoplast S-phase, the matured daughter basal body, together with its new flagellum, rotates anti-clockwise from its anterior position to posterior related to the mother basal body and old flagellum (Gluenz et al., 2011; Lacomble et al., 2010). A membranous structure protrudes between the two flagella, dividing the flagellar pocket into two (Lacomble et al., 2010). With the start of the nuclear S-phase new probasal bodies are formed (Woodward and Gull, 1990).

At nuclear G2-phase, basal bodies segregate, probably as a result of base-to-tip waves of the new flagellum (Absalon et al., 2007; Robinson and Gull, 1991). Due to basal bodies' TAC mediated linkage to the kinetoplast, its movement segregates the duplicated kinetoplast, resulting in 2K1N cells (Ogbadoyi et al., 2003; Robinson and Gull, 1991).

Introduction

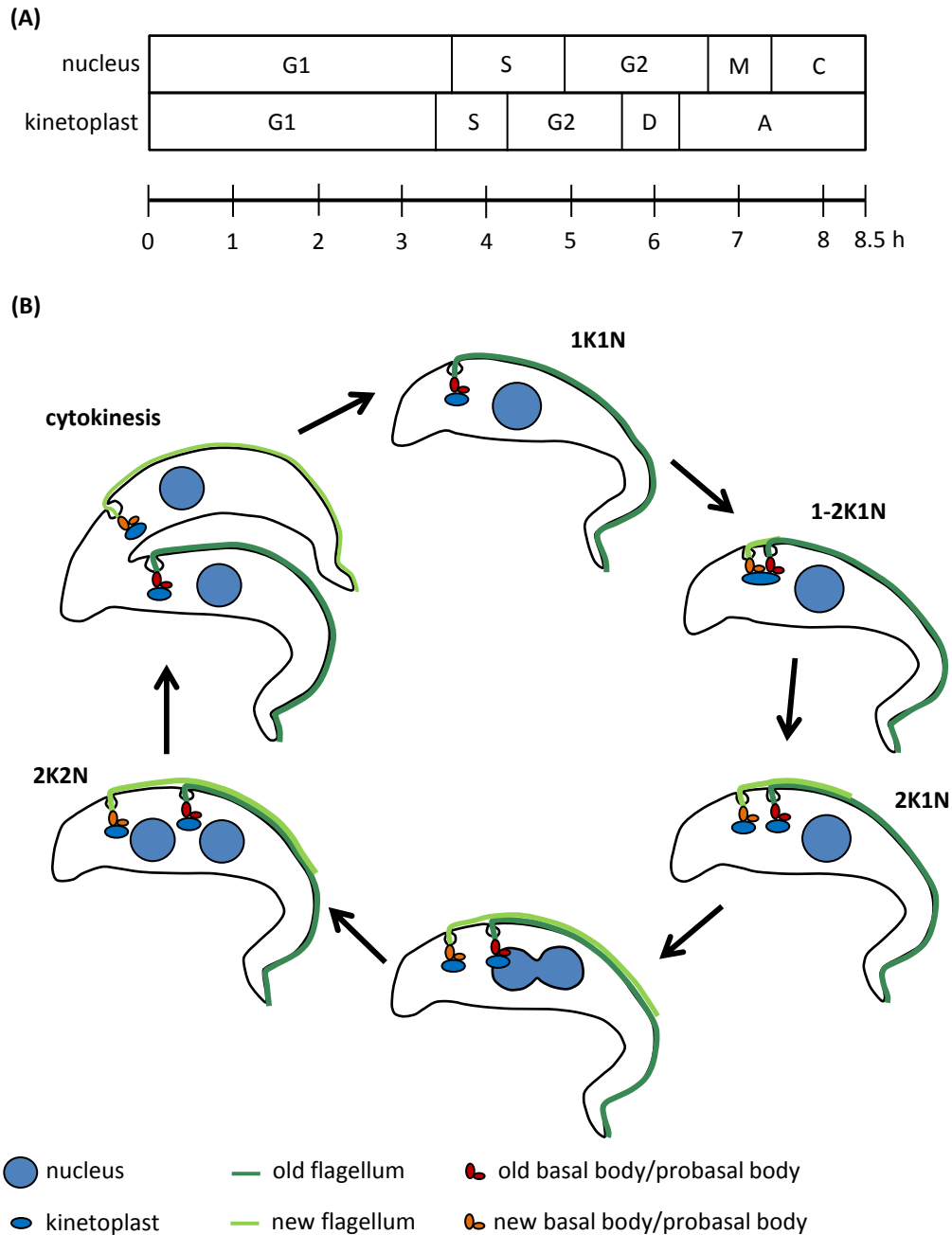


Figure 2: *T. brucei* cell cycle. (A) Exponentially growing procyclic *T. brucei* have a cell cycle of 8.5 hours. The cell cycle of the kinetoplast and the nucleus are shifted to one another. Kinetoplast S-phase (S) starts before and lasts shorter than the nuclear S-phase. Kinetoplast segregation (D) occurs before the onset of nuclear mitosis (M). In the kinetoplast apportioning (A) phase, separated kinetoplasts and the respective associated basal bodies continue to move apart. During cytokinesis (C) the cleavage furrow forms along the entire cell from anterior to posterior, running between the two flagella. Figure (A) is modified and adapted from Gull et al., 1990. (B) In G1-phase *T. brucei* contains one flagellum, one kinetoplast and one nucleus (1K1N). In S-phase the kinetoplast elongates (1-2K1N) and in G2-phase the basal bodies and the kinetoplast segregate (2K1N). Subsequently, nuclear mitosis occurs with an elongating nucleus, finally resulting in a cell with two kinetoplasts and two nuclei (2K2N). Cytokinesis runs longitudinally from anterior to posterior, leading to 1K1N cells.

Introduction

After completing the kinetoplast segregation, closed nuclear mitosis starts and ends in 2K2N cells, positioning the new nucleus between the two kinetoplasts (Robinson et al., 1995; Sherwin and Gull, 1989). Cytokinesis initiates at the distal tip of the new flagellum, running longitudinally through the cell, thereby following the new flagellum and FAZ as axis (Kohl et al., 2003; Sherwin and Gull, 1989). This yields two cells with one nucleus, one kinetoplast and one flagellum each (1K1N).

Cell cycle regulation differs in procyclic and bloodstream Trypanosomes. In procyclics initiation of cytokinesis depends primarily on the basal body/kinetoplast cycle (Hammarton et al., 2003; Li and Wang 2003; Ploubidou et al., 1999; Tu and Wang, 2004). Thus, mitotic block does not inhibit cytokinesis, resulting in anucleate cells (zoids (ON1K); Hammarton et al., 2003; Li and Wang 2003; Ploubidou et al., 1999; Tu and Wang, 2004). In contrast, mitotic block in bloodstream Trypanosomes leads to inhibition of cytokinesis but allows re-entry into G1- and S-phase (Hammarton et al., 2003; Tu and Wang, 2004). Kinetoplast duplication and segregation continues in these cells, resulting in cells with multiple kinetoplasts and an enlarged nucleus with high DNA content (Hammarton et al., 2003; Li and Wang, 2006; Tu and Wang, 2004).

1.2. Microtubules

Microtubules in Trypanosomes are involved in many essential cellular processes, like maintenance of cell shape, cell polarity, motility and mitosis. They form the subpellicular cytoskeleton, the axoneme of the flagellum, the mitotic spindle, and the basal body (Ogbadoyi et al., 2000; Robinson et al., 1995; Vickerman and Preston, 1970). In Trypanosomes six members (α , β , γ , δ , ϵ and ζ) of the tubulin superfamily are present (Scott et al., 1997; Vaughan et al., 2000). α - and β -tubulin protein sequences of *T. brucei* are similar to their mammalian homologues (Lama et al., 2012).

The $\alpha\beta$ -tubulin heterodimers are arranged in a head-to-tail fashion, forming longitudinal protofilaments (Desai and Mitchison, 1997). 13 protofilaments, laterally attached to one another, form the hollow cylindrical structure of a microtubule with a diameter of 25 nm. Microtubules are dynamic and are subject to a mechanism called 'dynamic instability', i.e. cycles of random shrinkage (catastrophe) and growth (rescue; Mitchison and Kirschner, 1984). This preferentially happens at the plus end, exposing β -tubulin. α -tubulin points towards the minus end, which is slowly growing (Figure 3 (A)).

Introduction

Microtubule nucleation of the minus end primarily occurs at MTOCs. They contain γ -tubulin, which is essential for nucleation. MTOCs differ among species: in animal cells this centre is primarily the cytoplasmic centrosome, consisting of a pair of centrioles surrounded by pericentriolar matrix. In *S. cerevisiae* the single MTOC is the spindle pole body, a trilaminar plaque located within the nuclear envelope, forming cytoplasmic microtubules and the spindle (King et al., 1982; Moens and Rapport, 1971; Robinow and Marak, 1966). In *T. brucei* there are at least two MTOCs. The first one is the basal body, which is located close to the kinetoplast and nucleates the flagellum. The second one are plaques within the nuclear envelope from which the mitotic spindle emerges (see 1.1.3.; Ogbadoyi et al., 2000). The microtubules of the subpellicular corset originate mainly from the anterior tip of the cell body and extend posterior. For them, no precise MTOCs have been identified. A study suggests that γ -tubulin accumulations at the anterior tip serve as their nucleation sites (Scott et al., 1997).

The motor of microtubule plus ends' dynamic instability is the hydrolysis of tubulin bound GTP. Each of the $\alpha\beta$ -tubulin dimer subunits binds GTP. GTP-tubulin has a straight conformation. This is deemed to favour its integration into straight microtubule protofilament ends (Wang and Nogales, 2005). Free GDP-tubulin exhibits a curved shape, incapable of binding to microtubule ends (Wang and Nogales, 2005).

In α -tubulin, the GTP binding site is located within the intradimer interface at the transition to β -tubulin (Figure 3 (B)). This burries the bound GTP and makes it non-exchangeable (N-site; Nogales et al., 1998). GTP bound to the E-site (exchangeable) of β -tubulin is exposed in unpolymerised tubulin dimers as well as at microtubule polymer plus ends (Mitchison, 1993). Upon assembly of a new $\alpha\beta$ -tubulin dimer, the α subunit contacts the E-site of the terminal microtubule β -tubulin, leading to hydrolysis of β -tubulin's GTP (Nogales et al., 1999). While phosphate is released, GDP remains bound to β -tubulin within the lattice (Carlier and Pantaloni, 1981). High-resolution cryo-EM studies revealed that the release of phosphate leads to a compaction of the E-site (Alushin et al., 2014). This results in an internal rearrangement of α -tubulin, reminiscent in structure of the formerly supposed and observed straight-to-bent transition (Alushin et al., 2014). It is supposed that this induces a conformational strain within the microtubule, which is relaxed by bending during depolymerisation (Alushin et al., 2014). Depolymerisation of microtubules occurs mainly by disassembly of oligomeres (Mandelkow et al., 1991).

Introduction

To prevent tubulin-GDP from depolymerisation within the polymerised microtubule, lateral side-by-side interactions are thought to stabilise them (Desai and Mitchison, 1997). The coupling of the polymerisation mechanism to GTP hydrolysis results in a GTP cap at the plus end, which should stabilise microtubules (Mitchison and Kirschner, 1984). Loss of the GTP cap leads to GDP-tubulin at the end of a protofilament, which exhibits less lateral interactions. This favours its curved conformation and subsequent depolymerisation (Desai and Mitchison, 1997).

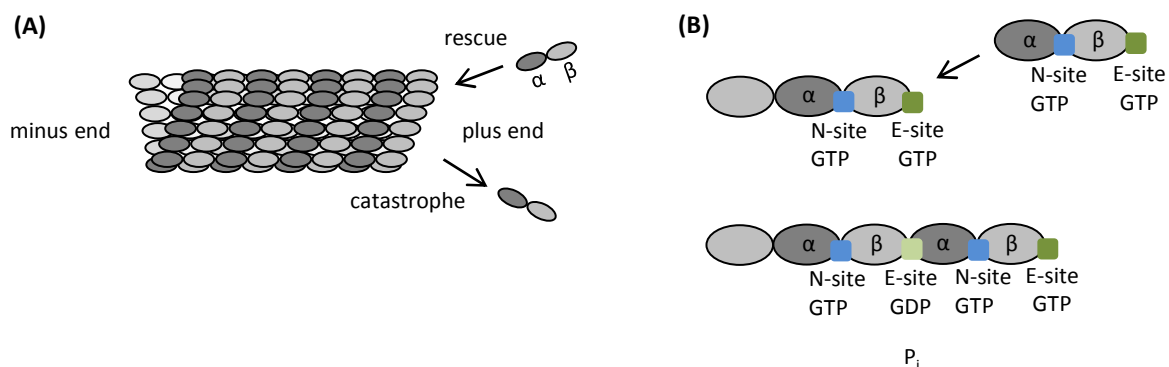


Figure 3: $\alpha\beta$ -tubulin heterodimers form microtubules. (A) A microtubulus consists of 13 protofilaments. Dynamic instability occurs mainly at the microtubule plus end with cycles of catastrophe and rescue. The plus end exposes β -tubulin, while the minus end exposes α -tubulin. **(B)** α - and β -tubulin dimer subunits both bind GTP. α -tubulin binds GTP within the intradimeric N-site (blue), where it is not hydrolysable; β -tubulin binds GTP in the E-site (green), in which it can be hydrolysed. $\alpha\beta$ -tubulin GTP has a straight conformation ready for incorporation into the microtubule end. During incorporation, α -tubulin of the free tubulin dimer binds to the E-site of the microtubule end β -tubulin, whose GTP is hydrolysed (light green); free phosphate is released. β -tubulin GTP at the microtubule plus end forms the stabilising GTP cap.

Stability of microtubules is also regulated by microtubule-associated proteins (MAPs). In Trypanosomes several MAPs link the subpellicular microtubules to each other and the cell membrane (Balaban and Goldman, 1992; Detmer et al., 1997; Hemphill et al., 1992; Vedrenne et al., 2002; Woods et al., 1992).

MAPs also include microtubule plus end tracking proteins (+TIPs), to which the family of end-binding (EB) proteins belongs. EB proteins interact with almost all other +TIPs and target them to microtubule plus ends. This mainly occurs via SxIP motifs in +TIPs (Honnappa et al., 2009). SxIP motif containing proteins form a family, whose most prominent member is the microtubule depolymerising Kinesin-13 protein MCAK (mitotic centromere associated kinesin; Honnappa et al., 2009). For the Kinesin-13 *TbKif13-1* in *T. brucei*, no SxIP site was detected. A *T. brucei* end-binding protein 1 (EB1) was identified (Sheriff et al., 2014). It

Introduction

localises posterior, where the subpellicular microtubule plus ends are supposed (Sheriff et al., 2014).

Microtubules from Trypanosomes are considered potential drug targets. Despite their protein sequence similarity to mammalian tubulin subunits, sufficient differences in tubulin structures are the reason for their exhibited selective drug sensitivity (Lama et al., 2012; Werbovetz et al., 2003). For instance, the tubulin binding site for colchicine, a drug that inhibits microtubule polymerisation by preventing curved tubulin to adopt a straight conformation in mammals, differs in *T. brucei* (Lama et al., 2012; Ravelli et al., 2004). Thus, colchicine sensitivity in *T. brucei* is strongly reduced (Lama et al., 2012). Nocodazole, which stabilises microtubule dynamics at low concentrations and promotes depolymerisation at high concentrations, also binds to the colchicine-domain and exhibits a significantly different impact on mammalian cells compared to *T. brucei* (Jordan et al., 1992; Lama et al., 2012). In contrast, taxol mediates microtubule stabilisation by straightening GDP-bound β -tubulin within the protofilament with the same sensitivity in mammalian cells and in *T. brucei* (Elie-Caille et al., 2007; Lama et al., 2012).

1.3. Kinesins

Eukaryotic cells contain three types of motor proteins: kinesins, dyneins and myosins. While myosins track on actin filaments, kinesins and dyneins use microtubules as surface. Of the three, only kinesins are ubiquitous to all eukaryotes (Kollmar, 2016; Richards and Cavalier-Smith, 2005; Wickstead and Gull, 2006; Wickstead and Gull, 2007). All three have in common to use energy from ATP hydrolysis for force generation, and to consist of many members, grouped into families. Most members are found within kinesins. According to phylogenetic analysis, kinesins were classified in up to 17 families (Dagenbach and Endow, 2004; Lawrence et al., 2004; Wickstead and Gull, 2006).

1.3.1. Kinesin architecture

Kinesins act as homo- or heterodimer or even higher-order complexes. They walk along the microtubule lattice in an unidirectional way, using the energy they produce by ATP hydrolysis. The ATP-binding site and the microtubule binding site are both located within the conserved globular motor domain, the head (Scholey et al., 1989). For ATP binding there are several conserved nucleotide binding motifs (N1-4) necessary within the motor domain (Sablin et al., 1996). The ATP adenine ring interacts with N4 RxRP, while α - and β -phosphate

Introduction

bind via the P-loop N1 GQTxSGKT (Sablin et al., 1996). γ -phosphate is bound via switch I N2 NxxSSRSH and switch II N3 DxxGxE. Both are assumed to be involved in γ -phosphate-sensing, i.e. sensing the presence or absence of γ -phosphate and triggering ATP hydrolysis and conformational changes within the motor structure (Kull and Endow, 2002; Naber et al., 2003; Sablin et al., 1996). Switch II is directly connected to the microtubule binding site within kinesins (Woehlke et al., 1997). This spatial proximity indicates how the information between the state of the bound nucleotide and the microtubule binding state is exchanged within the kinesin (Woehlke et al., 1997).

The location of the motor domain points to the direction of movement and used to serve as criterion for the first kinesin classification (Figure 4; Vale and Fletterick, 1997). Most kinesins (Kinesin-1 to -12) are plus end directed motors, possessing a N-terminal motor domain (N-type kinesins). Kinesin-14 members contain a C-terminal motor domain (C-type kinesins) and exhibit a minus end directed movement. N- and C-type kinesins act as transporters for various cargoes, like vesicles and organelles within the cell. They are specific to their cargo. N- and C-type kinesins contain two variable domains, the stalk and the tail. The tail, by itself or by association with adaptor or scaffold proteins, binds to cargo proteins. The stalk mediates dimerisation via its coiled-coil structure. It is connected to the motor by the positively charged neck. The neck assists the catalytic core with generation of the kinesin movement.

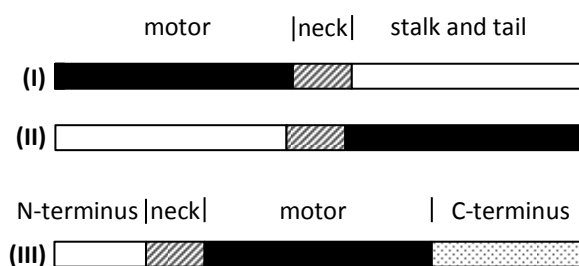


Figure 4: Model of kinesin types. (I) Plus end directed kinesin with a N-terminal motor domain. (II) Minus end directed kinesin with a C-terminal motor domain. Both kinesin types contain the catalytic motor domain (black) with conserved nucleotide binding motifs N1-N4 and the microtubule binding site; via the positively charged neck (grey stripes), that contributes to processivity; the motor domain is linked to the stalk and the tail (white); the stalk serves as dimerisation domain and the tail is used for interaction with cargo proteins. (III) Depolymerising kinesin with the motor domain in the middle. The motor domain contains in addition to the conserved nucleotide binding motifs N1-N4 and microtubule binding sites, the class specific elongated loop 2 with the KVD motif. The neck is located N-terminal to the catalytic core. It contributes to Kinesin-13's depolymerisation activity. Both, the N- (white) and the C-terminus (spotted) contribute to dimerisation and subcellular localisation.

In contrast, there are kinesins not transporting cargo, but using the energy of ATP hydrolysis to depolymerise microtubules from one of its two ends. To these belong other members of the Kinesin-14 family and the Kinesin-8 family (Endow et al., 1994; Gupta et al., 2006; Mayr et al., 2007). The members of the Kinesin-13 family have the ability to depolymerise microtubules from both ends (Desai et al., 1999). The Kinesin-13 family is needed for modulation of microtubule dynamics during mitosis (see 1.3.3.) and interphase (Mennella et al., 2005). Several types of cancer are associated with overexpression of the Kinesin-13 member MCAK/Kif2C (kif: kinesin superfamily; see 1.3.5.; Ishikawa et al., 2008).

Kinesin-13 members are mainly homodimers. Their motor domain is located within the middle (M-type kinesins). Elements like the nucleotide binding motifs within the motor domain are conserved. N-terminal to the motor domain is the positively charged neck domain located. These two domains were shown to be necessary and sufficient for MCAK's microtubule depolymerisation activity (Maney et al., 2001). Both, N- and C-terminal domain may contribute to MCAK's dimerisation. N- or C-terminus deleted constructs are dimeric, while the neck-motor construct remains a monomer (Burns et al., 2014; Maney et al., 2001; Talapatra et al., 2015). Also subcellular localisation depends on these two domains (Moore et al., 2005; Welburn and Cheeseman, 2012; Wordeman et al., 1999).

1.3.2. Kinesin-13 movement and microtubule depolymerisation

Kinesin-13 members do not walk along microtubules, but use unbiased one-dimensional (1D) diffusion to reach microtubules' ends (Helenius et al., 2006). Movement by diffusion could be beneficial for targeting both microtubule ends and for fast movement, accelerating depolymerisation reactions (Helenius et al., 2006). While diffusion initiation depends on ATP hydrolysis, diffusion itself occurs without energy obtained from ATP hydrolysis (Burns et al., 2014; Helenius et al., 2006).

Kinesin-13 activity is regulated by conformational changes during its catalytic cycle of diffusion, depolymerisation and ATP hydrolysis. The extreme C-terminal tail and the neck-motor domain are involved in these conformational changes, but also the state of the bound nucleotide is important (Burns et al., 2014; Ems-McClung et al., 2013). In solution MCAK's activity is regulated by the extreme C-terminus. It folds back to the motor domain in proximity to the neck, bringing the molecule into a stabilised, closed conformation after ATP binding (Figure 5 (A); Burns et al., 2014; Ems-McClung et al., 2013; Moore and Wordeman, 2004; Talapatra et al., 2015). The C-terminus does not interact with the nucleotide binding

Introduction

sites, but enables stabilisation of MCAK's dimeric nature (Talapatra et al., 2015; Zong et al., 2016). For the interaction, the conserved EExxS motif within the C-terminal tail is essential (Talapatra et al., 2015; Zong et al., 2016).

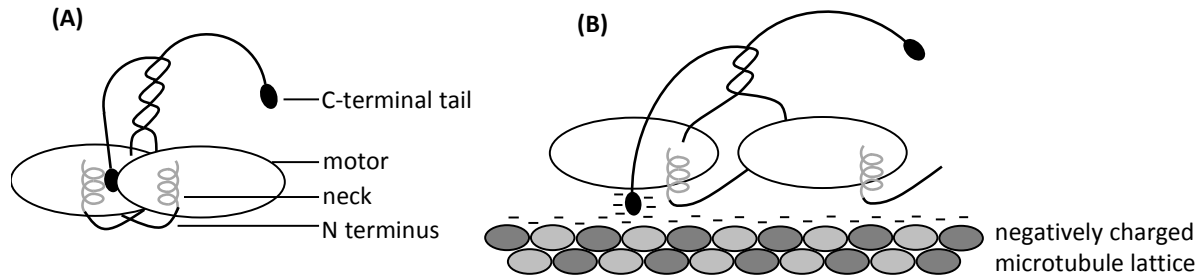


Figure 5: Model of closed and open conformation of the Kinesin-13 dimer. (A) In the closed conformation, the C-terminal tail with the EExxS motif interacts with the neck-motor domain and binds at the interface of two motor domains. The C-terminus, and to some extent also the N-terminus, contributes to dimerisation. (B) Motor domain binding to microtubules and to the C-terminus is mutually exclusive, inducing the open conformation. The negatively charged C-terminal EExxS motif and the negatively charged microtubule lattice contribute to 1D diffusion by electrostatic repulsion. Conformational change leads to settling of the neck domain to the microtubule lattice and the N-terminus delocalises. For simplification reasons two protofilaments represent the microtubule. The figure is modified and adapted from Talapatra et al., 2015.

The C-terminal tail and its attachment to the motor domain also regulates adequate lattice binding of MCAK. Mutants with deleted C-terminus or mutants unable to bind the motor domain exhibit increased lattice binding (Moore et al., 2005; Talapatra et al., 2015; Zong et al., 2016). Also the microtubule E-hook, which consists of an array of negatively charged amino acids within the C-termini of α - and β -tubulin subunits, has an influence on MCAK's lattice binding. While removal of the microtubule E-hook results in increased microtubule affinity of MCAK, it does not have an influence on the affinity of the mutant MCAK, in which the C-terminal tail is unable to bind to the motor (Talapatra et al., 2015). These results indicate that the neck-motor bound C-terminal tail and the E-hook cooperate in order to reduce MCAK's lattice binding affinity and to support its movement to the microtubule tips (Figure 5 (B); Moore et al., 2005; Talapatra et al., 2015). Thus, the electrostatic repulsion between the C-terminal tail and the E-hook could contribute to the 1D diffusion.

It was supposed that also electrostatic interactions between the positively charged neck and the tubulin E-hook are necessary for 1D diffusion (Helenius et al., 2006; Ovechkina et al., 2002). In contrast to conventional kinesins with the neck in parallel to or away from the microtubule, the helical neck domain of Kinesin-13 extends towards microtubules (Ogawa et al., 2004). Data suggest that conformational changes to the open conformation upon lattice

Introduction

binding induced ATP hydrolysis result in delocalisation of the N-terminus and in settling of the neck domain to the lattice (Burns et al., 2014; Cooper et al., 2010). Thus, by doing the initial step of lattice binding, the neck contributes to MCAK's delivery to the microtubule ends. But it was disproved that the neck itself is needed for diffusion (Cooper et al., 2010).

In solution MCAK is preferentially ATP bound and exists in a closed conformation (Ems-McClung et al., 2013; Friel and Howard, 2011; Helenius et al., 2006). Upon microtubule lattice binding, Kinesin-13 changes to an open conformation in a post-hydrolysis ADP-P_i state. The open conformation probably results from C-terminal tail dissociation. It is presumably induced by a conformational change within the motor's microtubule binding domain. C-terminal tail binding and microtubule binding to the motor domain are mutually exclusive (Talapatra et al., 2015). Thereby it is the lattice itself to trigger the release of the C-terminal tail and not the E-hook (Talapatra et al., 2015).

In the open state, Kinesin-13 is relaxed and binds weakly to the lattice, hence facilitating 1D diffusion (Figure 6; Asenjo et al., 2013; Burns et al., 2014; Ems-McClung et al., 2013; Helenius et al., 2006). This is in coincidence with MCAK's lattice stimulated ATPase activity (Moore and Wordeman, 2004). Deletion of the C-terminal tail increases ATPase activity, indicating again its regulatory function (Moore and Wordeman, 2004).

Reaching the microtubule ends by diffusion, nucleotide exchange from ADP to ATP is accelerated (Friel and Howard, 2011). This brings MCAK again into a high-affinity closed conformation (Burns et al., 2014; Ems-McClung et al., 2013). The C-terminal tail-neck interaction also contributes to the closed conformation. This could explain why the positive charges within the neck are essential for depolymerisation (Cooper et al., 2010; Ogawa et al., 2004; Ovechkina et al., 2002; Talapatra et al., 2015).

Introduction

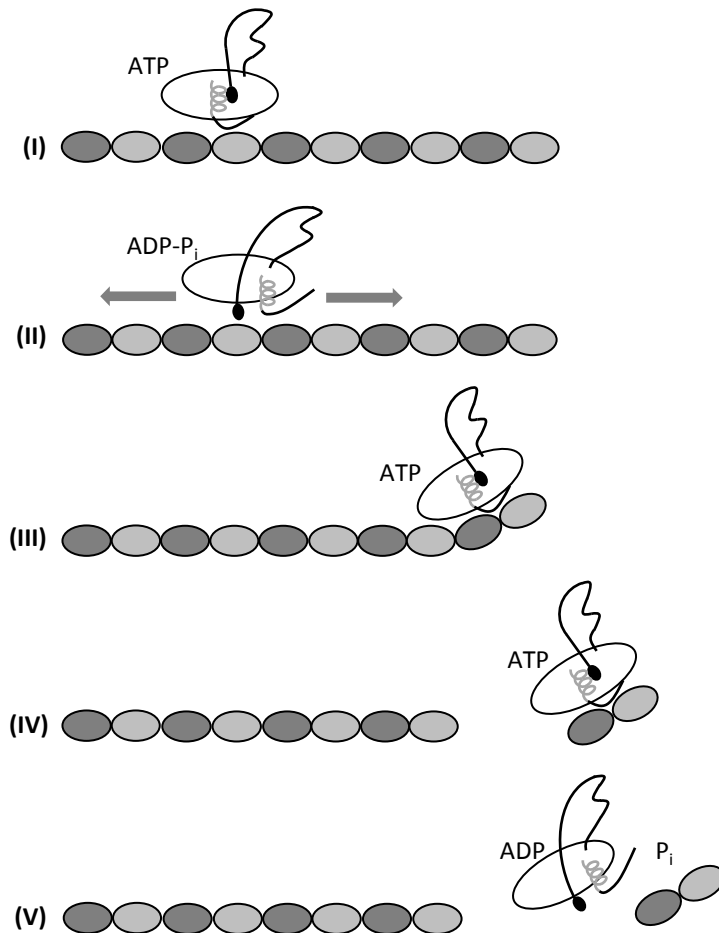


Figure 6: Model of the Kinesin-13 working cycle. In solution Kinesin-13 is in a ATP bound, closed conformation. **(I)** Binding to the microtubule lattice induces **(II)** ATP hydrolysis and a conformational change to the open conformation. In this conformation Kinesin-13 uses 1D diffusion by repulsion of the negatively charged C-terminal Kinesin-13 tail and the negatively charged microtubule lattice for reaching one of the two microtubule ends. **(III)** At a microtubule end, Kinesin-13-ADP exchanges ADP for ATP and changes to the closed conformation. Alternatively, Kinesin-13-ATP directly binds from solution to a microtubule end, **(IV)** binds tightly to tubulin and bends it until it finally peels off the protofilament. **(V)** The ternary Kinesin-13-ATP-tubulin complex is released by ATP hydrolysis, which brings Kinesin-13 again into the open conformation. In solution ADP is exchanged for ATP and the working cycle starts again. For simplification reasons a Kinesin-13 monomer is depicted instead of the dimer, the three areas for tubulin binding are not depicted and a protofilament represents the microtubule.

Kinesin-13-ATP binds to the tubulin intradimer interface (Asenjo et al., 2013; Moores et al., 2002). Three areas of the kinesin are necessary for binding (Figure 7 (A)): area 1 contains loop 8 and binds close to the interdimeric end of β -tubulin (Asenjo et al., 2013). Area 2 includes $\alpha 4$ and loop 11. Both belong to switch II. Switch II, in addition to switch I, changes conformation depending on the bound nucleotide species (Kull and Endow, 2002). Moreover, the KEC motif is located within this side. It is necessary for microtubule binding (Shiple et al., 2004). Area 2 binds at the intradimer interface of the $\alpha\beta$ -tubulin heterodimer

Introduction

(Asenjo et al., 2013). Area 3 is Kinesin-13 class specific and consists of loop 2. It contains the KVD motif necessary for binding, bending and depolymerising microtubule protofilaments (Asenjo et al., 2013; Ogawa et al., 2004; Shipley et al., 2004; Wang et al., 2015). The loop 2 associates with the microtubule interdimer interface. The lysine and valine of the KVD motif interact with α -tubulin of the tubulin heterodimer, while aspartate interacts with the β -tubulin of the subsequent tubulin heterodimer (Asenjo et al., 2013; Wang et al., 2015). The loop 2 mediated interaction with tubulin is missing for conventional kinesins and performs most of all the differences between walking along and bending microtubules (Asenjo et al., 2013).

The KVD interaction with the tubulin interdimer is essential for a conformational change in the depolymerising Kinesin-13-ATP upon microtubule end binding (Wang et al., 2015). Mutation of the switch II motif (DxxGxE) G495A in human MCAK inhibits this conformational change, keeping the kinesin in a pre-conformational change mimicking state (Wang et al., 2012). The mutant is characterised by the remaining ability to bind to microtubules but its failure to depolymerise them and abolished ATPase activity (Wagenbach et al., 2008; Wang et al., 2012).

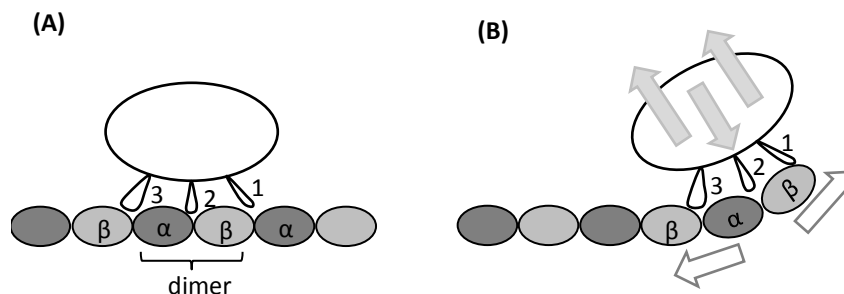


Figure 7: Kinesin-13 binds to the tubulin intradimer interface and facilitates bending at the end of microtubules. A monomeric Kinesin-13 motor domain is illustrated with the three areas interacting with tubulin: area 1 binds to β -tubulin close to the interdimer interface; area 2 binds to the intradimer interface; the class-specific KVD motif of area 3 binds with lysine and valine to α -tubulin of the tubulin heterodimer while aspartate binds to β -tubulin of the subsequent dimer. **(A)** At the straight microtubule lattice Kinesin-13 binds weakly with dominating interactions of area 2 and 3 with tubulin. **(B)** At the end of microtubules, Kinesin-13 binds tightly in a 'crossbow-type' leading to a curved-sheared tubulin conformation. Kinesin-13 pulling and pushing forces for tubulin bending are illustrated by light grey arrows, tubulin shearing forces are illustrated by white arrows. For simplification reasons a protofilament represents the microtubule.

At microtubule ends, Kinesin-13-ATP binds in a 'crossbow-type', bringing the tubulin dimer in a curved-sheared conformation (Figure 7 (B); Asenjo et al., 2013; Mandelkow et al., 1991; Moores et al., 2002). The three areas within the motor domain bend the tubulin dimer. They

pull the plus and minus ends of the tubulin dimer relative to the intradimer interface (Asenjo et al., 2013). The bent tubulin dimers are unable to undergo stabilising lateral interaction again and finally peel off the microtubule (Asenjo et al., 2013).

Instead of lattice diffusion by Kinesin-13-ADP-P_i, Kinesin-13-ATP may also directly bind from solution to the protofilament end and induce a curved conformation (Asenjo et al., 2013; Wang et al., 2012). One hypothesis why Kinesin-13 recognises microtubule ends is that there are lateral protofilament contacts missing, which enables their bending by Kinesin-13 (Asenjo et al., 2013). At the straight tubulin of the microtubule lattice, Kinesin-13 binding sites are too far apart and Kinesin-13 is unable to bind tightly (Asenjo et al., 2013).

Finally, depolymerisation releases a ternary complex of Kinesin-13-ATP-tubulin. This itself does not depend on ATP hydrolysis (Wang et al., 2015). Release of the ternary complex depends on ATP hydrolysis. It sets Kinesin-13 free, because Kinesins-13's affinity for tubulin is reduced in the open state and when bound to ADP (Ems-McClung et al., 2013; Wagenbach et al., 2008). This step is blocked by the switch II motif mutant E497A, the post-conformational change mimicking mutant, which keeps the ternary complex tightly bound (Wagenbach et al., 2008; Wang et al., 2015).

In solution the new Kinesin-13 catalytic cycle begins with binding of ATP (Ems-McClung et al., 2013).

1.3.3. Kinesin-13 family

The microtubule depolymerising Kinesin-13 family consists of four members within human and mouse: Kif2A, Kif2B, Kif2C/MCAK and Kif24. Kif24 and Kif2A act as microtubule depolymerisers at the formation of cilia or at the regulation of axonal growth cones (Homma et al., 2003; Kobayashi et al., 2011; Miyamoto et al., 2015). Mitotic functions were described for Kif2A, Kif2B and MCAK (Ganem and Compton, 2004; Manning et al., 2007).

During mitosis MCAK is located at centromeres and kinetochores, spindle poles and at microtubule plus ends, where it also localises in interphase (Moore et al., 2005; Wordeman and Mitchison, 1995). In the assembling bipolar spindle, it depolymerises non-kinetochore microtubule tips (Domnitz et al., 2012). This increases the amount of microtubules available for kinetochore attachments and thus, contributes to correct bipolar attachment (Domnitz et al., 2012). At low tension across the centromere, because of incorrect microtubule-kinetochore attachments, centromeric MCAK translocates to the kinetochore inner plate in

close proximity to microtubule binding sites (Kline-Smith et al., 2004). Depletion studies of centromeric MCAK indicate that it enhances microtubule turnover at kinetochores for error correction in metaphase (Bakhoun et al., 2009; Kline-Smith et al., 2004; Wordeman et al., 2007). In prometaphase this task is performed by Kif2B, which localises to kinetochores solely during this cell cycle phase (Bakhoun et al., 2009; Manning et al., 2007). However, MCAK is not directly involved in chromatid segregation during anaphaseA.

In contrast, studies in *D. melanogaster* early embryos revealed that Klp10A (kinesin like protein) and Klp59C, corresponding to Kif2A and MCAK, respectively, are needed for chromosome-to-pole movement (Buster et al., 2007; Rogers et al., 2004). Klp59C depolymerises microtubules' plus ends at kinetochores, contributing to the 'Pac-Man-model', while centrosomal Klp10A depolymerises microtubules at their minus ends, leading to a poleward flux of chromatids (Buster et al., 2007; Rogers et al., 2004).

Saccharomyces cerevisiae, like *Schizosaccharomyces pombe*, completely lacks Kinesin-13 members. Depolymerisation activity is carried out by Kinesin-14 members (Kar3p (karyogamy) in *S. cerevisiae*; Pkl1p and Klp2p in *S. pombe*) and Kinesin-8 members (Kip3p (kinesin related protein) in *S. cerevisiae*; Klp5p and Klp6p in *S. pombe*), which depolymerise microtubules solely from the minus or plus end, respectively (Endow et al., 1994; Troxell et al., 2001; Unsworth et al., 2008; Varga et al., 2006). By heterodimerisation with Cik1p (chromosome instability and karyogamy), Kar3p also targets microtubule plus ends (Chu et al., 2005; Sproul et al., 2005). Of the six kinesins in budding yeast, five were shown to be involved in mitosis (DeZwaan et al., 1997; Gupta et al., 2006; Hepperla et al., 2014; Hoyt et al., 1992; Huyett et al., 1998; Miller et al., 1998; Roof et al., 1992; Saunders et al., 1997; Straight et al., 1998; Tytell and Sorger, 2006).

1.3.4. Kinesin-13 family in *T. brucei*

Genome analysis revealed a large number of kinesin motor proteins in kinetoplastids (Berriman et al., 2005). In *T. brucei* (41) and in human (45) a similar quantity of kinesin family proteins was identified (Miki et al., 2001; Wickstead and Gull, 2006). In contrast to kinesins from vertebrates, only a few kinesins from Trypanosomes have yet been functionally characterised. Among the 41 kinesins in *T. brucei*, there are 13 kinetoplastid-specific and 15 orphan kinesins (Wickstead and Gull, 2006). Orphan kinesins do not belong to any known

Introduction

kinesin family. Kinetoplastid-specific and orphan kinesins could compensate the absence of conserved mitotic kinesins, like kinesin-5 and -7 (Wickstead and Gull, 2006).

A kinesin family that has been functionally characterised in *T. brucei* is the kinesin-13 family. In *T. brucei* sequence analysis revealed seven members of the Kinesin-13 family (Wickstead et al., 2010b). Based on phylogenetic typing of the catalytic domain and on protein architecture, *TbKif13-1*, -2, -3, -4a, -4b and -5 belong to the Kinesin-13A subfamily, while *TbKif13-6* is a Kinesin-13C subfamily member (Wickstead et al., 2010a). All of them possess the KEC motif, necessary for microtubule binding (see 1.3.2.; Shipley et al., 2004). The KVD motif of *TbKif13-1*, -5 and -6, necessary for microtubule depolymerisation, is changed to RVD in the flagellar *TbKif13-4a*, b and 13-2, and to KYD in the cytoplasmatic *TbKif13-3* (Shipley et al., 2004).

Localisation studies of the Kinesin-13 family in *T. brucei* showed that only *TbKif13-1* is located nuclear during closed mitosis and would thus be a possible mitotic kinesin (Chan et al., 2010; Wickstead et al., 2010a). Polyclonal antibody mediated staining of endogenous *TbKif13-1* showed its cell cycle specific appearance from S-phase until the end of mitosis (Chan et al., 2010). In contrast, direct fluorescence microscopy of endogenous C-terminal GFP tagged *TbKif13-1* detected it throughout the cell cycle (Wickstead et al., 2010a). Its mitotic localisation along the spindle differs to the spatially changing localisation of the vertebrate Kinesin-13B MCAK during mitosis (see 1.3.3.). Depletion of *TbKif13-1* resulted in long and bent spindle structures in *T. brucei*, leading to segregation defects of both megabase and minichromosomes, indicating its necessity for proper spindle formation (Chan et al., 2010; Wickstead et al., 2010a). It also resulted in an increase of G2/early mitosis arrested cells and zoids, supporting its mitotic or cytokinetic function (Wickstead et al., 2010a). After a few days, RNAi mediated *TbKif13-1* depletion led to cell death of *T. brucei* (Chan et al., 2010; Wickstead et al., 2010a). This was also observed in a mouse model, where inoculated mice did not show infection several days after *TbKif13-1* RNAi induction (Chan et al., 2010).

TbKif13-2 is expressed weakly in procyclics. Only ectopically expressed myc-tagged *TbKif13-2* was detected at the flagellar tip (Chan, 2008; Chan et al., 2010). Also its *Leishmania major* orthologue *LmjKin13-2* was only detectable after ectopic expression (Blaineau et al., 2007). In addition to the flagellar tip, *LmjKin13-2* was found at the flagellum base and occasionally

along the flagellum (Blaineau et al., 2007). *LmjKin13-2* regulates the length of the flagellum, whereas the function of *TbKif13-2* in flagellar length control is supposed to be insignificant (Blaineau et al., 2007; Chan and Ersfeld, 2010). However, it has an impact on the initial growth of the new flagellum (Chan and Ersfeld, 2010).

Alongside the flagellum, *TbKif13-4a* is located, but its function has not yet been identified (Chan, 2008; Chan et al., 2010).

It is supposed that flagellar length control in *T. brucei* occurs at different levels, including intraflagellar transport and other proteins (Absalon et al., 2008; Casanova et al., 2009).

The specific functions of the other *T. brucei* Kinesin-13 family members have not yet been determined. However, their subcellular localisations are determined. *TbKif13-3* and *TbKif13-5* locate throughout the cell body (Chan, 2008; Chan et al., 2010). *TbKif13-5* is detectable only after ectopic expression (Chan, 2008; Chan et al., 2010).

In immunofluorescence studies, *TbKif13-6* colocalises with the single mitochondrion in *T. brucei* (Chan, 2008). The failure of *TbKif13-6* depletion by RNAi, and the failure of a *TbKif13-6* double knock-out cell line generation, indicates its basic necessity for *T. brucei* (Chan, 2008; unpublished data).

1.3.5. Mitotic kinesins as anti-cancer drug targets

Cancer cells exhibit unregulated proliferation. This property is used by several anti-cancer drugs, focusing on mitotic proteins. Tubulin is one of the most used mitotic anti-cancer drug targets. Compounds that alter microtubule functions are e.g. vinca alkaloides and taxanes (Noble et al., 1958; Schiff et al., 1979; Wani et al., 1971). They are used for treatment of several cancer types (Mencoboni et al., 2017; Mukai et al., 2017; Scherz et al., 2017; Wagner et al., 2017).

Mitotic kinesins that interact with the microtubular spindle are also considered potential cancer drug targets. A frequently mentioned target is Eg5 (Kif11, a Kinesin-5 member), which is necessary for bipolar spindle assembly in prophase (Blangy et al., 1995; Kapitein et al., 2005). Many Eg5 inhibitor compounds have been tested in clinical trials, but failed to show sufficient clinical efficacy (Holen et al., 2011; Kantarjian et al., 2012; LoRusso et al., 2015; Purcell et al., 2010). Other Eg5 inhibitors, also in combination with additional drugs, are currently evaluated in clinical trials (Infante et al., 2017).

Anti-tumor activity is also shown for CENP-E (Kif10, a Kinesin-7 member) inhibitors (Bennet et al., 2015; Wood et al., 2010). CENP-E is required for progression from metaphase to anaphase because of its contribution to facilitating end-on attachments of laterally attached kinetochores (Ding et al., 2010; Schaar et al., 1997; Yen et al., 1991).

The kinesin-8 family member Kif18A was found overexpressed in breast and colorectal cancer (Nagahara et al., 2011; Zhang et al., 2010). It is located at kinetochore microtubules and contributes to correct chromosome congression as microtubule depolymeriser (Stumpff et al., 2008; Stumpff et al., 2011; Stumpff et al., 2012). Yet, there have only been identified *in vitro* Kif18A inhibitors (Braun et al., 2015; Catarinella et al., 2009).

Overexpression of the microtubule depolymeriser MCAK is found in colon, gastric and breast cancer, and it is associated with poor prognosis (Ishikawa et al., 2008; Nakamura et al., 2007; Shimo et al., 2008). Cell-based studies showed that MCAK overexpression mediates paclitaxel resistance, while its depletion increases sensitivity to anti-microtubule drugs (Ganguly et al., 2011a; Ganguly et al., 2011b; Hedrick et al., 2008). Thus, a combinatorial treatment of MCAK inhibition and paclitaxel addition is considered to overcome limiting success of sole paclitaxel treatment (Hedrick et al., 2008; Rizk et al., 2009). Identification of first potential drugs targeting MCAK occurred, but further studies are mandatory (Aoki et al., 2005).

1.4. Regulation of Kinesin-13

1.4.1. Aurora kinase

Regulation of proteins is achieved in part by modifications, like phosphorylation mediated by kinases. One known kinase family is that of Aurora-like kinases. They are essential for mitosis and cytokinesis in eukaryotes. Aurora-like kinases are serine/threonine kinases. In yeast there is only a single Aurora-like kinase, Ipl1p (increase in ploidy) in *S. cerevisiae* and Ark1p (actin regulating kinase) in *S. pombe*. In *D. melanogaster* there are already two Aurora-like kinases, AuroraA and AuroraB. In vertebrates there is a third one, AuroraC. The three Aurora-like kinases in *T. brucei* are TbAuk1, TbAuk2 and TbAuk3 (Tu et al., 2006).

AuroraB, like the single yeast Aurora kinases, forms the catalytic domain of the chromosomal passenger complex (CPC). In addition, the CPC contains the regulatory and subcellular targeting components INCENP (inner centromer protein), survivin and borealin (Cooke et al., 1987; Gassmann et al., 2004). INCENP contains a β -tubulin binding site within the N-

Introduction

terminus and an internal coiled-coil domain that is used for non-spindle microtubule binding (Ainsztein et al., 1998; Mackay et al., 1993; Wheatley et al., 2001). INCENP and survivin contain centromere targeting domains, and borealin contributes to chromosome and centromere binding (Ainsztein et al., 1998; Klein et al., 2006; Vader et al., 2006).

The mitotic localisation of the CPC is connected to its respective mitotic function. At the onset of mitosis, the CPC moves from condensing chromosome arms to centromeres (Jeyaprakash et al., 2007; Klein et al., 2006; Murata-Hori et al., 2002). There, AuroraB is involved in resolving mal-oriented kinetochore-microtubule interactions during metaphase (Cimini et al., 2006; Hauf et al., 2003; Kallio et al., 2002; Knowlton et al., 2006; Lampson et al., 2004). It is supposed to phosphorylate subunits of the KMN (Knl1 complex, Mis12 complex, Ndc80 complex) network (Cheeseman et al., 2006; Welburn et al., 2010). The KMN network is located at the outer kinetochore and is a keyplayer in kinetochore-microtubule attachments (Cheeseman et al., 2006). The fine tuning of correcting kinetochore-microtubule attachments is supposed to occur via the AuroraB substrate MCAK, which weakens the interaction (Wordeman et al., 2007).

At the metaphase to anaphase transition the CPC localises at the central spindle (Jeyaprakash et al., 2007; Murata-Hori et al., 2002). There, it contributes to anaphase onset, since AuroraB is involved in checkpoint signaling and recruits checkpoint proteins to kinetochores (Ditchfield et al., 2003; Kallio et al., 2002; Santaguida et al., 2011). Finally, the CPC moves to the midbody for cytokinesis (Jeyaprakash et al., 2007; Murata-Hori et al., 2002).

AuroraB regulates MCAK by phosphorylation of several sites within the N-terminus and the neck domain (Lan et al., 2004; Zhang et al., 2007). These affect MCAK's subcellular localisation and activity (Lan et al., 2004; Zhang et al., 2007). The major phosphoregulation site of MCAK is within its neck domain at S196 (*Xenopus laevis*), which is conserved. Phosphorylation at that serine inhibits MCAK's depolymerisation activity (Andrews et al., 2004; Lan et al., 2004). It prevents the interaction of the C-terminus and the neck domain and thus, the necessary conformational change for tight microtubule lattice binding and depolymerisation (Ems-McClung et al., 2013).

AuroraB phosphorylates MCAK also at other sites. These phosphorylations determine its inner centromeric or kinetochore localisation from prometa- to metaphase (Andrews et al., 2004; Knowlton et al., 2006; Lan et al., 2004; Wordeman et al., 2007; Zhang et al., 2007).

AuroraA mediated phosphorylation regulates MCAK's spindle association that enhances spindle bi-polarity (Zhang et al., 2008).

1.4.2. *T. brucei* Aurora kinase

Among the three Aurora-like kinases in *T. brucei*, there is only *TbAuk1* involved in mitosis and cytokinesis (Tu et al., 2006). *TbAuk1* is the catalytic domain of the CPC. The *T. brucei* CPC also consists of the regulatory subunits *TbCPC1* and *TbCPC2*, which do not have structural similarity to INCENP, survivin and borealin (Li et al., 2008a). The C-terminal tails of *TbCPC1* and *TbCPC2* serve for interaction with each other and for binding to the N- and C-terminus of *TbAuk1* (Hu et al., 2014). The *TbCPC1* C-terminus contains the IN-box motif that is necessary for *TbAuk1* binding and which is highly divergent from that in INCENP (Hu et al., 2014).

The IN-box mediated binding of INCENP to AuroraB already activates low levels of kinase activity (Honda et al., 2003). The binding induces a conformational switch of the AuroraB T-loop to the active state (Sessa et al., 2005). This enables AuroraB to phosphorylate the C-terminal TSS motif within INCENP and T232 in AuroraB, phosphorylations that are necessary for full kinase activity (Honda et al., 2003; Yasui et al., 2004). These phosphorylations are probably conducted *in trans* by nearby CPCs (Cormier et al., 2013; Sessa et al., 2005).

In *TbAuk1* phosphorylation of the T-loop T184, the T232 equivalent, is necessary for its full kinase activity (Hu et al., 2014). T188 phosphorylation contributes to *TbAuk1* activity, but to a lesser extent than T184 phosphorylation (Hu et al., 2014). Also the conserved lysine K58 is necessary for *TbAuk1*'s catalytic function (Li and Wang, 2006). Degradation of *TbAuk1* is facilitated by the ubiquitin-proteasome pathway, using at least two D-boxes (destruction) within the *TbAuk1* C-terminus (Hu et al., 2014). Like human AuroraB, *TbAuk1* ubiquitination requires the APC/C (anaphase-promoting complex/cyclosome; Hu et al., 2014; Stewart and Fang, 2005).

In procyclic and bloodstream *T. brucei* cells, *TbAuk1* is necessary for spindle formation, proper chromosome segregation and cytokinesis (Li and Wang, 2006; Li et al., 2008b; Li et al., 2009; Tu et al., 2006). These functions are associated with its respective subcellular localisation. *TbAuk1*, in conjunction with *TbCPC1* and *TbCPC2*, localises intranuclear in G2, is found at the mitotic spindle during metaphase and anaphaseA, and moves to the spindle midzone in anaphaseB (Li et al., 2008a; Li et al., 2008b). During anaphaseB the CPC starts to leave the nucleus and accumulates at the dorsal site of the cell (Li et al., 2008a). Recent

studies showed that *TbAuk1* is recruited to the new FAZ tip during late anaphase by the trypanosome-specific protein *TbCif1* (cytokinesis initiation factor; Zhou et al., 2016). Previously, *TbCif1* is phosphorylated by *TbPlk* (polo-like kinase), which targets it to the new FAZ (Zhou et al., 2016). During cytokinesis the CPC and *TbCif1* locate between the two separating anterior tips, travelling along the cleavage furrow (Li et al., 2008a; Zhou et al., 2016).

The CPC contributes to *TbAuk1*'s localisation. Studies with truncated CPC subunits that are unable to interact with the other CPC subunits, indicate a *TbCPC1*-dependent CPC localisation (Hu et al., 2014). In contrast, RNAi studies revealed that all CPC subunits contribute to its localisation (Li et al., 2008a; Li et al., 2009). However, there have not yet been identified microtubule-binding motifs within the CPC subunits (Hu et al., 2014).

Also the orphan kinesins *TbKIN-A* and *TbKIN-B*, that interact with *TbAuk1*, contribute to *TbAuk1*'s localisation (Li et al., 2008a; Li et al., 2008b). They are necessary for spindle segregation, chromosome segregation and cytokinesis (Li et al., 2008a). The Touseld-like kinase *TbTlk1* associates with *TbKIN-B* and the CPC and contributes to their localisation (Li et al., 2008b). *TbAuk1* cooperates with *TbTlk1* to regulate spindle assembly and chromosome segregation (Li et al., 2007). *TbTlk1* is a substrate of *TbAuk1*, but also autophosphorylates, and locates at the spindle poles during mitosis (Li et al., 2007). *TbAuk1* or *TbTlk1* depletion results in their mutual mislocalisation (Li et al., 2008b).

1.5. Nuclear protein import and export

The eukaryotic nucleus is delimited by a nuclear envelope. In Trypanosomes, the nuclear envelope is maintained even throughout mitosis, exhibiting closed mitosis. Thus, cell cycle-dependent import or export of proteins is a possible way of regulating the activity of nuclear proteins, such as *TbKif13-1*.

Nuclear pore complexes (NPC) allow energy-dependent nuclear import of proteins translated within the cytoplasm as well as nuclear export. For nuclear import, a heterodimer of $\alpha\beta$ -importin is used as transporter. α -importin binds to the nuclear localisation sequence (NLS) of the cargo protein (Görlich et al., 1995). Classical monopartite NLS consist of three or four basic amino acids with the sequence K(K/R)X(K/R), while bipartite NLS show two clusters of basic amino acids separated by a spacer of ten to twelve amino acids (Conti and Kuriyan, 2000; Dang and Lee, 1988; Hodel et al., 2001; Kalderon et al., 1984; Robbins et al.,

1991). These two kinds of NLS were also found in *T. brucei* (Lips et al., 1996; Marchetti et al., 2000). Noncanonical NLS have the sequence KRX(W/F/Y)XXAF, (P/R)XXKR(K/R) or LGKR(K/R)(W/F/Y) (Kosugi et al., 2009a).

β -importin binds the complex to the NPC and facilitates release of the cargo protein and α -importin within the nucleus by binding to Ran-GTP (Görlich et al., 1995; Lee et al., 2005). The nucleotide state of Ran is mediated by the Ran guanine nucleotide exchange factor (RanGEF) in the nucleus and the Ran GTPase-activating protein (RanGAP) in the cytoplasm (Becker et al., 1995; Bischoff and Ponstingl, 1991; Corbett et al., 1995; Klebe et al., 1995). Within *T. brucei* the key components of the nuclear transport machinery were identified by proteomic analysis and bioinformatics, but like for all apicomplexa no RanGAP was identified (DeGrasse et al., 2009; Frankel and Knoll, 2009; O'Reilly et al., 2011; Yahya et al., 2012). Probably this function is realised by another protein.

For nuclear export, cargo proteins are bound to exportin and RanGTP, whose hydrolysis to GDP within the cytoplasm sets cargo and exportin free (Askjaer et al., 1998; Fornerod et al., 1997). Export cargo proteins contain nuclear export sequences (NES). In general NES are characterised by leucine-rich domains or hydrophobic patterns interspersed by negatively charged amino acids (Hellman et al., 2007; la Cour et al., 2004; Xu et al., 2012).

1.6. Aims of the thesis

Human African trypanosomiasis depends on cell proliferation within the mammalian host. This makes its progression similar to cancer. When fighting cancer, small molecule inhibitors of mitotic kinesins are tested as chemotherapeutics (see 1.3.5.). In *T. brucei*, RNAi mediated depletion of mitotic *TbKif13-1* resulted in cell death and in prevention of infection in an inoculated mouse model (Chan et al., 2010; Wickstead et al., 2010a). This makes *TbKif13-1* an excellent potential drug target for fighting trypanosomiasis.

In the first section of the thesis, the aim is to establish the prerequisites for a heterologous *in vivo* assay and an *in vitro* assay for a high-throughput inhibitor screen. The basic idea for both is that *TbKif13-1* depolymerises microtubules, while an applied suitable small molecule inhibitor would prevent depolymerisation. As depolymerisation substrate should serve the cytoskeleton of HeLa cells in the heterologous *in vivo* assay, and the cytoskeleton of *T. brucei* cells in the *in vitro* assay. Analysis of the microtubule depolymerisation state shall occur via microscopy.

Introduction

- a) For the heterologous *in vivo* assay, a stable HeLa cell line shall be generated, inducibly overexpressing *TbKif13-1*, which is expected to result in cytoskeleton depolymerisation.
- b) For the *in vitro* assay, *T. brucei* cytoskeletons shall be prepared on 384-well plates that are depolymerisable by recombinantly purified *TbKif13-1*.

In the second section of the thesis, the aim is the functional characterisation of *TbKif13-1* domains. Several *TbKif13-1* deletion constructs and amino acid exchange mutants are constructed for *in vivo* and *in vitro* studies.

For *in vivo* studies, transgenic cell lines, ectopically expressing *TbKif13-1* deletion constructs, are generated for the following studies.

- a) Immunfluorescence studies throughout the cell cycle indicate *TbKif13-1* domains necessary for nuclear import and export.
- b) Cell cycle-dependent regulation of *TbKif13-1* is examined in terms of a proteasome-dependent degradation with an assay that inhibits translation and the proteasome.
- c) Toxicity of *TbKif13-1* domains is indicated by growth curves and flow cytometry analysis.
- d) Negative influence of the domains to spindle formation and maintenance is determined by staining of the mitotic spindle for immunfluorescence studies.
- e) The ability of the *TbKif13-1* domains to bind to spindle microtubules is examined via immunfluorescence microscopy of cytoskeleton preparations.

For *in vitro* studies, *TbKif13-1* deletion constructs are recombinantly purified and are used for the following studies.

- a) The microtubule binding ability of the *TbKif13-1* domains is determined *in vitro* via the tubulin sedimentation assay. In addition, this assay displays *TbKif13-1* domains necessary for microtubule depolymerisation.
- b) The microtubule depolymerisation activity of *TbKif13-1* domains is verified using *T. brucei* cytoskeletons as substrate for an immunfluorescence microscopy depolymerisation assay. The depolymerisation assays will allow determination of *TbKif13-1*'s minimal functional construct.
- c) The conservation of the decoupled mechanism for microtubule depolymerisation and ATPase activity is tested for *TbKif13-1*. Recombinantly purified *TbKif13-1* amino acid

Introduction

mutants are applied to the malachite green assay to determine the state of their ATPase activity. Using the tubulin sedimentation assay, their depolymerisation activity is tested.

In the third section of the thesis, the aim is to identify a possible phosphorylation and depolymerisation regulation of *TbKif13-1* by *TbAuk1*.

To this end, *in vitro* assays with recombinantly purified *TbKif13-1* and immunoprecipitated *TbAuk1* from *T. brucei* cell lysate are used.

- a) *TbAuk1* mediated *TbKif13-1* phosphorylation is examined with a ^{33}P phosphorylation assay.
- b) An inhibitory regulation of *TbKif13-1* by *TbAuk1* is determined using the tubulin sedimentation assay.

2. Results

2.1. Attempt to establish a procedure for a *TbKif13-1* high-throughput inhibitor screen

In this thesis it was tried to establish the prerequisites for a *TbKif13-1* high-throughput inhibitor screen, using a small molecule library. An *in vivo* and an *in vitro* assay were considered. Both assays were based on a substrate microtubule cytoskeleton, which was expected to be depolymerised by *TbKif13-1*.

For the heterologous *in vivo* assay, the substrate microtubule cytoskeleton was that of interphase HeLa cells. These HeLa cells should inducibly overexpress transgenic *TbKif13-1* for depolymerisation. For the *in vitro* assay, the substrate microtubule cytoskeleton were *T. brucei* cytoskeleton preparations, to which recombinantly purified *TbKif13-1* was added for depolymerisation.

Addition of an appropriate inhibitor would prevent the microtubule cytoskeleton depolymerisation in both assays (Figure 8). Results should be determined by image analysis.

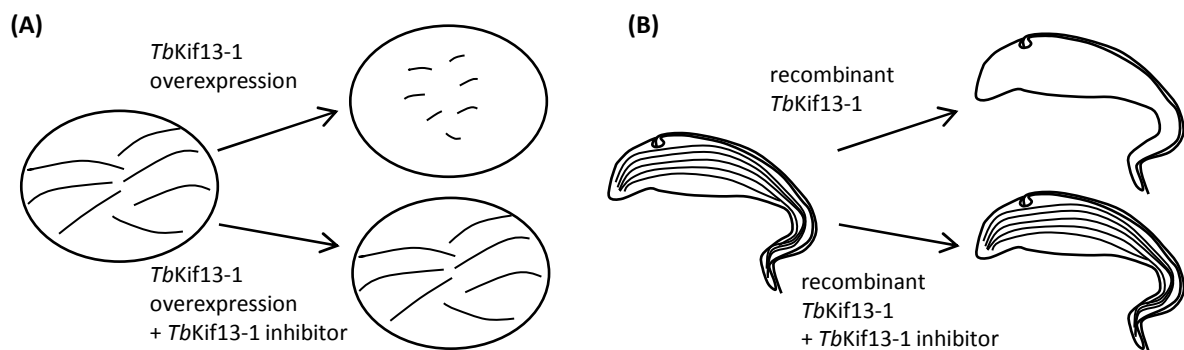


Figure 8: Schematic illustration of the heterologous *in vivo* and the *in vitro* assay. (A) Heterologous *in vivo* assay. Interphase HeLa cells exhibit a spread microtubule cytoskeleton (black lines). Inducible overexpression of the transgenic *TbKif13-1* is expected to lead to microtubule depolymerisation, while addition of an appropriate *TbKif13-1* inhibitor would rescue the microtubule cytoskeleton from depolymerisation. (B) *In vitro* assay. *T. brucei* cytoskeleton preparations (microtubules are illustrated as black lines) serve as depolymerisation substrate for recombinantly purified *TbKif13-1*. Addition of an appropriate *TbKif13-1* inhibitor would prevent cytoskeleton depolymerisation. Evaluation of both assays should occur via immunofluorescence microscopy of the microtubule cytoskeletons.

2.1.1. Heterologous *in vivo* assay

The prerequisite for the heterologous *in vivo* inhibitor screen assay was the generation of a stable HeLa cell line that inducibly overexpresses *TbKif13-1* for cytoskeleton depolymerisation. For easier microscopic visualisation of *TbKif13-1*, it was N-terminal eGFP

Results

tagged. Furthermore, a S143A mutation in *TbKif13-1* was introduced to prevent its inhibition, which is probably induced by AuroraB kinase mediated phosphorylation (see 1.4.1.; Figure S 1).

The basic functionality of the assay, regarding the ability of overexpressed ^{eGFP}*TbKif13-1* S143A to depolymerise the microtubule cytoskeleton of HeLa interphase cells, was tested. HeLa Flp-In cells were transiently transfected with *pcDNA5/FRT/TO*-^{eGFP}*TbKif13-1* S143A. HeLa cells with reduced microtubule cytoskeleton were observed already twelve hours after induction of ^{eGFP}*TbKif13-1* S143A overexpression (Figure 9). It seemed that a more intense ^{eGFP}*TbKif13-1* S143A signal correlated with a stronger cytoskeleton depolymerisation effect. Non transfected and non induced cells served as control. For verification, HeLa cells were transiently transfected with the vector *pCS2*-^{eGFP}*TbKif13-1* S143A. It allowed constitutive expression of the transgene, in contrast to the inducible expression allowed by *pcDNA5/FRT/TO*. Depolymerisation effects in these cells were the same (Figure S 2).

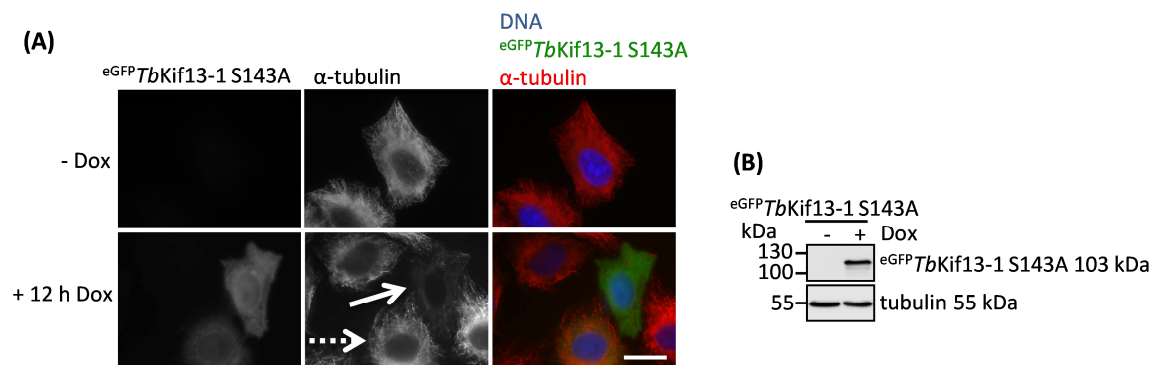


Figure 9: Microtubule cytoskeleton depolymerisation of HeLa Flp-In cells transiently transfected with *pcDNA5/FRT/TO*-^{eGFP}*TbKif13-1* S143A. (A) HeLa Flp-In cells transiently transfected with *pcDNA5/FRT/TO*-^{eGFP}*TbKif13-1* S143A, that overexpressed ^{eGFP}*TbKif13-1* S143A (green, autofluorescence), showed a reduced microtubule cytoskeleton (red, α-tubulin antibody TAT); white arrow: cell with reduced cytoskeleton; dashed arrow: cell with less reduced cytoskeleton, probably due to lower ^{eGFP}*TbKif13-1* S143A expression rate. The nucleus was DAPI (blue) stained. Cells were harvested 12 h after induction and fixed with methanol. Non transfected and non induced cells served as control. Scale bar 20 μm. (B) Westernblot of HeLa Flp-In cells transiently transfected with *pcDNA5/FRT/TO*-^{eGFP}*TbKif13-1* S143A, to verify the overexpression of ^{eGFP}*TbKif13-1* S143A after induction. ^{eGFP}*TbKif13-1* S143A was detected using α-GFP, tubulin was detected using α-tubulin antibody TAT.

The generation of a stable HeLa cell line, inducibly overexpressing ^{eGFP}*TbKif13-1* S143A, used the 'Flp-InTM T-REXTM System' with HeLa Flp-In cells and the vector *pcDNA5/FRT/TO*-

Results

eGFP^{TbKif13-1 S143A}. No reduced microtubule cytoskeleton was observed within successful stable transfected cells from twelve to 72 h after overexpression induction (Figure 10).

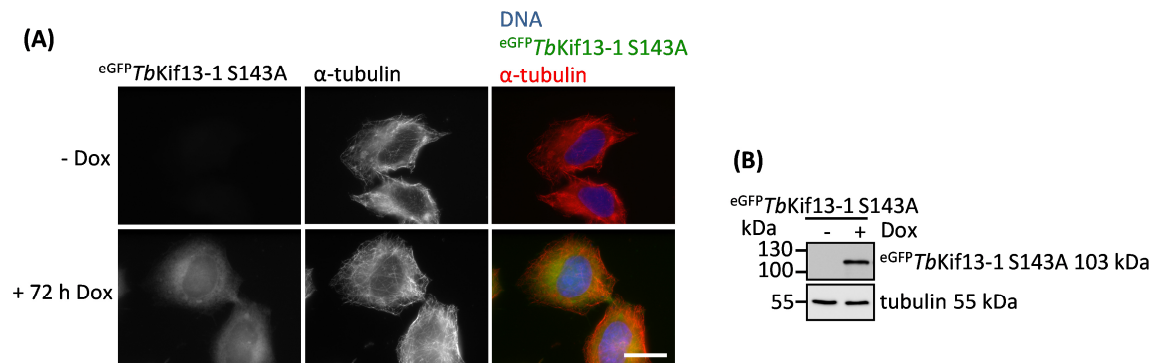


Figure 10: No microtubule cytoskeleton depolymerisation of HeLa Flp-In cells stable transfected with *pcDNA5/FRT/TO-eGFP^{TbKif13-1 S143A}* 72 h after induction. (A) HeLa Flp-In cells stable transfected with *pcDNA5/FRT/TO-eGFP^{TbKif13-1 S143A}* showed 72 h after induction of *eGFP^{TbKif13-1 S143A}* overexpression (green, autofluorescence) no reduced microtubule cytoskeleton (red, α-tubulin antibody TAT). The nucleus was DAPI (blue) stained. Cells were harvested 72 h after induction and fixed with methanol. Non induced cells served as control. Scale bar 20 μm. (B) Westernblot of *pcDNA5/FRT/TO-eGFP^{TbKif13-1 S143A}* stable transfected HeLa Flp-In cells to verify the expression of *eGFP^{TbKif13-1 S143A}* 72 h after induction. *eGFP^{TbKif13-1 S143A}* was detected using α-GFP, tubulin was detected using α-tubulin antibody TAT.

As a result of the observed correlation of the *eGFP^{TbKif13-1 S143A}* expression level and cytoskeleton depolymerisation effects within transiently transfected HeLa cells (Figure 9 and S 2), the stable cell line was transfected with the vector *pcDNA3.1-eGFP^{TbKif13-1 S143A}*. This caused an additional random genomic integration of the transgene. It was expected to increase the expression level of *eGFP^{TbKif13-1 S143A}*. Induction of *eGFP^{TbKif13-1 S143A}* from twelve hours to five days in these double stable cell line clones did not result in depolymerisation of the microtubule cytoskeleton (Figure S 3).

Addition of nocodazole to the single stable cell line was expected to support the *eGFP^{TbKif13-1 S143A}* mediated depolymerisation by weakening the microtubules. Varying nocodazole concentrations from 20 – 110 ng/mL were added to the cells. In one approach overexpression of *eGFP^{TbKif13-1 S143A}* was induced simultaneously with nocodazole addition. In another approach it was induced twelve hours prior to nocodazole addition (Figure S 4). Effects to microtubule cytoskeleton depolymerisation were observed from 40 ng/mL, while cells started to arrest in mitosis at 70 ng/mL nocodazole. However, the slight microtubule cytoskeleton depolymerisation in these cells deemed to be not sufficient for the

Results

high-throughput inhibitor screen that requires a robust readout by automated image analysis.

To conclude, the basic functionality of the heterologous *in vivo* assay was proven in transiently transfected HeLa cells. However, inducible overexpression of ^{eGFP}TbKif13-1 S143A in the required generated stable HeLa cell line did not result in a sufficient cytoskeleton depolymerisation for a readout by automated image analysis.

2.1.2. *In vitro* *T. brucei* cytoskeleton assay

The prerequisite of the *in vitro* inhibitor screen assay was the preparation of *T. brucei* cytoskeletons on 384-well plates that were depolymerisable by recombinantly purified ^{His6}TbKif13-1. *T. brucei* cytoskeleton preparations are detergent-extracted cells, in which freely diffusing proteins are removed and only the cytoskeleton, cytoskeleton associated proteins, chromatin, the nucleolus and the spindle remain.

The basic functionality of the assay, regarding the depolymerisation of *T. brucei* cytoskeletons by recombinantly purified ^{His6}TbKif13-1, was tested. *T. brucei* cells were detergent-extracted on top of microscopy slides, incubated with ^{His6}TbKif13-1 and ATP, methanol fixed and finally stained for immunofluorescence microscopy. A control occurred without addition of ATP. *T. brucei* cytoskeletons were depolymerised by ^{His6}TbKif13-1 in the presence of ATP (Figure 11). Only the flagellum was not depolymerised.

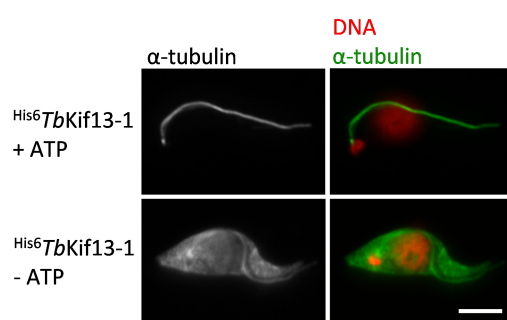


Figure 11: *In vitro* depolymerisation of *T. brucei* cytoskeletons by recombinantly purified ^{His6}TbKif13-1. *T. brucei* cytoskeletons were depolymerised by 0.5 μ M ^{His6}TbKif13-1 on microscopy slides. Control sample without ATP addition did not show cytoskeleton depolymerisation. The cytoskeleton tubulin (green) was stained with α -tubulin antibody (TAT). DNA was DAPI (red) stained. Scale bar 5 μ m.

The high-throughput inhibitor screen should occur on 384-well plates with bound cytoskeletons. The necessity of their preparation persisted. One approach was to distribute

Results

equal amounts of cytoskeletons to the wells of a plate and to dry them over night. Addition of recombinantly purified ^{His6}TbKif13-1 and ATP did not depolymerise these dried cytoskeletons. Another approach was to use cytoskeletons immediately after their detergent-extraction and distribution to the 384-well plate. Addition of ^{His6}TbKif13-1 and ATP resulted in depolymerisation of cytoskeletons, but those of one well were not equally depolymerised. This prevents a robust readout by automated image analysis.

The question persisted whether ^{His6}TbKif13-1 stuck to the well surface. The used 384-well plates were polystyrene low-binding plates. Polystyrene exhibits non-specific affinity for biomolecular reagents, but it is reduced in low-binding plates. Thus, these plates were expected to exhibit low non-specific binding of ^{His6}TbKif13-1 to the surface. In one approach it was tried to reduce the remaining non-specific binding to the plate's surface by blocking the wells with BSA before ^{His6}TbKif13-1 addition. This did not result in an equal depolymerisation of cytoskeletons.

Another problem, preventing a robust readout by automated image analysis, was the loss of a variable amount of cytoskeletons per well during the assay's procedure. The plate's surface probably also reduced the binding ability of cytoskeletons. However, the use of medium-binding plates did not result in a higher amount of bound cytoskeletons.

2.2. Functional dissection of TbKif13-1 domains

Several deletion mutants were generated for the functional characterisation of TbKif13-1 (Tb927.9.3650) domains (Figure 12). The approximate sections of the TbKif13-1 N-, motor and C-terminus were determined by using SMART (smart.embl-heidelberg.de). The neck domain is putative and was ascertained by comparison with results from MCAK studies in CHO cells (Maney et al., 2001). The APC/C recognition motif (D-box) was predicted by GPS-ARM (arm.biocuckoo.org).

Results

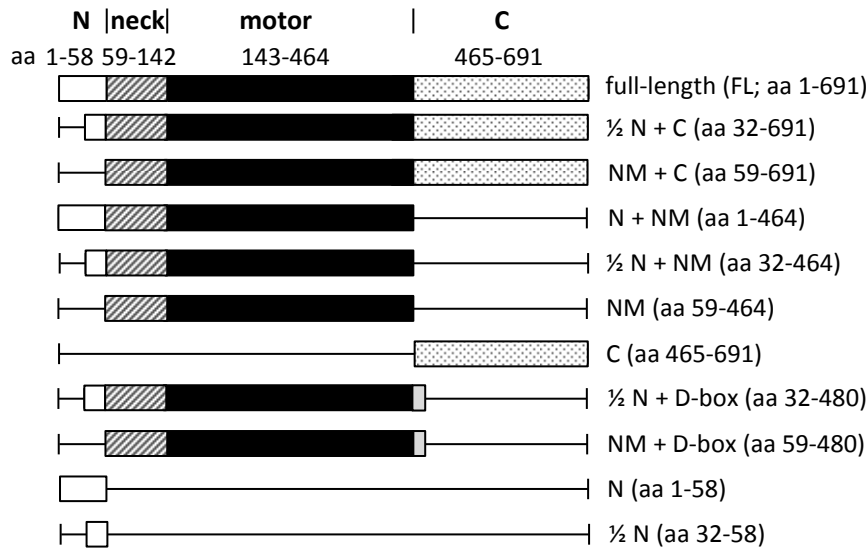


Figure 12: *TbKif13-1* deletion constructs. According amino acid (aa) numbers of the domains and the deletion constructs are stated. As depicted for the full-length construct: white box: N-terminus (N); striped grey box: putative neck domain; black box: motor domain, which forms together with the neck domain the neck-motor domain (NM); grey box: predicted APC/C recognition motif (D-box); spotted box: C-terminus (C). For *in vitro* studies constructs were supplied with a N-terminal His₆ tag. For *in vivo* studies constructs were N-terminal tagged with a myc tag, except for the constructs N and $\frac{1}{2}$ N, which were C-terminal GFP-myc tagged.

For *in vivo* studies in *T. brucei*, the coding sequences for the deletion constructs were inserted into the *pHD1801* vector. After transfection into *T. brucei*, this allowed their doxycycline-dependent ectopic expression with a N-terminal myc tag. Because the sole N-terminal myc tag did not result in a detectable fluorescence and Westernblot signal, in contrast to all other *TbKif13-1* constructs, the *TbKif13-1* N-terminus and the bisected N-terminus were expressed with a C-terminal GFP-myc tag. Their coding sequences were inserted into the *pHD1800^{GFP-myc}* vector. This allowed their doxycycline-dependent ectopic expression with a C-terminal GFP-myc tag after transfection.

For *in vitro* studies, the coding sequences for the deletion constructs were inserted into the *pTrcC FA* vector, which allowed IPTG-dependent overexpression with a N-terminal His₆ tag in transformed *E. coli*.

2.2.1. Localisation of *TbKif13-1* deletion constructs in *T. brucei*

^{myc}*TbKif13-1* deletion constructs were ectopically expressed in transgenic 449 procyclic *T. brucei* cells to identify NLS and NES within *TbKif13-1*. The localisation of the respective construct was tracked and visualised with an α -myc antibody throughout the cell cycle. Cytoskeleton samples were prepared in addition to whole cell samples. Cytoskeleton samples facilitated the analysis of the ^{myc}*TbKif13-1* constructs' binding to microtubule

Results

structures, such as the mitotic spindle. The cell cycle-specific expression of the constructs during G1-, S-, M- and G2-phase was analysed in whole cell samples. According to kinetoplast and nucleus positioning (Figure 2), 100 cells of each cell cycle stage were evaluated for expression of the respective ^{myc}*TbKif13-1* deletion construct. This gave a first hint for sites within *TbKif13-1*, necessary for cell cycle-dependent degradation.

^{myc}*TbKif13-1* FL was not detected in G1-phase (1K1N) cells, but in 75% of S-phase (1-2K1N) cells its nuclear localisation could be shown (Figure 13 (A) and (B)). All late G2/mitotic 2K1N cells showed ectopically expressed ^{myc}*TbKif13-1* FL in the nucleus, which reduced to 90% of 2K2N cells. Cytoskeleton samples revealed that ^{myc}*TbKif13-1* FL built a formation within the mitotic nucleus resembling the shape of the mitotic spindle (Figure 13 (C)).

A very similar localisation phenotype in whole cell samples and cytoskeleton samples was observed for ^{myc}*TbKif13-1* with the half reduced N-terminus (^{myc}*TbKif13-1* ½ N + C). In contrast, it was detected intranuclear already during G1-phase (1K1N) in almost half of the induced cells. It was found in all S-phase (1-2K1N) and late G2/mitotic 2K1N cells and within 75% of 2K2N cells (Figure S 5 (A), (B) and (C)).

Results

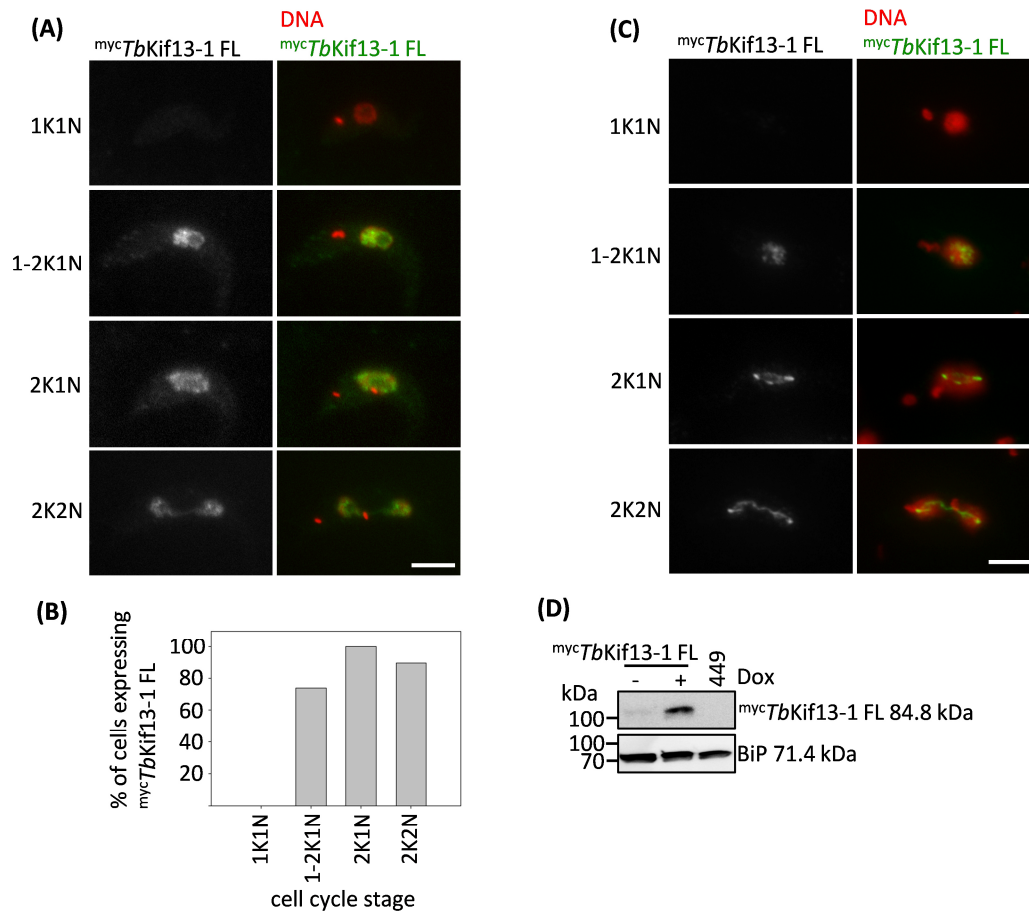


Figure 13: Nuclear localisation of *mycTbKif13-1 FL* in *T. brucei* from 1-2K1N to 2K2N cell stages. (A) Whole cell samples of transgenic 449 cells ectopically expressing *mycTbKif13-1 FL*. DNA was DAPI (red) stained, *mycTbKif13-1 FL* (green) was visualised using α -myc antibody. Scale bar 5 μ m. (B) Diagram shows percentage of cells with visual detectable ectopically expressed *mycTbKif13-1 FL* within each cell cycle stage, detected according to kinetoplast and nucleus postioning. (C) Cytoskeleton samples of transgenic 449 cells ectopically expressing *mycTbKif13-1 FL*. Staining and scale bar according to subfigure (A). (D) Westernblot analysis verifying doxycycline (Dox) inducible ectopic expression of *mycTbKif13-1 FL* in transgenic 449 cells with α -myc antibody. 449 cells were used as negative control, BiP staining was used as loading control.

The complete deletion of the *TbKif13-1* N-terminus resulted in the construct *mycTbKif13-1 NM + C*. It showed a slight staining within the cytoplasm in addition to nuclear staining within whole cell samples after ectopic expression (Figure 14 (A)). *mycTbKif13-1 NM + C* was seen in 35% of G1-phase (1K1N) cells, 91% of S-phase (1-2K1N) cells, all late G2/mitotic 2K1N cells and in 45% of 2K2N cells (Figure 14 (B)). Cytoskeleton 2K1N samples showed *mycTbKif13-1 NM + C* localised in a formation resembling the shape of the mitotic spindle (Figure 14 (C)).

Results

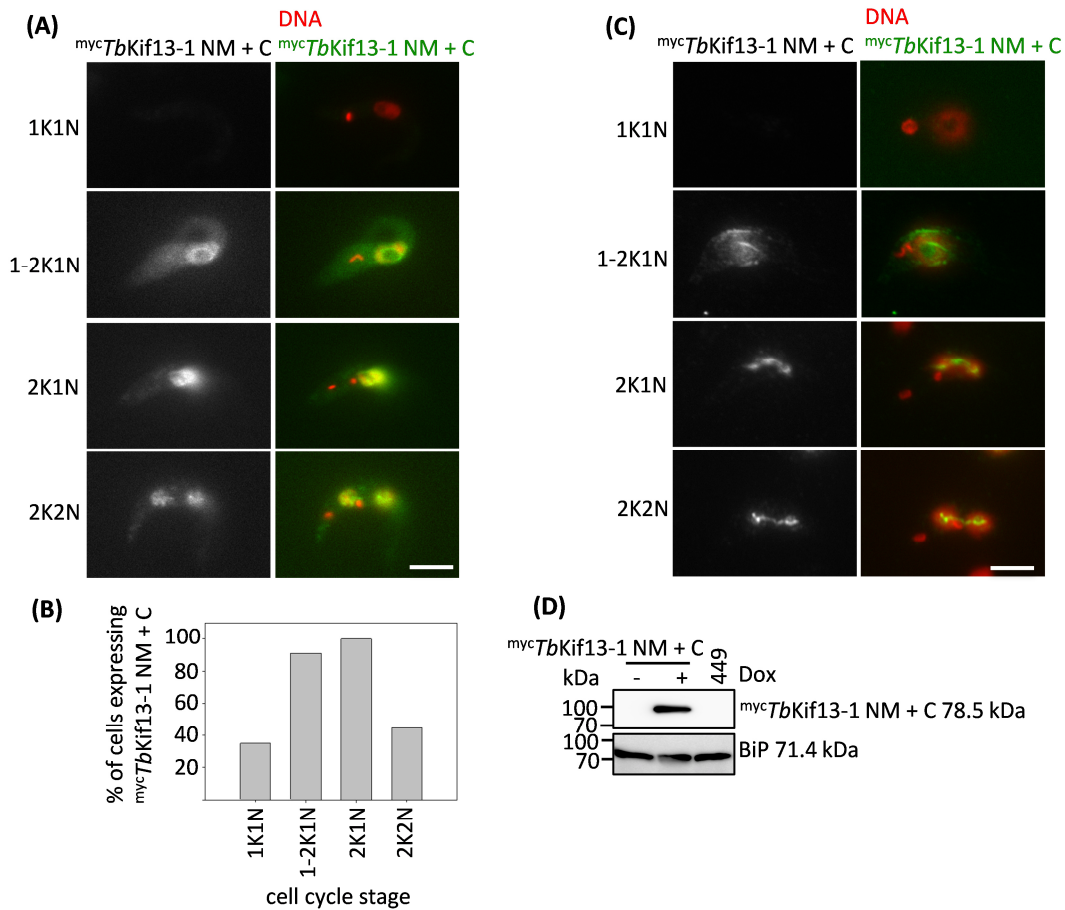


Figure 14: Nuclear and slight cytoplasmic localisation of *mycTbKif13-1 NM + C* in *T. brucei* from 1-2K1N to 2K2N cell stages. (A) Whole cell samples of transgenic 449 cells ectopically expressing *mycTbKif13-1 NM + C*. DNA was DAPI (red) stained, *mycTbKif13-1 NM + C* (green) was visualised using α -myc antibody. Scale bar 5 μ m. (B) Diagram shows percentage of cells with visual detectable ectopically expressed *mycTbKif13-1 NM + C* within each cell cycle stage, detected according to kinetoplast and nucleus positioning. (C) Cytoskeleton samples of transgenic 449 cells ectopically expressing *mycTbKif13-1 NM + C*. Staining and scale bar according to subfigure (A). (D) Westernblot analysis verifying doxycycline (Dox) inducible ectopic expression of *mycTbKif13-1 NM + C* in transgenic 449 cells with α -myc antibody. 449 cells were used as negative control, BiP staining was used as loading control.

The reduction of the C-terminus from the full-length construct resulted in the construct *mycTbKif13-1 N + NM*. It remained solely within the cytoplasm throughout the cell cycle after ectopic expression in the respective transgenic *T. brucei* cell line (Figure 15 (A)). It was seen in 80% of G1-phase (1K1N) and 2K2N cells and in all S-phase (1-2K1N) and late G2/mitotic 2K1N cells (Figure 15 (B)). *mycTbKif13-1 N + NM* was not found within cytoskeleton samples (Figure 15 (C)).

Results

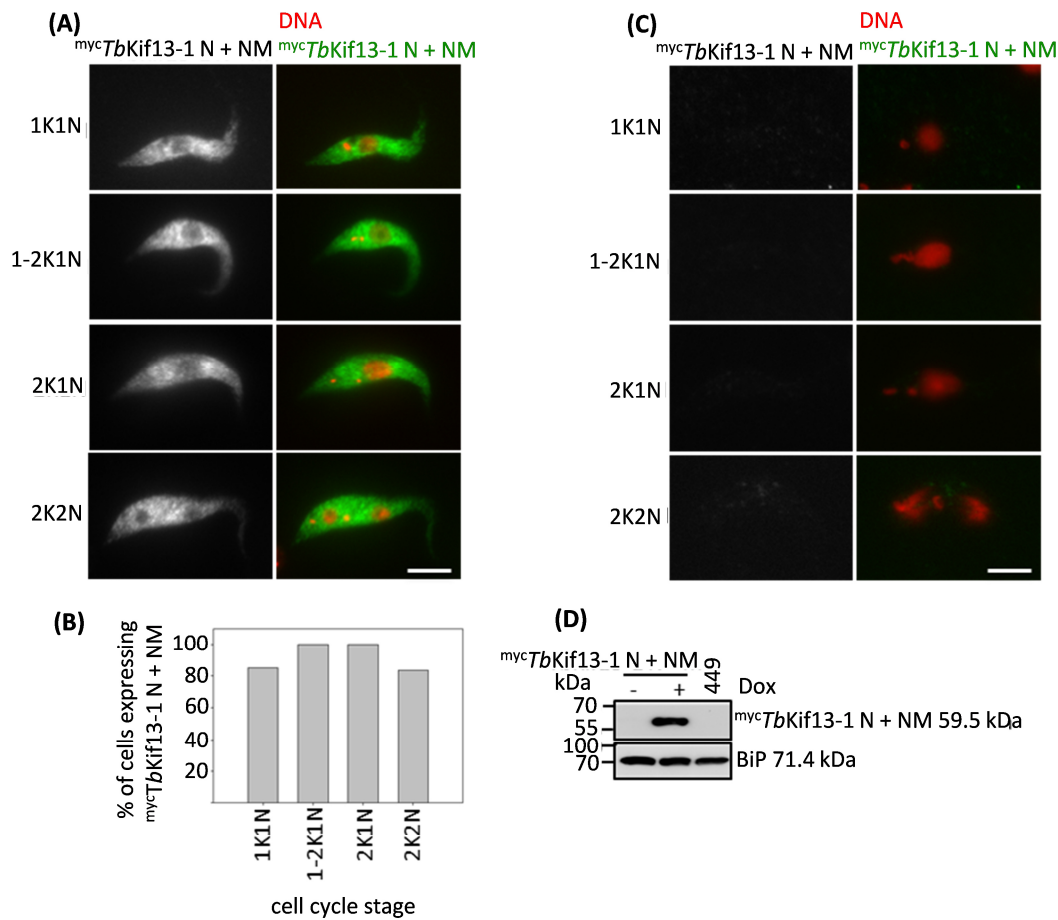


Figure 15: Cytoplasmic localisation of *mycTbKif13-1 N + NM* in *T. brucei* throughout the cell cycle. (A) Whole cell samples of transgenic 449 cells ectopically expressing *mycTbKif13-1 N + NM*. DNA was DAPI (red) stained, *mycTbKif13-1 N + NM* (green) was visualised using α -myc antibody. Scale bar 5 μ m. (B) Diagram shows percentage of cells with visual detectable ectopically expressed *mycTbKif13-1 N + NM* within each cell cycle stage, detected according to kinetoplast and nucleus postioning. (C) Cytoskeleton samples of transgenic 449 cells ectopically expressing *mycTbKif13-1 N + NM*. Staining and scale bar according to subfigure (A). (D) Westernblot analysis verifying doxycycline (Dox) inducible ectopic expression of *mycTbKif13-1 N + NM* in transgenic 449 cells with α -myc antibody. 449 cells were used as negative control, BiP staining was used as loading control.

mycTbKif13-1 ½ N + NM with a bisected N-terminus and missing C-terminus, in contrast, was nuclear and only slightly cytoplasmic localised (Figure S 6 (A)). *mycTbKif13-1 ½ N + NM* appeared throughout the cell cycle in whole cell samples, but it almost completely disappeared in cytoskeleton samples (Figure S 6 (B) and (C)).

This localisation pattern and cell cycle-dependent distribution was similar to that of *mycTbKif13-1 NM* (Figure 16 (A) and (B)), where only the neck and motor domain of *TbKif13-1* was ectopically expressed with a N-terminal myc tag. Compared to *mycTbKif13-1 ½ N + NM*, the neck-motor construct was more obvious within the nucleus in cytoskeleton samples

Results

(Figure 16 (C)). It appeared in all cell cycle stages within the nucleus, but not in a formation resembling the shape of the mitotic spindle.

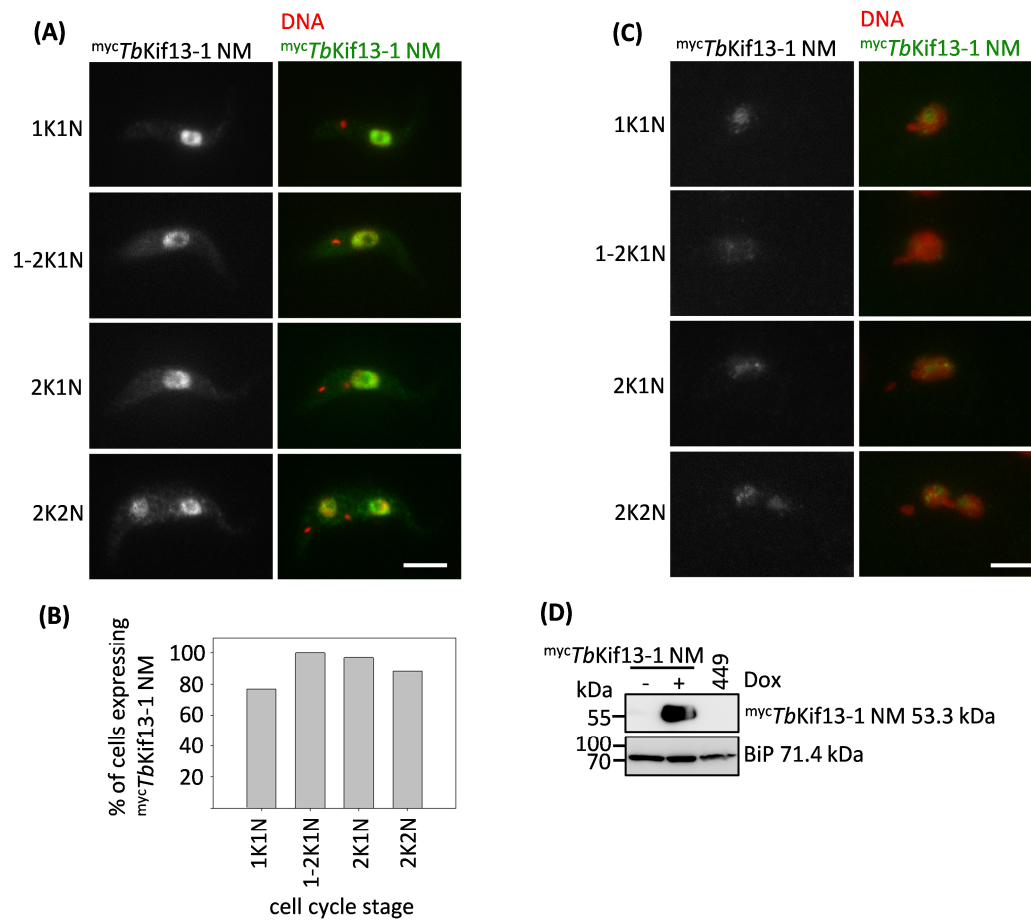


Figure 16: Nuclear and slight cytoplasmic localisation of *mycTbKif13-1* NM in *T. brucei* throughout the cell cycle. (A) Whole cell samples of transgenic 449 cells ectopically expressing *mycTbKif13-1* NM. DNA was DAPI (red) stained, *mycTbKif13-1* NM (green) was visualised using α -myc antibody. Scale bar 5 μ m. (B) Diagram shows percentage of cells with visual detectable ectopically expressed *mycTbKif13-1* NM within each cell cycle stage, detected according to kinetoplast and nucleus positioning. (C) Cytoskeleton samples of transgenic 449 cells ectopically expressing *mycTbKif13-1* NM. Staining and scale bar according to subfigure (A). (D) Westernblot analysis verifying doxycycline (Dox) inducible ectopic expression of *mycTbKif13-1* NM in transgenic 449 cells with α -myc antibody. 449 cells were used as negative control, BiP staining was used as loading control.

The ectopically expressed *TbKif13-1* myc tagged C-terminal domain construct *mycTbKif13-1* C localised within the nucleus in whole cell samples and cytoskeleton samples throughout the cell cycle (Figure 17 (A), (B) and (C)). Surprisingly, the *mycTbKif13-1* C signal in whole cell samples of late G2/mitotic 2K1N cells appeared in a more elongated shape than the full-length construct. This phenotype was seen in 65% of 2K1N cells 24 h after induction and in 71% of 2K1N cells 48 h after induction (Figure 17 (E)). Cytoskeleton samples of 2K1N cells confirmed this rather special elongated formation of *mycTbKif13-1* C (Figure 17 (C)).

Results

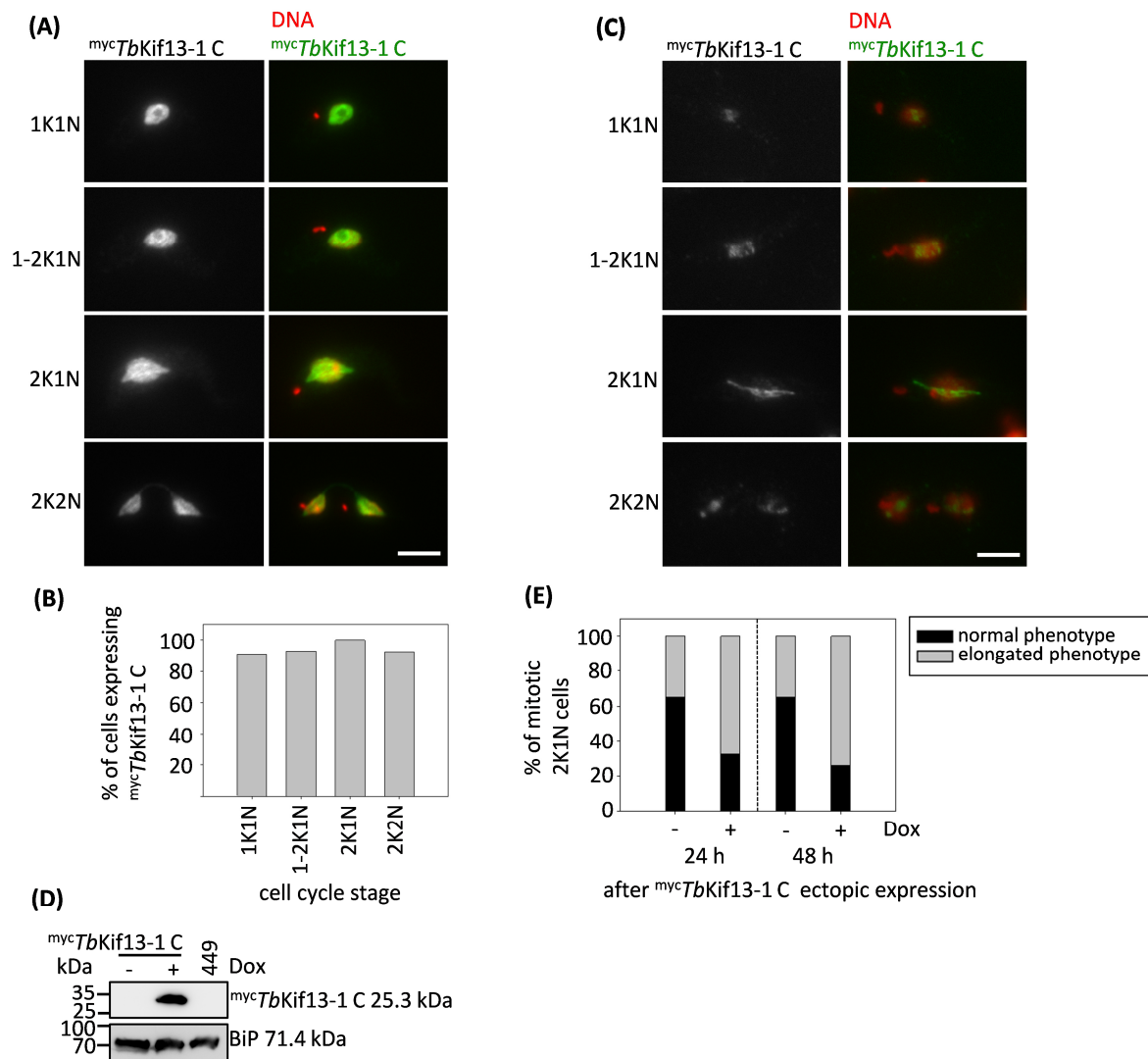


Figure 17: Nuclear localisation of *mycTbKif13-1 C* in *T. brucei* throughout the cell cycle. (A) Whole cell samples of transgenic 449 cells ectopically expressing *mycTbKif13-1 C*. DNA was DAPI (red) stained, *mycTbKif13-1 C* (green) was visualised using α -myc antibody. Scale bar 5 μ m. (B) Diagram shows percentage of cells with visual detectable ectopically expressed *mycTbKif13-1 C* within each cell cycle stage, detected according to kinetoplast and nucleus postioning. (C) Cytoskeleton samples of transgenic 449 cells ectopically expressing *mycTbKif13-1 C*. Staining and scale bar according to subfigure (A). (D) Westernblot analysis verifying doxycycline (Dox) inducible ectopic expression of *mycTbKif13-1 C* in transgenic 449 cells with α -myc antibody. 449 cells were used as negative control, BiP staining was used as loading control. (E) Percentage of mitotic 2K1N cells with normal or elongated phenotype of *mycTbKif13-1 C* 24 h and 48 h after doxycycline (Dox) dependent induction after its ectopic expression; black: normal phenotype; grey: elongated phenotype.

Ectopically expressed *TbKif13-1 N^{GFP-myc}* was detectable during all cell cycle stages in whole cell samples (Figure 18 (A) and (B)). In G1-phase (1K1N) and S-phase (1-2K1N) cells, *TbKif13-1 N^{GFP-myc}* was found in the cytoplasm, while it was additionally localised in the nucleus in late G2/mitotic 2K1N and 2K2N cells. *TbKif13-1 N^{GFP-myc}* was not detectable in cytoskeleton samples (Figure 18 (C)).

Results

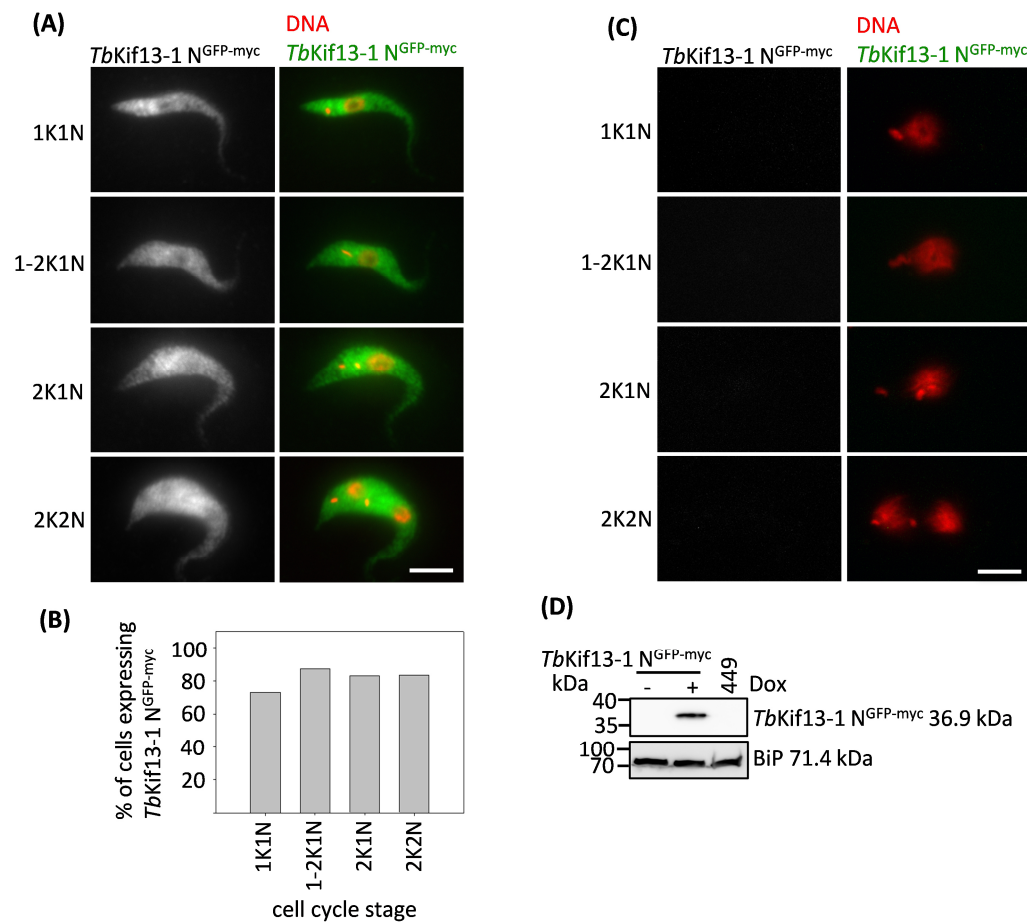


Figure 18: Cytoplasmic and nuclear localisation of *TbKif13-1* N^{GFP-myc} in *T. brucei* throughout the cell cycle. (A) Whole cell samples of transgenic 449 cells ectopically expressing *TbKif13-1* N^{GFP-myc}. DNA was DAPI (red) stained, *TbKif13-1* N^{GFP-myc} (green) was visualised using α-myc antibody. Scale bar 5 μm. (B) Diagram shows percentage of cells with visual detectable ectopically expressed *TbKif13-1* N^{GFP-myc} within each cell cycle stage, detected according to kinetoplast and nucleus positioning. (C) Cytoskeleton samples of transgenic 449 cells ectopically expressing *TbKif13-1* N^{GFP-myc}. Staining and scale bar according to subfigure (A). (D) Western blot analysis verifying doxycycline (Dox) inducible ectopic expression of *TbKif13-1* N^{GFP-myc} in transgenic 449 cells with α-myc antibody. 449 cells were used as negative control, BiP staining was used as loading control.

In contrast, *TbKif13-1* ½ N^{GFP-myc} was found solely in the cytoplasm throughout the cell cycle (Figure S 7 (A) and (B)). The exception were G1-phase (1K1N) cells, there it was in addition located to the nucleus. Like the whole N-terminal domain construct, *TbKif13-1* ½ N^{GFP-myc} was not detectable in cytoskeleton samples (Figure S 7 (C)).










Control cells, ectopically expressing GFP-myc, showed GFP-myc localisation in whole cell samples throughout the cell cycle within the cytoplasm and the nucleus (Figure S 8 (A) and (B)). The staining of GFP-myc was stronger in the nucleus than in the cytoplasm. In cytoskeleton samples GFP-myc was not detectable (Figure S 8 (C)).

Results

The localisation of the *TbKif13-1* deletion constructs is summarised in Table 1. Their nuclear and cytoplasmic localisation in whole cell samples, as well as their occurrence in cytoskeleton samples were taken into consideration.

To conclude, full-length ^{myc}*TbKif13-1* FL was found nuclear from 1-2K1N to 2K2N cells, but not in G1 (1K1N) cells. In mitotic 2K1N cells it localised in a shape resembling the mitotic spindle. Ectopic expression of ^{myc}*TbKif13-1* C localised in a shape resembling an elongated spindle in mitotic 2K1N cells.

Table 1: Localisation of the *TbKif13-1* deletion constructs in *T. brucei*. Nuclear and cytoplasmic localisation of the *TbKif13-1* deletion constructs in whole cell samples and their presence in cytoskeleton samples is stated. +: localisation; +/-: slight localisation; -: no localisation. The respective *TbKif13-1* deletion constructs are depicted. White box: N-terminus; striped grey box: putative neck domain; black box: motor domain; spotted box: C-terminus.

	<i>TbKif13-1</i> deletion construct	nucleus	cytoplasm	cytoskeleton
	FL	+	-	+
	½ N + C	+	-	+
	NM + C	+	+/-	+
	N + NM	-	+	-
	½ N + NM	+	+/-	+/-
	NM	+	+/-	+
	C	+	-	+
	N	+	+	-
	½ N	+/-	+	-

2.2.2. Proteasome-dependent degradation of *TbKif13-1*

Immunofluorescence studies gave a first hint about *TbKif13-1*'s cell cycle-dependent degradation. The question remained, whether this occurred proteasome-dependent and if so, which *TbKif13-1* domain was necessary for it.

To analyse this, the turnover of ^{myc}*TbKif13-1* FL was monitored. ^{myc}*TbKif13-1* FL was ectopically expressed for four hours in the corresponding transgenic 449 cell line. Subsequently, in one approach translation was inhibited by cycloheximide (CHX) and in the other approach the proteasome was inhibited by MG 132 in addition to CHX treatment.

Westernblot analysis from this assay revealed that ^{myc}*TbKif13-1* FL was degraded already two hours after translational inhibition (Figure 19). This degradation was prevented by inhibition of the proteasome, thus indicating its proteasome-dependent degradation.

Results

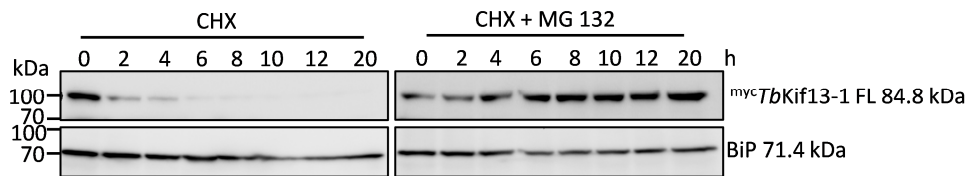


Figure 19: Proteasome-dependent degradation of *mycTbKif13-1* FL. In transgenic 449 cells ectopic expression of *mycTbKif13-1* FL was induced for four hours. Then cycloheximide (CHX) was added for translational inhibition (left Westernblot, CHX); in addition to CHX also MG 132 for proteasome inhibition was added (right Westernblot, CHX + MG 132). Westernblot samples were taken every two hours. Time point 0 marks when CHX or in addition MG 132 were added to the cell culture. For detection of *mycTbKif13-1* FL α -myc antibody was used; α -BiP served as loading control.

To determine the domain necessary for proteasomal degradation, the assay was applied to the transgenic 449 cell lines ectopically expressing the *mycTbKif13-1* deletion constructs.

For *mycTbKif13-1* $\frac{1}{2}$ N + C the same result was received as for the full-length construct (Figure S 9). In contrast, the missing of the whole N-terminus resulted in a non-degradable construct *mycTbKif13-1* NM + C (Figure S 10). Also the absence of the C-terminus from the full-length construct (*mycTbKif13-1* N + NM) led to no degradation (Figure 20).

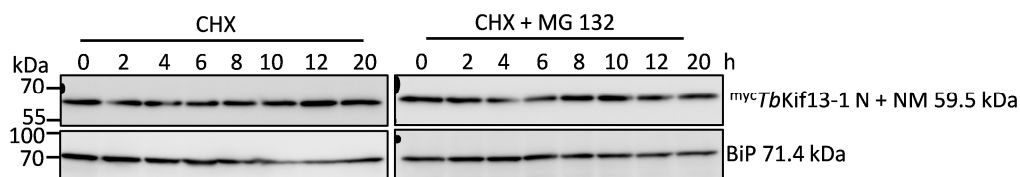


Figure 20: No degradation of *mycTbKif13-1* N + NM. In transgenic 449 cells ectopic expression of *mycTbKif13-1* N + NM was induced for four hours. Then cycloheximide (CHX) was added for translational inhibition (left Westernblot, CHX); in addition to CHX also MG 132 for proteasome inhibition was added (right Westernblot, CHX + MG 132). Westernblot samples were taken every two hours. Time point 0 marks when CHX or in addition MG 132 were added to the cell culture. For detection of *mycTbKif13-1* N + NM α -myc antibody was used; α -BiP served as loading control.

Bisection of the N-terminus in this construct resulted in *mycTbKif13-1* $\frac{1}{2}$ N + NM. It again was degraded in the approach with CHX treatment, while addition of MG 132 in the other approach prevented its degradation (Figure 21).

Results

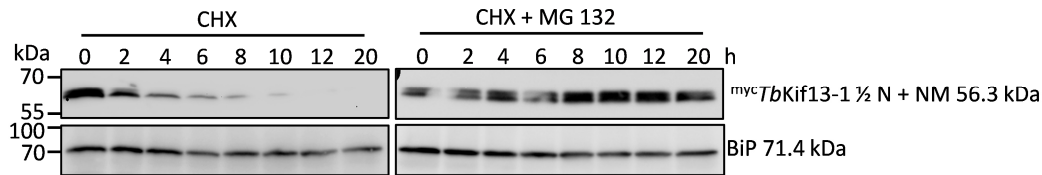


Figure 21: Proteasome-dependent degradation of *mycTbKif13-1 1/2 N + NM*. In transgenic 449 cells ectopic expression of *mycTbKif13-1 1/2 N + NM* was induced for four hours. Then cycloheximide (CHX) was added for translational inhibition (left Westernblot, CHX); in addition to CHX also MG 132 for proteasome inhibition was added (right Westernblot, CHX + MG 132). Westernblot samples were taken every two hours. Time point 0 marks when CHX or in addition MG 132 were added to the cell culture. For detection of *mycTbKif13-1 1/2 N + NM* α -myc antibody was used; α -BiP served as loading control.

Reduction of this half N-terminus in the construct *mycTbKif13-1 NM* again resulted in a protein, which was not degraded after inhibition of translation (Figure 22).

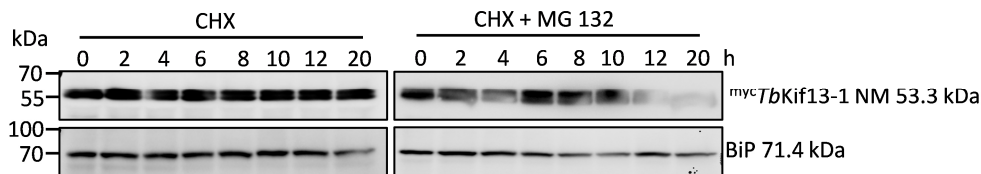


Figure 22: No degradation of *mycTbKif13-1 NM*. In transgenic 449 cells ectopic expression of *mycTbKif13-1 NM* was induced for four hours. Then cycloheximide (CHX) was added for translational inhibition (left Westernblot, CHX); in addition to CHX also MG 132 for proteasome inhibition was added (right Westernblot, CHX + MG 132). Westernblot samples were taken every two hours. Time point 0 marks when CHX or in addition MG 132 were added to the cell culture. For detection of *mycTbKif13-1 NM* α -myc antibody was used; α -BiP served as loading control.

The single C-terminus in the construct *mycTbKif13-1 C* showed proteasome-dependent degradation already two hours after CHX addition (Figure S 11). The single N-terminus *TbKif13-1 N^{GFP-myc}* also was found to be proteasomal degraded (Figure S 12). The second half of the N-terminus in the construct *TbKif13-1 1/2 N^{GFP-myc}* was proteasomal degradable, yet to a lesser extend than the whole N-terminus (Figure S 13). A cell line ectopically expressing GFP-myc was used as control. GFP-myc was not degraded (Figure S 14).

In addition, *TbKif13-1 FL* was checked for D-boxes or KEN-boxes via GPS-ARM. D- and KEN-boxes are recognition sequences for the E3 ubiquitin ligase APC/C. This revealed a single D-box shortly after the transition from the predicted motor domain to the C-terminus at aa 470-473.

Due to the experimental results, a transgenic 449 cell line ectopically expressing the neck-motor domain with the subsequent D-box motif (*mycTbKif13-1 NM + D-box*; Figure 12) was

Results

generated. This construct was used, because ^{myc}TbKif13-1 NM was found not degraded after inhibition of translation. This was expected to be changed by the addition of the predicted D-box. It was, however, found that ^{myc}TbKif13-1 NM + D-box was also not degraded after translational inhibition (Figure 23). Furthermore, immunfluorescence studies in *T. brucei* showed that the nuclear localised, ectopically expressed ^{myc}TbKif13-1 NM + D-box was not degraded during the cell cycle (Figure S 15 (A) and (B)).

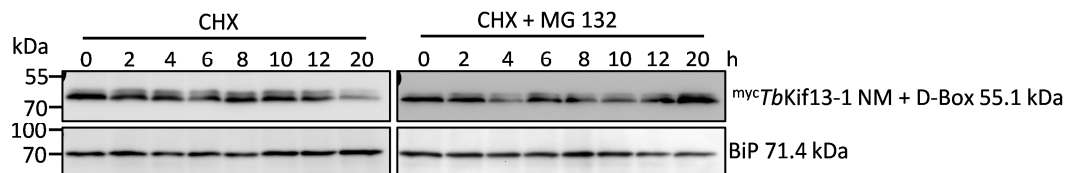


Figure 23: No degradation of ^{myc}TbKif13-1 NM + D-box. In transgenic 449 cells ectopic expression of ^{myc}TbKif13-1 NM + D-box was induced for four hours. Then cycloheximide (CHX) was added for translational inhibition (left Westernblot, CHX); in addition to CHX also MG 132 for proteasome inhibition was added (right Westernblot, CHX and MG 132). Westernblot samples were taken every two hours. Time point 0 marks when CHX or in addition MG 132 were added to the cell culture. For detection of ^{myc}TbKif13-1 NM + D-Box α -myc antibody was used; α -BiP served as loading control.












^{myc}TbKif13-1 ½ N + D-box was used as control. The addition of the D-box sequence to ^{myc}TbKif13-1 ½ N + NM did not have an influence on its proteasomal degradation and its appearance throughout the cell cycle in immunfluorescence studies (Figure S 16).

The results of a possible degradation of ^{myc}TbKif13-1 deletion constructs after inhibition of translation and their possible proteasome-dependent degradation, are summarised in Table 2.

^{myc}TbKif13-1 FL was proteasome-dependent degraded. Also the ^{myc}TbKif13-1 N-terminus and the ^{myc}TbKif13-1 C-terminus were proteasome-dependent degraded. The predicted D-box motif did not have an influence on degradation characteristics of the deletion constructs. N- and C-terminal degradation motifs were supposed.

Results

Table 2: Proteasome-dependent degradation of ^{myc}TbKif13-1 deletion constructs. Degradation of *TbKif13-1* deletion constructs was determined by inhibition of translation in the respective transgenic 449 cell line ectopically expressing ^{myc}*TbKif13-1* deletion constructs. Proteasome-dependent degradation was determined by additional inhibition of the proteasome. +: degradation; +/-: degradation not pronounced; -: no degradation. The respective *TbKif13-1* deletion constructs are depicted. White box: N-terminus; striped grey box: putative neck domain; black box: motor domain; grey box: predicted D-box motif; spotted box: C-terminus.

	<i>TbKif13-1</i> deletion construct	degradation after inhibition of translation	proteasome-dependent degradation
	FL	+	+
	½ N + C	+	+
	NM + C	-	-
	N + NM	-	-
	½ N + NM	+	+
	NM	-	-
	C	+	+
	N	+	+
	½ N	+/-	+/-
	NM + D-box	-	-
	½ N + D-box	+	+

2.2.3. Effect of *TbKif13-1* deletion constructs on cell cycle progression

The effects of *TbKif13-1* deletion constructs on cell cycle progression and cell viability give insight into functionality of *TbKif13-1* domains by analysing possible dominant-negative phenotypes. To this end, the tagged *TbKif13-1* deletion constructs were ectopically expressed in the respective transgenic procyclic 449 cell line and their growth was observed for six days. Moreover, cell cycle profiles of the cell lines were obtained via flow cytometry analysis at several days of ectopic expression. In cell lines exhibiting growth inhibition and increased zoid formation, spindle formation was observed for six days by staining microtubules with the KMX antibody, which recognises β -tubulin, and subsequent immunofluorescence microscopy.

Results

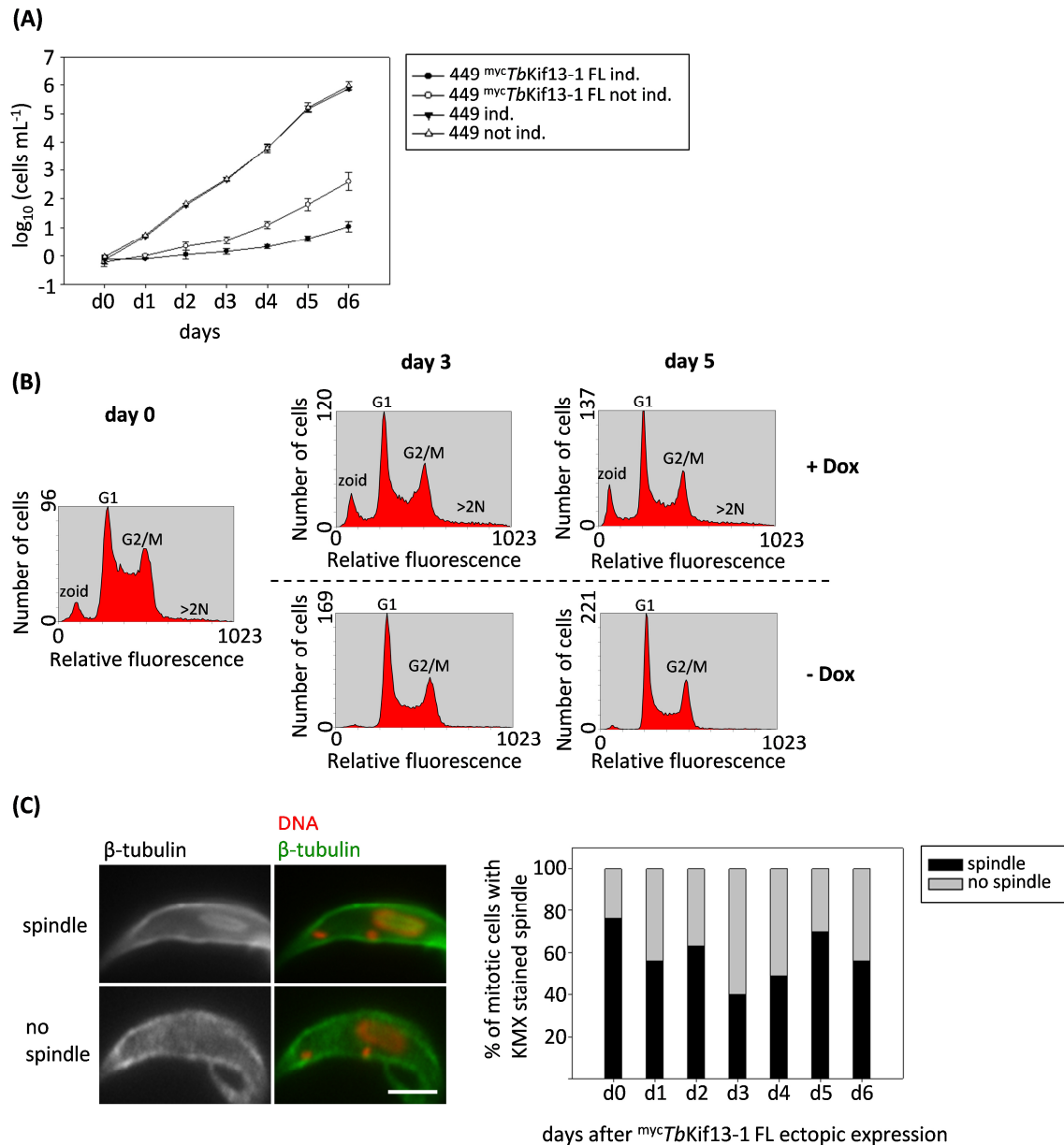


Figure 24: Reduced growth and increase of zoids and cells >2N in the cell line ectopically expressing *mycTbKif13-1 FL*. (A) Growth curve of the transgenic 449 cell line ectopically expressing *mycTbKif13-1 FL*; control cells: non induced and non transfected 449 cells. (B) Flow cytometry analysis of the transgenic 449 cell line ectopically expressing *mycTbKif13-1 FL* (+ Dox, upper panels), control cells: non induced (- Dox, lower panels). (C) Immunofluorescence analysis of mitotic 2K1N cells after ectopic expression of *mycTbKif13-1 FL*, depicting a cell with spindle formation (upper panel) and one without detectable spindle (lower panel). KMX antibody was used for β -tubulin staining (green), DNA was stained with DAPI (red). Scale bar 3 μ m. Diagram shows evaluation of spindle formation in mitotic 2K1N cells ectopically expressing *mycTbKif13-1 FL* from day 0 to day 6; black: spindle formation; grey: no spindle formation.

The ectopic expression of the full-length construct *mycTbKif13-1 FL* led to a reduced growth compared to non induced *mycTbKif13-1 FL* transgenic cells and non transfected 449 cells (Figure 24 (A)). Flow cytometry analysis showed for this cell line an increase in zoids and cells

Results

with >2N three and five days after induction (Figure 24 (B)). Flow cytometry results were confirmed via immunofluorescence microscopy. Based on kinetoplast and nucleus positioning, 100 cells were noted for their cell cycle stage (Figure S 17). Spindle staining with KMX antibody showed in mitotic 2K1N cells a reduced spindle formation by 10 to 40% one to six days after ectopic expression of *mycTbKif13-1* FL, compared to cells without ectopic expression (Figure 24 (C)).

Ectopic expression of the deletion constructs *mycTbKif13-1* ½ N + C and *mycTbKif13-1* NM + C, with bisected and reduced N-terminus respectively, also led to a growth defect (Figure S 18 (A) and 25 (A)).

Ectopic expression of *mycTbKif13-1* ½ N + C resulted in an increase of zoids and cells >2N three and five days after induction (Figure S 18 (B)). Flow cytometry data were confirmed via immunofluorescence microscopy (Figure S 18 (C)). KMX staining of the spindle in mitotic 2K1N cells showed a reduction in spindle formation by 20 to 60% within one to six days after ectopic expression of *mycTbKif13-1* ½ N + C, compared to non induced cells (Figure S 18 (D)).

In contrast, ectopic expression of *mycTbKif13-1* NM + C resulted in an increase of zoids three days after induction. However, they were no longer detectable at day five (Figure 25 (B); for fluorescence microscopy evaluation refer to Figure S 19). Instead, a peak of dead cells appeared in flow cytometry analysis. Spindle formation in mitotic 2K1N cells was reduced by a maximum of only 20%, compared to non induced cells (Figure 25 (C)). Also the formation of a diffuse spindle occurred.

Results

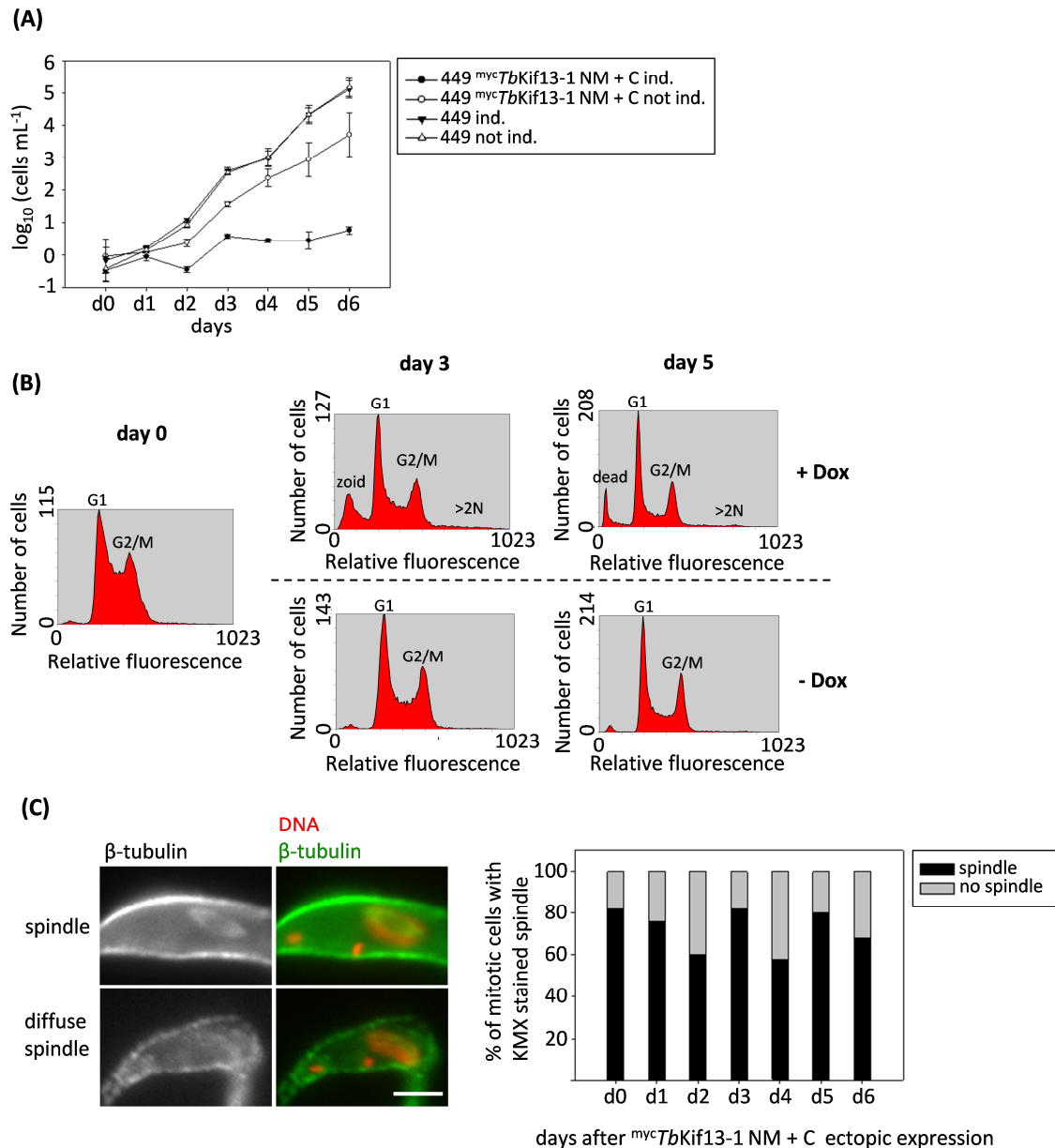


Figure 25: Reduced growth of the cell line ectopically expressing *mycTbKif13-1* NM + C. **(A)** Growth curve of the transgenic 449 cell line ectopically expressing *mycTbKif13-1* NM + C; control cells: non induced and non transfected 449 cells. **(B)** Flow cytometry analysis of the transgenic 449 cell line ectopically expressing *mycTbKif13-1* NM + C (+ Dox, upper panels), control cells: non induced (- Dox, lower panels). **(C)** Immunofluorescence analysis of mitotic 2K1N cells after ectopic expression of *mycTbKif13-1* NM + C, depicting a cell with spindle formation (upper panel) and one with a diffuse spindle (lower panel). KMX antibody was used for β -tubulin staining (green), DNA was stained with DAPI (red). Scale bar 3 μ m. Diagram shows evaluation of spindle formation in mitotic 2K1N cells ectopically expressing *mycTbKif13-1* NM + C from day 0 to day 6; black: spindle formation; grey: no spindle formation.

Compared to non induced cells, the ectopic expression of the construct without C-terminus, *mycTbKif13-1* N + NM, did not result in a growth defect. Despite both showed a growth reduction compared to non transfected 449 cells (Figure S 20 (A)). Flow cytometry analysis

Results

and fluorescence microscopy evaluation showed no divergent increase of zoids between ^{myc}TbKif13-1 N + NM induced and non induced cells (Figure S 20 (B) and (C)). The maximal observed reduction of spindle formation in mitotic 2K1N cells was by 20% at day one and six after ^{myc}TbKif13-1 N + NM induction, compared to day 0 (Figure S 20 (D)).

The bisection of the N-terminus within this construct led to ^{myc}TbKif13-1 ½ N + NM. Its ectopic expression resulted in a growth defect (Figure 26 (A)). Flow cytometry analysis showed a strong increase in zoids and >2N cells up to three days after induction of ^{myc}TbKif13-1 ½ N + NM ectopic expression (Figure 26 (B); for fluorescence microscopy evaluation refer to Figure S 21). This effect was reduced at day five after induction. KMX staining revealed a reduction of spindle formation in ectopically expressing ^{myc}TbKif13-1 ½ N + NM cells by 10 to 50% one to six days after induction (Figure 26 (C)).

Ectopic expression of the neck-motor construct ^{myc}TbKif13-1 NM also resulted in a growth defect (Figure 27 (A)). Flow cytometry analysis showed an unusual distribution of the cells within the cell cycle (Figure 27 (B); for fluorescence microscopy evaluation refer to Figure S 22 (B)). After twelve hours of ^{myc}TbKif13-1 NM ectopic expression, there was an increase of zoids, cell cycle stage shift from G1 to G2/M and an increasing amount of >2N cells. The only strong peak of the flow cytometry analysis was found for zoids. After five days of ectopic expression, most cells were dead (Figure S 22 (A)). KMX spindle staining showed that after twelve hours of ^{myc}TbKif13-1 NM ectopic expression, only 8% of mitotic 2K1N cells formed a spindle. After 24 hours of ^{myc}TbKif13-1 NM ectopic expression, there was no spindle detectable in mitotic 2K1N cells (Figure 27 (C)).

Results

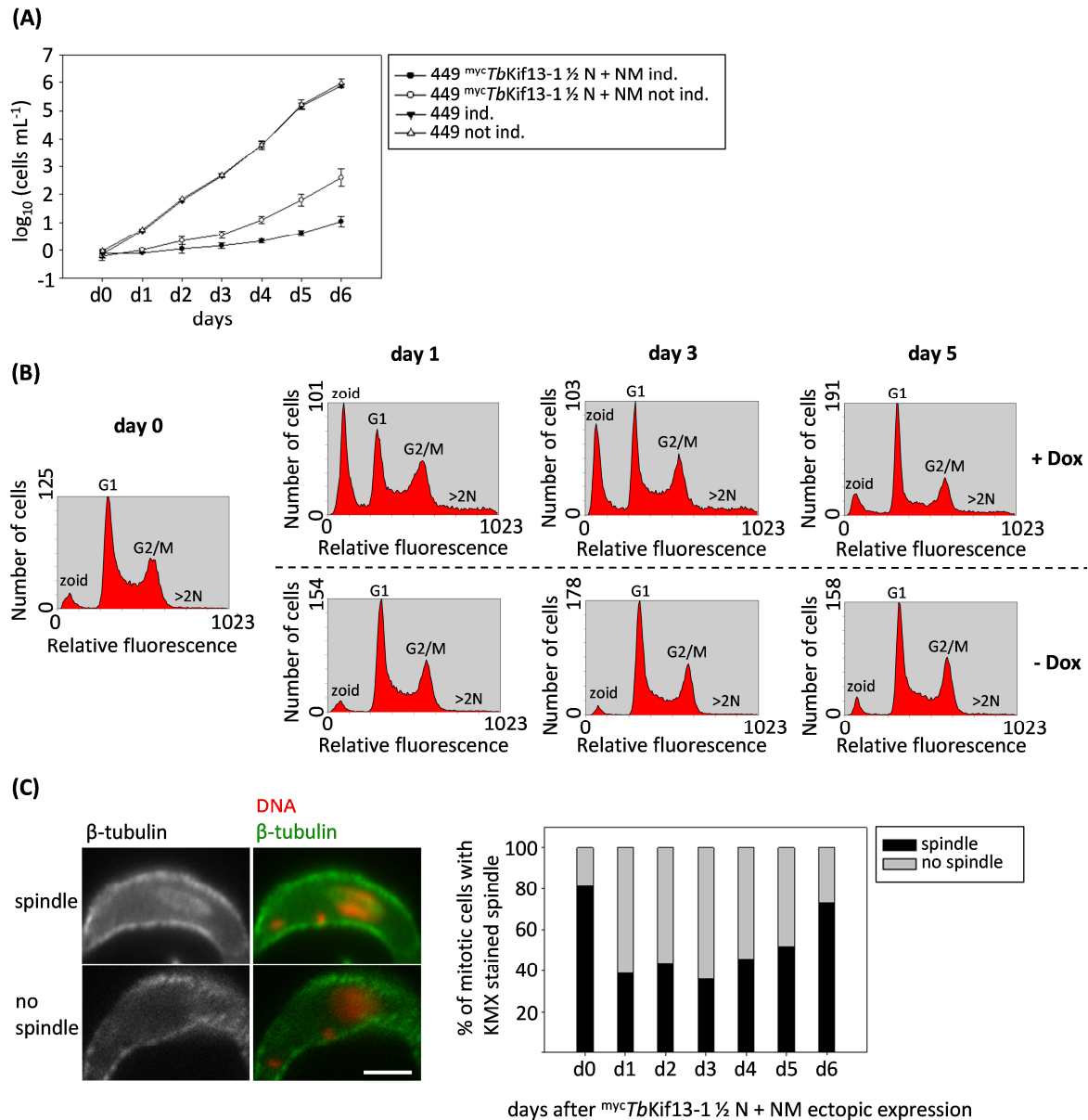


Figure 26: Reduced growth of the cell line ectopically expressing *mycTbKif13-1* ½ N + NM. **(A)** Growth curve of the transgenic 449 cell line ectopically expressing *mycTbKif13-1* ½ N + NM; control cells: non induced and non transfected 449 cells. **(B)** Flow cytometry analysis of the transgenic 449 cell line ectopically expressing *mycTbKif13-1* ½ N + NM (+ Dox, upper panels), control cells: non induced (- Dox, lower panels). **(C)** Immunofluorescence analysis of mitotic 2K1N cells after ectopic expression of *mycTbKif13-1* ½ N + NM, depicting a cell with spindle formation (upper panel) and one without detectable spindle (lower panel). KMX antibody was used for β -tubulin staining (green), DNA was stained with DAPI (red). Scale bar 3 μ m. Diagram shows evaluation of spindle formation in mitotic 2K1N cells ectopically expressing *mycTbKif13-1* ½ N + NM from day 0 to day 6; black: spindle formation; grey: no spindle formation.

Results

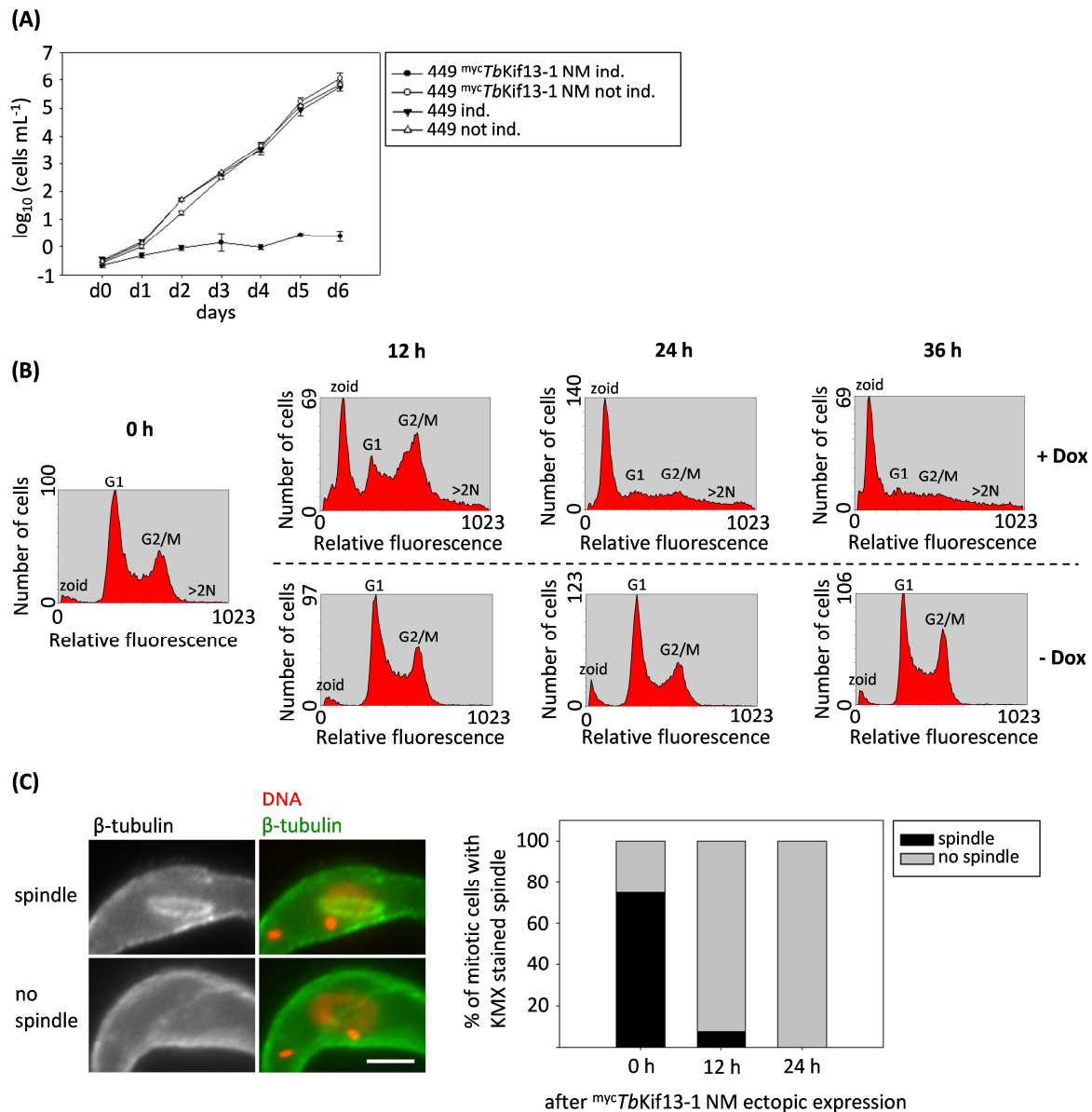


Figure 27: Reduced growth of the cell line ectopically expressing *mycTbKif13-1* NM. **(A)** Growth curve of the transgenic 449 cell line ectopically expressing *mycTbKif13-1* NM; control cells: non induced and non transfected 449 cells. **(B)** Flow cytometry analysis of the transgenic 449 cell line ectopically expressing *mycTbKif13-1* NM (+ Dox, upper panels), control cells: non induced (- Dox, lower panels). **(C)** Immunofluorescence analysis of mitotic 2K1N cells after ectopic expression of *mycTbKif13-1* NM, depicting a cell with spindle formation (upper panel) and one without detectable spindle (lower panel). KMX antibody was used for β -tubulin staining (green), DNA was stained with DAPI (red). Scale bar 3 μ m. Diagram shows evaluation of spindle formation in mitotic 2K1N cells ectopically expressing *mycTbKif13-1* NM at day 0 and 12 h and 24 h after induction; black: spindle formation; grey: no spindle formation.

In comparison to non induced cells, ectopic expression of the *mycTbKif13-1* C-terminus did not result in a growth defect (Figure S 23 (A)). Also flow cytometry analysis did not show a divergent distribution of cells within the cell cycle from induced, ectopically expressing *mycTbKif13-1* C to non induced cells (Figure S 23 (B)); for fluorescence microscopy evaluation

Results

refer to Figure S 23 (C)). KMX staining of mitotic 2K1N cells ectopically expressing ^{myc}*TbKif13-1 C* showed that there was no reduction in spindle formation (Figure 28 (A) and (B)). However, more than half of the observed spindles had an elongated phenotype from day one to day six after ectopic expression of ^{myc}*TbKif13-1 C* (Figure 28 (C)).

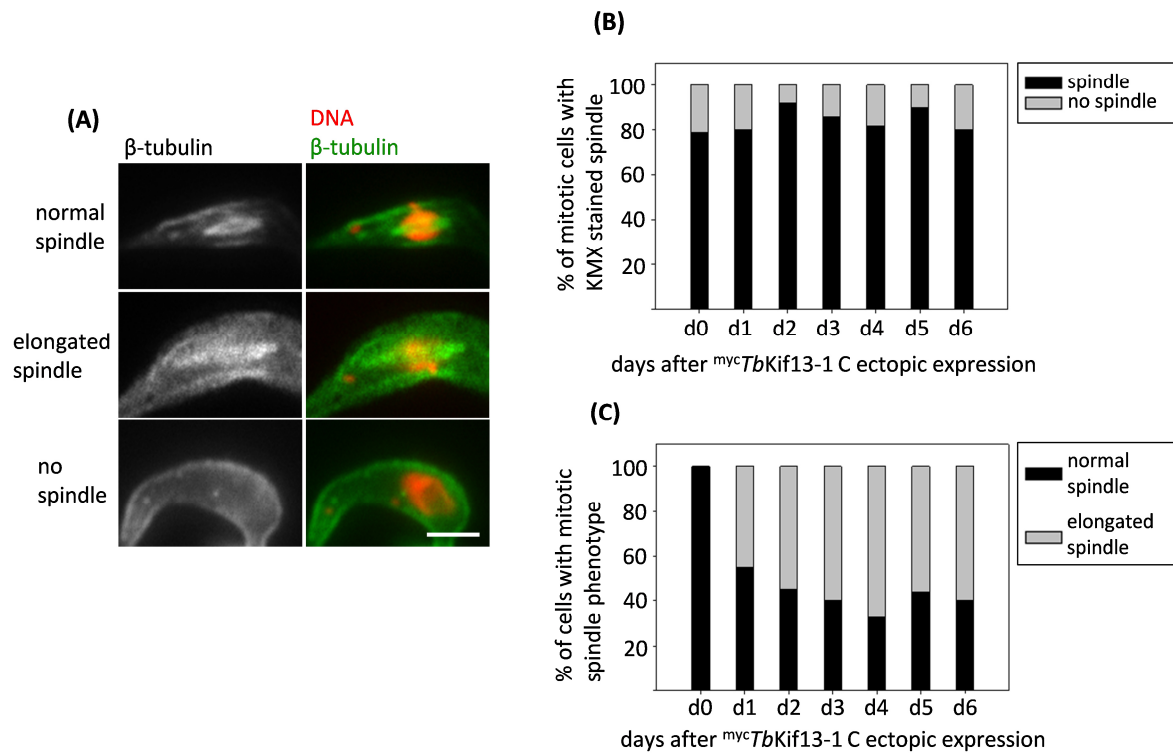


Figure 28: Ectopic expression of ^{myc}*TbKif13-1 C* led to an elongated spindle phenotype. (A) Immunofluorescence analysis of mitotic 2K1N after ectopic expression of ^{myc}*TbKif13-1 C*, depicting a cell with normal spindle formation (upper panel), with an elongated spindle phenotype (middle panel) or with no detectable spindle (lower panel). KMX antibody was used for β -tubulin staining (green), DNA was stained with DAPI (red). Scale bar 3 μ m. (B) Evaluation of spindle formation in mitotic 2K1N cells ectopically expressing ^{myc}*TbKif13-1 C* from day 0 to day 6; black: spindle formation; grey: no spindle formation. (C) Evaluation of normal and elongated spindle phenotype in mitotic 2K1N cells ectopically expressing ^{myc}*TbKif13-1 C* from day 0 to day 6; black: normal spindle phenotype; grey: elongated spindle phenotype.








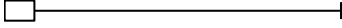
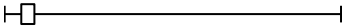
The ectopic expression of the N-terminus or the bisected N-terminus (*TbKif13-1* N^{GFP-myc} and ½ N^{GFP-myc}) within the corresponding transgenic cell lines, did not result in growth inhibition (Figure S 24 (A) and S 25 (A)). Also flow cytometry analysis did not show any shift in cell cycle stage distribution (Figure S 24 (B) and (C), S 25 (B) and (C)). Spindle staining of mitotic 2K1N cells ectopically expressing *TbKif13-1* ½ N^{GFP-myc} did not show any reduced spindle formation (Figure S 25 (D)).

Results

The influence of the ectopically expressed *TbKif13-1* deletion constructs to the cell cycle progression in the respective transgenic 449 cell line is summarised in Table 3. Focus was put on the dominant-negative phenotypes reduced growth of the respective cell lines, formation of zoids and missing spindle formation.

To conclude, ectopic expression of full-length ^{myc}*TbKif13-1* reduced the growth of the respective transgenic cell line, and led to zoid formation and a reduction in spindle formation. The ectopic expression of the ^{myc}*TbKif13-1* neck-motor domain had a massive dominant-negative influence on cell viability and spindle formation. The ectopic expression of the ^{myc}*TbKif13-1* C-terminus led to an elongation of the spindle, but did not have a dominant-negative influence on cell viability.

Table 3: Effects of ectopic expression of the *TbKif13-1* deletion constructs on the cell cycle. Results were gained from growth curves and immunfluorescence microscopy. The dominant-negative phenotypes reduced growth, zoid formation and the missing spindle formation were considered. +: reduced growth, zoid formation or missing spindle formation; +/-: reduced growth, zoid formation or missing spindle formation is not pronounced; -: no reduced growth, no zoid formation or no missing spindle formation; enhanced effects are marked with repetitive signs; n.d.: not determined. The respective *TbKif13-1* deletion constructs are depicted. White box: N-terminus; striped grey box: putative neck domain; black box: motor domain; spotted box: C-terminus.

	<i>TbKif13-1</i> deletion construct	reduced growth	zoid formation	missing spindle formation
	FL	+	+	+
	½ N + C	+	+	++
	NM + C	+	+	+/-
	N + NM	-	-	+/-
	½ N + NM	+	++	++
	NM	+++	+++	+++
	C	-	-	- elongated spindle
	N	-	-	n.d.
	½ N	-	-	-

2.2.4. *TbKif13-1* domains necessary for microtubule binding and depolymerisation

Microtubule binding sites are essential for *TbKif13-1*'s depolymerisation activity. To identify necessary microtubule binding and depolymerisation domains *in vitro*, *TbKif13-1* deletion constructs that contain a motor domain were N-terminal His₆ tagged and recombinantly

Results

purified from *E. coli*. To determine their functional purification, the ATPase activity of the purified ^{His6}TbKif13-1 constructs was analysed using the malachite green assay.

The tubulin sedimentation assay was used for *in vitro* microtubule binding and depolymerisation determination. To this end, the recombinantly purified ^{His6}TbKif13-1 constructs were incubated with taxol-stabilised microtubules and ATP. After binding to microtubules some constructs were able to depolymerise them. Subsequent centrifugation pelleted polymerised microtubules with bound ^{His6}TbKif13-1 while depolymerised tubulin and unbound ^{His6}TbKif13-1 were found in the supernatant. SDS PAGE analysis was done for visualisation of the results.

An assay with *T. brucei* cytoskeleton preparations as depolymerisation substrate was done to verify the microtubule depolymerisation activity of purified ^{His6}TbKif13-1 constructs. In this assay recombinantly purified ^{His6}TbKif13-1 constructs and ATP, or without ATP for control, were added to cytoskeletons. Subsequent immunfluorescence microscopy monitored a possible depolymerisation.

The full-length construct ^{His6}TbKif13-1 FL depolymerised microtubules in the tubulin sedimentation assay and the cytoskeleton assay (Figure 29 (A) and 11). In the tubulin sedimentation assay, ^{His6}TbKif13-1 FL was found together with polymerised tubulin in the pellet fraction of the control approach without ATP (Figure 29 (A)). This indicates its tubulin binding ability. The malachite green assay showed the ATPase activity of ^{His6}TbKif13-1 FL, which increased with increasing ^{His6}TbKif13-1 FL concentration (Figure 29 (B)).

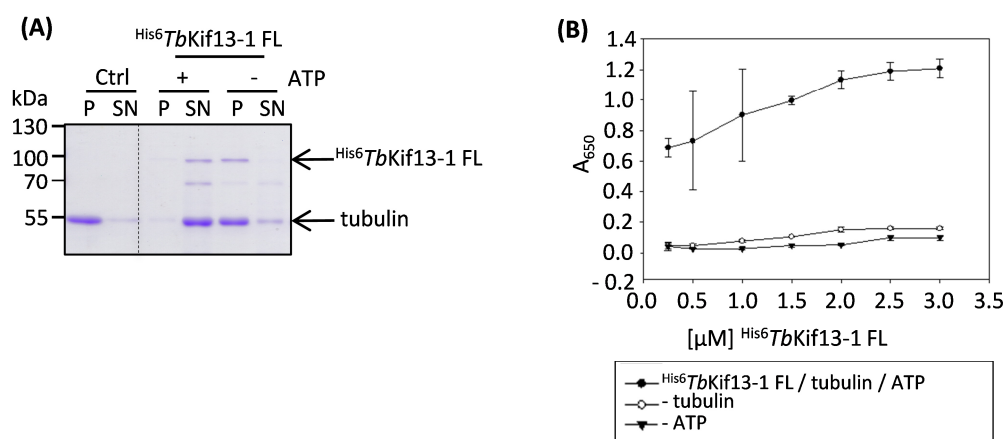


Figure 29: ^{His6}TbKif13-1 FL is a microtubule depolymeriser. (A) Tubulin sedimentation assay. 1.5 μM ^{His6}TbKif13-1 FL were used. Substrate were 3 μM taxol-stabilised microtubules. Control (Ctrl) sample was not treated with recombinantly purified ^{His6}TbKif13-1 FL. P: pellet; SN: supernatant; SDS-PAGE analysis. **(B)** Malachite green assay for ^{His6}TbKif13-1 FL. ATPase activity of ^{His6}TbKif13-1 FL increased with increasing ^{His6}TbKif13-1 FL concentration. Approaches without tubulin or ATP served as control.

Results

The recombinantly purified constructs ^{His6}TbKif13-1 ½ N + C and ^{His6}TbKif13-1 NM + C also depolymerised Trypanosome cytoskeletons (Figure S 26 (B) and S 27 (B)) and microtubules in the sedimentation assay (Figure S 26 (A) and S 27 (A)). Both deletion constructs were found with polymerised tubulin in the pellet fraction of the control approaches without ATP (Figure S 26 (A) and S 27(A)). This indicates their tubulin binding ability. The malachite green assays for ^{His6}TbKif13-1 ½ N + C and ^{His6}TbKif13-1 NM + C showed their increasing ATPase activity with increasing concentrations of ^{His6}TbKif13-1 ½ N + C and ^{His6}TbKif13-1 NM + C, respectively (Figure S 26 (C) and S 27 (C)).

In contrast, the ^{His6}TbKif13-1 deletion constructs with missing C-terminus, ^{His6}TbKif13-1 N + NM, ^{His6}TbKif13-1 ½ N + NM and ^{His6}TbKif13-1 NM, were neither able to depolymerise microtubules within the tubulin sedimentation assay, nor to depolymerise Trypanosome cytoskeletons, despite concentrations between 1 µM and 5 µM were used (Figure 30 (A) and (C), S 28 (A) and (C), S 29 (A) and (C)). Malachite green assays confirmed the ATPase activity of these deletion constructs (Figure 30 (D), S 28 (D) and S 29 (D)). Hence, their missing depolymerisation activity did not result from ATPase inactivity.

Westernblot analysis of their tubulin sedimentation assay samples was conducted to identify a microtubule binding ability of these deletion constructs, because of the similar molecular weight of ^{His6}TbKif13-1 N + NM, ^{His6}TbKif13-1 ½ N + NM, ^{His6}TbKif13-1 NM and tubulin. There were contradictory results of a possible microtubule binding ability of the ^{His6}TbKif13-1 deletion constructs. In the approaches with ATP, the deletion constructs were found in the supernatant, while polymerised microtubules were found in the pellet fraction (Figure 30 (B), S 28 (B) and S 29 (B)). In the control approaches without ATP, the deletion constructs were also found in the pellet fraction with polymerised microtubules.

Results

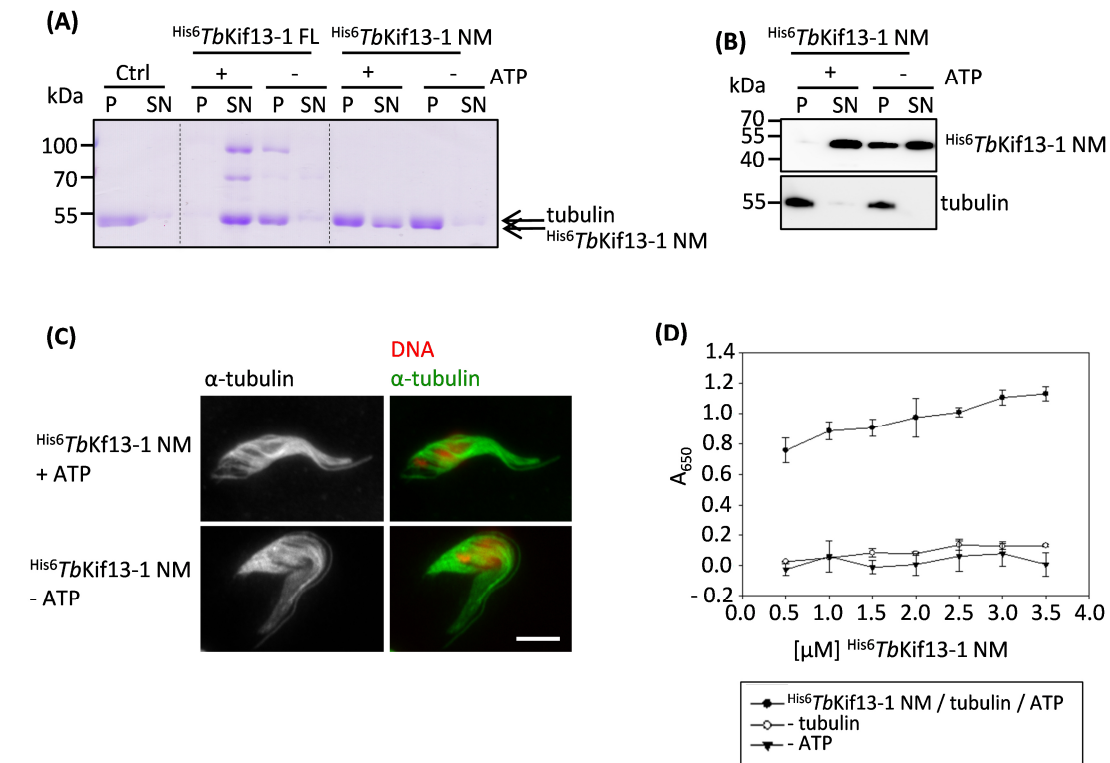








Figure 30: *His6TbKif13-1 NM* is no microtubule depolymeriser but retains ATPase activity. **(A)** Tubulin sedimentation assay. 1.5 μM *His6TbKif13-1 NM* were used. 1.5 μM *His6TbKif13-1 FL* were used as positive control. Substrate were 3 μM taxol-stabilised microtubules. Control (Ctrl) sample was not treated with recombinantly purified *His6TbKif13-1 NM*. P: pellet; SN: supernatant; SDS-PAGE analysis. **(B)** Westernblot analysis of the tubulin sedimentation assay samples. *His6TbKif13-1 NM* was detected using α-His antibody; tubulin was detected using α-tubulin antibody. **(C)** Cytoskeleton depolymerisation assay. 1 μM *His6TbKif13-1 NM* was used. Cytoskeleton tubulin (green) was stained with α-tubulin antibody. DNA was DAPI (red) stained. Scale bar 5 μm. **(D)** Malachite green assay for *His6TbKif13-1 NM*. ATPase activity of *His6TbKif13-1 NM* increased with increasing *His6TbKif13-1 NM* concentration. Approaches without tubulin or ATP served as control.

The ability of the *His6TbKif13-1* deletion constructs to depolymerise the Trypanosome cytoskeleton and microtubules within the tubulin sedimentation assay, and their ability to bind to microtubules is summarised in Table 4.

Results indicate that the neck-motor domain in conjunction with the C-terminus is necessary for *TbKif13-1*'s microtubule binding and depolymerisation activity.

Table 4: Microtubule binding and depolymerisation ability of ^{His6}TbKif13-1 deletion constructs. The results were received from the tubulin sedimentation assay and the cytoskeleton depolymerisation assay. +: depolymerisation/binding to microtubules; -: no depolymerisation/no binding to microtubules. White box: N-terminus; striped grey box: putative neck domain; grey box: predicted APC/C recognition motif; black box: motor domain; spotted box: C-terminus.

	<i>TbKif13-1</i> deletion construct	depolymerisation	microtubule binding
	FL	+	+
	½ N + C	+	+
	NM + C	+	+
	N + NM	-	-
	½ N + NM	-	-
	NM	-	-

2.2.5. Essential amino acids for depolymerisation and ATPase activity within the motor domain of *TbKif13-1*

Studies with MCAK found that microtubule depolymerisation and ATPase activity are not interdependent (Wagenbach et al., 2008; Wang et al., 2012; Wang et al., 2015). The switch II motif (DxxGxE) within the motor domain plays an essential role in this issue (see 1.3.2.). Mutation of the switch II motif glycine in MCAK G495A resulted in a pre-conformational change-mimicking mutant. This mutant is able to bind to microtubules, but unable to hydrolyse ATP and to depolymerise microtubules (Wagenbach et al., 2008; Wang et al., 2012). MCAK E497A was shown to be a post-conformational change-mimicking mutant, that is nearly ATPase deficient and able to depolymerise microtubules concentration-dependent (Wagenbach et al., 2008; Wang et al., 2015).

Both amino acids are conserved within the *TbKif13-1* motor domain, G371 and E373. It should be determined, whether they were also essential for its depolymerisation and ATPase activity, and whether both mechanisms were also not interdependent within *TbKif13-1*.

^{His6}*TbKif13-1* FL G371A and ^{His6}*TbKif13-1* FL E373A were recombinantly purified to test this hypothesis. Malachite green assays were individually performed with both proteins to check their ATPase activity. Tubulin sedimentation assays were carried out to check their depolymerisation activity.

It was found that ^{His6}*TbKif13-1* FL G371A abolished ATPase activity, while ^{His6}*TbKif13-1* FL E373A was almost completely ATPase deficient (Figure 31 (A) and (B)). The pre-

Results

conformational change-mimicking mutant G371A did not depolymerise microtubules, even at increased $\text{His}_6\text{TbKif13-1 FL G371A}$ concentrations (5 μM). But it was able to bind to microtubules (Figure 31 (C)). By contrast, the post-conformational change-mimicking mutant E373A depolymerised microtubules, an effect which was evident at higher (5 μM) $\text{His}_6\text{TbKif13-1 FL E373A}$ concentrations (Figure 31 (D)). $\text{His}_6\text{TbKif13-1 FL E373A}$ depolymerised microtubules independent of the presence of ATP (Figure 31 (D)).

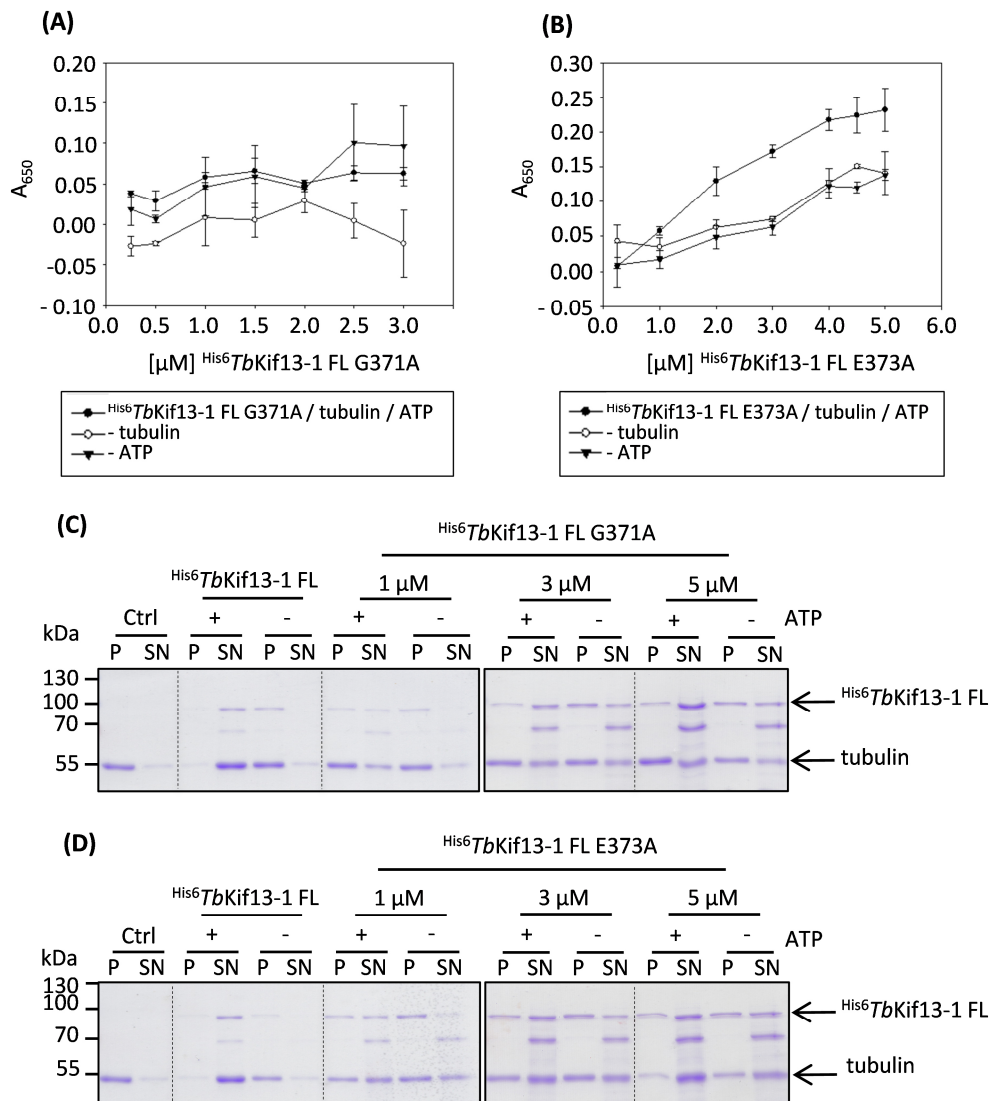


Figure 31: $\text{His}_6\text{TbKif13-1 FL G371A}$ inhibits ATPase and depolymerisation activity, while $\text{His}_6\text{TbKif13-1 FL E373A}$ is ATPase deficient but depolymerises tubulin. (A) Malachite green assay for $\text{His}_6\text{TbKif13-1 FL G371A}$. (B) Malachite green assay for $\text{His}_6\text{TbKif13-1 FL E373A}$. (C) Tubulin sedimentation assay. 1 to 5 μM $\text{His}_6\text{TbKif13-1 FL G371A}$ were used. 1 μM $\text{His}_6\text{TbKif13-1 FL}$ was used as positive control. Substrate were 3 μM taxol-stabilised microtubules. Control (Ctrl) sample was not treated with recombinantly purified $\text{His}_6\text{TbKif13-1 FL G371A}$. P: pellet; SN: supernatant. (D) Tubulin sedimentation assay. 1 to 5 μM $\text{His}_6\text{TbKif13-1 FL E373A}$ were used. 1 μM $\text{His}_6\text{TbKif13-1 FL}$ was used as positive control. Substrate were 3 μM taxol-stabilised microtubules. Control (Ctrl) sample was not treated with recombinantly purified $\text{His}_6\text{TbKif13-1 FL E373A}$. P: pellet; SN: supernatant.

2.3. *TbAuk1* and *TbKif13-1*

Mammalian MCAK is phosphorylated by AuroraB kinase for regulatory localisation and activity reasons (see 1.4.1.). The mitotic *TbAuk1* is necessary for proper mitosis and cytokinesis and is located at the spindle during metaphase in *T. brucei*. This indicates that in *T. brucei*, *TbAuk1* could regulate *TbKif13-1*'s activity by phosphorylation.

To test this hypothesis, an *in vitro* ^{33}P γATP phosphorylation assay was conducted with $^{\text{myc}}\text{TbAuk1}$ received from immunoprecipitation and $^{\text{His6}}\text{TbKif13-1}$ received from recombinant purification.

In a first step, a transgenic 449 cell line ectopically expressing $^{\text{myc}}\text{TbAuk1}$ (*Tb927.11.8220*) was generated. Two transgenic 449 cell lines ectopically expressing published kinase-dead $^{\text{myc}}\text{TbAuk1}$ K58R and $^{\text{myc}}\text{TbAuk1}$ T184A, respectively, were generated for use as negative controls (silver staining of IP products (Figure S 30); Hu et al., 2014; Li and Wang, 2006). In order to confirm phosphorylation activity of immunoprecipitated $^{\text{myc}}\text{TbAuk1}$ and abolished phosphorylation activity in the immunoprecipitated kinase-dead mutants $^{\text{myc}}\text{TbAuk1}$ K58R and $^{\text{myc}}\text{TbAuk1}$ T184A, a ^{33}P γATP phosphorylation assay using recombinantly purified *TbHistoneH3*^{His6} as substrate was conducted.

Autoradiography analysis revealed that immunoprecipitated $^{\text{myc}}\text{TbAuk1}$ was able to phosphorylate *TbHistoneH3*^{His6} (Figure 32). However, for the published kinase-dead mutants $^{\text{myc}}\text{TbAuk1}$ K58R and $^{\text{myc}}\text{TbAuk1}$ T184A, *TbHistoneH3*^{His6} phosphorylation was also detected, despite to only about one third of the extend of $^{\text{myc}}\text{TbAuk1}$ mediated phosphorylation (Figure 32). Applied myc-coupled protein G-sepharose from immunoprecipitation of wild type 449 cell lysate also led to a weak phosphorylation of *TbHistoneH3*^{His6}. For mock IP, protein G-sepharose without additional antibody was used in 449 wild type lysate. This did not result in *TbHistoneH3*^{His6} phosphorylation. To confirm addition of $^{\text{myc}}\text{TbAuk1}$, $^{\text{myc}}\text{TbAuk1}$ K58R and *TbHistoneH3*^{His6}, Westernblot analysis with the samples was conducted (Figure S 31).

Results

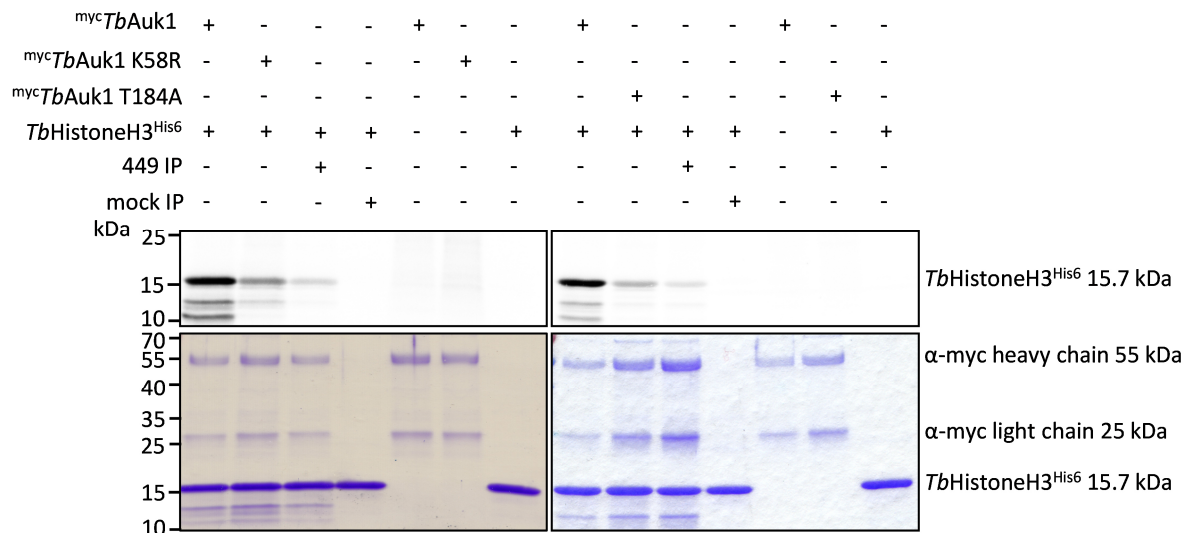


Figure 32: *mycTbAuk1* phosphorylates *TbHistoneH3*^{His6}, but also kinase-dead *mycTbAuk1* K58R and *mycTbAuk1* T184A are able to phosphorylate *TbHistoneH3*^{His6}, even though to a lesser extend. Autoradiography of *mycTbAuk1* and kinase-dead *mycTbAuk1* K58R and *mycTbAuk1* T184A ³³P γATP kinase assay. *mycTbAuk1* and its mutants were immunoprecipitated from transgenic *T. brucei* cell lysates. As control, IP of 449 wild type cell lysates and mock IP without addition of antibody were conducted. The phosphorylation substrate was recombinantly purified *TbHistoneH3*^{His6} (1.5 μg). Phosphorylation occurred in the presence of ³³P γATP. Coomassie stained gels served as loading control.

Another ³³P γATP phosphorylation assay was used to check whether *mycTbAuk1* and its mutants *mycTbAuk1* K58R and *mycTbAuk1* T184A are able to phosphorylate *TbKif13-1*^{His6}. Previous studies with AuroraB kinase had shown that it needed microtubules for *in vitro* activation and that microtubules accelerate its kinase activity (Noujaim et al., 2014; Rosasco-Nitcher et al., 2008). The ³³P γATP phosphorylation assay was conducted with and without additional taxol-stabilised microtubules to test, whether this was also true for *TbAuk1*.

The immunoprecipitated *mycTbAuk1*, *mycTbAuk1* K58R or *mycTbAuk1* T184A was incubated with recombinantly purified *TbKif13-1*^{His6}, ³³P γATP and with or without taxol-stabilised microtubules. Autoradiography analysis showed that *mycTbAuk1*, like its mutants *mycTbAuk1* K58R and *mycTbAuk1* T184A, phosphorylated *TbKif13-1*^{His6} independent of the presence of microtubules (Figure 33). Microtubules were also phosphorylated by *mycTbAuk1*, *mycTbAuk1* K58R and *mycTbAuk1* T184A (Figure 33). Westernblot analysis of the samples showed that tubulin was also contained to a little extend in samples where no microtubules were added (Figure S 32). Samples with *mycTbAuk1* T184A showed an autophosphorylation signal (Figure 33). Beads from wild type 449 cell lysate immunoprecipitation and mock IP served as negative controls.

Results

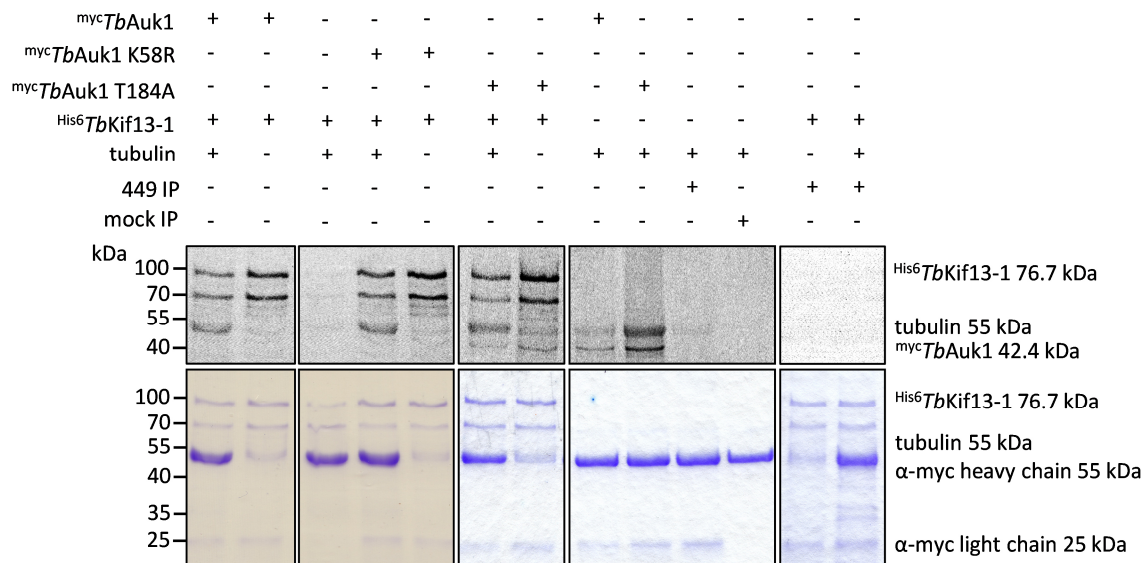


Figure 33: mycTbAuk1, mycTbAuk1 K58R and mycTbAuk1 T184A phosphorylate His6TbKif13-1 independent of the presence of microtubules. Prior to autoradiography analysis, immunoprecipitated mycTbAuk1, mycTbAuk1 K58R or mycTbAuk1 T184A, respectively, was incubated with recombinantly purified His6TbKif13-1 (0.75 μM), ³³P γATP and with or without taxol-stabilised microtubules. Coomassie stained gels served as loading control. IP from wild type 449 cell lysate and mock IP served as negative control.

Finally, it was tested whether mycTbAuk1 mediated phosphorylation inhibits the depolymerisation activity of His6TbKif13-1 *in vitro*. A tubulin sedimentation assay was conducted and mycTbAuk1 or mycTbAuk1 T184A, respectively, was added to the depolymerisation approach. It was found that addition of immunoprecipitated mycTbAuk1 did not inhibit His6TbKif13-1's depolymerisation activity in the assay (Figure 34). mycTbAuk1 T184A, which was added as negative control, did also not inhibit His6TbKif13-1's depolymerisation activity in the assay. Pre-incubation of mycTbAuk1 and His6TbKif13-1 in the presence of ATP before addition of taxol-stabilised microtubules, did also not result in inhibition of His6TbKif13-1's depolymerisation activity in the assay (Figure S 33).

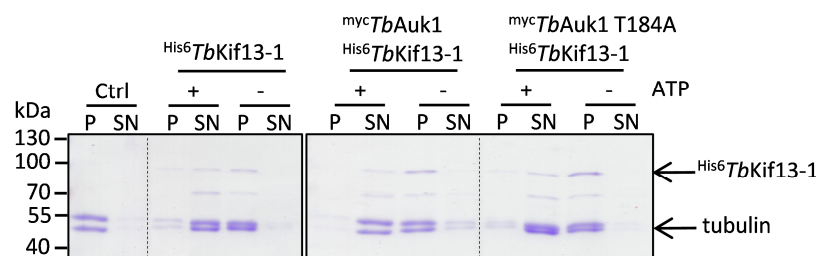


Figure 34: No inhibition of His6TbKif13-1's depolymerisation activity by the product of mycTbAuk1 IP. A depolymerisation assay with added immunoprecipitated mycTbAuk1 or mycTbAuk1 T184A, respectively, was conducted. 1 μM His6TbKif13-1 was used. Control (Ctrl) sample was not treated with recombinantly purified His6TbKif13-1. P: pellet; SN: supernatant.

Results

To conclude, immunoprecipitated ^{myc}TbAuk1 was active and phosphorylated TbHistoneH3^{His6}. Also the immunoprecipitated kinase-dead ^{myc}TbAuk1 K58R and ^{myc}TbAuk1 T184A, and wild type 449 immunoprecipitation products showed phosphorylation of TbHistoneH3^{His6}, but to a lesser extend. ^{His6}TbKif13-1 was phosphorylated by ^{myc}TbAuk1, but also by ^{myc}TbAuk1 K58R and ^{myc}TbAuk1 T184A. ^{myc}TbAuk1 did not inhibit ^{His6}TbKif13-1's depolymerisation activity in the tubulin sedimentation assay.

3. Discussion

3.1. Attempt to establish a procedure for a *TbKif13-1* high-throughput inhibitor screen

The failure of existing drugs against trypanosomiasis, difficulties in their administration and arising resistances, emphasise the urgent need for new drugs in the fight against trypanosomiasis. New drug targets include *T. brucei* proteins essential for their survival and best unique to Trypanosomes, thus reducing adverse side effects in the mammalian host. Drug libraries are screened for proper small molecule inhibitors in high-throughput assays (Smith et al., 2016; Volkov et al., 2017; Zimmermann et al., 2016). However, *in vitro* identified inhibitors from target-based approaches that screen the isolated protein, are not always reliable compounds *in vivo*. These *in vitro* identified compounds are not tested for membrane permeability and drug conversion in human cells, and in the case of anti-parasitic drugs for toxicity against the human host. Thus, the high-throughput phenotypic screening on cellular basis is more attractive. Two compounds against *T. b. gambiense* and *T. b. rhodesiense* were already found in phenotypic screens and entered clinical trials by DNDi (drugs for neglected diseases initiative; dndi.org; Jacobs et al., 2011; Kaiser et al., 2011; Torreele et al., 2010).

In this thesis the attempt was made to establish the prerequisites for a heterologous *in vivo* high-throughput inhibitor screen. The promising drug target in this assay is the mitotic kinesin *TbKif13-1*. Previous studies showed that *TbKif13-1* is necessary for proper mitotic spindle assembly and *T. brucei* survival, both in cell culture and in a mouse model (Chan et al., 2010; Wickstead et al., 2010a). Since trypanosomiasis' progression and pathogenicity is caused by massive cell proliferation within the human host, it is supposed that prevention of trypanosomes' proliferation could cure trypanosomiasis. A scenario reminding of fighting cancer, where mitotic kinesins came into focus as drug targets (see 1.3.5.).

The principal setting of the heterologous *in vivo* assay in this thesis is simple and elaborate. Usually, inhibitor screens for kinesins are done using ATPase assays (DeBonis et al., 2004; Sakowicz et al., 2004). The heterologous *in vivo* assay has several advantages compared to *in vitro* assays. In contrast to those, the *in vivo* assay is able to identify inhibitors not only acting on the ATPase activity. Moreover, this assay selects for an inhibitor that is not cytotoxic for

Discussion

HeLa cells, indicating that such an inhibitor is potentially also not cytotoxic to the human host. As a potential small molecule inhibitor from this screen would be membrane-permeable, it could also be applied for intracellular *Leishmania* or *T. cruzi*, causing Leishmaniasis or Chagas disease, respectively. The disadvantage of the assay is its high selectivity towards a potential drug. Compounds that would need a chemical modification, like a functional group for inhibiting *TbKif13-1*, are not coming into focus.

In *Xenopus* MCAK, S196 is an inhibitory phosphorylation site for AuroraB kinase, inhibiting MCAK's microtubule depolymerisation effect (Andrews et al., 2004; Lan et al., 2004). Preliminary tests in this thesis also confirmed that mutation of the corresponding S143 in ^{eGFP}*TbKif13-1* is necessary for its microtubule depolymerisation activity in HeLa cells (Figure S 1). While the assay's functionality was proved in HeLa cells transiently transfected and expressing ^{eGFP}*TbKif13-1* S143A, stable HeLa cell lines inducibly overexpressing ^{eGFP}*TbKif13-1* S143A, did not show cytoskeleton microtubule depolymerisation (Figure 9, 10 and S 2).

Experimental data from transiently transfected cells indicated that a higher ^{eGFP}*TbKif13-1* S143A expression rate resulted in better microtubule cytoskeleton depolymerisation rates (Figure 9 and S 2). Hence, it was considered to integrate additional ^{eGFP}*TbKif13-1* S143A copies into the genome of HeLa cells. However, also its additional random genomic integration into already single stable cells, did not result in the desired cytoskeleton depolymerisation (Figure S 3). High expression rates in mammalian cells are in general gained by an alternative transfection option, the lentiviral system (Mao et al., 2015; Varma et al., 2011). Vectors with the highest published expression rates contain the *cytomegalovirus* (CMV) promoter (Mao et al., 2015; Varma et al., 2011). This is the same promoter like in the vector used in this study for the generation of a stable cell line. However, the lentiviral system allows integration of several gene copies and could therefore allow higher expression rates.

A correlation of the expression rate of depolymerising kinesin and cytoskeleton depolymerisation was also seen in stable CHO cells overexpressing MCAK (Ganguly et al., 2011a). Interestingly, there seems to be a correlation between microtubule depolymerisation induced by MCAK and the cellular tubulin expression level. Cytoskeleton depolymerisation by overexpressed MCAK in CHO cells at first increases the amount of unpolymerised free tubulin, but then the level declines below that of free tubulin in control

cells (Ovechkina et al., 2002). The reason for this is supposed to be an autoregulation mechanism of tubulin. Microtubule depolymerising drugs that increase the level of free tubulin lead to decreasing mRNA levels of α - and β -tubulin (Cleveland et al., 1981; Gonzalez-Garay and Cabral, 1996; Ovechkina et al., 2002).

Moreover, CHO cells with high levels of overexpressed MCAK showed an increased sensitivity to microtubule depolymerising drugs, like colcemid (Ganguly et al., 2011a). Conversely, they also exhibited resistance to microtubule stabilising drugs, like paclitaxel (Ganguly et al., 2011a). This effect was not seen within this thesis. The stable HeLa cells, overexpressing ^{eGFP}TbKif13-1 S143A, did not show a sufficient microtubule destabilising effect by nocodazole for use in a high-throughput assay (Figure S 4). This could be due to the expression level of ^{eGFP}TbKif13-1 S143A. Low expression of MCAK did also not result in an increased sensitivity to colcemid in CHO cells (Ganguly et al., 2011a).

Resistance to microtubule stabilising or destabilising drugs depends in addition to other mechanisms, like expression of a different tubulin isotype, on $\alpha\beta$ -tubulin mutations (Gonzalez-Garay et al., 1999; Hari et al., 2003a; He et al., 2001; Schibler and Cabral, 1986). Cell lines with mutations in α - and β -tubulin, resulting in resistance to microtubule stabilising drugs, also showed less assembled microtubule polymers compared to wild type cells (Barlow et al., 2002; Minotti et al., 1991). Conversely, cells with resistance to microtubule destabilising drugs, contain hyperstable microtubules and more microtubule polymers compared to wild type cells (Barlow et al., 2002; Minotti et al., 1991). In both cases the increased or decreased amount of microtubule polymers does not depend on varying tubulin expression levels (Barlow et al., 2002).

It is unlikely that the stable HeLa cells within this thesis are resistant to the used microtubule depolymerising drug nocodazole, because cells started to arrest in mitosis already at addition of 70 ng/mL nocodazole. It is more likely that the maximal usable nocodazole concentration in conjunction with the level of overexpressed ^{eGFP}TbKif13-1 S143A is not sufficient for microtubule depolymerisation, like it was mentioned above for MCAK expression levels in stable CHO cells and colcemid sensitivity (Ganguly et al., 2011a).

Interestingly, in CHO cells addition of microtubule destabilising drugs at a level that does not result in mitotic arrest, decreases the dynamic instability of microtubules, making them more static (Yang et al., 2010). At higher concentrations, microtubule minus ends are released from centrosomes, resulting in microtubule fragments and mitotic arrest (Yang et

al., 2010). Cytoplasmic microtubules are depolymerised only at even higher drug concentrations (Yang et al., 2010).

As an alternative to the *in vivo* assay, an *in vitro* assay for a high-throughput inhibitor screen is possible. In this thesis the prerequisite for such an assay, regarding the depolymerisation of *T. brucei* cytoskeletons by recombinantly purified ^{His6}TbKif13-1 within 384-well plates, should be established. The basic idea of the *in vitro* assay worked well. *T. brucei* cytoskeletons were depolymerisable by recombinantly purified ^{His6}TbKif13-1 (Figure 11). However, providing 384-well plates with depolymerisable cytoskeletons is a challenging task. In this thesis it was found out that on-well-dried cytoskeletons are not depolymerisable. This diminishes the possibility to supply 384-well plates with on-well-dried cytoskeletons for the assay. This is regrettable since their use was much more practical for a high-throughput screen compared to cytoskeletons that are prepared immediately before usage.

However, there was also found no possibility for a robotic readout by automated image analysis for cytoskeletons that were prepared shortly before addition of ^{His6}TbKif13-1. The problems here were unequal depolymerisation of cytoskeletons within one well and the loss of variable amounts of cytoskeletons throughout the operating process. Possibly the use of 384-well plates consisting of another polymer could solve these problems.

As these issues make the assay impractical for a high-throughput screen, a classical *in vitro* ATPase assay, like the enzyme-coupled assay, could be taken into consideration (Huang and Hackney, 1994). However, enzyme-coupled assays are at risk to exhibit off-target inhibition of the used enzymes that couple the reaction to a measurable product. In addition, an *in vitro* target-based assay would necessitate high amounts of recombinantly purified TbKif13-1.

In general, the heterologous *in vivo* assay is preferred. Possibly using another cell line, transfection plasmid or transfection method would generate an appropriate stable cell line clone. Possibly an approach according to the study in CHO cells overexpressing MCAK, which resulted in sufficient cytoskeleton depolymerisation, could generate an appropriate stable cell line (Ganguly et al., 2011a).

3.2. Functional characterisation of TbKif13-1

In this study more insight was gained into domains important for TbKif13-1's subcellular localisation, cell cycle-dependent regulation, microtubule binding and depolymerisation

activity. To this end, *TbKif13-1* deletion constructs were designed and several assays were conducted.

3.2.1. *TbKif13-1* nuclear import and export sequences regulate its subcellular localisation

This study, like two others, showed that full-length *TbKif13-1* is solely nuclear and colocalises with the mitotic spindle (Figure 13; Chan et al., 2010; Wickstead et al., 2010a). Also the *L. major* orthologue *LmjKin13-1* is strictly nuclear (Dubessay et al., 2005). In contrast, mammalian MCAK and its *X. laevis* homologue XKCM1 (*Xenopus* kinesin central motor 1) are equally distributed within the cytoplasm and the nucleus during interphase (Walczak et al., 1996; Wordeman and Mitchison, 1995). Towards mitosis the MCAK level increases and it is recruited to the nucleus (Wordeman et al., 1999).

For MCAK data suggest that its localisation depends on a balance of NLS and NES (Wordeman et al., 1999). The strict nuclear localisation of *LmjKin13-1* depends on an atypical NLS with widely distributed NLS residues within its C-terminus (Dubessay et al., 2005). Also ^{myc}*TbKif13-1* deletion constructs containing the C-terminal domain were essentially nuclear, suggesting a NLS within (Figure 13, 14, 17 and S 5). Within the amino acid sequence of the C-terminal domain there was a potential monopartite NLS found located at aa 562-565 (KRSR; Figure 35). But its functionality remains to be verified by polyalanine substitutions.

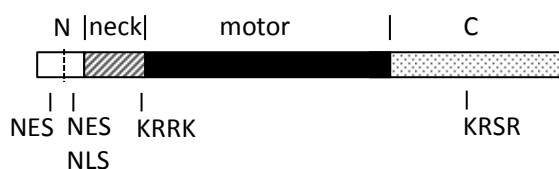


Figure 35: Model for the localisation of (putative) NLS and NES in *TbKif13-1*. In the C-terminus there is a strong NLS KRSK (aa 562-565). The predicted NLS KRRK (aa 139-142) at the supposed neck-motor transition is in competition with the two putative N-terminal NES. Within the N-terminus there is a putative weak NLS. In full-length *TbKif13-1* NLS dominate. White box: N-terminus (N); striped grey box: putative neck domain; black box: motor domain; spotted box: C-terminus (C).

Another NLS sequence is supposed within the neck-motor domain, because the ^{myc}*TbKif13-1* NM construct was essentially nuclear (Figure 16). At the supposed neck-motor transition there is a predicted NLS at aa 139-142 (KRRK; Kosugi et al., 2009b). Also within the motor domain of MCAK there is a predicted NLS, which was verified to be necessary in conjunction with the C-terminal NLS for MCAK's complete nuclear localisation (Wordeman et al., 1999).

Discussion

In contrast, in *LmjKin13-1* the motor domain was found localised essentially in the cytoplasm and weakly in the nucleus (Dubessay et al., 2005).

Also the single N-terminus of *LmjKin13-1* localises within the cytoplasm (Dubessay et al., 2005). For MCAK there was a NES identified within the second half of the bisected N-terminus (Wordeman et al., 1999). Results from this thesis indicate that the second half of the *TbKif13-1* N-terminus (*TbKif13-1* ½ N^{GFP-myc}) also contains a NES and a weak NLS. *TbKif13-1* ½ N^{GFP-myc} localised within the cytoplasm throughout the cell cycle and was additionally nuclear in G1 (1K1N cells; Figure S 7). The small size of *TbKif13-1* ½ N^{GFP-myc} (36.9 kDa) could also raise the question of passive transport through the NPC. Its exclusive cytoplasmic localisation from S-phase to the end of mitosis (1-2K1N to 2K2N cells), however, indicates its active export. Unchanged essential nuclear localisation of the neck-motor construct after addition of the bisected N-terminus (construct^{myc} *TbKif13-1* ½ N + NM) supposes that the N-terminal NES is weaker than the NLS in the neck-motor domain together with the supposed NLS within the second half of the N-terminus (Figure 35 and S 6). Control ectopic expression of the used GFP-myc tag, and GFP tags from other studies, showed that both are cytoplasmic and nuclear throughout the cell cycle (Figure S 8; Marchetti et al., 2000). This supports the existence of the NES within *TbKif13-1* ½ N^{GFP-myc}.

The nuclear and cytoplasmic localisation of *TbKif13-1* N^{GFP-myc} could be due to the supposed NLS and NES within the second half of the N-terminus (Figure 18). There also has to be another NES within the N-terminus, because^{myc} *TbKif13-1* N + NM was strictly cytoplasmic, in contrast to the essentially nuclear localisation of^{myc} *TbKif13-1* ½ N + NM (Figure 15 and S 6). Within the *TbKif13-1* N-terminus several leucines are found, which could indicate a NES (la Cour et al., 2004; Hellman et al., 2007). However, no NES was predicted. Localisation studies of leucine-to-alanine substituted or of smaller fragmented N-terminal parts could shed more light on this topic.

The data indicate that subcellular localisation of *TbKif13-1*, like shown for MCAK, depends on an interplay of NLS and NES, but NLS dominate the full-length *TbKif13-1* localisation (Wordeman et al., 1999).

3.2.2. Cell cycle-specific and proteasome-dependent degradation of *TbKif13-1*

In trypanosomatids, like in all other eukaryotes, misfolded and cell cycle specific proteins are degraded by the 26S proteasome (Hua et al., 1996; Li et al., 2002; Mutomba et al., 1997;

Discussion

Wang et al., 2003). Proteins for degradation are marked with multiubiquitin chains using in general the D-box motif (RxxL) or the KEN-box motif (KEN) as recognition signal for the E3 ubiquitin ligase APC/C with its activator Cdc20 (cell division cycle) or Cdh1 (cdc20 homologue; Fang et al., 1998; Glotzer et al., 1991; Pfleger and Kirschner, 2000; Visintin et al., 1997).

During mitosis APC/C^{Cdc20} ubiquitinates MCAK, which subsequently is degraded at the metaphase-anaphase transition (Ganguly et al., 2008; Sanhaji et al., 2014). APC/C^{Cdc20} binds to the D-box motif RxxL within the MCAK neck domain (Sanhaji et al., 2014). The D-box is made accessible for this by a conformational switch induced by Plk1 phosphorylation of the MCAK C-terminal S621 (Sanhaji et al., 2014).

In *T. brucei* there were found APC/C subunit homologues, additional non-core proteins and a Cdc20 homologue (Bessat, 2014; Bessat et al., 2013; Kumar and Wang, 2005). Functional analysis indicated that APC/C acts on its own, because the Cdc20 homologue was not found associated to it (Bessat et al., 2013).

In this thesis, a cell cycle-specific and proteasome-dependent degradation of *TbKif13-1* was analysed. Studies using inhibition of translation and of the proteasome in the transgenic cell lines ectopically expressing ^{myc}*TbKif13-1* FL showed its proteasome-dependent degradation (Figure 19). Its cell cycle-specific degradation is supported by immunofluorescence microscopy analysis, showing its appearance from S-phase until the end of mitosis (1-2K1N to 2K2N cells), but not in G1-phase (1K1N cells; Figure 13). This is in accordance with a *T. brucei* study localising endogenous *TbKif13-1* with a polyclonal antibody (Chan et al., 2010). In contrast, another *T. brucei* study using direct fluorescence microscopy of endogenous C-terminal GFP tagged *TbKif13-1* (*TbKif13-1*^{GFP}), found *TbKif13-1* not cell cycle regulated with its appearance throughout the cell cycle (Wickstead et al., 2010a).

The *L. major* orthologue *LmjKin13-1* is cell cycle-specific regulated by degradation, with its increase at the beginning of mitosis and its degradation at the end of mitosis (Dubessay et al., 2005). In *LmjKin13-1* the C-terminus is necessary and sufficient for proteasomal degradation, though no D-box or KEN-box motif was identified (Dubessay et al., 2005).

PEST sequences (sequences enriched in proline (P), glutamic acid (E), serine (S), threonine (T), and aspartic acid (D)) are a motif to direct ubiquitin-mediated proteasomal degradation by being phosphorylated (Marchal et al., 1998; Meyer et al., 2011; Rogers et al., 1986; Schnupf et al., 2006). Identified C- and N-terminal PEST sequences in *LmjKin13-1* were found not necessary for degradation (Dubessay et al., 2005). This is consistent with proteins of

Discussion

other organisms, showing that PEST is no destruction motif or that it is necessary but not sufficient, making a PEST sequence not a reliable indicator of proteasomal degradation (Pakdel et al., 1993; Salama et al., 1994). In *TbKif13-1* a PEST motif was predicted within the putative neck domain at aa 64-115 (<http://emboss.bioinformatics.nl/cgi-bin/emboss/pepfind>). However, the neck-motor construct (^{myc}*TbKif13-1* NM) was not degraded after inhibition of translation (Figure 22). This indicates that the PEST motif is also not a reliable proteasomal degradation indicator in *TbKif13-1*.

The results from this thesis indicate that there are several degradation signals within *TbKif13-1* (Figure 36). Two motifs indicative of a proteasomal degradation signal are within the N-terminus of *TbKif13-1*. One is supposed in the first half and one in the second half of the N-terminus. There is also at least one degradation signal supposed within the C-terminus of *TbKif13-1*. The *TbKif13-1* C-terminus (^{myc}*TbKif13-1* C) and the N-terminus (*TbKif13-1* N^{GFP-myc}) were proteasome-dependent degraded (Figure S 11 and S 12). Yet, each in conjunction with the non-degradable neck-motor domain (^{myc}*TbKif13-1* N + NM and ^{myc}*TbKif13-1* NM + C) was not degraded (Figure 20 and S 10). The addition of the half N-terminus within both constructs (^{myc}*TbKif13-1* ½ N + NM and ^{myc}*TbKif13-1* ½ N + C) led to their proteasome-dependent degradation (Figure 21 and S 9). Proteasomal degradation of the second half of the N-terminus (*TbKif13-1* ½ N^{GFP-myc}) was not as pronounced as that one of the single N-terminus (Figure S 13).

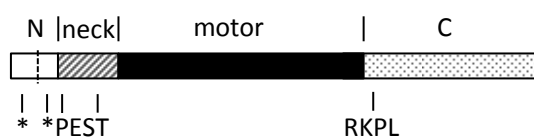


Figure 36: Putative locations for proteasome-dependent degradation signals within *TbKif13-1*. There are three degradation motifs supposed, one within the first and one within the second half of the N-terminus, and one within the C-terminus (marked with *). The marked PEST motif within the putative neck domain at aa 64-115 is predicted, but evidence for its necessity in *TbKif13-1*'s proteasomal degradation is missing. Within the C-terminus at aa 470-473 there is a predicted D-box motif (RKPL), but positive evidence for its functionality is missing. White box: N-terminus (N); striped grey box: putative neck domain; black box: motor domain; spotted box: C-terminus (C).

It is probable that the assumed degradation motifs cooperate for cell cycle-dependent proteasomal degradation. A single D-box motif (RKPL) was predicted at aa 470-473 within the *TbKif13-1* C-terminus, shortly downstream of the neck-motor domain. It was shown to be not sufficient for proteasome-dependent degradation of the *TbKif13-1* neck-motor

Discussion

construct (^{myc}*TbKif13-1* NM + D-box; Figure 23). This could be a result of missing lysine residues for ubiquitination within this construct. Identification of ubiquitination sites remains to be done. Whether the predicted D-box motif within the C-terminus serves as a signal for proteasomal degradation of the C-terminal construct (^{myc}*TbKif13-1* C), could be analysed by mutation or deletion of the D-box motif within this construct.

This brings the supposed two N-terminal and one C-terminal degradation signals again into focus. The proposed destruction motif within the second half of the N-terminus could be a strong signal due to the gained results. Because no canonical destruction motifs were found within the N-terminus, and because the initial results indicate that the predicted D-box motif within the C-terminus is possibly not sufficient for degradation, it could be non-canonical motifs. These were also identified within several proteins of other organisms, like in *S. cerevisiae* within members of the bimC family of kinesins, Cin8p (chromosome instability protein) and Kip1p, and in *L. major* *LmjKin13-1*. In these proteins a NLS was shown to be necessary but not sufficient for APC/C-dependent degradation (Dubessay et al., 2006; Gordon and Roof, 2001; Hildebrandt and Hoyt, 2001). Maybe this is also true for *TbKif13-1*. There is a supposed NLS within the second half of the N-terminus and a predicted NLS within the C-terminus (Figure 35). Mutation of lysines and arginines within the second half of the N-terminus and mutation of the predicted NLS within the C-terminus would give a hint for their role as possible non-canonical degradation signal.

Interestingly, the *TbKif13-1* neck-motor construct with the C-terminus (^{myc}*TbKif13-1* NM + C) appeared cell cycle-dependent degraded in immunofluorescence microscopy studies, while inhibition of translation did not lead to its reduction in Westernblot analysis (Figure 14 and S 10). So far these results cannot be explained.

To conclude, *TbKif13-1* degradation signals are supposed in its C- and N-terminus, with the strongest in the second half of the N-terminus. Further studies are necessary to localise them. A predicted D-box motif within the C-terminus possibly does not function as degradation signal according to initial study results. Deletion or mutation studies could give more information about it.

Further information about *TbKif13-1* domains necessary for APC/C-dependent ubiquitination could be gained from immunoprecipitation of the respective *TbKif13-1* deletion constructs

from cell lysates with inhibited proteasomal degradation. Their Westernblot analysis with an α -ubiquitin antibody (e.g. U5379, Sigma; P4D1, Santa Cruz Biotechnology) could identify ubiquitinated *TbKif13-1* domains. For specific localisation of the ubiquitination sites mass spectrometry could be used (Kaiser and Wohlschlegel, 2005; Xu et al., 2013).

3.2.3. Ectopic expression of the *TbKif13-1* neck-motor domain has a dominant-negative effect on cell cycle progression

The analysis of dominant-negative phenotypes from transgenic 449 cell lines ectopically expressing *TbKif13-1* deletion constructs was expected to reveal the functionality of *TbKif13-1* domains.

Ectopic expression of the depolymerising full-length ^{myc}*TbKif13-1* resulted in reduced growth in the respective transgenic 449 cell line (Figure 24). This is probably due to reduced spindle formation and hence unsuccessful mitosis, but occurring cytokinesis, leading to zoids and >2N cells (Figure 24). Reduced spindle formation after ectopic expression corresponds to the phenotype of long, bent spindles after RNAi mediated *TbKif13-1* depletion (Chan et al., 2010; Wickstead et al., 2010a). Due to varying cellular functions, the effect of ectopically expressed MCAK in CHO cells is slightly different. It results in a reduced microtubule cytoskeleton, multinucleate cells and an accumulation of multipolar prometaphase-like spindles (Ganguly et al., 2011a; Maney et al., 2001).

Growth curves and flow cytometry analysis showed that ectopic expression of the ^{myc}*TbKif13-1* C-terminus did not have a retarding effect on the cell cycle compared to non induced transgenic cells, but compared to wild type cells (Figure S 23). Maybe this is due to leaky expression in non induced cells. More than 50% of mitotic cells ectopically expressing ^{myc}*TbKif13-1* C exhibited an elongated spindle (Figure 28). This is conform with data from ^{myc}*TbKif13-1* C staining in this cell line. In whole cell and cytoskeleton samples, ^{myc}*TbKif13-1* C resembled the shape of the mitotic spindle, but in a more elongated kind (Figure 17). A double staining of the spindle and ^{myc}*TbKif13-1* C could determine a definite colocalisation and thus a possible binding of ^{myc}*TbKif13-1* C to spindle microtubules. KMX and α -myc double staining was not possible due to the experimental procedure.

Ectopic expression of ^{myc}*TbKif13-1* C occurred within the wild type background. A possible explanation for the phenotype of the elongated spindle could be a simple competition of the endogenous *TbKif13-1* with the non functional ^{myc}*TbKif13-1* C-terminus. An increased binding

Discussion

of the *TbKif13-1* C-terminus to the spindle could reduce binding of endogenous *TbKif13-1* and thus, reduce its spatial functionality. This possibility also corresponds to the *TbKif13-1* RNAi phenotype with long and bent spindles (Chan et al., 2010; Wickstead et al., 2010a). Despite the binding of ^{myc}*TbKif13-1* C resembling in shape the mitotic spindle in cytoskeleton preparation, direct evidence for its microtubule binding ability is missing (Figure 17). Tubulin sedimentation assays with recombinantly purified *TbKif13-1* C could clarify its possible binding ability. To figure out a possible competition, the tubulin binding affinities of full-length and C-terminal *TbKif13-1* could be determined in a varied tubulin sedimentation assay (Hertzer et al., 2006). This assay uses doubly stabilised microtubules to minimise depolymerisation. Increasing amounts of them are added to the respective kinesin. SDS-PAGE analysis of the centrifugated pellet and supernatant samples, and subsequent quantification shows microtubule binding affinities.

Another explanation for the elongated spindle phenotype is the binding of ^{myc}*TbKif13-1* C to wild type *TbKif13-1*. This construct could be less productive compared to a wild type *TbKif13-1* dimer because of just one motor domain. Also this possibility is conform with the *TbKif13-1* RNAi phenotype (Chan et al., 2010; Wickstead et al., 2010a). MCAK was shown to be a more potent depolymeriser as dimer, compared to the monomeric neck-motor construct (Cooper et al., 2010; Hertzer et al., 2006). In addition to two motor domains within the dimeric full-length MCAK, it is mainly proposed that its release from detached tubulin dimers after depolymerisation is more promoted as dimer, facilitating repeated rounds of depolymerisation (Cooper et al., 2010; Hertzer et al., 2006).

The MCAK C-terminus contributes to dimerisation by binding with its conserved EExxS motif at the interface of two motor domains (Ems-McClung et al., 2013; Talapatra et al., 2015). While the EExxS motif is conserved from *Drosophila* Klp10A to human MCAK, in *TbKif13-1* only the two glutamic acids are conserved (Talapatra et al., 2015). Instead of the conserved serine there is a cysteine within the sequence of *TbKif13-1*. Talapatra et al. (2015) showed that a larger side chain compared to serine would cause steric hindrance of C-terminus binding to the motor domain. The same side chain size of serine and cysteine probably does not prevent binding. Thus, there is a possibility that the spindle binding phenotype of ^{myc}*TbKif13-1* C is attributed to its binding to the wild type *TbKif13-1*.

In vitro pull down assays and size exclusion chromatography using recombinantly purified full-length *TbKif13-1*, neck-motor domain *TbKif13-1* and *TbKif13-1* C, as well as substitution

Discussion

or deletion mutants of the EE_{xx}C motif, could provide more knowledge about a possible C-terminal interaction with the neck-motor domain.

The most dominant-negative phenotype exhibited ectopically expressed ^{myc}*TbKif13-1* NM. The ectopic expression of the neck-motor construct did have a massive negative influence on cell viability and spindle formation within the transgenic 449 cell line (Figure 27). These effects were already indicated by ectopic expression of the neck-motor domain with the half N-terminus (^{myc}*TbKif13-1* ½ N + NM; Figure 26). The ectopic expression of the neck-motor construct resulted in a strong growth defect due to missing spindles in mitotic cells already twelve hours after induction, a massive increase in zoids and multinuclear cells, and finally cell death five days after induction (Figure 27 and S 22). The subcellular localisation and phenotype of the basal body, flagellum and FAZ were analysed via immunofluorescence twelve and 24 hours after induction (data not shown). But there were found no abnormalities throughout the cell cycle, making the missing spindle the only hint.

In cytoskeleton preparations of ectopically expressing ^{myc}*TbKif13-1* NM cells, the neck-motor construct was still found within the nucleus, even though not in a spindle-resembling shape (Figure 16). The earliest microscopy analysis of these cells was done twelve hours after induction, a time at which almost no spindle was found anymore within this cell line. This could indicate that the neck-motor domain could have bound to nuclear tubulin either by itself or, which is more likely due to data from its missing *in vitro* microtubule binding ability in the presence of ATP, via another protein within the nucleus, possibly endogenous *TbKif13-1* (Figure 30). Dimerisation could occur as shown for MCAK via the C-terminus, which is able to bind two motor domains (Ems-McClung et al., 2013; Talapatra et al., 2015). Pull down assays and size exclusion chromatography would give more information about this possibility in *TbKif13-1*.

One explanation for the dominant-negative phenotype could be that a possible *TbKif13-1* full-length and neck-motor dimer was more active than wild type *TbKif13-1* due to missing regulatory sites. This could comprise conformational switches involving the C-terminus and the motor domain, which were shown to control conformation within the MCAK wild type dimer (Talapatra et al., 2015). But this could also comprise phosphoregulation sites due to their occurrence only once within such a chimeric dimer. For *TbKif13-1* there have not yet been identified phosphoregulation sites. For MCAK there are several phosphoregulation

Discussion

sites known within the N- and C-terminus, necessary for its localisation and activity (Lan et al., 2004; Shao et al., 2015; Zhang et al., 2007; Zhang et al., 2011).

A possible dimerisation is conform with results from ectopic expression of the *TbKif13-1* neck-motor domain with the full or half N-terminus. Ectopic expression of ^{myc}*TbKif13-1* N + NM did not have an obvious effect on growth behaviour, the cell cycle or spindle assembly (Figure S 20). Moreover, it was not found within the nucleus in cytoskeleton preparations and *in vitro* it did not bind to microtubules (Figure 15 and S 28). Possibly, it could mainly dimerise with itself via its N-terminus. The N-terminus is also a dimerisation domain in MCAK (Maney et al., 2001). It is supported by data from ectopic expression of *TbKif13-1* N^{GFP-myc}, which was not found within the nucleus of cytoskeleton preparations (Figure 18).

Reducing more than half of the MCAK N-terminus led to a quite reduced dimerisation ability of the N-terminus (Maney et al., 2001). In *TbKif13-1* the neck-motor domain together with the half N-terminus (^{myc}*TbKif13-1* ½ N + NM) led to a growth defect with an increase of zoids and >2N cells (Figure 26). These effects are probably due to the analysed up to 50% reduction in mitotic spindle formation (Figure 26). Based on data for reduced dimerisation ability of MCAK's half N-terminus, it is possible that this *TbKif13-1* construct also dimerises with itself to some extent, but that it also would dimerise with the endogenous wild type *TbKif13-1* (Maney et al., 2001). A competition with endogenous *TbKif13-1* should be excluded, because *TbKif13-1* ½ N + NM was not found associated to microtubules within the tubulin sedimentation assay and did also not bind in a shape resembling the mitotic spindle in cytoskeleton preparations (Figure S 6 and S 29).

This endogenous *TbKif13-1* - ^{myc}*TbKif13-1* ½ N + NM chimeric dimer could, like it is supposed for the endogenous-neck-motor chimeric dimer, not be regulated sufficiently by phosphorylation or conformational changes. Unfortunately, there are no data available for *TbKif13-1* regulatory sites. Phosphorylation sites could be identified using microcapillary liquid chromatography/tandem mass spectrometry (LC-MS/MS). Moreover data for dimerisation domains could be achieved by yeast-two-hybrid assays, pull down assays and size-exclusion chromatography.

Another explanation for the ectopic expression phenotype of the neck-motor construct could be its possible inhibitory binding to another protein necessary for spindle assembly or maintenance. *TbAuk1* was shown to be essential for spindle assembly, and endogenous

tagged *TbAuk1*^{HA3} was found at the central spindle and in the spindle midzone (Tu et al., 2006; Li and Wang, 2006; Li et al., 2008a). RNAi of proteins necessary for correct *TbAuk1* localisation resulted in a missing spindle. Among them are *TbKIN-A*, *TbKIN-B*, the chromosomal passenger complex proteins *TbCPC1* and *TbCPC2* and the *TbAuk1* substrate activator *TbTlk1* (Li et al., 2007; Li et al., 2008a; Li et al., 2008b). *TbKIN-A*, *TbKIN-B*, *TbCPC1* and *TbCPC2* are distributed throughout the nucleus during interphase and *TbTlk1* forms a focal point in the interphase nucleus (Li et al., 2007; Li et al., 2008a; Li et al., 2008b). Also the ectopically expressed *TbKif13-1* neck-motor construct localised throughout the nucleus (Figure 16). To get more information about a possible interaction of the *TbKif13-1* neck-motor construct with these proteins, a yeast-two-hybrid assays, pull down assays and size-exclusion chromatography could be conducted.

To conclude, further studies are necessary to understand the dominant-negative phenotype of ectopically expressed ^{myc}*TbKif13-1* NM and the elongated spindle phenotype of ectopically expressed ^{myc}*TbKif13-1* C. Of interest are studies concerning a possible microtubule binding competition with wild type *TbKif13-1*, as well as possible dimerisation domains, phosphoregulation sites and binding partners of *TbKif13-1*.

3.2.4. *TbKif13-1* neck-motor domain and C-terminus are necessary for *in vitro* microtubule binding and depolymerisation

The depolymerisation mechanism of Kinesin-13 family members depends on their ability to bind to microtubules (Asenjo et al., 2013; Burns et al., 2015; Ems-McClung et al., 2013; Moore and Wordeman, 2004).

This study confirmed that *TbKif13-1* binds to isolated microtubules and that it is a potent microtubule depolymeriser in an ATP-dependent manner (Figure 11 and 29; Chan et al., 2010). Recombinantly purified ^{His6}*TbKif13-1* depolymerised Trypanosome cytoskeletons *in vitro* (Figure 11). The flagellum and possibly the FAZ remained. Both structures are known to remain even after high salt and detergent treatment, removing all other cytoskeleton components (Sherwin and Gull, 1989).

The question persisted which *TbKif13-1* domains are necessary for microtubule binding and depolymerisation. The *Plasmodium falciparum* KinI motor domain alone is sufficient for microtubule binding and depolymerisation (Moores et al., 2002). In MCAK the motor domain is sufficient for microtubule binding, while for depolymerisation the addition of the neck is

necessary (Maney et al., 2001). That is not true for *TbKif13-1*. The *TbKif13-1* neck-motor domain alone (^{myc}*TbKif13-1* NM) or together with the N-terminus (^{myc}*TbKif13-1* N + NM) is not sufficient for *in vitro* microtubule binding or depolymerisation (Figure 30 and S 28). This study showed that for *in vitro* microtubule binding in the presence of ATP and for depolymerisation, the neck-motor domain in conjunction with the C-terminus is necessary (^{myc}*TbKif13-1* NM + C; Figure S 27 and 37).

It would be interesting to get more insight into which parts of the C-terminus in conjunction with the neck-motor domain are necessary for microtubule binding and depolymerisation. To analyse this, deletion constructs of the C-terminus in conjunction with the neck-motor domain would be necessary.

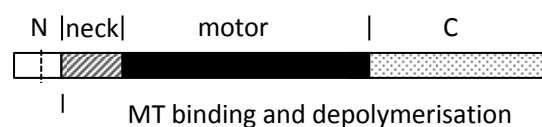


Figure 37: Model depicting necessary *TbKif13-1* domains for microtubule binding and microtubule depolymerisation. The *TbKif13-1* neck-motor domain in conjunction with the C-terminus is necessary for microtubule binding and microtubule depolymerisation. White box: N-terminus (N); striped grey box: putative neck domain; black box: motor domain; spotted box: C-terminus (C).

The neck-motor construct was shown to exhibit *in vitro* ATPase activity, but only when stimulated by added microtubules (Figure 30). ATPase activity of MCAK was shown to occur when it settles onto the microtubule lattice and when the MCAK-ATP-tubulin complex dissociates after depolymerisation (Burns et al., 2015; Ems-McClung et al., 2013; Moore and Wordeman, 2004). Because an *in vitro* depolymerisation activity of the neck-motor construct is missing, it is supposed that its ATPase activity here is attributed to the construct's lattice binding. ATP hydrolysis weakens the binding of the kinesin to the lattice, which could explain why it was not found tightly bound to microtubules (Figure 30; Burns et al., 2014; Ems-McClung et al., 2013). This would be in agreement with data from the neck-motor construct of MCAK, which was shown to bind more often to microtubules, but also to dissociate more rapidly than full-length MCAK (Cooper et al., 2010).

Interestingly, results showed that the *TbKif13-1* neck-motor domain with or without the half or whole N-terminus is able to bind to microtubules *in vitro* in the absence of ATP, but not in its presence (Figure 30, S 28 and S 29). Probably, this is due to a conformational difference of the motor when having ATP bound or not. Cryomicroscopy of Kar3, a depolymerising kinesin-14 family member, in different nucleotide states showed that the nucleotide-free

state differs structurally from the others in that the $\alpha 4$ and loop 11 of switch II change conformation, resulting in strong binding to the tubulin intradimer (Hirose et al., 2006). The nucleotide-free state of full-length and C-terminal truncated MCAK leads to bundled microtubules decorated with the respective MCAK molecules (Moore and Wordeman, 2004). These data and those received in this thesis might imply that the nucleotide-free state of ^{myc}TbKif13-1 NM, ^{myc}TbKif13-1 N + NM and ^{myc}TbKif13-1 ½ N + NM binds stronger to tubulin possibly by nucleotide-dependent conformational changes.

3.2.5. Conserved decoupled mechanism of microtubule depolymerisation and ATP hydrolysis in TbKif13-1

Kinesins, myosins and G proteins have conserved structures for ATP binding and hydrolysis, and change of the bound nucleotide state is accompanied by change in conformation (Bourne et al., 1990; Bourne et al., 1991; Kikkawa et al., 2001; Kull et al., 1996; Kull et al., 1998; Sablin et al., 1996). The switch II (DxxGxE) is an important motif for ATP binding and hydrolysis, and it is directly connected to the microtubule binding site within kinesins (Woehlke et al., 1997).

At microtubule ends, MCAK-ATP undergoes a conformational change that is necessary for microtubule bending and subsequent depolymerisation and ATP hydrolysis activity (Wang et al., 2015). Mutation of the switch II motif (Dxx**G**xE) G495A in human MCAK inhibits this conformational change, keeping the kinesin in a pre-conformational change state (Wang et al., 2012). The mutant is characterised by the remaining ability to bind to microtubules, but its failure to depolymerise them and abolished ATPase activity (Wagenbach et al., 2008; Wang et al., 2012).

The same effects were seen for ^{His6}TbKif13-1 FL G371A (Figure 31). ^{His6}TbKif13-1 FL G371A did not depolymerise microtubules within the tubulin sedimentation assay, independent of its concentration (Figure 31 (C)). In this assay it was found in the pellet fraction with polymerised microtubules, indicating its microtubule binding ability. The ATPase deficiency of ^{His6}TbKif13-1 FL G371A was shown by the malachite green assay (Figure 31 (A)).

Mutation of the glycine within the switch II motif abolishes a hydrogen bond to the ATP γ -phosphate. Because the motif is conserved, glycine mutation also results within conventional kinesins and myosins in abolished ATPase activity (Kull et al., 1998; Rice et al., 1999; Sasaki et al., 1998; Trivedi et al., 2012).

Discussion

After the conformational change, MCAK-ATP is able to depolymerise microtubules, i.e. releases a ternary complex of MCAK-ATP-tubulin, which is afterwards dissolved by ATP hydrolysis. This step is blocked by the switch II motif mutant E497A and the ternary complex is kept tightly bound (Wagenbach et al., 2008; Wang et al., 2015). MCAK E497A was found nearly completely ATPase deficient, but it was still found sensitive to stimulation by microtubules (Wagenbach et al., 2008; Wang et al., 2015). The same effect was seen for *TbKif13-1* E497A. In the malachite green assay, *TbKif13-1* E497A exhibited almost no ATPase activity, but depending on higher microtubule concentration it increased slightly (Figure 31 (B)).

TbKif13-1 E497A was able to depolymerise microtubules, which was more evident at higher kinesin concentrations (Figure 31 (D)). This is also seen for MCAK E497A (Wagenbach et al., 2008; Wang et al., 2015). The depolymerisation behaviour of the mutant differs from the wild type MCAK. In wild type MCAK a maximum is reached when protofilament ends are saturated (Hunter et al., 2003). This lower motor to tubulin ratio necessary for depolymerisation was also seen for wild type *TbKif13-1* (Figure 31 (C) and (D)).

In contrast, efficient depolymerisation by MCAK E497A is only possible when the microtubule lattice is saturated with the kinesin. MCAK E497A is not able to do several rounds of depolymerisation (Wagenbach et al., 2008). This necessitates a saturated concentration of MCAK E497A along the microtubule lattice for efficient depolymerisation. Moreover, negative staining electron microscopy showed that at saturated levels, pelletable tubulin oligomers or rings occur because of the kinesin's longitudinally linking (Wang et al., 2015). At an unsaturated level of MCAK E497A only two tubulin heterodimers are linked, peel off the microtubule and are found soluble (Wang et al., 2015).

The conserved switch II glutamic acid (DxxGxE) and the switch I arginine (NxxSSR) form a salt bridge in kinesins and myosins (Furch et al., 1999; Onishi et al., 1998; Yun et al., 2001). The effects seen in MCAK E497A are similar to those in myosins and other kinesins, pointing to the conserved communication mechanism between the switch motifs' conformational changes and state of the bound nucleotide, even though ATPase cycles and according motor-microtubule/actin interactions differ between motors. In myosin, mutation of the corresponding amino acids inhibits ATP hydrolysis (Furch et al., 1999; Onishi et al., 1998; Sasaki et al., 1998; Shimada et al., 1997; Trivedi et al., 2012). Also in the *S. cerevisiae* minus-end directed microtubule depolymerising kinesin Kar3, mutation of the glutamic acid

resulted in stronger binding to microtubules compared to the wild type, probably because of the displacement of loop 8, and loss of microtubule activated ATPase activity (Yun et al., 2001). Conventional kinesin with mutated switch II glutamic acid is also ATPase deficient, but the conformational change necessary for the subsequent forward step of the partner head occurs (Rice et al., 1999).

In general kinesins, myosins and G-proteins are evolutionary linked because of several conserved core motifs and secondary elements, which show similar but different mechanisms (Kull et al., 1998; Sablin et al., 1996). In this study the conserved decoupled mechanism of microtubule depolymerisation and ATP hydrolysis of Kinesin-13 family members was confirmed for *T. brucei* TbKif13-1.

3.3. TbAuk1 and TbKif13-1

MCAK is phosphorylated by AuroraB at several sites within the N-terminus and the neck domain for localisation and activity reasons (Lan et al., 2004; Zhang et al., 2007). Little is known about a possible regulation of TbKif13-1 in *T. brucei*. One issue of this thesis was to analyse whether TbKif13-1 was phosphorylated by the mitotic Aurora-like kinase TbAuk1 and whether this phosphorylation inhibited TbKif13-1's depolymerisation activity.

In a first step, ^{myc}TbAuk1 was immunoprecipitated from a transgenic 449 cell line ectopically expressing ^{myc}TbAuk1 in an active state, being able to phosphorylate TbHistoneH3^{His6} (Figure 32). The N-terminus of TbHistoneH3 lacks phosphorylation sites corresponding to mammalian S10 and S28, which are phosphorylated by AuroraB. LC/MS/MS revealed that TbHistoneH3 is phosphorylated by TbAuk1 at T116 within the C-terminal domain (Jetton et al., 2009).

The published kinase-dead mutants ^{myc}TbAuk1 K58R and ^{myc}TbAuk1 T184A were chosen as negative controls. However, both mutants were able to phosphorylate TbHistoneH3^{His6} to some extent (Figure 32; Hu et al., 2014; Li and Wang, 2006). There was no TbHistoneH3^{His6} phosphorylation by the product of the mock IP, in which the protein G-sepharose was applied to wild type 449 cell lysate without antibody. This control excludes the possibility that contaminations of the cell lysate were responsible for the phosphorylation.

The control IP product from wild type 449 cell lysate also showed slight TbHistoneH3^{His6} phosphorylation, but to an even lesser extent than the kinase-dead controls (Figure 32). This

Discussion

indicates that the myc-antibody bound protein G-sepharose purified a protein from Trypanosomes' cell lysate capable of phosphorylating *TbHistoneH3*^{His6} to a small degree. The, in comparison, slightly increased *TbHistoneH3*^{His6} phosphorylation by the kinase-dead ^{myc}*TbAuk1* K58R and ^{myc}*TbAuk1* T184A mutants suggests the possibility of additional co-immunoprecipitation of a protein able to oligomerise with ^{myc}*TbAuk1*. Yeast-two-hybrid assays showed that *TbAuk1* does not dimerise with itself but it does with *TbTlk1* (Li et al., 2007). *TbTlk1* was already found co-immunoprecipitated with *TbAuk1* from *T. brucei* cell lysates and it was shown to phosphorylate *TbHistoneH3* *in vitro* (Li et al., 2007). Westernblot analysis or mass spectrometry of the immunoprecipitated products could determine whether *TbTlk1* is contained in the IP products and whether other possible kinases were immunoprecipitated.

In a next step, the product from ^{myc}*TbAuk1* IP was shown to phosphorylate ^{His6}*TbKif13-1* (Figure 33). This occurred independent of microtubule addition. At first sight it suggests that *TbAuk1*, in contrast to AuroraB kinase, would not need tubulin for *in vitro* activity (Rosasco-Nitcher et al., 2008). However, Westernblot analysis showed tubulin to a minor degree also in samples where microtubules were not added (Figure S 32). This could be the result of a spillover during gel loading. Another possibility is that it confirms studies where PTP mediated purification of *TbAuk1* from *T. brucei* cell lysates also isolated tubulin, which could be due to *TbAuk1*'s association to spindle microtubules (Li et al., 2008a; Tu et al., 2006). Hence, as previously supposed for AuroraB kinase, *TbAuk1* could have an increased activity towards other microtubule-bound proteins like *TbKif13-1*, compared to non-bound proteins (Noujaim et al., 2014).

^{myc}*TbAuk1* K58R and ^{myc}*TbAuk1* T184A resulted in the same phosphorylation effects, while wild type 449 IP product did not phosphorylate ^{His6}*TbKif13-1* and tubulin. One explanation could be the possibility that the published kinase-dead mutants are not entirely devoid of kinase activity. Another explanation could be the previously mentioned possibility of co-purification of other kinases, capable to oligomerise with ^{myc}*TbAuk1*. In addition to *TbTlk1*'s ability to phosphorylate *TbHistoneH3*, there is nothing known about its ability to phosphorylate *TbAuk1* or *TbKif13-1* (Li et al., 2007). MCAK's motor domain phosphorylation by Cdk1 (cyclin-dependent kinase) diminishes its depolymerisation activity and contributes to spindle formation and chromosome positioning (Sanhaji et al., 2010). Cdk1 also phosphorylates unpolymerised tubulin (Fourest-Lieuvain et al., 2006). For the *T. brucei* Cdk1

Discussion

homologue *TbCrk3* (cdc2-related kinase) no interaction with tubulin, *TbKif13-1* or *TbAuk1* has yet been identified (Hammarton et al., 2003; Tu and Wang, 2004).

Furthermore, MCAK is also phosphorylated at five residues within the C-terminal domain by Plk1, stimulating its depolymerisation activity during early phases of mitosis (Shao et al., 2015; Zhang et al., 2011). Such an stimulating effect of *TbPlk* to *TbKif13-1* could explain the absent inhibition of ^{His6}*TbKif13-1*'s depolymerisation activity by the ^{myc}*TbAuk1* IP product (Figure 34). However, for *TbPlk* an interaction with *TbAuk1* or *TbKif13-1* has not yet been shown. *TbPlk* is excluded from the nucleus throughout the cell cycle and does not play a role during mitosis, but during cytokinesis (Hammarton et al., 2007; Kumar and Wang, 2006). *TbPlk*, together with its substrates, is necessary for basal body segregation, Golgi and bilobe biogenesis and flagellum inheritance (de Graffenried et al., 2008; Hammarton et al., 2007; Hu et al., 2015; Ikeda and de Graffenried, 2012; McAllaster et al., 2015). Also for mammalian Plk1 there is nothing known about a AuroraB kinase phosphorylation.

Other possible explanations could be that the used ^{myc}*TbAuk1* concentration in comparison to ^{His6}*TbKif13-1* was insufficient or that *TbAuk1* simply does not inhibit *TbKif13-1*'s depolymerisation activity.

To conclude, data from this thesis suggest a *TbAuk1* mediated phosphorylation of *TbKif13-1* that does not inhibit its microtubule depolymerisation activity. However, mass spectrometry analysis of the immunoprecipitated products could figure out a possible co-immunoprecipitation of other kinases. This will provide more information about the detected *TbKif13-1* phosphorylation and the possible involvement of *TbAuk1*.

4. Material and methods

4.1. Materials

4.1.1. Hard- and software

This work was written on an Asus N56V (ASUSTeK COMPUTER INC., Taiwan, China) using Microsoft Word 2010 (Microsoft Corporation, Redmond, WA, USA). For the design of diagrams Sigma Plot 11.0 (Systat Software Inc., San José, CA, USA) was used. Chemiluminescence signals were detected with the 'LAS-4000' system (Fujifilm Europe, Düsseldorf). Autoradiographies were digitized using the 'FLA-7000' phosphorimager (Fuji Film Europe, Düsseldorf). Absorbance measurements on well plates were done using 'FLUOstar Omega' (BMG Labtech, Ortenberg) according with its own control software and 'MARS data analysis' software. Images were processed with 'Adobe Photoshop CS4' (Adobe Systems Inc., San Jose, CA, USA). Figures were generated using Microsoft PowerPoint 2010 (Microsoft Corporation, Redmond, WA, USA). *T. brucei* DNA and protein sequences were received from www.genedb.org. Analysis of DNA sequences and virtual design of plasmids was done with 'DNASTAR Lasergene' (GATC Biotch, Konstanz). For sequence alignments a service of the European Bioinformatics Institute ('EMBOSS needle pairwise sequence alignment' algorithm, www.ebi.ac.uk) was used. Prediction of APC/C recognition motif was done with 'GPS-ARM 1.0' (the cuckoo workgroup, China, arm.biocuckoo.org). For analysis of protein domain architecture the European Molecular Biology Laboratory online tool 'SMART' (smart.embl-heidelberg.de) was used. The National Center for Biotechnology Information (www.ncbi.nlm.nih.gov/) provided electronic online services for literature research.

4.1.2. Chemicals, reagents and kits

All chemicals and reagents were purchased, unless noticed otherwise, from AppliChem (Darmstadt), BioRad (Munich), Calbiochem (via Merck, Darmstadt), Fermentas (St. Leon-Rot), GE Healthcare (München), Merck (Darmstadt), Invitrogen (via Thermo Scientific, Schwerte), Macherey-Nagel (Düren), New England Biolabs (NEB, Frankfurt a. M.), Qiagen (Hilden), Roth (Karlsruhe), Serva (Heidelberg), Sigma-Aldrich (Steinheim) and Thermo Scientific (Schwerte).

For all solutions, de-ionized sterile water was used. If needed, solutions were sterilised and sterile flasks were used.

4.1.3. Antibodies

Commercial and self-made antibodies were used in this study as follows (Table 5 and 6).

Table 5: Primary antibodies.

antibody	class and species	antigen	dilution	source/reference
BiP	mouse monoclonal	BiP	1:3000 WB	Gertrud Lallinger-Kube, Molecular Parasitology, University of Bayreuth
GFP	IgG mouse monoclonal	GFP	1:1000 WB	Markus Hermann, Genetics, University of Bayreuth
His	IgG1 mouse monoclonal	Histidin	1:2000 WB	Santa Cruz Biotechnology, Dallas, TX, USA
KMX	IgG2b mouse monoclonal	β -Tubulin/ spindle	1:2000 IF	Birkett et al., 1985
TAT1	IgG2b mouse monoclonal	α -Tubulin	1:1000 IF 1:10000 WB	Woods et al., 1989
<i>Tb</i> Histone H3	rabbit	<i>Tb</i> Histone H3	1:50000 WB	kind gift from Prof. Dr. Christian Janzen, Cell and Developmental Biology, University of Würzburg
9E10	IgG mouse monoclonal	myc	1:200 IF 1:500 WB	SeraLab, London, UK

Table 6: Secondary antibodies.

antibody	antigen and species	dilution	source
Atto 488 FITC labelled	α -mouse IgG (whole molecule), polyclonal, produced in goat	1:500 IF	Sigma-Aldrich, Steinheim
Atto 550 Cy3 labelled	α -mouse IgG (whole molecule), polyclonal, produced in goat	1:500 IF	Sigma-Aldrich, Steinheim
mouse-HRP	α -mouse IgG (whole molecule), polyclonal, produced in rabbit	1:80000 WB	Sigma-Aldrich, Steinheim
rabbit-HRP	α -rabbit IgG (H+L) conjugated, polyclonal, produced in goat	1:20000 WB	Zymed via Invitrogen, Thermo Scientific, Schwerte

4.1.4. DNA oligonucleotides

DNA oligonucleotides for this study were received from Microsynth (Balgach, Switzerland). Their design was as follows (Table 7, 8 and 9).

Table 7: DNA oligonucleotides for changing multiple cloning sites and tags in vectors.

oligonucleotide	sequence 5'->3'	purpose
MluIFseIPvuIAscIBamHI_for2	5'-CGC GTC GGG CCG GCC CGA TCG GGC GCG CCG-3'	<i>MluI FseI PvuI AscI BamHI</i> changing MCS of pHD1701 to pHD1801; forward
MluIFseIPvuIAscIBamHI_rev2	5'-GAT CCG GCG CGC CCG ATC GGG CCG GCC CGA-3'	<i>MluI FseI PvuI AscI BamHI</i> changing MCS of pHD1701 to pHD1801; reverse
FseIAscIApaIMluIBamHI_for	5'-CCA TTA TTG GGC GCG CCA TTG GGC CCA TTA CGC GTA TTG-3'	<i>FseI AscI ApaI MluI BamHI</i> changing MCS of pHD1800; forward
FseIAscIApaIMluIBamHI_rev	5'-GAT CCA ATA CGC GTA ATG GGC CCA ATG GCG CGC CAA TGG CCG G-3'	<i>FseI AscI ApaI MluI BamHI</i> changing MCS of pHD1800; reverse
GFP_Mlu_for	5'-ATA <u>ACG CGT</u> ATG GTG AGC AAG GGC GAG GAG C-3'	GFP; with startcodon; <i>MluI</i> ; forward; for cloning <i>GFP</i> into pHD1800, resulting in pHD1800-GFPmyc
GFP_BamHI_re	5'-ATA <u>GGA TCC</u> CTT GTA CAG CTC GTC CAT GCC G-3'	GFP; without stopcodon; <i>BamHI</i> ; reverse; for cloning <i>GFP</i> into pHD1800, resulting in pHD1800-GFPmyc

Table 8: DNA oligonucleotides for *TbKif13-1* constructs.

oligonucleotide	sequence 5'->3'	purpose
pCS2tag_Kif13_1f Fse	5'-ATA <u>GGC CGG CCG</u> GCG AAG TGG GAA TTA AAG CTG-3'	<i>TbKif13-1 N-terminus</i> , without startcodon; starts at 4 th base of <i>TbKif13-1</i> , <i>FseI</i> ; forward; pHD1801, pTrc C FA, pcDNA5, pcDNA3.1, pCS2-eGFP
pHD1800Kif13.1forFse	5'-ATA <u>GGC CGG CCA</u> TGG CGA AGT GGG AAT TAA AGC T-3'	<i>TbKif13-1 N-terminus</i> , with startcodon; starts at 1 st base of <i>TbKif13-1</i> , <i>FseI</i> ; forward; pHD1801-GFPmyc
13-1 NES_ATG_forFs	5'- ATA <u>GGC CGG CCA</u> TGG AAG AGT TCG TAG CCC TG-3'	<i>TbKif13-1 ½ N-terminus</i> , with startcodon; <i>FseI</i> ; forward; pHD1800- GFPmyc
NES for	5'-ATA <u>GGC CGG CCG</u> GAA GAG TTC GTA GCC CTG CAG-3'	<i>TbKif13-1 ½ N-terminus</i> , without startcodon; starts at 94 th base of <i>TbKif13-1</i> ; <i>FseI</i> ; forward; pHD1801, pTrc C FA
pCS2tag_Kif13_1MfFse	5'-ATA <u>GGC CGG CCC</u> GCC ATA AAG AAG CTG CGC GGG-3'	<i>TbKif13-1 neck/motor domain</i> , without startcodon; starts at 175 th base of <i>TbKif13-1</i> ; <i>FseI</i> ; forward; pHD1801, pTrc C FA
Tag-13-1 C-ter fF	5'-ATA <u>GGC CGG CCG</u> AAA AGC CGT AGT GAA AGA AAG CC-3'	<i>TbKif13-1 C-terminus</i> , without startcodon; starts at 1396 th base of <i>TbKif13-1</i> ; <i>FseI</i> ; forward; pHD1801

Material and methods

Kif13.1MycEGFPprev	5'- <u>GGC GCG CCC</u> TAA ATC CCG TTT TGC TCG AGA-3'	<i>TbKif13-1 C-terminus</i> , with stopcodon; ends at 2073 rd base of <i>TbKif13-1</i> ; Ascl; reverse; pHD1801, pTrc C FA, pcDNA5, pcDNA3.1, pCS2-eGFP
pCS2tag_Kif13_1MrAsc	5'- <u>GGC GCG CCT</u> TAC TTT AAC TCC TTC ACA CGA TCA GCG TA-3'	<i>TbKif13-1 neck/motor domain</i> , with stopcodon; ends at 1392 nd base of <i>TbKif13-1</i> ; Ascl; reverse; pHD1801, pTrc C FA
Kif13_1DBox_rev_Asc	5'- <u>GGC GCG CCT</u> TAC TCA GAT TGC TCA TTT TCC TCT AGA GG-3'	<i>TbKif13-1 DBox</i> , with stopcodon; ends at 2073 th base of <i>TbKif13-1</i> ; Ascl; reverse; pHD1801
13-1 N-term GFP_re	5'-ATA <u>GGC GCG CCC</u> GTG ATA CAA ATT CAC CGT ATC CTC-3'	<i>TbKif13-1 N-terminus</i> , without stopcodon; ends at 174 th base of <i>TbKif13-1</i> ; Ascl; reverse; pHD1800- GFPmyc
Kif13.1 143SA for	5'-GGG AGG TTA AAC GGC GTA AAG <u>CCC</u> GCA TCG TGG-3'	<i>TbKif13-1 S143A</i> mutation within the motordomain; in order to prevent inhibitory phosphorylation of that serine; forward; pcDNA5, pcDNA3.1, pCS2-eGFP
Kif13.1 143SA rev	5'-CCA CGA TGC GGG <u>CTT</u> TAC GCC GTT TAA CCT CCC-3'	<i>TbKif13-1 S143A</i> mutation within the motordomain; in order to prevent inhibitory phosphorylation of that serine; reverse; pcDNA5, pcDNA3.1, pCS2-eGFP
Kif13-1 G371A for	5'-CTT TTA TTG ATC TCG CTG <u>CGA</u> GTG AGC GTG GG-3'	<i>TbKif13-1 G371A</i> mutation within one ATP binding motif in the motordomain; in order to prevent ATPase activity; forward; pTrc C FA
Kif13-1 G371A rev	5'-CCC ACG CTC ACT <u>CGC</u> AGC GAG ATC AAT AAA AG-3'	<i>TbKif13-1 G371A</i> mutation within one ATP binding motif in the motordomain; in order to prevent ATPase activity; reverse; pTrc C FA
Kif13-1 E373A for	5'-CGC TGG GAG TGC GCG TGG GGC GG-3'	<i>TbKif13-1 E373A</i> mutation within one ATP binding motif in the motordomain; in order to prevent ATPase activity and maintain depolymerisation activity; forward; pTrc C FA
Kif13-1 E373A rev	5'-CCG CCC CAC GCG CAC TCC CAG CG-3'	<i>TbKif13-1 E373A</i> mutation within one ATP binding motif in the motordomain; in order to prevent ATPase activity and maintain depolymerisation activity; reverse; pTrc C FA

Table 9: DNA oligonucleotides for *TbAuk1* constructs.

oligonucleotide	sequence 5'->3'	purpose
pET-Auk1-forFseI	5'-ATA <u>G</u> G <u>C</u> <u>C</u> G <u>G</u> <u>C</u> C <u>G</u> AGG TCA ACT GAG GTC GGG CGT-3'	<i>TbAuk1</i> N-terminus, without startcodon; starts at 4 th base of <i>TbAuk1</i> ; FseI; forward; pHD1801
pET-Auk1-revAscl	5'- <u>G</u> G <u>C</u> <u>G</u> C <u>G</u> <u>C</u> C <u>T</u> TAA TTC TCT TTC CCT GCA GTT GGC-3' TC	<i>TbAuk1</i> C-terminus, with stopcodon; ends at 927 nd base of <i>TbAuk1</i> ; Ascl; reverse; pHD1801
<i>TbAuk</i> K58R for	5'-GCA ATT TTG TTT GCG CGC TGA <u>G</u> AA GGT TGT CCA TTA AAA AAC T-3'	<i>TbAuk1</i> K58R mutation; kinase-dead mutant; forward; pHD1801
<i>TbAuk</i> K58R rev	5'-AGT TTT TTA ATG GAC AAC CTT <u>C</u> TC AGC GCG CAA ACA AAA TTG C-3'	<i>TbAuk1</i> K58R mutation; kinase-dead mutant; reverse; pHD1801
<i>TbAuk</i> T184A for	5'-ACC GTC GCA AG <u>G</u> CAT CTT GCG GGA CG- 3'	<i>TbAuk1</i> T184A mutation; kinase-dead mutant; forward; pHD1801
<i>TbAuk</i> T184A rev	5'- CGT CCC GCA AGA TG <u>C</u> CTT GCG ACG GT- 3'	<i>TbAuk1</i> T184A mutation; kinase-dead mutant; forward; pHD1801

4.1.5. Plasmids

The multiple cloning sites (MCS) of all used vectors were provided with unique *FseI* and *Ascl* sites for easier and more rapid subcloning. Sequencing of PCR product inserts was done by Macrogen (Macrogen Europe, Amsterdam, the Netherlands) according to their instructions. The following vectors and plasmids were used during this study (Table 10 and 11).

Table 10: Vectors.

vector	tag	description and origin
pTrc C FA	N-His ₆	inducible expression vector in <i>E. coli</i> ; <i>trc</i> promoter; ampicillin resistance; Thermo Scientific (Schwerte); modified by Bianca Kakoschky, Molecular Parasitology, University of Bayreuth
pHD1800 ^{GFP-myc}	GFP-myc-C	inducible expression vector in <i>T. brucei</i> ; <i>procyclin</i> promoter; ampicillin and hygromycin resistance; origin pHD1700, Dr. Voncken, University of Hull; modified in this study
pHD1800	myc-C	inducible expression vector in <i>T. brucei</i> ; <i>procyclin</i> promoter; ampicillin and hygromycin resistance; origin pHD 1700, Dr. Voncken, University of Hull; modified in this study
pHD1801	N-myc	inducible expression vector in <i>T. brucei</i> ; <i>procyclin</i> promoter; ampicillin and hygromycin resistance; origin pHD1701, Dr. Voncken, University of Hull; modified in this study
pCS2-eGFP	N-eGFP	constitutive expression vector in mammalian cells; <i>simian cytomegalovirus (CMV) IE94</i> enhancer/promoter; ampicillin and hygromycin resistance; Turner and Weintraub (1994); modified by department of Genetics, University of Bayreuth
pcDNA TM 5/FRT/TO-eGFP-FA	N-eGFP	inducible expression vector for the 'Flp-In TM T-REx TM System' (Invitrogen); hybrid <i>human CMV/TetO₂</i> enhancer/promoter; contains FLP recombination site (<i>FRT</i>) for Flp recombinase-mediated integration into the genome; ampicillin and hygromycin resistance; Invitrogen via Thermo Scientific (Schwerte); modified by department of Genetics, University of Bayreuth
pcDNA TM 3.1-eGFP-FA	N-eGFP	inducible expression vector in mammalian cells, hybrid <i>human CMV/TetO₂</i> enhancer/promoter, ampicillin and neomycin resistance; Invitrogen via Thermo Scientific (Schwerte); modified by department of Genetics, University of Bayreuth and in this study

Table 11: Plasmids.

plasmid	insert	tag	vector	origin
pTrc-TbKif13-1 FL	TbKif13-1 FL	N-His ₆	pTrc C FA	this study
pTrc-TbKif13-1 ½ N + C	TbKif13-1 ½ N + C	N-His ₆	pTrc C FA	this study
pTrc-TbKif13-1 NM + C	TbKif13-1 NM + C	N-His ₆	pTrc C FA	this study
pTrc-TbKif13-1 NM	TbKif13-1 NM	N-His ₆	pTrc C FA	this study
pTrc-TbKif13-1 N + M	TbKif13-1 N + M	N-His ₆	pTrc C FA	this study
pTrc-TbKif13-1 ½ N + M	TbKif13-1 ½ N + M	N-His ₆	pTrc C FA	this study
pTrc-TbKif13-1 N + D-box	TbKif13-1 N + D-box	N-His ₆	pTrc C FA	this study
pTrc-TbKif13-1 ½ N + D-box	TbKif13-1 ½ N + D-box	N-His ₆	pTrc C FA	this study
pTrc-TbKif13-1 FL G371A	TbKif13-1 FL G371A	N-His ₆	pTrc C FA	this study
pTrc-TbKif13-1 FL E373A	TbKif13-1 FL E373A	N-His ₆	pTrc C FA	this study
pHD1800-GFPmyc	GFP	myc-C	pHD1800	this study
pHD1800-TbKif13-1 N ^{GFP-myc}	TbKif13-1 N	GFP-myc-C	pHD1800 ^{GFP} -myc	this study
pHD1800-TbKif13-1 ½ N ^{GFP-myc}	TbKif13-1 ½ N	GFP-myc-C	pHD1800 ^{GFP} -myc	this study
pHD1801-TbKif13-1 FL	TbKif13-1 FL	N-myc	pHD1801	this study
pHD1801-TbKif13-1 ½ N + C	TbKif13-1 ½ N + C	N-myc	pHD1801	this study
pHD1801-TbKif13-1 NM + C	TbKif13-1 NM + C	N-myc	pHD1801	this study
pHD1801-TbKif13-1 NM	TbKif13-1 NM	N-myc	pHD1801	this study
pHD1801-TbKif13-1 N + M	TbKif13-1 N + M	N-myc	pHD1801	this study
pHD1801-TbKif13-1 ½ N + M	TbKif13-1 ½ N + M	N-myc	pHD1801	this study
pHD1801-TbKif13-1 C	TbKif13-1 C	N-myc	pHD1801	this study
pHD1801-TbAuk1	TbAuk1	N-myc	pHD1801	this study
pHD1801-TbAuk1 K58R	TbAuk1 K58R	N-myc	pHD1801	this study
pHD1801-TbAuk1 T184A	TbAuk1 T184A	N-myc	pHD1801	this study
pQE60-TbHistoneH3	TbHistoneH3	His ₆ -C	pQE60	Larry Ruben, Southern Methodist University, Dallas, USA
pCS2-eGFP-TbKif13-1 FL S143A	TbKif13-1 FL S143A	N-eGFP	pCS2-eGFP	this study
pcDNA5/FRT/TO-eGFP TM TbKif13-1 S143A	TbKif13-1 FL S143A	N-eGFP	pcDNA5-FRT-TO-eGFP	this study
pcDNA TM 3.1-eGFP TM TbKif13-1 S143A	TbKif13-1 FL S143A	N-eGFP	pcDNA TM 3.1-eGFP	this study
pAG1786	Flp-recominase	-	pCS2	Genetics, University of Bayreuth

4.2. Microbiological techniques

4.2.1. *E. coli* strains and media

E. coli strains for molecular cloning or recombinant protein expression were used as follows (Table 12).

Table 12: *E. coli* strains.

<i>E. coli</i> strain	genotype	purpose
XL1-blue	<i>endA1 gyrA96(nal^R) thi-1 recA1 relA1 lac glnV44 F' [::Tn10 proAB⁺ lacI^q Δ(lacZ)M15] hsdR17(r_K⁻ m_K⁺)</i>	molecular cloning
BL21	<i>F⁻ ompT gal dcm lon hsdS_B(r_B⁻ m_B⁻) λ(DE3 [lacI lacUV5-T7 gene 1 ind1 sam7 nin5])</i>	recombinant protein expression

E. coli cells were grown in LB-media or on LB-agar plates.

LB medium

1% (w/v) tryptone

0.5% (w/v) yeast extract

0.5% (w/v) NaCl

LB-agar

LB medium + 1.5% (w/v) agar

4.2.2. Cultivation of *E. coli*

E. coli strains were grown in LB media at 37°C or 18°C (protein expression) by shaking at about 130 rpm. LB-agar plates were incubated at 37°C. Selection of transformed bacteria was done with 100 µg/mL ampicillin in LB medium/-agar. Cell culture density was measured via absorbance at a wavelength of 600 nm (OD₆₀₀; BioPhotometer, Eppendorf, Hamburg). Cultures on LB-agar plates were stored at 4°C for up to 30 days.

4.2.3. Transformation of plasmid DNA into chemical competent *E. coli*

Frozen, chemical competent *E. coli* strains were thawed on ice. For transformation, 300 ng of plasmid DNA or 3 µL of ligation product were mixed with 200 µL of cells and incubated on ice for 30 min. A heat shock occurred at 42°C for 45 sec. Subsequently 1 mL of LB medium without antibiotics was added and cells recovered from that treatment for 1 h at 37°C with shaking. For liquid cultures, these cells were subsequently put to 20-50 mL of LB with antibiotics and grown by shaking at 37°C over night. For cultivation on plates, 100 µL, 10 µL and the resuspended bacterial pellet (13.200 rpm, 1 min; 5415 D, rotor F45-24-11, Eppendorf, Hamburg) were plated on LB-agar plates with antibiotics and grown at 37°C over night.

4.2.4. Recombinant protein expression in *E. coli*

After transformation of the desired plasmid into *E. coli* BL21, 1.5 L of LB were inoculated with 15 mL of the over night culture (see 4.2.3.) and grown at 37°C with shaking. At OD₆₀₀ 0.4 - 0.6 (BioPhotometer, Eppendorf, Hamburg) selection with 100 µg/mL ampicillin and induction with 0.1 mM IPTG were started. Cells were grown for 16 h at 18°C with shaking for receiving overexpressed soluble protein, while for overexpressed protein in inclusion bodies cells were grown for 12 h at 30°C with shaking. Cultures were harvested at 5.500 rpm for 15 min (Avanti J-26 XP Centrifuge, rotor JA 10, Beckman Coulter, Krefeld).

4.3. Molecular biological methods

Centrifugation within molecular biological methods occurred within a bench-top centrifuge (5415 D, rotor F45-24-11, Eppendorf, Hamburg).

4.3.1. Isolation of plasmid DNA from *E. coli* XL1-blue

GTE buffer	Lysis buffer	TE
50 mM glucose	0.2 N NaOH	10 mM Tris-HCl, pH 7.4
25 mM Tris-HCl, pH 8.0	1% (v/v) SDS	1 mM EDTA
10 mM EDTA, pH 8.0		
100 µg/mL boiled RNase		

For identification of a positive colony, containing the right plasmid after ligation (see 4.3.9.), XL1-blue single colonies were picked from LB-agar plates and grown in 3 mL LB with 100 µg/mL ampicillin over night at 37°C with shaking. After harvesting cells (13.200 rpm, 1 min), plasmid DNA was isolated via alkaline lysis. Cell pellets were resuspended in 150 µL ice-cold GTE buffer by mixing properly and subsequently lysed with 200 µL lysis buffer on ice for 5 min. 150 µL of 3 M KAc (pH 4.8) precipitated high molecular *E. coli* DNA within 5 min on ice. Chromosomal *E. coli* DNA was pelleted via centrifugation at 13.200 rpm for 5 min. Plasmid DNA remaining in the supernatant was precipitated by addition of 900 µL 100% (v/v) ethanol and pelleted by centrifugation at 13.200 rpm for 15 min. Plasmid DNA was washed with 200 µL 70% (v/v) ethanol, centrifuged at 13.200 rpm for 5 min, dried at RT for 10 min and finally dissolved in 50 µL TE.

In order to receive plasmid DNA for sequencing, purification took place with the 'GeneJET Plasmid Miniprep Kit' (Thermo Scientific, Schwerte) according to manufacturer's instruction.

Material and methods

Higher concentrations of plasmid DNA were received by harvesting a 50 mL LB ampicillin (100 µg/mL) culture of the desired clone. Purification was done with the 'Qiagen Plasmid Plus Midi Kit' (Qiagen, Hilden) according to manufacturer's instruction.

4.3.2. Determination of DNA concentration

DNA concentration was determined by measuring the absorbance at a wavelength of 260 nm (OD₂₆₀) with a 'ND-1000 Spectrophotometer' (Peglab, Erlangen). An OD₂₆₀ 1 equates 50 µg/mL DNA.

4.3.3. Restriction hydrolysis of DNA

Site-specific endonucleases were received from Fermentas (St. Leon-Rot) or NEB (Frankfurt a. M.) and used according to manufacturer's instruction. 1 - 3 µg of DNA were hydrolysed with 1 - 10 units of restriction enzymes for 2 h at 37°C. For DNA hydrolysis with two endonucleases not suitable within the same buffer conditions, a sequential restriction was applied with a change of buffers using 'NucleoSpin® Gel and PCR Clean-up' (Macherey-Nagel, Düren) according to manufacturer's instructions. Restriction hydrolysis was stopped by addition of loading dye. DNA hydrolysed for molecular cloning was separated on an agarose gel and subsequently purified (see 4.3.7. and 4.3.8.) in order to receive pure DNA fragments of desired weight.

4.3.4. Polymerase chain reaction

For amplification of specific DNA fragments or genes out of genomic *T. brucei* DNA (strain 449) or plasmids, polymerase chain reaction (PCR) was applied. Therefore 0.6 units 'Phusion High-Fidelity DNA Polymerase' (Fermentas, St. Leon-Rot) within a 50 µL approach were used. 0.2 µM (each) specific DNA oligonucleotides flanking the DNA region of interest (see 4.1.4.), 0.4 mM (each) deoxynucleotides (dNTPs, NEB, Frankfurt a. M.), 250 ng template DNA and supplied buffer (Fermentas, St. Leon-Rot) were added.

PCR was performed in 'MyCycler™ Thermocycler' (BioRad, Hercules, CA, USA). In general, the initial and first denaturation step during each cycle at 98°C leads to single stranded DNA, to which in the following annealing step single stranded DNA oligonucleotides can bind at complementary sites. This step is done 5 - 10°C underneath the melting temperature of the DNA oligonucleotides. During elongation within each cycle and the final elongation step, DNA is polymerised by integrating dNTPs. This takes place at a temperature specific for the

Material and methods

used polymerase. 'Phusion High Fidelity Polymerase' works best at 72°C, at which it elongates 1 kb within 15 - 30 sec. PCR products were analysed on an agarose gel and purified using 'NucleoSpin® Gel and PCR Clean-up' (Macherey-Nagel, Düren) according to manufacturer's instructions.

4.3.5. Mutagenesis of multiple cloning sites in plasmid DNA

Mutagenesis of multiple cloning sites in vector DNA was used to insert additional restriction sites. DNA oligonucleotides were created containing sticky overhangs according to the respective endonuclease restriction sites at the 5' and 3' ends, via which they were ligated into the appropriate hydrolysed vector (see 4.1.4. and 4.3.3.). To this end, DNA oligonucleotides were phosphorylated at 5', which is essential for subsequent ligation. For phosphorylation, 4 µM oligonucleotide were mixed with 1 mM dATP, 1x 'T4 Polynucleotide Kinase buffer' and 15 units 'T4 Polynucleotide Kinase' (NEB, Frankfurt a. M.) within 25 µL and incubated at 37°C for 30 min. Phosphorylated oligonucleotides were unified and kept for their hybridisation in a thermocycler (Techne, TC-512, Bibby Scientific Limited, Stone, UK) for 5 min at 98°C, slowly cooled down to 65°C and held for 10 min at 65°C. The phosphorylated, hybridised oligonucleotides were diluted 1:20 and 1:100 in de-ionized sterile water and 1 µL of each was ligated with the desired endonuclease hydrolysed and dephosphorylated vector of choice. 5' dephosphorylation of linearised vectors is necessary to inhibit religation. 1 µg vector was dephosphorylated by 5 units 'Antarctic Phosphatase' (NEB, Frankfurt a. M) within 1 h at 37°C.

4.3.6. Site-specific mutagenesis of plasmid DNA

In order to introduce site-specific point mutations into plasmid DNA the 'QuikChange Lightning Site-Directed Mutagenesis Kit' (Agilent Technologies, Santa Clara, CA, USA) was used according to manufacturer's instructions. The underlying principle is a PCR based amplification of the whole plasmid, whereby complementary oligonucleotides contain the desired basepair exchange (see 4.1.4.). Elongation is provided by the 'QuickChange Lightning enzyme', which is a blend containing a derivative of 'PfuUltra high fidelity DNA polymerase'. After temperature cycling, *DpnI* was added. This endonuclease (target sequence 5'-Gm⁶ATC-3') specifically hydrolyses methylated and hemimethylated DNA. As DNA isolated from almost all *E. coli* strains is methylated, template DNA will be hydrolysed. The newly synthesised

Material and methods

mutagenetic plasmid DNA was afterwards transformed into *E. coli* cells. In this study, *E. coli* XL1-blue cells were used, differing from manufacturer's instruction.

4.3.7. Separation of DNA fragments by agarose gelelectrophoresis

1x TAE	6x Loading dye
0.04 M Tris	0.09% (w/v) bromphenol blue
0.1142% (v/v) acetic acid	0.09% (w/v) xylene cyanol FF
1.3 mM EDTA	60% (v/v) glycerol
pH 8.5 with acetic acid	60 mM EDTA

For analytical and preparative reasons, DNA was mixed with loading dye (to 1x) and loaded onto agarose gels (1- 2% agarose (SeaKem® LE agarose, Lonza, Rockland, ME, USA) in 1x TAE). Gels were run at 80 - 100 V in 1x TAE in an electrophoresis chamber ('HU6 Mini Horizontal', Scie-Plas Limited, Cambridge, UK) and subsequently stained in an ethidium bromide (0.5 µg/mL) 1x TAE bath for 10 min. Gels were analysed with an UV transilluminator ('GenoSmart Compact Imaging System', VWR, Darmstadt). DNA size was estimated according to the self-made DNA ladder, received by *EcoRI*-restriction hydrolysed *SPP1* bacteriophage DNA (Karin Angermann, Molecular Parasitology, University of Bayreuth).

4.3.8. Isolation of DNA from agarose gels

For isolation of DNA from agarose gels, staining did not occur with ethidium bromide, but with 'SYBR Safe® DNA gel stain' (Invitrogen via Thermo Scientific, Schwerte) in 1x TAE according to manufacturer's instruction. 'SYBR Safe®' is less mutagenetic than ethidium bromide and mutagenesis by UV light is circumvented because DNA is made visible with an excitation maximum of 502 nm and an emission maximum of 530 nm. A 'dark reader blue' transilluminator (Clare Chemical Research, Dolores, CO, USA) was used. DNA was cut from gels with 'X-tracta II' (Biozym Scientific, Hessisch Oldendorf). For purification of DNA from agarose gels, 'NucleoSpin® Gel and PCR Clean-up' (Macherey-Nagel, Düren) was applied according to manufacturer's instruction.

4.3.9. Ligation

Ligation serves for insertion of endonuclease hydrolysed DNA fragments, received from PCR or plasmids, into other linearised vectors or plasmids. A molar ratio vector to fragment of 1:6 was used, which was estimated on an agarose gel. For ligation 5 units 'T4 DNA ligase'

Material and methods

(Fermentas, St. Leon-Rot), supplied 1x 'T4 DNA ligase buffer', linearised vector and hydrolysed fragment were combined within 10 µL for 2 h at RT or over night at 18°C.

4.3.10. Linearisation of plasmid DNA for transformation of *T. brucei*

For homologous recombination of plasmid DNA with genomic *T. brucei* DNA, plasmid DNA had to be linearised. A unique *NotI* endonuclease cutting site within the plasmid's rRNA locus, that is homologous to the rRNA locus within the genomic DNA, was used for linearisation. Therefore 30 ng plasmid DNA, 20 units endonuclease and supplied buffer (1x) were mixed within a total of 40 µL and hydrolysis occurred for 16 h at 37°C. The linearised plasmid DNA was precipitated with 2 vol 100% (v/v) ice-cold ethanol and 1/10 vol 3 M sodium acetate. After 10 min of centrifugation at 13.200 rpm, DNA was washed with 70% (v/v) ethanol and centrifuged again for 5 min at 13.200 rpm. The pellet was dried underneath a laminar flow (ScanLaf, Mars Safety Class, LaboGene, Lynge, DK) before being resuspended in 75 µL de-ionized sterile water. 2 µL were analysed for linearisation on an agarose gel.

4.4. Protein biochemical methods

4.4.1. Denaturing sodium dodecyl sulfate polyacrylamide gelelectrophoresis (SDS-PAGE)

2x Laemmli	1x SDS-PAGE buffer
125 mM Tris-HCl pH 6.8	25 mM Tris
5% (v/v) glycerol	0,2 M glycine
4% (v/v) SDS	0,001% (v/v) SDS
5% (v/v) β-mercaptoethanol	
some crystals of bromphenol blue	

Material and methods

10% Polyacrylamid gel

30% (w/v) acrylamide-bisacrylamid solution, 37.5:1 (Serva, Heidelberg) was used for all polyacrylamid gels.

Resolving gel (30 mL)

10 mL 30% (w/v) acrylamide-bisacrylamid
7.5 mL 1.5 M Tris-HCl (pH 8.8)
0.3 mL 10% (w/v) SDS
12 mL ddH₂O
15 µL TEMED
0.15 mL 10% (w/v) APS

Stacking gel (14.65 mL)

2 mL 30% (w/v) acrylamide-bisacrylamid
3.25 mL 0.5 M Tris-HCl (pH 6.8)
0.15 mL 10% (w/v) SDS
9.15 mL ddH₂O
15 µL TEMED
75 µL 10% (w/v) APS

Gradient gel 8% - 17%

8% solution (28 mL)

7 mL 30% (w/v) acrylamide-bisacrylamid
7 mL 1.5 M Tris-HCl (pH 8.8)
32 µL 10% (w/v) SDS
13.4 mL ddH₂O
11.2 µL TEMED
0.128 mL 10% (w/v) APS

17% solution (30 mL)

17 mL 30% (w/v) acrylamide-bisacrylamid
7.5 mL 1.5 M Tris-HCl (pH 8.8)
1.6 mL 2.5 M sucrose
32 µL 10% (w/v) SDS
3.7 mL ddH₂O
8.8 µL TEMED
0.128 mL 10% (w/v) APS

Stacking gel (39 ml):

9.12 mL 30% (w/v) acrylamide-bisacrylamid
4.92 mL 1 M Tris-HCl (pH 6.8)
48 µL 10% (w/v) SDS
24.7 mL ddH₂O
12 µL TEMED
0.192 mL 10% (w/v) APS

For separating proteins under denaturing conditions, a discontinuous SDS-PAGE was performed (Laemmli, 1970). This method separates proteins depending on their molecular mass and independent of their initial charge within an electric field. As protein samples are mixed with hot Laemmli (to 1x) and boiled at 99°C for 10 min, proteins are negatively

Material and methods

charged by SDS and are unfolded upon, whereas β -mercaptoethanol reduces their disulfide bridges.

For proteins with a molecular mass <30 kDa 8 - 17% gradient gels and for proteins >30 kDa 10% polyacrylamid gels were used. As molecular weight ladder 'PageRuler Prestianed Protein Ladder' (Fermentas, St. Leon-Rot) was used.

After loading of samples onto the stacking gel, they were run with 80 V until reaching the resolving gel, where it was turned to 130 V. 1x SDS-PAGE buffer was used as running buffer.

4.4.2. Methanol-chloroform precipitation of protein samples

Protein samples for SDS-PAGE analysis containing GuaHCl or urea were methanol-chloroform precipitated. 4 volumes methanol (100% (v/v)) and 1 volume chloroform (100% (v/v)) were added to the sample and mixed properly. 3 volumes of ddH₂O were added and the sample mixed. Centrifugation was done at 12.300 rpm for 5 min (5415 D, rotor F45-24-11, Eppendorf, Hamburg). The protein precipitate forms at the interphase of a bottom layer with chloroform, containing lipids and a top aqueous layer, containing detergens etc. After removal of the aqueous phase, 3 volumes methanol (100% (v/v)) were added, the sample mixed and centrifuged at 12.300 rpm for 5 min (5415 D, rotor F45-24-11, Eppendorf, Hamburg). Methanol was removed completely and the pellets dried for 10 min at RT before being boiled for 10 min at 99°C with Laemmli (to 1x).

4.4.3. Determination of protein concentration in solution

In order to determine protein concentrations, a defined volume of the protein of interest in Laemmli (to 1x) was loaded onto an SDS-PAGE next to lanes where 1 μ g, 0.5 μ g and 0.25 μ g BSA in Laemmli (to 1x) were loaded. After coomassie staining and destaining (see 4.4.5.) bands were compared to each other.

In addition, recombinantly purified protein concentrations were measured via a Bradford assay (BioRad, Munich) according to manufacturer's instruction. This colorimetric assay is based on the binding of a Coomassie Brilliant Blue G-250 solution dye to protein, which causes a shift in the absorption maximum of the dye from 465 nm to 595 nm (Bradford, 1976). It measures total protein concentrations. A photometer (BioPhotometer, Eppendorf, Hamburg) was used.

4.4.4. Westernblot (Immunoblot)

1x Blotting buffer	1x PBS	1x PBS-T
25 mM Tris	0.14 M NaCl	1x PBS
0.2 M glycine	2.7 mM KCl	0.1% (v/v) Tween-20
10% (v/v) methanol	8.5 mM Na ₂ HPO ₄ x 2H ₂ O	
	pH 7.4	
 Blocking buffer	 Ponceau S solution	 Stripping buffer
5% milk powder in PBS-T	3.3 mM ponceau S	0.1 M NaOH
(Magermilchpulver, Sucofin,	40% (v/v) methanol	2% (w/v) SDS
TSI, Zeven)	15% (v/v) acetic acid	0.5% (w/v) DTT

For immunoblotting, proteins separated by SDS-PAGE, were transferred to a polyvinylidene difluoride (PVDF) membrane (Serva, Heidelberg). Prior to use, PVDF membranes are activated using 100% (v/v) methanol for 20 min and equilibrated in 1x blotting buffer. The activation step ensures that the membrane exposes its full protein binding capacity when aqueous buffers are used for immunoblotting.

The electrophoretic transfer of the SDS gel-bound proteins to the membrane occurred via wet blotting within a 'Mini Trans-Blot® cell' (BioRad, Munich). Transfer occurred at 250 mA for 2 h while the blotting chamber was cooled by a surrounding ice box.

The membrane was stained for a few seconds with Ponceau S solution to visualise blotted proteins as loading control. Non specific binding sites were blocked with blocking buffer twice for 15 min. Incubation with the primary and the secondary antibody, diluted in blocking buffer, occurred for 1 h at RT. After each antibody treatment, the membrane was washed three times for 10 min in PBS-T. The membrane was stored in PBS until detection.

Detection was done with 'HRP-juice' (PJK, Kleinblittersdorf) or 'Lumigen ECL Ultra' (Lumigen, Southfield, MI, USA), both of which are chemiluminescent systems detecting horseradish peroxidase. Visualisation was done with the 'LAS-4000' detection system (Fujifilm Europe, Düsseldorf).

In order to strip the PVDF membrane for a second time of primary antibody binding, it was incubated with stripping buffer for 1 h at 55°C under rotation. Stringent washing three times with 1x PBS-T for 10 min followed before primary antibody was admitted as described above.

4.4.5. Coomassie staining and destaining

Staining solution

3 mM Coomassie Brilliant Blue R 250
45.4% (v/v) methanol
0.92% (v/v) acetic acid

Destain solution

35% (v/v) methanol
5% (v/v) acetic acid

In order to stain proteins after SDS-PAGE on the gel, it was put into Coomassie staining solution for 20 min with soft shaking. Afterwards it was destained until clear bands were seen.

4.4.6. Silver staining

Fix solution

50% (v/v) methanol
12% (v/v) acetic acid
0.05% (v/v) formaldehyde (fresh)

Stain solution

11.8 mM AgNO₃
0.076% (v/v) formaldehyde (fresh)
on ice

Developing solution

0.57 mM Na₂CO₃
0.05% (v/v) formaldehyde (fresh)
0.025 mM Na₂S₂O₃

Stop solution

50% (v/v) methanol
12% (v/v) acetic acid

Silver staining of proteins separated by SDS-PAGE facilitates a more sensitive detection of proteins than Coomassie staining.

After SDS-PAGE, gels were fixed for 2 h or over night in fix solution before they were washed three times for 20 min with 35% (v/v) ethanol. Alternatively, Coomassie stained and destained SDS gels (see 4.4.5.) were washed extensively with ddH₂O. Subsequently, gels were sensitised for 2 min with 1.26 mM Na₂S₂O₃ and washed three times for 5 min with ddH₂O. Staining occurred for 20 min with stain solution. Afterwards, gels were washed two times for 1 min with ddH₂O, developed with developing solution for as long as necessary and staining was stopped with stop solution for 5 min. Gels were stored in 1% (v/v) acetic acid.

4.4.7. Autoradiography

After SDS-PAGE, Coomassie staining and destaining, gels were washed with water for 10 min. Thereby proteins were fixed and unincorporated ³³P was washed out. Drying of gels on chromatography paper (Whatman™ 3 MM Chr, GE Healthcare, Little Chalfont, UK) was done

Material and methods

in a 'slab gel dryer' (GD2000, Hoefer, Holliston, MA, USA). Exposition to a film (BioMax MR, Kodak) lasted 4 h to 4 days, depending on the intensity of the expected signals. Digitisation occurred with a 'FLA-7000' phosphorimager (Fujifilm Europe, Düsseldorf).

4.4.8. Ni²⁺-NTA affinity purification of His₆ tagged proteins

His₆ tagged, recombinantly expressed proteins were purified, both under native and denaturing conditions, using 'HisPur™ Ni-NTA Superflow Agarose' (Thermo Scientific, Schwerte). Ni²⁺ is bound to the NTA matrix in a way that one or more of its coordination sites are available for interacting with alkaline amino acids like histidine.

4.4.8.1. Native conditions

Lysis and wash buffer	High salt buffer	Elution buffer
0.1 M PIPES, pH 6.9	0.1 M PIPES, pH 6.9	0.1 M PIPES, pH 6.9
0.1 M NaCl	0.5 M NaCl	0.1 M NaCl
1 mM MgCl ₂	1 mM MgCl ₂	1 mM MgCl ₂
10 mM imidazol	10 mM imidazol	0.25 M imidazol
pH 6.9	pH 6.9	pH 6.9
add before use:	add before use:	add before use:
1 mM ATP (lysis buffer)/	0.01 mM ATP	0.01 mM ATP
0.01 mM ATP (wash buffer)	1 mM β-mercaptoethanol	1 mM β-mercaptoethanol
1 mM β-mercaptoethanol	0.2 mM PMSF	0.2 mM PMSF
0.2 mM PMSF		

Due to native purification, all used buffers were ice-cold and purification occurred within a 4°C room. Harvested bacterial pellet (see 4.2.4.) was resuspended in 10 mL lysis buffer per g pellet. Cells were crushed for 20 min using a high pressure homogeniser ('EmulsiFlex-C5', Avestin, Ottawa, Canada). Soluble proteins were separated from non soluble cell material by centrifugation at 11.500 rpm at 4°C for 15 min (Avanti J-26 XP Centrifuge, rotor JA 25.50, Beckman Coulter, Krefeld) and subsequently incubated with 1 mL lysis buffer equilibrated 'HisPur™ Ni-NTA Superflow Agarose' resin for 30 min at 4°C under rotation. For purification, 'Econo-Pac® Chromatography Columns' (BioRad, Munich) were used. His₆ tagged proteins bound to Ni²⁺-NTA beads were washed with 10 bed volumes (bv) wash buffer, 10 bv high salt buffer to reduce non specific bound proteins and again with 10 bv wash buffer. Elution occurred with high concentration of imidazol, which competes with histidine for binding to

Material and methods

Ni²⁺. 2x 5 bv elution buffer were used and fractions of 0.5 mL were collected. Protein concentration within fractions was determined (see 4.4.3.) and those containing highest concentrations of protein were pooled. Aliquots with 50% (v/v) glycerol were snap frozen in liquid N₂ and stored at -80°C.

4.4.8.2. Denaturing conditions

Lysis buffer	Extraction buffer	Wash buffer B
50 mM HEPES, pH 6.9	100 mM sodium phosphate	100 mM sodium phosphate
100 mM NaCl	10 mM Tris	10 mM Tris
1 mM MgCl ₂	6 M GuaHCl	8 M urea
pH 6.9	pH 8.0	pH 8.0
add just before use:	add just before use:	add just before use:
1 mM PMSF	1 mM PMSF	1 mM PMSF
1 mM β-mercaptoethanol	1 mM β-mercaptoethanol	1 mM β-mercaptoethanol

Wash buffer C	Elution buffer
100 mM sodium phosphate	100 mM sodium phosphate
10 mM Tris	10 mM Tris
8 M urea	8 M urea
pH 6.3	pH 4.3
add just before use:	add just before use:
1 mM PMSF	1 mM PMSF
1 mM β-mercaptoethanol	1 mM β-mercaptoethanol

Denaturing purification occurred at RT. Harvested bacterial pellet (see 4.2.4.) was resuspended in 10 mL lysis buffer per g pellet. Cells were crushed for 20 min using a high pressure homogeniser ('EmulsiFlex-C5', Avestin, Ottawa, Canada). Due to the relatively high density of inclusion bodies, they were pelleted with non soluble cell components by centrifugation at 11.500 rpm for 15 min (Avanti J-26 XP Centrifuge, rotor JA 25.50, Beckman Coulter, Krefeld). The pellet was resuspended in 10 mL extraction buffer per g pellet and kept under rotation for 2 h to solubilise proteins of the inclusion bodies. By subsequent centrifugation at 11.400 rpm for 30 min (Avanti J-26 XP Centrifuge, rotor JA 25.50, Beckman Coulter, Krefeld), remaining aggregates were removed. The supernatant was incubated with 0.5 mL extraction buffer equilibrated 'HisPur™ Ni-NTA Superflow Agarose' resin for 3 h at RT

Material and methods

under rotation. For purification, 'Poly-Prep® Chromatography Columns' (BioRad, Munich) were used. His₆ tagged proteins bound to Ni²⁺-NTA beads were washed with 10 bv wash buffer B and 10 bv wash buffer C. The decreased pH of wash buffer C reduces non specific bound proteins. Elution occurred with a decreased pH 4.3, which leads to a protonation of histidine and thus, to a weaker or no binding of the resin to Ni²⁺. 2x 5 bv elution buffer were used and fractions of 0.5 mL were collected. Protein fractions containing the desired protein were detected via Westernblot (see 4.4.4.) and those containing the highest concentrations of protein were pooled and dialysed against ddH₂O ('SnakeSkin® Dialysis Tubing', cut off 3.5 kDa, Thermo Scientific, Schwerte). Dialysate concentration was determined (see 4.4.3.). Aliquots were snap frozen in liquid N₂ and stored at -80°C.

4.4.9. Tubulin sedimentation assay

Polymerisation buffer (PME)

80 mM PIPES, pH 6.9

2 mM MgCl₂

0.5 mM EGTA

pH 6.9

Kinase buffer

20 mM HEPES, pH 7.4

150 mM KCl

5 mM MgCl₂

Microtubule depolymerisation activity of recombinantly purified His₆TbKif13-1 protein constructs was monitored using a tubulin sedimentation assay. Tubulin was isolated from pig brain according to the method of Borisy et al. (1975). The tubulin sedimentation assay was adopted from Desai and Walczak (2001).

1 mg tubulin was thawed on ice. For promotion of polymerisation 1 mM GTP and DTT were added. Gradually increasing concentrations of taxol – 0.1 µM, 1 µM for five min each and 10 µM for 15 min at 37°C - were added to stabilise microtubules. Following centrifugation at 84.000 rpm for 15 min at 30°C (Beckman Optima TL-100 Benchtop Ultracentrifuge, rotor TLA 100.1, tubes ref. 343776, Beckman Coulter, Krefeld), the pellet was resuspended in 2 mL 37°C prewarmed PME buffer containing 1 mM DTT, 1mM GTP and 10 µM taxol.

In order to test depolymerisation activity of the purified kinesin variants, PME buffer, 0.5 mM DTT, 1.5 mM ATP, 50 mM KCl, 8.25 µg taxol stabilised microtubules and varying concentrations of kinesin variants were combined within 50 µL. As control the same approaches were done without ATP. After incubation for 30 min at 37°C the depolymerisation solution was spun at 84.000 rpm for 10 min at 23°C (Beckman Optima TL-

Material and methods

100 Benchtop Ultracentrifuge, rotor TLA 100.1, tubes ref. 343776, Beckman Coulter, Krefeld). While the supernatant was boiled with Laemmli (to 1x), the pellet was dissolved in 50 μ L PME, 5 mM CaCl_2 , 50 mM KCl and kept on ice for ten minutes prior to that. Samples were analysed using SDS-PAGE (see 4.4.1.) and subsequent Coomassie staining (see 4.4.5.).

To test whether $^{\text{His6}}$ TbKif13-1 was inhibited by $^{\text{myc}}$ TbAuk1 and its kinase-dead mutant T184A, two slightly modified versions of the tubulin sedimentation assay were used. In one 10 μ L of protein G-sepharose bound kinase, 1 μ M $^{\text{His6}}$ TbKif13-1 and 1.5 mM ATP were pre-incubated in kinase buffer for 1 h at RT before all other depolymerisation activity testing components and 5 mM phosphatase inhibitor NaF were added for another 30 min at 37°C. The second approach unified all of these components without pre-incubation. After centrifugation (84.000 rpm for 10 min at 23°C; Beckman Optima TL-100 Benchtop Ultracentrifuge, rotor TLA 100.1, tubes ref. 343776, Beckman Coulter, Krefeld) and separation of pellet and supernatant, samples were boiled in Laemmli (to 1x) as described above.

4.4.10. Malachite green assay

Malachite green solution

1 part 4.2% (w/v) ammonium-molybdate in 4 M HCl

3 parts 0.045% (w/v) malachite green oxalate salt in ddH₂O

incubated over night at 4°C under rotation, filtered through 0.2 μ m filter (Sarstedt, Nürnbrecht), storage at 4°C, put to RT 1 h before use, keep dark

BRB80

80 mM PIPES, pH 6.8 with KOH

1 mM MgCl_2

1 mM EGTA, pH 6.8 with KOH

The malachite green assay is a phosphatase assay, extremely sensitive to phosphate, which is why no glass ware was used and plastic equipment was not autoclaved. The assay was done on med-binding 384-well plates (781096, Greiner bio one, Frickenhausen).

The malachite green assay is based on the complex formed between malachite green, ammonium-molybdate, and inorganic phosphate (P_i) under acidic conditions. Kinesin's activity depends on its ability to hydrolyse ATP within its motor domain. This releases P_i from ATP, which in turn forms a complex with ammonium-molybdate in a solution of perchloric

Material and methods

acid. The subsequent formation of the malachite green phosphomolybdate complex is measured at 650 nm. Accordingly, this complex is directly related to the P_i concentration. Thus, it is possible to quantify the ATPase activity of the recombinantly purified ^{His6}TbKif13-1 variants.

1 mg tubulin, isolated from pig brain (see 4.4.9.), was thawed on ice and centrifuged at 84.000 rpm for 15 min at 30°C (Beckman Optima TL-100 Benchtop Ultracentrifuge, rotor TLA 100.1, tubes ref. 343776, Beckman Coulter, Krefeld). The pellet was resuspended in BRB80. Its concentration was determined by denaturing 20 µL in 80 µL 6M GuaHCl and measuring its absorbance at A_{280} using a photometer (BioPhotometer, Eppendorf, Hamburg). Taking the tubulin extinction coefficient of 115.000, the layer thickness of the cuvette and the dilution into consideration, one can calculate the tubulin concentration via the Lambert-Beer law.

395 nM tubulin, varying concentrations of ^{His6}TbKif13-1 deletion constructs and 100 µM ATP were incubated in BRB80 (total volume 30 µL) for 18 min at RT. To stop kinesin's ATP hydrolysis, 60 µL of 1.2 M (0.8 M final) ice-cold perchloric acid were added and 30 µL of the mix were put to 40 µL of malachite green solution. The reaction lasted 20 min at RT. The absorbance at A_{650} was measured using the plate reader 'FLUOstar Omega' (BMG Labtech, Ortenberg).

4.4.11. Immunoprecipitation

Lysis buffer	Wash buffer	Kinase buffer
50 mM HEPES, pH 7.4	50 mM HEPES, pH 7.4	20 mM HEPES, pH 7.4
100 mM KCl	100 mM KCl	150 mM KCl
add just before use:	add just before use:	5 mM MgCl ₂
1% (v/v) NP40	1 mM DTT	add just before use:
1 mM DTT	1 mM PMSF	1 mM DTT
1 mM PMSF	1x protease inhibitor	1 mM PMSF
1x protease inhibitor		1x protease inhibitor

(cOmplete, EDTA-free, Roche, Basel, Switzerland)

Immunoprecipitation was done using *T. brucei* 449 cell lines, ectopically expressing myc^{TbAuk1} or its mutant variants. After ectopic expression for 16 h 1×10^9 cells were harvested by centrifugation at 3.000 rpm for 20 min (5702 R, rotor A-4-38, Eppendorf, Hamburg). Cell pellet was washed twice in 1x PBS. Lysis was done in 1 mL ice-cold lysis buffer

Material and methods

for 15 min on ice. To separate soluble from non soluble lysis compartments, the lysate was centrifuged at 10.400 rpm for 15 min at 4°C (Mikro 200R, rotor 2424, Hettich, Tuttlingen). The supernatant was pre-cleared with 40 µL resin of wash buffer equilibrated protein G-sepharose ('Protein G SepharoseTM 4 Fast Flow', GE Healthcare Bio-Sciences AB, Uppsala, Sweden) for 2 h at 4°C with rotation, in order to reduce non specific binding to the resin. The pre-cleared beads were removed by centrifugation at 500 rpm for 2 min at 4°C (Mikro 200R, rotor 2424, Hettich, Tuttlingen). 50 µg myc antibody were added and incubated with the pre-cleared lysate for 3.5 h at 4°C under rotation to allow binding of the myc-tagged protein of interest. Myc is recognised by the antibody's antigen binding site (paratope) consisting of three β -strand loops (complementary determining regions, CDRs) each on the light (V_L) and heavy (V_H) chains of the variable domains (F_V). 120 µL wash buffer equilibrated protein G-sepharose was subjoined and incubated over night at 4°C under rotation. The F_c region of IgGs binds with high affinity to three homologous binding domains within the C-terminus of matrix bound protein G. Protein G-sepharose was settled by centrifugation at 500 rpm for 2 min at 4°C (Mikro 200R, rotor 2424, Hettich, Tuttlingen) and subsequently washed twice with 10 bv ice-cold wash buffer. An equal volume of ice-cold kinase buffer was added to the protein G bound protein resin in preparation for its fresh use in further kinase assays.

4.4.12. ³³P kinase assays

The kinase assay for testing phosphorylation activity of ^{myc}*TbAuk1* or its kinase-dead mutants used 5 µCi ³³P γ ATP (10 µCi/µL, Hartmann Analytic, Braunschweig), 6.5 µL protein G-sepharose coupled kinase (see 4.4.11.), 1.5 µg *TbHistoneH3*^{His6} and 5 mM NaF to inhibit phosphatases, in a total of 10 µL within kinase buffer. Incubation occurred for 30 min at RT, afterwards samples were boiled for 10 min at 99°C with Laemmli (to 1x).

The kinase assay for testing the ability of ^{myc}*TbAuk1* or its kinase-dead mutants to phosphorylate recombinantly purified ^{His6}*TbKif13-1* was done similar to the tubulin sedimentation assay (see 4.4.9.). Taxol stabilised microtubules were obtained according to 4.4.9. All components of the microtubule sedimentation assay were used and 5 µCi ³³P γ ATP (10 µCi/µL, Hartmann Analytic, Braunschweig), 10 µL protein G-sepharose coupled kinase (see 4.4.11.), 0.75 µM ^{His6}*TbKif13-1* and 5 mM phosphatase inhibitor NaF were added and incubated for 30 min at RT. Samples were boiled for 10 min at 99°C with Laemmli (to 1x).

4.4.13. Immunfluorescence

Visualisation of immunfluorescence labelled samples occurred with an 'Axio Imager 2' (Zeiss, Oberkochen) microscope, a 100x oil objective (Plan-Apochromat 100x/1.40 Oil Ph3 M27, Zeiss, Oberkochen), a 'SPOT Pursuit' camera (SPOT ImagingTM, Sterling Heights, MI, USA) and 'VisiView®' software (Visitron Systems, Puchheim). Microscopic analysis of 384-well plates occurred with the microscope 'DMI 6000' equipped with a digital camera and 100x/0.4 oil objective ('HCX PL FUOTAR L'; Leica Microsystems, Wetzlar).

4.4.13.1. *T. brucei*

For immunostaining of specific cell structures in *T. brucei*, two different approaches were used. Whole cell microscopy samples were formaldehyd fixed. Preparation of cytoskeleton samples included extraction of *T. brucei* cells and subsequent methanol fixation.

Fixed samples on poly L lysine (0.1 mg/mL poly L lysine hydrobromide (Sigma-Aldrich, Steinheim) in ddH₂O) coated slides (Thermo Scientific Gerhard Menzel, Braunschweig) were incubated with primary and afterwards secondary antibody, diluted in 1x PBS-T (see 4.1.3.). Staining occurred for 1 h at RT within a wet chamber. After each antibody incubation, washing of the slide coated samples was done three times for 5 min at RT within coplin jars using 1x PBS-T Tween-20 within PBS-T is a detergent, reducing non specific antibody binding. To remove salts from the samples, washing with ddH₂O occurred in a final step. DNA was stained with DAPI, which is already contained within the applied 5 µL mounting medium ('Vectashield mounting medium with DAPI', Vector Laboratories, Burlingame, CA, USA). Cover slips (Marienfeld-Superior, Lauda-Königshafen) were fixed with nail polish.

All centrifugation steps occurred at 1.600 rpm for 5 min in a bench-top centrifuge (5415 D, rotor F45-24-11, Eppendorf, Hamburg).

Whole cell samples

For whole cell samples 15×10^6 cells were washed twice with PBS. Fixation was done within 1 mL 3.7% (v/v) formaldehyde (diluted in 1x PBS) for 20 min under rotation at 5 rpm ('Intelli-Mixer', Elmi laboratory equipment, Riga, Latvia). Formaldehyde cross-links proteins. Pellets were resuspended in 1x PBS, settled on poly L lysine coated slides for 10 min and washed in 1x PBS. In order to keep *T. brucei* cells within a certain area on the slides, surrounding squares were drawn with the 'ImmEdge Hydrophobic Barrier Pen' (Vector Laboratories, Burlingame, CA, USA). To permeabilise formaldehyde fixed cells for antibodies, they were

Material and methods

treated with 0.1% (v/v) Triton-X100 in 1x PBS for 3 min at RT. Samples were washed with 1x PBS before antibody treatment.

Cytoskeleton samples

PEME buffer

0.1 M PIPES

2 mM EGTA

1 mM MgSO₄

0.1 mM EDTA

pH 6.9

5x 10⁶ cells were washed twice with PEME, settled on poly L lysine coated slides for 10 min at RT and washed with PEME. To receive cytoskeleton samples, cells were extracted with 1% (v/v) NP40 in PEME for 5 min on ice. Slides were washed with PEME before cells were fixed with 100% (v/v) ice-cold methanol within a coplin jar for at least 15 min at -20°C. Methanol is a precipitative fixative, reducing the solubility of proteins and disrupting hydrophobic interactions within them. Cells were rehydrated by 1x PBS for 5 min. Staining with antibodies followed as described above.

Spindle staining with KMX

To stain spindles of mitotic *T. brucei* cells using KMX antibody, samples were treated like whole cell samples (see above). But it was necessary to use a fresh stock of formaldehyde for fixation. Permeabilisation occurred with 0.1% (v/v) NP40 for 5 min at RT. Dilution of antibodies and washing steps were done in 1x PBS.

4.4.13.2. Mammalian cells

Cover slips (ø12 mm, Marienfeld-Superior, Lauda-Königshofen), whereon HeLa cells had settled, were washed in 1x PBS for 5 min and fixed in 100% (v/v) ice-cold methanol for at least 15 min at -20°C in six-well plates (Cellstar®, Greiner bio one, Frickenhausen). Cells were rehydrated in 1x PBS for 5 min at RT. They were placed on top of a 'Parafilm' (Sigma-Aldrich, Steinheim) covered glass plate within a wet chamber. For staining with primary and secondary antibody, diluted in PBS-T (see 4.1.3.), they were put upside-down to reduce the required antibody volume. Washing of the cover slips occurred three times with 1 mL 1x PBS-T, which was slowly run over them. DNA was stained with DAPI, being part of the 5 µL

Material and methods

mounting medium ('Vectashield mounting medium with DAPI', Vector Laboratories, Burlingame, CA, USA) used to put cover slips upside-down onto slides (Thermo Scientific Gerhard Menzel, Braunschweig). Nail polish sealed cover slips at slides.

4.4.13.3. Microscopic enumeration of *T. brucei* cells

Several enumerations of *T. brucei* cells occurred via microscopy. When necessary, specific subcellular proteins were stained for immunofluorescence before.

To study cell cycle specific expression of ectopically expressed ^{myc}TbKif13-1 deletion constructs in *T. brucei*, for each cell cycle stage 100 cells were counted after 16 h of ectopic expression for expression or no expression.

To verify *T. brucei* flow cytometry analysis results, 100 cells in total were counted for the given timepoints and their respective cell cycle stages were reported.

For checking the assembly of a mitotic spindle in mitotic 2K1N cells after ectopic expression of the different ^{myc}TbKif13-1 deletion constructs in *T. brucei*, 100 mitotic cells were counted at each timepoint for spindle formation.

4.4.14. *In vitro* degradation of *T. brucei* cytoskeletons

For *in vitro* degradation of *T. brucei* cytoskeletons strain 427 was used. Samples were prepared as described for cytoskeleton samples (see 4.4.13.1.). After extraction and subsequent PEME and ddH₂O wash, varying concentrations of recombinantly purified ^{His6}TbKif13-1 deletion constructs, 1.5 mM ATP and polymerisation buffer were put on top of the slide-bound cytoskeletons within a total of 80 µL per square. Incubation occurred within a wet chamber at 37°C for 30 min. Fixation and antibody staining was done as described above (see 4.4.13.1.).

For the *in vitro* high-throughput inhibitor screen, PEME washed *T. brucei* cells (strain 427) were extracted with 0.5% (v/v) NP40 in PEME in an incubation tube on ice for 5 min. Cytoskeletons were resolved in ddH₂O and settled on 384 well plates (781096, Greiner bio one, Frickenhausen) with 1x 10⁶ cells per well. The remaining supernatant was removed. In one approach possible protein binding sites at the plastic surface of the plate should be blocked by addition of 3% (w/v) BSA for 1 h. After a ddH₂O wash, varying concentrations of recombinantly purified ^{His6}TbKif13-1 FL, 1.5 mM ATP and polymerisation buffer in a total of 40 µL were put on top of the cytoskeletons. Degradation occurred at 37°C for 30 min. Wells

were ddH₂O washed and subsequent fixation and antibody staining occurred as described above (see 4.4.13.1).

4.5. Cell biological methods

4.5.1. *T. brucei* cell lines and cultivation

In this study different *T. brucei* strains were used (Table 13).

Table 13: *T. brucei* strains.

cell line	description and origin
427	procyclic wild type
449	procyclic; inducible cell line; constitutively expressing <i>tet</i> repressor from plasmid <i>pHD 449</i> integrated at the tubulin locus; selection is kept with 5 µg/mL phleomycin; Biebinger et al., 1997

The procyclic wild type cell line 427 was maintained in a semi-defined medium (SDM-79; Brun and Schönenberger, 1979; Gibco® by Life Technologies™, Carlsbad, CA, USA) supplemented with 10% (v/v) heat-inactivated (30 min 56°C) fetal bovine serum (Sigma-Aldrich, Steinheim) and 7.5 mg/L hemin (Sigma-Aldrich, Steinheim) at 27°C (MIR-154, Sanyo, Moriguchi, Japan).

For ectopic expression, the procyclic cell line 449 was used, which constitutively expresses the tetracycline repressor (tetR). Therein, transgenic constructs from *pHD1800* and *pHD1801* are put into non-transcribed spacers of the rRNA repeat via homologous recombination. Their orientation is opposite to that of the rRNA transcription (Biebinger et al., 1997). Transgenic 449 cell lines being transformed with *pHD1800* or *pHD1801* are held under selection with 50 µg/mL hygromycin (Invivogen, San Diego, CA, USA) in addition.

Cultivation of *T. brucei* occurred in suspension culture flasks (Cellstar®, Greiner bio one, Frickenhausen) with regular splitting in a 1:50 – 1:100 ratio.

Counting of *T. brucei* cells was provided by 'Casy® Cell Counter and Analyser System Modell TT' (Roche Innovatis, Bielefeld).

4.5.2. Mammalian cell lines and cultivation

Depending on the purpose of the experiment, different mammalian cell types were used (Table 14).

Table 14: Mammalian cell lines.

cell line	description and origin
HeLa L	human cervix epithelial adenocarcinoma; transformed by humanpathogene Papilloma virus, subclone L
HeLa Flp-In	human cervix epithelial cells; modified according to 'Flp-In™ T-REx™ System' (Invitrogen, Thermo Scientific, Schwerte); stable integration of a pFRT/ <i>lacZeo</i> plasmid (Invitrogen) carrying the <i>FRT</i> (Flp-recombinase target) recognition site for site specific transgene integration by Flp-recombinase (mediates zeocin resistance), and <i>pcDNA6/TR</i> ® plasmid (Invitrogen; modified by replacing the <i>blastR</i> gene with a <i>puroR</i> gene), for constitutive expression of the <i>tet</i> repressor (mediates puromycin resistance) under the control of the <i>human CMV</i> promotor; integration of both plasmids is random and occurs independently; this host cell line was kindly provided by Thomas U. Mayer (Department of Biology, University of Konstanz)

HeLa cells were cultivated in Dulbecco's Modified Eagle Medium (DMEM; Gibco® by Life Technologies™, Carlsbad, CA, USA) supplemented with 10% (v/v) heat-inactivated (30 min 56°C) fetal bovine serum (Sigma-Aldrich, Steinheim). Cultivation occurred in cell culture dishes (Cellstar®, Greiner bio one, Frickenhausen) at 37°C in 5% CO₂ atmosphere ('Innova CO-170', New Brunswick Scientific, Eppendorf, Hamburg). For splitting/diluting, cells were washed with 1x PBS and subsequently incubated with 16 µl/cm² Trypsin/EDTA solution (PAA, Pasching, Austria) at 37°C for 5 min, which proteolytically cleaves cell surface proteins. Fresh medium was repeatedly pipetted to dissolve cells. After centrifugation at 1.200 rpm for 3 min (5810R, rotor A-4-62, Eppendorf, Hamburg), pelleted cells were resolved in fresh medium and a dilution was added to a new cell culture dish.

For the purpose of immunfluorescence samples, cover slips were washed and sterilised in 70% (v/v) ethanol, dried within the laminar flow and put to the dishes'ground. Then, medium and cells were added.

4.5.3. Transformation of *T. brucei*

2x Transformation buffer

60 mM Na₃PO₄

3.3 mM KCl

0.1 mM CaCl₂

33.3 mM HEPES

pH 7.3

Material and methods

Stable transformation of linearised DNA (see 4.3.10.) into the genome of *T. brucei* occurs via homologous recombination. In this study the *pHD* vector was used, which allows inducible, ectopic expression under the control of the procyclin promotor. For homologous recombination the rRNA locus is used (see 4.5.1.).

Electroporation of linearised plasmid DNA in transformation buffer (to 1x) was done using the 'Nucleofector II®' (Amaxa biosystems, via Lonza, Basel, Switzerland) with sterile electroporation cuvettes (732-1136, VWR, Radnor, PA, USA). For transformation 25×10^6 procyclic 449 cells were centrifuged at 1.600 rpm for 5 min (5702 R, rotor A-4-38, Eppendorf, Hamburg) and resuspended in 150 µL linearised plasmid in transformation buffer. For recovery reasons, cells were put to 10 mL SDM-79 without new antibiotic selection over night at 27°C. Cells were diluted 1:5 and 1:50 in final volumes of 50 mL containing all necessary selection antibiotics, and were plated on 24 well plates (Cellstar®, Greiner bio one, Frickenhausen) for selection of positive clones.

4.5.4. Transfection of mammalian cells

4.5.4.1. Transient transfection

Within transiently transfected mammalian cells plasmid DNA is not integrated into the genome, but genes may be ectopically expressed after induction.

For transient transfection of HeLa cells, a culture confluency of 60% was needed. For 2 mL medium covering cells, 160 µL DMEM (Gibco® by Life Technologies™, Carlsbad, CA, USA) with 10% (v/v) FCS (Sigma-Aldrich, Steinheim) and 2.5 µg plasmid DNA were incubated for 5 min at RT. 10 µg polyethylenimine (PEI) were put to the solution, mixed well and after 15 min at RT added dropwise all over the dish. Incubation occurred for 24 h at 37°C and 5% CO₂ atmosphere before changing medium. PEI is a polycation and therefore binds to negatively charged DNA (Boussif et al., 1995). Incorporation of that complex is assumed to happen via endocytosis. The needed dissociation of the complex within the cell or the nucleus is not yet understood.

4.5.4.2. Stable transfection

Stable transfected cells have integrated a transgene into their genome. In this study this was done primarily using the 'Flp-In™ T-REx™ System' (Invitrogen via Thermo Scientific, Schwerte). Therein site-specific integration of transgenic DNA into the genome occurred via *FRT* sites within the genome of HeLa Flp-In cells and *FRT* sites flanking the gene of interest in

the plasmid *pcDNA5TM/FRT/TO*. Recombination is facilitated by Flp-recombinase, which is encoded at the cotransfected *pAG1786*. For transfection HeLa Flp-Ins with a culture confluency of 60% on a \varnothing 145 mm dish (Cellstar®, Greiner bio one, Frickenhausen) were used. 4 μ g *pcDNA5TM/FRT/TO* containing the gene of interest, 40 μ g *pAG1786* and 2 mL Opti-MEM GlutamaxTM (Life Technologies, via Thermo Scientific, Schwerte) were incubated for 5 min at RT. 140 μ g PEI were added, mixed well, incubated for 1 h at RT and added dropwise to the cells. 24 h later cells were trypsinised (see 4.5.2.) and distributed to 4 dishes. After another 24 h 250 μ g/mL hygromycin were added for selection. After three weeks of regular medium change to remove died off cells, cell clones became visible. They were trypsinised using small glass rings put around them and transferred to single well plates until grown for testing.

To enhance expression of the transgene, a second transgenic plasmid was introduced into the generated single stable cell line. *pcDNATM3.1* (see 4.1.5.) was used, which allows random integration into the genome. 30 μ g of *pcDNATM3.1* containing the gene of interest were linearised with 20 units *PvuI* at 37°C for 16 h and subsequently purified as described in 4.3.10. Linearisation minimises the risk that integration of the vector disrupts elements necessary for expression in mammalian cells. The linearised plasmid was mixed with 2 mL Opti-MEM GlutamaxTM (Life Technologies, via Thermo Scientific, Schwerte), incubated for 5 min at RT, mixed well with 140 μ g PEI and incubated for 1 h at RT. The mixture was added dropwise all over the \varnothing 145 mm dish (Cellstar®, Greiner bio one, Frickenhausen), containing cells with a culture confluency of 60%. 24 h later cells were distributed to 4 dishes and after another 24 h 400 μ g/mL neomycin were added for selection.

4.5.5. Subcloning of *T. brucei*

Subcloning of *T. brucei* cells was done for receiving monoclonal cell cultures. Transgenic cell lines were plated to 96 well plates (Cellstar®, Greiner bio one, Frickenhausen) in a dilution of 0.5 – 1 cell per well in appropriate cultivation medium with selection antibiotics and 20% (v/v) conditioned medium. Conditioned medium was received by centrifugation (10 min 1.600 rpm; 5702 R, rotor A-4-38, Eppendorf, Hamburg) of logarithmically grown 427 wild type cells.

4.5.6. Storage of *T. brucei* and mammalian cells

Freezing medium *T. brucei*

SDM-79

10% (v/v) FCS

7% (v/v) glycerol

sterile filtered

Freezing medium mammalian cells

FCS

10% (v/v) DMSO

For storage of logarithmically growing *T. brucei*, cell cultures of 10 mL were centrifuged for 5 min at 1.600 rpm (5702 R, rotor A-4-38, Eppendorf, Hamburg) and resuspended in 0.5 mL freezing medium.

Mammalian cells with a confluency of 70% were trypsinised (see 4.5.2.) and after centrifugation (1.200 rpm for 3 min; 5810R, rotor A-4-62, Eppendorf, Hamburg) resuspended in 1 mL freezing medium.

T. brucei and mammalian cells in freezing medium were put in 'Cryogenic Vials' (VWR, Radnor, PA, USA) and cooled slowly to -80°C in 'Nalgene® Cryo 1°C' (Nalge Nunc, Rochester, NY, USA) freezing containers. Long term storage occurred in -80°C liquid N₂.

4.5.7. Ectopic expression in *T. brucei* and mammalian cells

For inducible, ectopic expression in *T. brucei* and mammalian cells 1 µg/mL doxycycline was used.

4.5.8. Growth curves

For *T. brucei* growth curves 0.5x 10⁶ cells/mL were seeded in 6 well plates (Cellstar®, Greiner bio one, Frickenhausen) within 2 mL. Seeding occurred as triplicates. For six days the cell number was determined via 'Casy® Cell Counter and Analyser System Modell TT' (Roche Innovatis, Bielefeld). At a density of about 1.3x 10⁷ cells were diluted.

4.5.9. Flow cytometry analysis

Possible effects of ectopically expressed ^{myc}*TbKif13-1* deletion constructs on the *T. brucei* cell cycle were examined by flow cytometry analysis. 5x 10⁶ cells of logarithmically growing cell cultures were washed with 1x PBS, fixed first with 0.5% formaldehyde in 1x PBS for 5 min on ice and then with 70% (v/v) ice-cold ethanol under continuous shaking. After 1 h at 4°C cells were centrifuged at 3.000 rpm for 5 min (5702 R, rotor A-4-38, Eppendorf, Hamburg) and the

Material and methods

pellet resuspended in 1x PBS containing 50 µg propidium iodide (Sigma-Aldrich, Steinheim) and 50 µg RNaseA (Sigma-Aldrich, Steinheim). For RNA degradation, samples were put to a 37°C water bath for 30 min prior to flow cytometry. Analysis was done with 'Cytomics FC 500' (Beckman Coulter, Krefeld) and associated 'CXP' software.

4.5.10. Proteasome degradation assay

To test APC/C-dependent proteasomal degradation of ^{myc}TbKif13-1 deletion constructs *in vivo*, appropriate transgenic 449 *T. brucei* cells lines were induced for ectopic expression with 1 µg/mL doxycycline 4.5 h prior to addition of 50 µg/mL cycloheximide (CHX; AppliChem, Darmstadt) solely or in combination with 50 µM MG 132 (Sigma Aldrich, Steinheim).

CHX inhibits translation by blocking the translocation step during the elongation phase at ribosomes. The binding of CHX to the E-site of the 60S ribosome together with a deacylated tRNA stops translocation and leads to an arrest of the ribosome at the second codon (Schneider-Poetsch et al., 2010). MG 132 blocks the proteolytic activity of the 26S proteasome by primarily binding covalently to the active site of the beta subunits of the chymotrypsin-like site within the 20S proteasome (Goldberg, 2012).

Samples of 4.5×10^6 cells were 1x PBS washed and boiled in hot Laemmli (to 1x) at the given timepoints.

5. Abbreviations

APC/C	anaphase-promoting complex/cyclosome
apoL-I	apolipoprotein L-I
APS	ammonium persulfate
Ark1	actin regulating kinase 1
Auk	Aurora-like kinase
Cdc20	cell division cycle 20
Cdh1	cdc20 homologue 1
Cdk1	cyclin-dependent kinase
CENP	centromere protein
CHO	chinese hamster ovary
CHX	cycloheximide
Cif	cytokinesis initiation factor
Cik	chromosome instability and karyogamy
Cin	Chromosome instability protein
CPC	chromosomal passenger complex
Crk	cdc2-related kinase
DAPI	4',6-diamidino-2-phenylindole
D-box	destruction-box
DMEM	Dulbecco's Modified Eagle Medium
EB	end-binding protein
FAZ	flagellar attachment zone
FCS	fetal calf serum
GP	glycoprotein
HeLa	Henrietta Lacks
HpHbR	haptoglobin-haemoglobin receptor
Hpr	haptoglobin-related protein
Ig	immunoglobulin
INCENP	inner centromere protein
Ip11	increase in ploidy 1
IPTG	Isopropyl β -D-1-thiogalactopyranoside

Abbreviations

Kar	karyogamy
Kif	kinesin superfamily
Kip	kinesin related protein
Klp	kinesin like protein
Kn1	kinetochore null protein 1
MAP	microtubule-associated protein
MCAK	mitotic centromere associated kinesin
MCS	multiple cloning site
Mis12	mis-segregation 12
MTOC	microtubule organising centre
MtQ	microtubule quartet
Ndc80	nuclear division cycle 80
NES	nuclear export sequence
NLS	nuclear localisation sequence
NPC	nuclear pore complex
Nuf2	nuclear filament-containing protein 2
PCR	polymerase chain reaction
PFR	paraflagellar rod
Plk	polo-like kinase
PVDF	polyvinylidene difluoride
Ran	ras-related nuclear protein
RanGAP	Ran GTPase-activating protein
RanGEF	Ran guanine nucleotide exchange factor
SDM	semi-defined medium
SDS-PAGE	sodium dodecyl sulfate polyacrylamid gelectrophoresis
SRA	serum resistance-associated
TAC	tripartite attachment complex
+TIP	microtubule plus end tracking protein
TLF	trypanosome lytic factor
Tlk	touseld-like kinase
VSG	variant surface glycoprotein
XKCM1	<i>Xenopus</i> kinesin central motor 1

6. References

- Absalon, S., Blisnick, T., Kohl, L., Toutirais, G., Doré, G., Julkowska, D., Tavenet, A., Bastin, P. (2008): Intraflagellar transport and functional analysis of genes required for flagellum formation in trypanosomes. *Mol Biol Cell* 19, 929-944.
- Absalon, S., Kohl, L., Branche, C., Blisnick, T., Toutirais, G., Rusconi, F., Cosson, J., Bonhivers, M., Robinson, D., Bastin, P. (2007): Basal body positioning is controlled by flagellum formation in *Trypanosoma brucei*. *PLoS One* 2, e437.
- Ainsztein, A. M., Kandels-Lewis, S. E., Mackay, A. M., Earnshaw, W. C. (1998): INCENP centromere and spindle targeting: identification of essential conserved motifs and involvement of heterochromatin protein HP1. *J Cell Biol* 143, 1763-1774.
- Akiyoshi, B., Gull, K. (2014): Discovery of unconventional kinetochores in kinetoplastids. *Cell* 156, 1247-1258.
- Alushin, G. M., Lander, G. C., Kellogg, E. H., Zhang, R., Baker, D., Nogales, E. (2014): High-resolution microtubule structures reveal the structural transitions in $\alpha\beta$ -tubulin upon GTP hydrolysis. *Cell* 157, 1117-1129.
- Andrews, P. D., Ovechkina, Y., Morrice, N., Wagenbach, M., Duncan, K., Wordeman, L., Swedlow, J. R. (2004): Aurora B regulates MCAK at the mitotic centromere. *Dev Cell* 6, 253-268.
- Aoki, S., Ohta, K., Yamazaki, T., Sugawara, F., Sakaguchi, K. (2005): Mammalian mitotic centromere-associated kinesin (MCAK): a new molecular target of sulfoquinovosylacylglycerols novel antitumor and immunosuppressive agents. *FEBS J* 272, 2132-2140.
- Asenjo, A. B., Chatterjee, C., Tan, D., DePaoli, V., Rice, W. J., Diaz-Avalos, R., Silvestry, M., Sosa, H. (2013): Structural model for tubulin recognition and deformation by kinesin-13 microtubule depolymerases. *Cell Rep* 3, 759-768.
- Askjaer, P., Jensen, T. H., Nilsson, J., Englmeier, L., Kjems, J. (1998): The specificity of the CRM1-Rev nuclear export signal interaction is mediated by RanGTP. *J Biol Chem* 273, 33414-33422.
- Bakhoun, S. F., Thompson, S. L., Manning, A. L., Compton, D. A. (2009): Genome stability is ensured by temporal control of kinetochore-microtubule dynamics. *Nat Cell Biol* 11, 27-35.
- Balaban, N., Goldman, R. (1992): Isolation and characterization of a unique 15 kilodalton trypanosome subpellicular microtubule-associated protein. *Cell Motil Cytoskeleton* 21, 138-146.

References

- Balasegaram, M., Young, H., Chappuis, F., Priotto, G., Raguenaud, M. E., Checchi, F. (2009): Effectiveness of melarsoprol and eflornithine as first-line regimens for *gambiense* sleeping sickness in nine Médecins Sans Frontières programmes. *Trans R Soc Trop Med Hyg* 103, 280-290.
- Barlow, S. B., Gonzalez-Garay, M. L., Cabral, F. (2002): Paclitaxel-dependent mutants have severely reduced microtubule assembly and reduced tubulin synthesis. *J Cell Sci* 115, 3469-3478.
- Bastin, P., Sherwin, T., Gull, K. (1998): Paraflagellar rod is vital for trypanosome motility. *Nature* 391, 548.
- Becker, J., Melchior, F., Gerke, V., Bischoff, F. R., Ponstingl, H., Wittinghofer, A. (1995): RNA1 encodes a GTPase-activating protein specific for Gsp1p, the Ran/TC4 homologue of *Saccharomyces cerevisiae*. *J Biol Chem* 270, 11860-11865.
- Bennett, A., Bechi, B., Tighe, A., Thompson, S., Procter, D. J., Taylor, S. S. (2015): Cenp-E inhibitor GSK923295: Novel synthetic route and use as a tool to generate aneuploidy. *Oncotarget* 6, 20921-20932.
- Berberof, M., Pérez-Morga, D., Pays, E. (2001): A receptor-like flagellar pocket glycoprotein specific to *Trypanosoma brucei gambiense*. *Mol Biochem Parasitol* 113, 127-138.
- Bessat, M. (2014): Knockdown of APC/C-associated genes and its effect on viability and cell cycle of protozoan parasite of *Trypanosoma brucei*. *Parasitol Res* 113, 1555-1562.
- Bessat, M., Knudsen, G., Burlingame, A. L., Wang, C. C. (2013): A minimal anaphase promoting complex/cyclosome (APC/C) in *Trypanosoma brucei*. *PLoS One* 8, e59258.
- Biebinger, S., Wirtz, L. E., Clayton, C. E. (1997): Vectors for inducible over-expression of potentially toxic gene products in bloodstream and procyclic *Trypanosoma brucei*. *Mol Biochem Parasitol* 85, 99-112.
- Birkett, C. R., Foster, K. E., Johnson, L., Gull, K. (1985): Use of monoclonal antibodies to analyse the expression of a multi-tubulin family. *FEBS Lett* 187, 211-218.
- Bischoff, F. R., Ponstingl, H. (1991): Catalysis of guanine nucleotide exchange on Ran by the mitotic regulator RCC1. *Nature* 354, 80-82.
- Blaineau, C., Tessier, M., Dubessay, P., Tasse, L., Crobu, L., Pagès, M., Bastien, P. (2007): A novel microtubule-depolymerizing kinesin involved in length control of a eukaryotic flagellum. *Curr Biol* 17, 778-782.
- Blangy, A., Lane, H. A., d'Hérin, P., Harper, M., Kress, M., Nigg, E. A. (1995): Phosphorylation by p34cdc2 regulates spindle association of human Eg5, a kinesin-related motor essential for bipolar spindle formation in vivo. *Cell* 83, 1159-1169.

References

- Borisy, G. G., Marcum, J. M., Olmsted, J. B., Murphy, D. B., Johnson, K. A. (1975): Purification of tubulin and associated high molecular weight proteins from porcine brain and characterization of microtubule assembly in vitro. *Ann N Y Acad Sci* 253, 107-132.
- Bourne, H. R., Sanders, D. A., McCormick, F. (1990): The GTPase superfamily: a conserved switch for diverse cell functions. *Nature* 348, 125-132.
- Bourne, H. R., Sanders, D. A., McCormick, F. (1991): The GTPase superfamily: conserved structure and molecular mechanism. *Nature* 349, 117-127.
- Boussif, O., Lezoualc'h, F., Zanta, M. A., Mergny, M. D., Scherman, D., Demeneix, B., Behr, J. P. (1995): A versatile vector for gene and oligonucleotide transfer into cells in culture and in vivo: polyethylenimine. *Proc Natl Acad Sci* 92, 7297-7301.
- Bradford, M. M. (1976): A rapid and sensitive method for the quantification of microgram quantities of protein utilizing the principle of protein-dye binding. *Anal Biochem* 72, 248-254.
- Braun, J., Möckel, M. M., Strittmatter, T., Marx, A., Groth, U., Mayer, T. U. (2015): Synthesis and biological evaluation of optimized inhibitors of the mitotic kinesin Kif18A. *ACS Chem Biol* 10, 554-560.
- Briggs, L. J., McKean, P. G., Baines, A., Moreira-Leite, F., Davidge, J., Vaughan, S., Gull, K. (2004): The flagella connector of *Trypanosoma brucei*: an unusual mobile transmembrane junction. *J Cell Sci* 117, 1641-1651.
- Broadhead, R., Dawe, H. R., Farr, H., Griffiths, S., Hart, S. R., Portman, N., Shaw, M. K., Ginger, M. L., Gaskell, S. J., McKean, P. G., Gull, K. (2006): Flagellar motility is required for the viability of the bloodstream trypanosome. *Nature* 440, 224-227.
- Brun, R., Schönenberger, M. (1979): Cultivation and in vitro cloning of procyclic culture forms of *Trypanosoma brucei* in a semi-defined medium. Short communication. *Acta Trop* 36, 289-292.
- Bullard, W., Kieft, R., Capewell, P., Veitch, N. J., Macleod, A., Hajduk, S. L. (2012): Haptoglobin-hemoglobin receptor independent killing of African trypanosomes by human serum and trypanosome lytic factors. *Virulence* 3, 72-76.
- Burns, K. M., Wagenbach, M., Wordeman, L., Schriemer, D. C. (2014): Nucleotide exchange in dimeric MCAK induces longitudinal and lateral stress at microtubule ends to support depolymerization. *Structure* 22, 1173-1183.
- Buster, D. W., Zhang, D., Sharp, D. J. (2007): Poleward tubulin flux in spindles: regulation and function in mitotic cells. *Mol Biol Cell* 18, 3094-3104.

References

- Capewell, P., Clucas, C., DeJesus, E., Kieft, R., Hajduk, S., Veitch, N., Steketee, P. C., Cooper, A., Weir, W., MacLeod, A. (2013): The TgsGP gene is essential for resistance to human serum in *Trypanosoma brucei gambiense*. PLoS Pathog 9, e1003686.
- Capewell, P., Cren-Travaillé, C., Marchesi, F., Johnston, P., Clucas, C., Benson, R. A., Gorman, T. A., Calvo-Alvarez, E., Crouzols, A., Jouvion, G., Jamonneau, V., Weir, W., Stevenson, M. L., O'Neill, K., Cooper, A., Swar, N. K., Bucheton, B., Ngoyi, D. M., Garside, P., Rotureau, B., MacLeod, A. (2016): The skin is a significant but overlooked anatomical reservoir for vector-borne African trypanosomes. Elife, e17716
- Carrier, M. F., Pantaloni, D. (1981): Kinetic analysis of guanosine 5'-triphosphate hydrolysis associated with tubulin polymerization. Biochemistry 20, 1918-1924.
- Casanova, M., Crobu, L., Blaineau, C., Bourgeois, N., Bastien, P., Pagès, M. (2009): Microtubule-severing proteins are involved in flagellar length control and mitosis in Trypanosomatids. Mol Microbiol 71, 1353-1370.
- Catarinella, M., Grüner, T., Strittmatter, T., Marx, A., Mayer, T. U. (2009): BTB-1: a small molecule inhibitor of the mitotic motor protein Kif18A. Angew Chem Int Ed Engl 48, 9072-9076.
- Chan, K. Y. (2008): The characterisation of family-13 kinesins in *Trypanosoma brucei*. Diss. University of Hull.
- Chan, K. Y., Ersfeld, K. (2010): The role of the Kinesin-13 family protein TbKif13-2 in flagellar length control of *Trypanosoma brucei*. Mol Biochem Parasitol 174, 137-140.
- Chan, K. Y., Matthews, K. R., Ersfeld, K. (2010): Functional characterisation and drug target validation of a mitotic kinesin-13 in *Trypanosoma brucei*. PLoS Pathog 6, e1001050.
- Chappuis, F., Udayraj, N., Stietenroth, K., Meussen, A., Bovier, P. A. (2005): Eflornithine is safer than melarsoprol for the treatment of second-stage *Trypanosoma brucei gambiense* human African trypanosomiasis. Clin Infect Dis 41, 748-751.
- Checchi, F., Filipe, J. A., Haydon, D. T., Chandramohan, D., Chappuis, F. (2008): Estimates of the duration of the early and late stage of *gambiense* sleeping sickness. BMC Infect Dis 8, 16.
- Checchi, F., Piola, P., Ayikoru, H., Thomas, F., Legros, D., Priotto, G. (2007): Nifurtimox plus Eflornithine for late-stage sleeping sickness in Uganda: a case series. PLoS Negl Trop Dis 1, e64.
- Cheeseman, I. M., Chappie, J. S., Wilson-Kubalek, E. M., Desai, A. (2006): The conserved KMN network constitutes the core microtubule-binding site of the kinetochore. Cell 127, 983-997.
- Chu, H. M., Yun, M., Anderson, D. E., Sage, H., Park, H. W., Endow, S. A. (2005): Kar3 interaction with Cik1 alters motor structure and function. EMBO J 24, 3214-3223.

References

- Cimini, D., Wan, X., Hirel, C. B., Salmon, E. D. (2006): Aurora kinase promotes turnover of kinetochore microtubules to reduce chromosome segregation errors. *Curr Biol* 16, 1711-1718.
- Cleveland, D. W., Lopata, M. A., Sherline, P., Kirschner, M. W. (1981): Unpolymerized tubulin modulates the level of tubulin mRNAs. *Cell* 25, 537-546.
- Conti, E., Kuriyan, J. (2000): Crystallographic analysis of the specific yet versatile recognition of distinct nuclear localization signals by karyopherin alpha. *Structure* 8, 329-338.
- Cooke, C. A., Heck, M. M., Earnshaw, W. C. (1987): The inner centromere protein (INCENP) antigens: movement from inner centromere to midbody during mitosis. *J Cell Biol* 105, 2053-2067.
- Cooper, J. R., Wagenbach, M., Asbury, C. L., Wordeman, L. (2010): Catalysis of the microtubule on-rate is the major parameter regulating the depolymerase activity of MCAK. *Nat Struct Mol Biol* 17, 77-82.
- Corbett, A. H., Koepp, D. M., Schlenstedt, G., Lee, M. S., Hopper, A. K., Silver, P. A. (1995): Rna1p, a Ran/TC4 GTPase activating protein, is required for nuclear import. *J Cell Biol* 130, 1017-1026.
- Cormier, A., Drubin, D. G., Barnes, G. (2013): Phosphorylation regulates kinase and microtubule binding activities of the budding yeast chromosomal passenger complex *in vitro*. *J Biol Chem* 288, 23203-23211.
- Dagenbach, E. M., Endow, S. A. (2004): A new kinesin tree. *J Cell Sci* 117, 3-7.
- Dang, C. V., Lee, W. M. (1988): Identification of the human c-myc protein nuclear translocation signal. *Mol Cell Biol* 8, 4048-4054.
- D'Archivio, S., Wickstead, B. (2017): Trypanosome outer kinetochore proteins suggest conservation of chromosome segregation machinery across eukaryotes. *J Cell Biol* 216, 379-391.
- DeBonis, S., Skoufias, D. A., Lebeau, L., Lopez, R., Robin, G., Margolis, R. L., Wade, R. H., Kozielski, F. (2004): *In vitro* screening for inhibitors of the human mitotic kinesin Eg5 with antimitotic and antitumor activities. *Mol Cancer Ther* 3, 1079-1090.
- Deflorin, J., Rudolf, M., Seebeck, T. (1994): The major components of the paraflagellar rod of *Trypanosoma brucei* are two similar, but distinct proteins which are encoded by two different gene loci. *J Biol Chem* 269, 28745-28751.
- de Graffenried, C. L., Ho, H. H., Warren, G. (2008): Polo-like kinase is required for Golgi and bilobe biogenesis in *Trypanosoma brucei*. *J Cell Biol* 181, 431-438.

References

- DeGrasse, J. A., DuBois, K. N., Devos, D., Siegel, T. N., Sali, A., Field, M. C., Rout, M. P., Chait, B. T. (2009): Evidence for a shared nuclear pore complex architecture that is conserved from the last common eukaryotic ancestor. *Mol Cell Proteomics* 8, 2119-2130.
- DeGreef, C., Hamers, R. (1994): The serum resistance-associated (SRA) gene of *Trypanosoma brucei rhodesiense* encodes a variant surface glycoprotein-like protein. *Mol Biochem Parasitol* 68, 277-284.
- DeJesus, E., Kieft, R., Albright, B., Stephens, N. A., Hajduk, S. L. (2013): A single amino acid substitution in the group 1 *Trypanosoma brucei gambiense* haptoglobin-hemoglobin receptor abolishes TLF-1 binding. *PLoS Pathog* 9, e1003317.
- Desai, A., Mitchison, T. J. (1997): Microtubule polymerization dynamics. *Annu Rev Cell Dev Biol* 13, 83-117.
- Desai, A., Verma, S., Mitchison, T. J., Walczak, C. E. (1999): Kin I kinesins are microtubule-destabilizing enzymes. *Cell* 96, 69-78.
- Desai, A., Walczak, C. E. (2001): Assays for microtubule-destabilizing kinesins. *Methods Mol Biol* 164, 109-121.
- Detmer, E., Hemphill, A., Müller, N., Seebeck, T. (1997): The *Trypanosoma brucei* autoantigen I/6 is an internally repetitive cytoskeletal protein. *Eur J Cell Biol* 72, 378-384.
- DeZwaan, T. M., Ellingson, E., Pellman, D., Roof, D. M. (1997): Kinesin-related KIP3 of *Saccharomyces cerevisiae* is required for a distinct step in nuclear migration. *J Cell Biol* 138, 1023-1040.
- Ding, X., Yan, F., Yao, P., Yang, Z., Wan, W., Wang, X., Liu, J., Gao, X., Abrieu, A., Zhu, T., Zhang, J., Dou, Z., Yao, X. (2010): Probing CENP-E function in chromosome dynamics using small molecule inhibitor syntelin. *Cell Res* 20, 1386-1389.
- Ditchfield, C., Johnson, V. L., Tighe, A., Ellston, R., Haworth, C., Johnson, T., Mortlock, A., Keen, N., Taylor, S. S. (2003): Aurora B couples chromosome alignment with anaphase by targeting BubR1, Mad2, and Cenp-E to kinetochores. *J Cell Biol* 161, 267-280.
- Domnitz, S. B., Wagenbach, M., Decarreau, J., Wordeman, L. (2012): MCAK activity at microtubule tips regulates spindle microtubule length to promote robust kinetochore attachment. *J Cell Biol* 197, 231-237.
- Drain, J., Bishop, J. R., Hajduk, S. L. (2001): Haptoglobin-related protein mediates trypanosome lytic factor binding to trypanosomes. *J Biol Chem* 276, 30254-30260.

References

- Dubessay, P., Blaineau, C., Bastien, P., Tasse, L., Van Dijk, J., Crobu, L., Pagès, M. (2006): Cell cycle-dependent expression regulation by the proteasome pathway and characterization of the nuclear targeting signal of a *Leishmania major* Kin-13 kinesin. *Mol Microbiol* 59, 1162-1174.
- Elie-Caille, C., Severin, F., Helenius, J., Howard, J., Muller, D. J., Hyman, A. A. (2007): Straight GDP-tubulin protofilaments form in the presence of taxol. *Curr Biol* 17, 1765-1770.
- Ems-McClung, S. C., Hainline, S. G., Devare, J., Zong, H., Cai, S., Carnes, S. K., Shaw, S. L., Walczak, C. E. (2013): Aurora B inhibits MCAK activity through a phosphoconformational switch that reduces microtubule association. *Curr Biol* 23, 2491-2499.
- Endow, S. A., Kang, S. J., Satterwhite, L. L., Rose, M. D., Skeen, V. P., Salmon, E. D. (1994): Yeast Kar3 is a minus-end microtubule motor protein that destabilizes microtubules preferentially at the minus ends. *EMBO J* 13, 2708-2713.
- Engstler, M., Pfohl, T., Herminghaus, S., Boshart, M., Wiegertjes, G., Heddergott, N., Overath, P. (2007): Hydrodynamic flow-mediated protein sorting on the cell surface of trypanosomes. *Cell* 131, 505-515.
- Engstler, M., Thilo, L., Weise, F., Grünfelder, C. G., Schwarz, H., Boshart, M., Overath, P. (2004): Kinetics of endocytosis and recycling of the GPI-anchored variant surface glycoprotein in *Trypanosoma brucei*. *J Cell Sci* 117, 1105-1115.
- Ersfeld, K., Gull, K. (1997): Partitioning of large and minichromosomes in *Trypanosoma brucei*. *Science* 276, 611-614.
- Esson, H. J., Morriswood, B., Yavuz, S., Vidilaseris, K., Dong, G., Warren, G. (2012): Morphology of the trypanosome bilobe, a novel cytoskeletal structure. *Eukaryot Cell* 11, 761-772.
- Fang, G., Yu, H., Kirschner, M. W. (1998): Direct binding of CDC20 protein family members activates the anaphase-promoting complex in mitosis and G1. *Mol Cell* 2, 163-171.
- Fornerod, M., Ohno, M., Yoshida, M., Mattaj, I. W. (1997): CRM1 is an export receptor for leucine-rich nuclear export signals. *Cell* 90, 1051-1060.
- Fourest-Lieuvin, A., Peris, L., Gache, V., Garcia-Saez, I., Juillan-Binard, C., Lantéz, V., Job, D. (2006): Microtubule regulation in mitosis: tubulin phosphorylation by the cyclin-dependent kinase Cdk1. *Mol Biol Cell* 17, 1041-1050.
- Frankel, M. B., Knoll, L. J. (2009): The ins and outs of nuclear trafficking: unusual aspects in apicomplexan parasites. *DNA Cell Biol* 28, 277-284.
- Friel, C. T., Howard, J. (2011): The kinesin-13 MCAK has an unconventional ATPase cycle adapted for microtubule depolymerization. *EMBO J* 30, 3928-3939.

References

- Fuge, H. (1969): Electron microscopic studies on the intra-flagellar structures of trypanosomes. *J Protozool* 16, 460-466.
- Furch, M., Fujita-Becker, S., Geeves, M. A., Holmes, K. C., Manstein, D. J. (1999): Role of the salt-bridge between switch-1 and switch-2 of Dictyostelium myosin. *J Mol Biol* 290, 797-809.
- Ganem, N. J., Compton, D. A. (2004): The KinI kinesin Kif2a is required for bipolar spindle assembly through a functional relationship with MCAK. *J Cell Biol* 166, 473-478.
- Ganguly, A., Bhattacharya, R., Cabral, F. (2008): Cell cycle dependent degradation of MCAK: evidence against a role in anaphase chromosome movement. *Cell Cycle* 7, 3187-3193.
- Ganguly, A., Yang, H., Cabral, F. (2011a): Overexpression of mitotic centromere-associated kinesin stimulates microtubule detachment and confers resistance to paclitaxel. *Mol Cancer Ther* 10, 929-937.
- Ganguly, A., Yang, H., Pedroza, M., Bhattacharya, R., Cabral, F. (2011b): Mitotic centromere-associated kinesin (MCAK) mediates paclitaxel resistance. *J Biol Chem* 286, 36378-36384.
- Gassmann, R., Carvalho, A., Henzing, A. J., Ruchaud, S., Hudson, D. F., Honda, R., Nigg, E. A., Gerloff, D. L., Earnshaw, W. C. (2004): Borealin: a novel chromosomal passenger required for stability of the bipolar mitotic spindle. *J Cell Biol* 166, 179-191.
- Glötzter, M., Murray, A. W., Kirschner, M. W. (1991): Cyclin is degraded by the ubiquitin pathway. *Nature* 349, 132-138.
- Gluenz, E., Povelones, M. L., Englund, P. T., Gull, K. (2011): The kinetoplast duplication cycle in *Trypanosoma brucei* is orchestrated by cytoskeleton-mediated cell morphogenesis. *Mol Cell Biol* 31, 1012-1021.
- Goldberg, A. L. (2012): Development of proteasome inhibitors as research tools and cancer drugs. *J Cell Biol* 199, 583-588.
- Gonzalez-Garay, M. L., Cabral, F. (1996): alpha-Tubulin limits its own synthesis: evidence for a mechanism involving translational repression. *J Cell Biol* 135, 1525-1534.
- Gonzalez-Garay, M. L., Chang, L., Blade, K., Menick, D. R., Cabral, F. (1999): A beta-tubulin leucine cluster involved in microtubule assembly and paclitaxel resistance. *J Biol Chem* 274, 23875-23882.
- Gordon, D. M., Roof, D. M. (2001): Degradation of the kinesin Kip1p at anaphase onset is mediated by the anaphase-promoting complex and Cdc20p. *Proc Natl Acad Sci* 98, 12515-12520.
- Görlich, D., Kostka, S., Kraft, R., Dingwall, C., Laskey, R. A., Hartmann, E., Prehn, S. (1995): Two different subunits of importin cooperate to recognize nuclear localization signals and bind them to the nuclear envelope. *Curr Biol* 5, 383-392.

References

- Gull, K., Alsford, S., Ersfeld, K. (1998): Segregation of minichromosomes in trypanosomes: implications for mitotic mechanisms. *Trends Microbiol* 6, 319-323.
- Gull, K., Birkett, C., Gerke-Bonet, R., Parma, A., Robinson, D., Sherwin, T., Woodward, R. (1990): The cell cycle and cytoskeletal morphogenesis in *Trypanosoma brucei*. *Biochem Soc Trans* 18, 720-722.
- Gupta, M. L. Jr, Carvalho, P., Roof, D. M., Pellman, D. (2006): Plus end-specific depolymerase activity of Kip3, a kinesin-8 protein, explains its role in positioning the yeast mitotic spindle. *Nat Cell Biol* 8, 913-923.
- Hammarton, T. C., Clark, J., Douglas, F., Boshart, M., Mottram, J. C. (2003): Stage-specific differences in cell cycle control in *Trypanosoma brucei* revealed by RNA interference of a mitotic cyclin. *J Biol Chem* 278, 22877-22886.
- Hammarton, T. C., Kramer, S., Tetley, L., Boshart, M., Mottram, J. C. (2007): *Trypanosoma brucei* polo-like kinase is essential for basal body duplication, kDNA segregation and cytokinesis. *Mol Microbiol* 65, 1229-1248.
- Hari, M., Wang, Y., Veeraraghavan, S., Cabral F. (2003a): Mutations in alpha- and beta-tubulin that stabilize microtubules and confer resistance to colcemid and vinblastine. *Mol Cancer Ther* 2, 597-605.
- Hauf, S., Cole, R. W., LaTerra, S., Zimmer, C., Schnapp, G., Walter, R., Heckel, A., van Meel, J., Rieder, C. L., Peters, J. M. (2003): The small molecule Hesperadin reveals a role for Aurora B in correcting kinetochore-microtubule attachment and in maintaining the spindle assembly checkpoint. *J Cell Biol* 161, 281-294.
- He, C. Y., Pypaert, M., Warren, G. (2005): Golgi duplication in *Trypanosoma brucei* requires Centrin2. *Science* 310, 1196-1198.
- He, L., Yang, C. P., Horwitz, S. B. (2001): Mutations in beta-tubulin map to domains involved in regulation of microtubule stability in epothilone-resistant cell lines. *Mol Cancer Ther* 1, 3-10.
- Hedrick, D. G., Stout, J. R., Walczak, C. E. (2008): Effects of anti-microtubule agents on microtubule organization in cells lacking the kinesin-13 MCAK. *Cell Cycle* 7, 2146-2156.
- Helenius, J., Brouhard, G., Kalaidzidis, Y., Diez, S., Howard, J. (2006): The depolymerizing kinesin MCAK uses lattice diffusion to rapidly target microtubule ends. *Nature* 441, 115-119.
- Hellman, K., Prohaska, K., Williams, N. (2007): *Trypanosoma brucei* RNA binding proteins p34 and p37 mediate NOPP44/46 cellular localization via the exportin 1 nuclear export pathway. *Eukaryot Cell* 6, 2206-2213.

References

- Hemphill, A., Affolter, M., Seebeck, T. (1992): A novel microtubule-binding motif identified in a high molecular weight microtubule-associated protein from *Trypanosoma brucei*. *J Cell Biol* 117, 95-103.
- Hepperla, A. J., Willey, P. T., Coombes, C. E., Schuster, B. M., Gerami-Nejad, M., McClellan, M., Mukherjee, S., Fox, J., Winey, M., Odde, D. J., O'Toole, E., Gardner, M. K. (2014): Minus-end-directed Kinesin-14 motors align antiparallel microtubules to control metaphase spindle length. *Dev Cell* 31, 61-72.
- Hertzer, K. M., Ems-McClung, S. C., Kline-Smith, S. L., Lipkin, T. G., Gilbert, S. P., Walczak, C. E. (2006): Full-length dimeric MCAK is a more efficient microtubule depolymerase than minimal domain monomeric MCAK. *Mol Biol Cell* 17, 700-710.
- Hildebrandt, E. R., Hoyt, M. A. (2001): Cell cycle-dependent degradation of the *Saccharomyces cerevisiae* spindle motor Cin8p requires APC(Cdh1) and a bipartite destruction sequence. *Mol Biol Cell* 12, 3402-3416.
- Higgins, M. K., Tkachenko, O., Brown, A., Reed, J., Raper, J., Carrington, M. (2013): Structure of the trypanosome haptoglobin-hemoglobin receptor and implications for nutrient uptake and innate immunity. *Proc Natl Acad Sci* 110, 1905-1910.
- Hildebrandt, E. R., Hoyt, M. A. (2001): Cell cycle-dependent degradation of the *Saccharomyces cerevisiae* spindle motor Cin8p requires APC(Cdh1) and a bipartite destruction sequence. *Mol Biol Cell* 12, 3402-3416.
- Hirose, K., Akimaru, E., Akiba, T., Endow, S. A., Amos, L. A. (2006): Large conformational changes in a kinesin motor catalyzed by interaction with microtubules. *Mol Cell* 23, 913-923.
- Hodel, M. R., Corbett, A. H., Hodel, A. E. (2001): Dissection of a nuclear localization signal. *J Biol Chem* 276, 1317-1325.
- Holen, K. D., Belani, C. P., Wilding, G., Ramalingam, S., Volkman, J. L., Ramanathan, R. K., Vasist, L. S., Bowen, C. J., Hodge, J. P., Dar, M. M., Ho, P. T. (2011): A first in human study of SB-743921, a kinesin spindle protein inhibitor, to determine pharmacokinetics, biologic effects and establish a recommended phase II dose. *Cancer Chemother Pharmacol* 67, 447-454.
- Homma, N., Takei, Y., Tanaka, Y., Nakata, T., Terada, S., Kikkawa, M., Noda, Y., Hirokawa, N. (2003): Kinesin superfamily protein 2A (KIF2A) functions in suppression of collateral branch extension. *Cell* 114, 229-239.
- Honda, R., Körner, R., Nigg, E. A. (2003): Exploring the functional interactions between Aurora B, INCENP, and survivin in mitosis. *Mol Biol Cell* 14, 3325-3341.
- Honnappa, S., Gouveia, S. M., Weisbrich, A., Damberger, F. F., Bhavesh, N. S., Jawhari, H., Grigoriev, I., van Rijssel, F. J., Buey, R. M., Lawera, A., Jelesarov, I., Winkler, F. K., Wüthrich, K., Akhmanova, A., Steinmetz, M. O. (2009): An EB1-binding motif acts as a microtubule tip localization signal. *Cell* 138, 366-376.

References

- Hoyt, M. A., He, L., Loo, K. .K, Saunders, W. S. (1992): Two *Saccharomyces cerevisiae* kinesin-related gene products required for mitotic spindle assembly. *J Cell Biol* 118, 109-120.
- Hu, H., Yu, Z., Liu, Y., Wang, T., Wie, Y., Li, Z. (2014): The Aurora B kinase in *Trypanosoma brucei* undergoes post-translational modifications and is targeted to various subcellular locations through binding to *TbCPC1*. *Mol Microbiol* 91, 256-274.
- Hu, H., Zhou, Q., Li, Z. (2015): A novel basal body protein that is a polo-like kinase substrate is required for basal body segregation and flagellum adhesion in *Trypanosoma brucei*. *J Biol Chem* 290, 25012-25022.
- Hua, S., To, W. Y., Nguyen, T. T., Wong, M. L., Wang, C. C. (1996): Purification and characterization of proteasomes from *Trypanosoma brucei*. *Mol Biochem Parasitol* 78, 33-46.
- Huang, T. G., Hackney, D. D. (1994): *Drosophila* kinesin minimal motor domain expressed in *Escherichia coli*. Purification and kinetic characterization. *J Biol Chem* 269, 16493-16501.
- Huyett, A., Kahana, J., Silver, P., Zeng, X., Saunders, W. S. (1998): The Kar3p and Kip2p motors function antagonistically at the spindle poles to influence cytoplasmic microtubule numbers. *J Cell Sci* 111, 295-301.
- Ikeda, K. N., de Graffenried, C. L. (2012): Polo-like kinase is necessary for flagellum inheritance in *Trypanosoma brucei*. *J Cell Sci* 125, 3173-3184.
- Infante, J. R., Patnaik, A., Verschraegen, C. F., Olszanski, A. J., Shaheen, M., Burris, H. A., Tolcher, A. W., Papadopoulos, K. P., Beeram, M., Hynes, S. M., Leohr, J., Lin, A. B., Li, L. Q., McGlothlin, A., Farrington, D. L., Westin, E. H., Cohen, R. B. (2017): Two Phase 1 dose-escalation studies exploring multiple regimens of litronesib (LY2523355), an Eg5 inhibitor, in patients with advanced cancer. *Cancer Chemother Pharmacol* 79, 315-326.
- Ishikawa, K., Kamohara, Y., Tanaka, F., Haraguchi, N., Mimori, K., Inoue, H., Mori, M. (2008): Mitotic centromere-associated kinesin is a novel marker for prognosis and lymph node metastasis in colorectal cancer. *Br J Cancer* 98, 1824-1829.
- Jacobs, R. T., Nare, B., Wring, S. A., Orr, M. D., Chen, D., Sligar, J. M., Jenks, M. X., Noe, R. A., Bowling, T. S., Mercer, L. T., Rewerts, C., Gaukel, E., Owens, J., Parham, R., Randolph, R., Beaudet, B., Bacchi, C. J., Yarlett, N., Plattner, J. J., Freund, Y., Ding, C., Akama, T., Zhang, Y. K., Brun, R., Kaiser, M., Scandale, I., Don, R. (2011): SCYX-7158, an orally-active benzoxaborole for the treatment of stage 2 human African trypanosomiasis. *PLoS Negl Trop Dis* 5, e1151.
- Jetton, N., Rothberg, K. G., Hubbard, J. G., Wise, J., Li, Y., Ball, H. L., Ruben, L. (2009): The cell cycle as a therapeutic target against *Trypanosoma brucei*: Hesperadin inhibits Aurora kinase-1 and blocks mitotic progression in bloodstream forms. *Mol Microbiol* 72, 442-458.

References

- Jeyapragash, A. A., Klein, U. R., Lindner, D., Ebert, J., Nigg, E. A., Conti, E. (2007): Structure of a Survivin-Borealin-INCENP core complex reveals how chromosomal passengers travel together. *Cell* 131, 271-285.
- Jordan, M. A., Thrower, D., Wilson, L. (1992): Effects of vinblastine, podophyllotoxin and nocodazole on mitotic spindles. Implications for the role of microtubule dynamics in mitosis. *J Cell Sci* 102, 401-416.
- Kaiser, M., Bray, M. A., Cal, M., Bourdin Trunz, B., Torreele, E., Brun, R. (2011): Antitrypanosomal activity of fexinidazole, a new oral nitroimidazole drug candidate for treatment of sleeping sickness. *Antimicrob Agents Chemother* 55, 5602-5608.
- Kaiser, P., Wohlschlegel, J. (2005): Identification of ubiquitination sites and determination of ubiquitin-chain architectures by mass spectrometry. *Methods Enzymol* 399, 266-277.
- Kalderon, D., Roberts, B. L., Richardson, W. D., Smith, A. E. (1984): A short amino acid sequence able to specify nuclear location. *Cell* 39, 499-509.
- Kallio, M. J., McClelland, M. L., Stukenberg, P. T., Gorbsky, G. J. (2002): Inhibition of aurora B kinase blocks chromosome segregation, overrides the spindle checkpoint, and perturbs microtubule dynamics in mitosis. *Curr Biol* 12, 900-905.
- Kantarjian, H. M., Padmanabhan, S., Stock, W., Tallman, M. S., Curt, G. A., Li, J., Osmukhina, A., Wu, K., Huszar, D., Borthukar, G., Faderl, S., Garcia-Manero, G., Kadia, T., Sankhala, K., Odenike, O., Altman, J. K., Minden, M. (2012): Phase I/II multicenter study to assess the safety, tolerability, pharmacokinetics and pharmacodynamics of AZD4877 in patients with refractory acute myeloid leukemia. *Invest New Drugs* 30, 1107-1115.
- Kapitein, L. C., Peterman, E. J., Kwok, B. H., Kim, J. H., Kapoor, T. M., Schmidt, C. F. (2005): The bipolar mitotic kinesin Eg5 moves on both microtubules that it crosslinks. *Nature* 435, 114-118.
- Kieft, R., Capewell, P., Turner, C. M., Veitch, N. J., MacLeod, A., Hajduk, S. (2010): Mechanism of *Trypanosoma brucei gambiense* (group 1) resistance to human trypanosome lytic factor. *Proc Natl Acad Sci* 107, 16137-16141.
- Kikkawa, M., Sablin, E. P., Okada, Y., Yajima, H., Fletterick, R. J., Hirokawa, N. (2001): Switch-based mechanism of kinesin motors. *Nature* 411, 439-445.
- King, S. M., Hyams, J. S., Luba, A. (1982): Absence of microtubule sliding and an analysis of spindle formation and elongation in isolated mitotic spindles from the yeast *Saccharomyces cerevisiae*. *J Cell Biol* 94, 341-349.
- Klebe, C., Prinz, H., Wittinghofer, A., Goody, R. S. (1995): The kinetic mechanism of Ran--nucleotide exchange catalyzed by RCC1. *Biochemistry* 34, 12543-12552.

References

- Klein, U. R., Nigg, E. A., Gruneberg, U. (2006): Centromere targeting of the chromosomal passenger complex requires a ternary subcomplex of Borealin, Survivin, and the N-terminal domain of INCENP. *Mol Biol Cell* 17, 2547-2558.
- Kline-Smith, S. L., Khodjakov, A., Hergert, P., Walczak, C. E. (2004): Depletion of centromeric MCAK leads to chromosome congression and segregation defects due to improper kinetochore attachments. *Mol Biol Cell* 15, 1146-1159.
- Knowlton, A. L., Lan, W., Stukenberg, P. T. (2006): Aurora B is enriched at merotelic attachment sites, where it regulates MCAK. *Curr Biol* 16, 1705-1710.
- Kobayashi, T., Tsang, W. Y., Li, J., Lane, W., Dynlacht, B. D. (2011): Centriolar kinesin Kif24 interacts with CP110 to remodel microtubules and regulate ciliogenesis. *Cell* 145, 914-925.
- Kohl, L., Robinson, D., Bastin, P. (2003): Novel roles for the flagellum in cell morphogenesis and cytokinesis of trypanosomes. *EMBO J* 22, 5336-5346.
- Kohl, L., Sherwin, T., Gull, K. (1999): Assembly of the paraflagellar rod and the flagellum attachment zone complex during the *Trypanosoma brucei* cell cycle. *J Eukaryot Microbiol* 46, 105-109.
- Kollmar, M. (2016): Fine-Tuning Motile Cilia and Flagella: Evolution of the dynein motor proteins from plants to humans at high resolution. *Mol Biol Evol* 33, 3249-3267.
- Kosugi, S., Hasebe, M., Matsumura, N., Takashima, H., Miyamoto-Sato, E., Tomita, M., Yanagawa, H. (2009a): Six classes of nuclear localization signals specific to different binding grooves of importin alpha. *J Biol Chem* 284, 478-485.
- Kosugi, S., Hasebe, M., Tomita, M., Yanagawa, H. (2009b): Systematic identification of cell cycle-dependent yeast nucleocytoplasmic shuttling proteins by prediction of composite motifs. *Proc Natl Acad Sci* 106, 10171-10176.
- Kull, F. J., Endow, S. A. (2002): Kinesin: switch I & II and the motor mechanism. *J Cell Sci* 115, 15-23.
- Kull, F. J., Sablin, E. P., Lau, R., Fletterick, R. J., Vale, R. D. (1996): Crystal structure of the kinesin motor domain reveals a structural similarity to myosin. *Nature* 380, 550-555.
- Kull, F. J., Vale, R. D., Fletterick, R. J. (1998): The case for a common ancestor: kinesin and myosin motor proteins and G proteins. *J Muscle Res Cell Motil* 19, 877-886.
- Kumar, P., Wang, C. C. (2005): Depletion of anaphase-promoting complex or cyclosome (APC/C) subunit homolog APC1 or CDC27 of *Trypanosoma brucei* arrests the procyclic form in metaphase but the bloodstream form in anaphase. *J Biol Chem* 280, 31783-31791.
- Kumar, P., Wang, C. C. (2006): Dissociation of cytokinesis initiation from mitotic control in a eukaryote. *Eukaryot Cell* 5, 92-102.

References

- Lacomble, S., Vaughan, S., Deghelt, M., Moreira-Leite, F. F., Gull, K. (2012): A *Trypanosoma brucei* protein required for maintenance of the flagellum attachment zone and flagellar pocket ER domains. *Protist* 163, 602-615.
- Lacomble, S., Vaughan, S., Gadelha, C., Morphew, M. K., Shaw, M. K., McIntosh, J. R., Gull, K. (2010): Basal body movements orchestrate membrane organelle division and cell morphogenesis in *Trypanosoma brucei*. *J Cell Sci* 123, 2884-2891.
- la Cour, T., Kiemer, L., Mølgaard, A., Gupta, R., Skriver, K., Brunak, S. (2004): Analysis and prediction of leucine-rich nuclear export signals. *Protein Eng Des Sel* 17, 527-536.
- Laemmli, U. K. (1970): Cleavage of structural proteins during the assembly of the head bacteriophage T4. *Nature* 227, 680-685.
- Lama, R., Sandhu, R., Zhong, B., Li, B., Su, B. (2012): Identification of selective tubulin inhibitors as potential anti-trypanosomal agents. *Bioorg Med Chem Lett* 22, 5508-5516.
- Lampson, M. A., Renduchitala, K., Khodjakov, A., Kapoor, T. M. (2004): Correcting improper chromosome-spindle attachments during cell division. *Nat Cell Biol* 6, 232-237.
- Lan, W., Zhang, X., Kline-Smith, S. L., Rosasco, S. E., Barrett-Wilt, G. A., Shabanowitz, J., Hunt, D. F., Walczak, C. E., Stukenberg, P. T. (2004): Aurora B phosphorylates centromeric MCAK and regulates its localization and microtubule depolymerization activity. *Curr Biol* 14, 273-286.
- Lawrence, C. J., Dawe, R. K., Christie, K. R., Cleveland, D. W., Dawson, S. C., Endow, S. A., Goldstein, L. S., Goodson, H. V., Hirokawa, N., Howard, J., Malmberg, R. L., McIntosh, J. R., Miki, H., Mitchison, T. J., Okada, Y., Reddy, A. S., Saxton, W. M., Schliwa, M., Scholey, J. M., Vale, R. D., Walczak, C. E., Wordeman, L. (2004): A standardized kinesin nomenclature. *J Cell Biol* 167, 19-22.
- Lee, S. J., Matsuura, Y., Liu, S. M., Stewart, M. (2005): Structural basis for nuclear import complex dissociation by RanGTP. *Nature* 435, 693-696.
- Legros, D., Fournier, C., Gastellu Etchegorry, M., Maiso, F., Szumilin, E. (1999): Therapeutic failure of melarsoprol among patients treated for late stage *T.b. gambiense* human African trypanosomiasis in Uganda. *Bull Soc Pathol Exot* 92, 171-172.
- Li, Z., Gourguechon, S., Wang, C. C. (2007): Tousled-like kinase in a microbial eukaryote regulates spindle assembly and S-phase progression by interacting with Aurora kinase and chromatin assembly factors. *J Cell Sci* 120, 3883-3894.
- Li, Z., Lee, J. H., Chu, F., Burlingame, A. L., Günzl, A., Wang, C. C. (2008a): Identification of a novel chromosomal passenger complex and its unique localization during cytokinesis in *Trypanosoma brucei*. *PLoS One* 3, e2354.

References

- Li, Z., Umeyama, T., Wang, C. C. (2008b): The chromosomal passenger complex and a mitotic kinesin interact with the Tousled-like kinase in trypanosomes to regulate mitosis and cytokinesis. *PLoS One* 3, e3814.
- Li, Z., Umeyama, T., Wang, C. C. (2009): The Aurora Kinase in *Trypanosoma brucei* plays distinctive roles in metaphase-anaphase transition and cytokinetic initiation. *PLoS Pathog* 5, e1000575.
- Li, Z., Wang, C. C. (2003): A PHO80-like cyclin and a B-type cyclin control the cell cycle of the procyclic form of *Trypanosoma brucei*. *J Biol Chem* 278, 20652-20658.
- Li, Z., Wang, C. C. (2006): Changing roles of aurora-B kinase in two life cycle stages of *Trypanosoma brucei*. *Eukaryot Cell* 5, 1026-1035.
- Li, Z., Zou, C. B., Yao, Y., Hoyt, M. A., McDonough, S., Mackey, Z. B., Coffino, P., Wang, C. C. (2002): An easily dissociated 26 S proteasome catalyzes an essential ubiquitin-mediated protein degradation pathway in *Trypanosoma brucei*. *J Biol Chem* 277, 15486-15498.
- Lips, S., Geuskens, M., Paturiaux-Hanocq, F., Hanocq-Quertier, J., Pays, E. (1996): The esag 8 gene of *Trypanosoma brucei* encodes a nuclear protein. *Mol Biochem Parasitol* 79, 113-117.
- LoRusso, P. M., Goncalves, P. H., Casetta, L., Carter, J. A., Litwiler, K., Roseberry, D., Rush, S., Schreiber, J., Simmons, H. M., Ptaszynski, M., Sausville, E. A. (2015): First-in-human phase 1 study of filanesib (ARRY-520), a kinesin spindle protein inhibitor, in patients with advanced solid tumors. *Invest New Drugs* 33, 440-449.
- MacGregor, P., Savill, N. J., Hall, D., Matthews, K. R. (2011): Transmission stages dominate trypanosome within-host dynamics during chronic infections. *Cell Host Microbe* 9, 310-318.
- Mackay, A. M., Eckley, D. M., Chue, C., Earnshaw, W. C. (1993): Molecular analysis of the INCENPs (inner centromere proteins): separate domains are required for association with microtubules during interphase and with the central spindle during anaphase. *J Cell Biol* 123, 373-385.
- Mandelkow, E. M., Mandelkow, E., Milligan, R. A. (1991): Microtubule dynamics and microtubule caps: a time-resolved cryo-electron microscopy study. *J Cell Biol* 114, 977-991.
- Maney, T., Wagenbach, M., Wordeman, L. (2001): Molecular dissection of the microtubule depolymerizing activity of mitotic centromere-associated kinesin. *J Biol Chem* 276, 34753-34758.
- Manning, A. L., Ganem, N. J., Bakhoum, S. F., Wagenbach, M., Wordeman, L., Compton, D. A. (2007): The kinesin-13 proteins Kif2a, Kif2b, and Kif2c/MCAK have distinct roles during mitosis in human cells. *Mol Biol Cell* 18, 2970-2979.

References

- Mao, Y., Yan, R., Li, A., Zhang, Y., Li, J., Du, H., Chen, B., Wie, W., Zhang, Y., Summers, C., Zheng, H., Li, H. (2015): Lentiviral vectors mediate long-term and high efficiency transgene expression in HEK 293T cells. *Int J Med Sci* 12, 407-415.
- Marchal, C., Haguenauer-Tsapis, R., Urban-Grimal, D. (1998): A PEST-like sequence mediates phosphorylation and efficient ubiquitination of yeast uracil permease. *Mol Cell Biol* 18, 314-321.
- Marchetti, M. A., Tschudi, C., Kwon, H., Wolin, S. L., Ullu, E. (2000): Import of proteins into the trypanosome nucleus and their distribution at karyokinesis. *J Cell Sci* 113, 899-906.
- Matovu, E., Enyaru, J. C., Legros, D., Schmid, C., Seebeck, T., Kaminsky, R. (2001): Melarsoprol refractory *T. b. gambiense* from Omugo, north-western Uganda. *Trop Med Int Health* 6, 407-411.
- Mayr, M. I., Hümmer, S., Bormann, J., Grüner, T., Adio, S., Woehlke, G., Mayer, T. U. (2007): The human kinesin Kif18A is a motile microtubule depolymerase essential for chromosome congression. *Curr Biol* 17, 488-498.
- McAllaster, M. R., Ikeda, K. N., Lozano-Núñez, A., Anrather, D., Unterwurzacher, V., Gossenreiter, T., Perry, J. A., Crickley, R., Mercadante, C. J., Vaughan, S., de Graffenried, C. L. (2015): Proteomic identification of novel cytoskeletal proteins associated with *TbPLK*, an essential regulator of cell morphogenesis in *Trypanosoma brucei*. *Mol Biol Cell* 26, 3013-3029.
- Mencoboni, M., Filiberti, R. A., Taveggia, P., Del Corso, L., Del Conte, A., Covesnon, M. G., Puccetti, C., Donati, S., Auriati, L., Amoroso, D., Camerini, A. (2017): Safety of first-line chemotherapy with metronomic single-agent oral vinorelbine in elderly patients with NSCLC. *Anticancer Res* 37, 3189-3194.
- Mennella, V., Rogers, G. C., Rogers, S. L., Buster, D. W., Vale, R. D., Sharp, D. J. (2005): Functionally distinct kinesin-13 family members cooperate to regulate microtubule dynamics during interphase. *Nat Cell Biol* 7, 235-245.
- Meyer, R. D., Srinivasan, S., Singh, A. J., Mahoney, J. E., Gharahassanlou, K. R., Rahimi, N. (2011): PEST motif serine and tyrosine phosphorylation controls vascular endothelial growth factor receptor 2 stability and downregulation. *Mol Cell Biol* 31, 2010-2025.
- Miki, H., Setou, M., Kaneshiro, K., Hirokawa, N. (2001): All kinesin superfamily protein, KIF, genes in mouse and human. *Proc Natl Acad Sci* 98, 7004-7011.
- Miller, R. K., Heller, K. K., Frisén, L., Wallack, D. L., Loayza, D., Gammie, A. E., Rose, M. D. (1998): The kinesin-related proteins, Kip2p and Kip3p, function differently in nuclear migration in yeast. *Mol Biol Cell* 9, 2051-2068.

References

- Minotti, A. M., Barlow, S. B., Cabral, F. (1991): Resistance to antimitotic drugs in Chinese hamster ovary cells correlates with changes in the level of polymerized tubulin. *J Biol Chem* 266, 3987-3994.
- Mitchison, T. J. (1993): Localization of an exchangeable GTP binding site at the plus end of microtubules. *Science* 261, 1044-1047.
- Mitchison, T., Kirschner, M. (1984): Dynamic instability of microtubule growth. *Nature* 312, 237-242.
- Miyamoto, T., Hosoba, K., Ochiai, H., Royba, E., Izumi, H., Sakuma, T., Yamamoto, T., Dynlacht, B. D., Matsuura, S. (2015): The microtubule-depolymerizing activity of a mitotic kinesin protein KIF2A drives primary cilia disassembly coupled with cell proliferation. *Cell Rep* 10, 664–673.
- Moens, P. B., Rapport, E. (1971): Spindles, spindle plaques, and meiosis in the yeast *Saccharomyces cerevisiae* (Hansen). *J Cell Biol* 50, 344-361.
- Moore, A. T., Rankin, K. E., von Dassow, G., Peris, L., Wagenbach, M., Ovechkina, Y., Andrieux, A., Job, D., Wordeman, L. (2005): MCAK associates with the tips of polymerizing microtubules. *J Cell Biol* 169, 391-397.
- Moore, A., Wordeman, L. (2004): C-terminus of mitotic centromere-associated kinesin (MCAK) inhibits its lattice-stimulated ATPase activity. *Biochem J* 383, 227-235.
- Moore, C. A., Yu, M., Guo, J., Beraud, C., Sakowicz, R., Milligan, R. A. (2002): A mechanism for microtubule depolymerization by KinI kinesins. *Mol Cell* 9, 903-909.
- Moreira-Leite, F. F., Sherwin, T., Kohl, L., Gull, K. (2001): A trypanosome structure involved in transmitting cytoplasmic information during cell division. *Science* 294, 610-612.
- Morrison, L. J., Majiwa, P., Read, A. F., Barry, J. D. (2005): Probabilistic order in antigenic variation of *Trypanosoma brucei*. *Int J Parasitol* 35, 961-972.
- Mukai, H., Hagiwara, Y., Imi, K., Isaka, H., Watanabe, K., Matsuyama, Y.; SELECT BC Study Group (2017): The impact of treatment preferences in second-line chemotherapy on the prognosis of HER2-negative metastatic breast cancer. *Oncology* 10.1159/000479033.
- Mumba Ngoyi, D., Lejon, V., Pyana, P., Boelaert, M., Ilunga, M., Menten, J., Mulunda, J. .P, Van Nieuwenhove, S., Muyembe Tamfum, J. J., Büscher, P. (2010): How to shorten patient follow-up after treatment for *Trypanosoma brucei gambiense* sleeping sickness. *J Infect Dis* 201, 453-463.
- Murata-Hori, M., Tatsuka, M., Wang, Y. L. (2002): Probing the dynamics and functions of aurora B kinase in living cells during mitosis and cytokinesis. *Mol Biol Cell* 13, 1099-1108.

References

- Mutomba, M. C., To, W. Y., Hyun, W. C., Wang, C. C. (1997): Inhibition of proteasome activity blocks cell cycle progression at specific phase boundaries in African trypanosomes. *Mol Biochem Parasitol* 90, 491-504.
- Naber, N., Minehardt, T. J., Rice, S., Chen, X., Grammer, J., Matuska, M., Vale, R. D., Kollman, P. A., Car, R., Yount, R. G., Cooke, R., Pate, E. (2003): Closing of the nucleotide pocket of kinesin-family motors upon binding to microtubules. *Science* 300, 798-801.
- Nagahara, M., Nishida, N., Iwatsuki, M., Ishimaru, S., Mimori, K., Tanaka, F., Nakagawa, T., Sato, T., Sugihara, K., Hoon, D. S., Mori, M. (2011): Kinesin 18A expression: clinical relevance to colorectal cancer progression. *Int J Cancer* 129, 2543-2552.
- Nakamura, Y., Tanaka, F., Haraguchi, N., Mimori, K., Matsumoto, T., Inoue, H., Yanaga, K., Mori, M. (2007): Clinicopathological and biological significance of mitotic centromere-associated kinesin overexpression in human gastric cancer. *Br J Cancer* 97, 543-549.
- Nerusheva, O. O., Akiyoshi, B. (2016): Divergent polo box domains underpin the unique kinetoplastid kinetochore. *Open Biol* 6, pii: 150206.
- Noble, R. L., Beer, C. T., Cuttis, J. H. (1958): Role of chance observations in chemotherapy: *Vinca rosea*. *Ann N Y Acad Sci* 76, 882-894.
- Nogales, E., Whittaker, M., Milligan, R. A., Downing, K. H. (1999): High-resolution model of the microtubule. *Cell* 96, 79-88.
- Nogales, E., Wolf, S. G., Downing, K. H. (1998): Structure of the alpha beta tubulin dimer by electron crystallography. *Nature* 391, 199-203.
- Noujaim, M., Bechstedt, S., Wiczeorek, M., Brouhard, G. J. (2014): Microtubules accelerate the kinase activity of Aurora-B by a reduction in dimensionality. *PLoS One* 9, e86786.
- Obado, S. O., Bot, C., Nilsson, D., Andersson, B., Kelly, J. M. (2007): Repetitive DNA is associated with centromeric domains in *Trypanosoma brucei* but not *Trypanosoma cruzi*. *Genome Biol* 8, R37.
- Oberholzer, M., Marti, G., Baresic, M., Kunz, S., Hemphill, A., Seebeck, T. (2007): The *Trypanosoma brucei* cAMP phosphodiesterases *TbrPDEB1* and *TbrPDEB2*: flagellar enzymes that are essential for parasite virulence. *FASEB J* 21, 720-731.
- Odiit, M., Kansime, F., Enyaru, J. C. (1997): Duration of symptoms and case fatality of sleeping sickness caused by *Trypanosoma brucei rhodesiense* in Tororo, Uganda. *East Afr Med J* 74, 792-795.
- Ogawa, T., Nitta, R., Okada, Y., Hirokawa, N. (2004): A common mechanism for microtubule destabilizers-M type kinesins stabilize curling of the protofilament using the class-specific neck and loops. *Cell* 116, 591-602.

References

- Ogbadoyi, E., Ersfeld, K., Robinson, D., Sherwin, T., Gull, K. (2000): Architecture of the *Trypanosoma brucei* nucleus during interphase and mitosis. *Chromosoma* 108, 501-513.
- Ogbadoyi, E. O., Robinson, D. R., Gull, K. (2003): A high-order trans-membrane structural linkage is responsible for mitochondrial genome positioning and segregation by flagellar basal bodies in trypanosomes. *Mol Biol Cell* 14, 1769-1779.
- Onishi, H., Kojima, S., Katoh, K., Fujiwara, K., Martinez, H. M., Morales, M. F. (1998): Functional transitions in myosin: formation of a critical salt-bridge and transmission of effect to the sensitive tryptophan. *Proc Natl Acad Sci* 95, 6653-6658.
- O'Reilly, A. J., Dacks, J. B., Field, M. C. (2011): Evolution of the karyopherin- β family of nucleocytoplasmic transport factors; ancient origins and continued specialization. *PLoS One* 6, e19308.
- Ovechkina, Y., Wagenbach, M., Wordeman, L. (2002): K-loop insertion restores microtubule depolymerizing activity of a "neckless" MCAK mutant. *J Cell Biol* 159, 557-562.
- Pakdel, F., Le Goff, P., Katzenellenbogen, B. S. (1993): An assessment of the role of domain F and PEST sequences in estrogen receptor half-life and bioactivity. *J Steroid Biochem Mol Biol* 46, 663-672.
- Pépin, J., Milord, F., Khonde, A., Niyonsenga, T., Loko, L., Mpia, B. (1994): *Gambiense* trypanosomiasis: frequency of, and risk factors for, failure of melarsoprol therapy. *Trans R Soc Trop Med Hyg* 88, 447-452.
- Pérez-Morga, D., Vanhollebeke, B., Paturiaux-Hanocq, F., Nolan, D. P., Lins, L., Homblé, F., Vanhamme, L., Tebabi, P., Pays, A., Poelvoorde, P., Jacquet, A., Brasseur, R., Pays, E. (2005): Apolipoprotein L-I promotes trypanosome lysis by forming pores in lysosomal membranes. *Science* 309, 469-472.
- Peris, L., Wagenbach, M., Lafanechère, L., Brocard, J., Moore, A. T., Kozielski, F., Job, D., Wordeman, L., Andrieux, A. (2009): Motor-dependent microtubule disassembly driven by tubulin tyrosination. *J Cell Biol* 185, 1159-1166.
- Pfleger, C. M., Kirschner, M. W. (2000): The KEN box: an APC recognition signal distinct from the D box targeted by Cdh1. *Genes Dev* 14, 655-665.
- Ploubidou, A., Robinson, D. R., Docherty, R. C., Ogbadoyi, E. O., Gull, K. (1999): Evidence for novel cell cycle checkpoints in trypanosomes: kinetoplast segregation and cytokinesis in the absence of mitosis. *J Cell Sci* 112, 4641-4650.

References

- Priotto, G., Kasparian, S., Mutombo, W., Ngouama, D., Ghorashian, S., Arnold, U., Ghabri, S., Baudin, E., Buard, V., Kazadi-Kyanza, S., Ilunga, M., Mutangala, W., Pohlig, G., Schmid, C., Karunakara, U., Torreele, E., Kande, V. (2009): Nifurtimox-eflornithine combination therapy for second-stage African *Trypanosoma brucei gambiense* trypanosomiasis: a multicentre, randomised, phase III, non-inferiority trial. *Lancet* 374, 56-64.
- Purcell, J. W., Davis, J., Reddy, M., Martin, S., Samayoa, K., Vo, H., Thomsen, K., Bean, P., Kuo, W. L., Ziyad, S., Billig, J., Feiler, H. S., Gray, J. W., Wood, K. W., Cases, S. (2010): Activity of the kinesin spindle protein inhibitor ispinesib (SB-715992) in models of breast cancer. *Clin Cancer Res* 16, 566-576.
- Raper, J., Fung, R., Ghiso, J., Nussenzweig, V., Tomlinson, S. (1999): Characterization of a novel trypanosome lytic factor from human serum. *Infect Immun* 67, 1910-1916.
- Ravelli, R. B., Gigant, B., Curmi, P. A., Jourdain, I., Lachkar, S., Sobel, A., Knossow, M. (2004): Insight into tubulin regulation from a complex with colchicine and a stathmin-like domain. *Nature* 428, 198-202.
- Rice, S., Lin, A. W., Safer, D., Hart, C. L., Naber, N., Carragher, B. O., Cain, S. M., Pechatnikova, E., Wilson-Kubalek, E. M., Whittaker, M., Pate, E., Cooke, R., Taylor, E. W., Milligan, R. A., Vale, R. D. (1999): A structural change in the kinesin motor protein that drives motility. *Nature* 402, 778-784.
- Richards, T. A., Cavalier-Smith, T. (2005): Myosin domain evolution and the primary divergence of eukaryotes. *Nature* 436, 1113-1118.
- Rizk, R. S., Bohannon, K. P., Wetzel, L. A., Powers, J., Shaw, S. L., Walczak, C. E. (2009): MCAK and paclitaxel have differential effects on spindle microtubule organization and dynamics. *Mol Biol Cell* 20, 1639-1651.
- Robays, J., Nyamowala, G., Sese, C., Betu Ku Mesu Kande, V., Lutumba, P., Van der Veken, W., Boelaert, M. (2008): High failure rates of melarsoprol for sleeping sickness, Democratic Republic of Congo. *Emerg Infect Dis* 14, 966-967.
- Robbins, J., Dilworth, S. M., Laskey, R. A., Dingwall, C. (1991): Two interdependent basic domains in nucleoplasmin nuclear targeting sequence: identification of a class of bipartite nuclear targeting sequence. *Cell* 64, 615-623.
- Robinow, C. F., Marak, J. (1966): A fiber apparatus in the nucleus of the yeast cell. *J Cell Biol* 29, 129-151.
- Robinson, N. P., Burman, N., Melville, S. E., Barry, J. D. (1999): Predominance of duplicative VSG gene conversion in antigenic variation in African trypanosomes. *Mol Cell Biol* 19, 5839-5846.

References

- Robinson, D. R., Gull, K. (1991): Basal body movements as a mechanism for mitochondrial genome segregation in the trypanosome cell cycle. *Nature* 352, 731-733.
- Robinson, D. R., Sherwin, T., Ploubidou, A., Byard, E. H., Gull, K. (1995): Microtubule polarity and dynamics in the control of organelle positioning, segregation, and cytokinesis in the trypanosome cell cycle. *J Cell Biol* 128, 1163-1172.
- Rogers, G. C., Rogers, S. L., Schwimmer, T. A., Ems-McClung, S. C., Walczak, C. E., Vale, R. D., Scholey, J. M., Sharp, D. J. (2004): Two mitotic kinesins cooperate to drive sister chromatid separation during anaphase. *Nature* 427, 364-370.
- Rogers, S., Wells, R., Rechsteiner, M. (1986): Amino acid sequences common to rapidly degraded proteins: the PEST hypothesis. *Science* 234, 364-368.
- Roof, D. M., Meluh, P. B., Rose, M. D. (1992): Kinesin-related proteins required for assembly of the mitotic spindle. *J Cell Biol* 118, 95-108.
- Rosasco-Nitcher, S. E., Lan, W., Khorasanizadeh, S., Stukenberg, P. T. (2008): Centromeric Aurora-B activation requires TD-60, microtubules, and substrate priming phosphorylation. *Science* 319, 469-472.
- Rotureau, B., Subota, I., Buisson, J., Bastin, P. (2012): A new asymmetric division contributes to the continuous production of infective trypanosomes in the tsetse fly. *Development* 139, 1842-1850.
- Sablin, E. P., Kull, F. J., Cooke, R., Vale, R. D., Fletterick, R. J. (1996): Crystal structure of the motor domain of the kinesin-related motor ncd. *Nature* 380, 555-559.
- Sakowicz, R., Finer, J. T., Beraud, C., Crompton, A., Lewis, E., Fritsch, A., Lee, Y., Mak, J., Moody, R., Turincio, R., Chabala, J. C., Gonzales, P., Roth, S., Weitman, S., Wood, K. W. (2004): Antitumor activity of a kinesin inhibitor. *Cancer Res* 64, 3276–3280.
- Salama, S. R., Hendricks, K. B., Thorner, J. (1994): G1 cyclin degradation: the PEST motif of yeast Cln2 is necessary, but not sufficient, for rapid protein turnover. *Mol Cell Biol* 14, 7953-7966.
- Sanhaji, M., Friel, C. T., Kreis, N. N., Krämer, A., Martin, C., Howard, J., Strebhardt, K., Yuan, J. (2010): Functional and spatial regulation of mitotic centromere-associated kinesin by cyclin-dependent kinase 1. *Mol Cell Biol* 30, 2594-2607.
- Sanhaji, M., Ritter, A., Belsham, H. R., Friel, C. T., Roth, S., Louwen, F., Yuan, J. (2014): Polo-like kinase 1 regulates the stability of the mitotic centromere-associated kinesin in mitosis. *Oncotarget* 5, 3130-3144.

References

- Santaguida, S., Vernieri, C., Villa, F., Ciliberto, A., Musacchio, A. (2011): Evidence that Aurora B is implicated in spindle checkpoint signalling independently of error correction. *EMBO J* 30, 1508-1519.
- Sasaki, N., Shimada, T., Sutoh, K. (1998): Mutational analysis of the switch II loop of *Dictyostelium* myosin II. *J Biol Chem* 273, 20334-20340.
- Saunders, W., Hornack, D., Lengyel, V., Deng, C. (1997): The *Saccharomyces cerevisiae* kinesin-related motor Kar3p acts at preanaphase spindle poles to limit the number and length of cytoplasmic microtubules. *J Cell Biol* 137, 417-431.
- Schaar, B. T., Chan, G. K., Maddox, P., Salmon, E. D., Yen, T. J. (1997): CENP-E function at kinetochores is essential for chromosome alignment. *J Cell Biol* 139, 1373-1382.
- Scherz, A., Feller, K., Berezowska, S., Genitsch, V., Zweifel, M. (2017): Successful treatment of pituitary germinoma with etoposide, cisplatin, vincristine, methotrexate and bleomycin chemotherapy without radiotherapy. *Anticancer Res* 37, 3111-3115.
- Schibler, M. J., Cabral, F. (1986): Taxol-dependent mutants of Chinese hamster ovary cells with alterations in alpha- and beta-tubulin. *J Cell Biol* 102, 1522-1531.
- Schlaeppli, K., Deflorin, J., Seebeck, T. (1989): The major component of the paraflagellar rod of *Trypanosoma brucei* is a helical protein that is encoded by two identical, tandemly linked genes. *J Cell Biol* 109, 1695-1709.
- Schnupf, P., Portnoy, D. A., Decatur, A. L. (2006): Phosphorylation, ubiquitination and degradation of listeriolysin O in mammalian cells: role of the PEST-like sequence. *Cell Microbiol* 8, 353-264.
- Scholey, J. M., Heuser, J., Yang, J. T., Goldstein, L. S. (1989): Identification of globular mechanochemical heads of kinesin. *Nature* 338, 355-357.
- Scott, V., Sherwin, T., Gull, K. (1997): Gamma-tubulin in trypanosomes: molecular characterisation and localisation to multiple and diverse microtubule organising centres. *J Cell Sci* 110, 157-168.
- Schiff, P. B., Fant, J., Horwitz, S. B. (1979): Promotion of microtubule assembly in vitro by taxol. *Nature* 277, 665-667.
- Sessa, F., Mapelli, M., Ciferri, C., Tarricone, C., Areces, L. B., Schneider, T. R., Stukenberg, P. T., Musacchio, A. (2005): Mechanism of Aurora B activation by INCENP and inhibition by hesperadin. *Mol Cell* 18, 379-391.
- Shao, H., Huang, Y., Zhang, L., Yuan, K., Chu, Y., Dou, Z., Jin, C., Garcia-Barrio, M., Liu, X., Yao, X. (2015): Spatiotemporal dynamics of Aurora B-PLK1-MCAK signaling axis orchestrates kinetochore bi-orientation and faithful chromosome segregation. *Sci Rep* 5:12204.

References

- Sheriff, O., Lim, L. F., He, C. Y. (2014): Tracking the biogenesis and inheritance of subpellicular microtubule in *Trypanosoma brucei* with inducible YFP- α -tubulin. *Biomed Res Int* 893272.
- Sherwin, T., Gull, K. (1989): The cell division cycle of *Trypanosoma brucei brucei*: timing of event markers and cytoskeletal modulations. *Philos Trans R Soc Lond B Biol Sci* 323, 573-88.
- Shimada, T., Sasaki, N., Ohkura, R., Sutoh, K. (1997): Alanine scanning mutagenesis of the switch I region in the ATPase site of *Dictyostelium discoideum* myosin II. *Biochemistry* 36, 14037-14043.
- Shimo, A., Tanikawa, C., Nishidate, T., Lin, M. L., Matsuda, K., Park, J. H., Ueki, T., Ohta, T., Hirata, K., Fukuda, M., Nakamura, Y., Katagiri, T. (2008): Involvement of kinesin family member 2C/mitotic centromere-associated kinesin overexpression in mammary carcinogenesis. *Cancer Sci* 99, 62-70.
- Shipley, K., Hekmat-Nejad, M., Turner, J., Moores, C., Anderson, R., Milligan, R., Sakowicz, R., Fletterick, R. (2004): Structure of a kinesin microtubule depolymerization machine. *EMBO J* 23, 1422-1432.
- Smith, P., Ho, C. K., Takagi, Y., Djaballah, H., Shuman, S. (2016): Nanomolar inhibitors of *Trypanosoma brucei* RNA triphosphatase. *MBio* 7:e00058-16.
- Sproul, L. R., Anderson, D. J., Mackey, A. T., Saunders, W. S., Gilbert, S. P. (2005): Cik1 targets the minus-end kinesin depolymerase kar3 to microtubule plus ends. *Curr Biol* 15, 1420-1427.
- Stephens, N. A., Hajduk, S. L. (2011): Endosomal localization of the serum resistance-associated protein in African trypanosomes confers human infectivity. *Eukaryot Cell* 10, 1023-1033.
- Stewart, S., Fang, G. (2005): Destruction box-dependent degradation of aurora B is mediated by the anaphase-promoting complex/cyclosome and Cdh1. *Cancer Res* 65, 8730-8735.
- Straight, A. F., Sedat, J. W., Murray, A. W. (1998): Time-lapse microscopy reveals unique roles for kinesins during anaphase in budding yeast. *J Cell Biol* 143, 687-694.
- Stumpff, J., Du, Y., English, C. A., Maliga, Z., Wagenbach, M., Asbury, C. L., Wordeman, L., Ohi, R. (2011): A tethering mechanism controls the processivity and kinetochore-microtubule plus-end enrichment of the kinesin-8 Kif18A. *Mol Cell* 43, 764-775.
- Stumpff, J., von Dassow, G., Wagenbach, M., Asbury, C., Wordeman, L. (2008): The kinesin-8 motor Kif18A suppresses kinetochore movements to control mitotic chromosome alignment. *Dev Cell* 14, 252-262.

References

- Stumpff, J., Wagenbach, M., Franck, A., Asbury, C. L., Wordeman, L. (2012): Kif18A and chromokinesins confine centromere movements via microtubule growth suppression and spatial control of kinetochore tension. *Dev Cell* 22, 1017-1029.
- Talapatra, S. K., Harker, B., Welburn, J. P. (2015): The C-terminal region of the motor protein MCAK controls its structure and activity through a conformational switch. *Elife* 4, e06421.
- Tetley, L., Vickerman, K. (1985): Differentiation in *Trypanosoma brucei*: host-parasite cell junctions and their persistence during acquisition of the variable antigen coat. *J Cell Sci* 74, 1-19.
- Torreele, E., Bourdin Trunz, B., Tweats, D., Kaiser, M., Brun, R., Mazué, G., Bray, M. A., Pécoul, B. (2010): Fexinidazole--a new oral nitroimidazole drug candidate entering clinical development for the treatment of sleeping sickness. *PLoS Negl Trop Dis* 4, e923.
- Trindade, S., Rijo-Ferreira, F., Carvalho, T., Pinto-Neves, D., Guegan, F., Aresta-Branco, F., Bento, F., Young, S. A., Pinto, A., Van Den Abbeele, J., Ribeiro, R. M., Dias, S., Smith, T. K., Figueiredo, L. M. (2016): *Trypanosoma brucei* parasites occupy and functionally adapt to the adipose tissue in mice. *Cell Host Microbe* 19, 837-848.
- Trivedi, D. V., David, C., Jacobs, D. J., Yengo, C. M. (2012): Switch II mutants reveal coupling between the nucleotide- and actin-binding regions in myosin V. *Biophys J* 102, 2545-2555.
- Troxell, C. L., Sweezy, M. A., West, R. R., Reed, K. D., Carson, B. D., Pidoux, A. L., Cande, W. Z., McIntosh, J. R. (2001): pkl1(+) and klp2(+): Two kinesins of the Kar3 subfamily in fission yeast perform different functions in both mitosis and meiosis. *Mol Biol Cell* 12, 3476-3488.
- Tu, X., Kumar, P., Li, Z., Wang, C. C. (2006): An aurora kinase homologue is involved in regulating both mitosis and cytokinesis in *Trypanosoma brucei*. *J Biol Chem* 281, 9677-9687.
- Tu, X., Wang, C. C. (2004): The involvement of two cdc2-related kinases (CRKs) in *Trypanosoma brucei* cell cycle regulation and the distinctive stage-specific phenotypes caused by CRK3 depletion. *J Biol Chem* 279, 20519-20528.
- Turner, D. L., Weintraub, H. (1994): Expression of achaete-scute homolog 3 in *Xenopus* embryos converts ectodermal cells to a neural fate. *Genes Dev* 8, 1434-1447.
- Tytell, J. D., Sorger, P. K. (2006): Analysis of kinesin motor function at budding yeast kinetochores. *J Cell Biol* 172, 861-874.
- Unsworth, A., Masuda, H., Dhut, S., Toda, T. (2008): Fission yeast kinesin-8 Klp5 and Klp6 are interdependent for mitotic nuclear retention and required for proper microtubule dynamics. *Mol Biol Cell* 19, 5104-5115.

References

- Uzureau, P., Uzureau, S., Lecordier, L., Fontaine, F., Tebabi, P., Homblé, F., Grélard, A., Zhendre, V., Nolan, D. P., Lins, L., Crowet, J. M., Pays, A., Felu, C., Poelvoorde, P., Vanhollebeke, B., Moestrup, S. K., Lyngsø, J., Pedersen, J. S., Mottram, J. C., Dufourc, E. J., Pérez-Morga, D., Pays, E. (2013): Mechanism of *Trypanosoma brucei gambiense* resistance to human serum. *Nature* 501, 430-434.
- Vader, G., Kauw, J. J., Medema, R. H., Lens, S. M. (2006): Survivin mediates targeting of the chromosomal passenger complex to the centromere and midbody. *EMBO Rep* 7, 85-92.
- Vale, R. D., Fletterick, R. J. (1997): The design plan of kinesin motors. *Annu Rev Cell Dev Biol* 13, 745-777.
- Van der Ploeg, L. H., Cornelissen, A. W., Barry, J. D., Borst, P. (1984a): Chromosomes of kinetoplastida. *EMBO J* 3, 3109-3115.
- Van der Ploeg, L. H., Schwartz, D. C., Cantor, C. R., Borst, P. (1984b): Antigenic variation in *Trypanosoma brucei* analyzed by electrophoretic separation of chromosome-sized DNA molecules. *Cell* 37, 77-84.
- Vanhamme, L., Paturiaux-Hanocq, F., Poelvoorde, P., Nolan, D. P., Lins, L., van den Abbeele, J., Pays, A., Tebabi, P., van Xong, H., Jacquet, A., Moguelevsky, N., Dieu, M., Kane, J. P., De Baetselier, P., Brasseur, R., Pays, E. (2003): Apolipoprotein L-I is the trypanosome lytic factor of human serum. *Nature* 422, 83-87.
- Vanhollebeke, B., De Muylder, G., Nielsen, M. J., Pays, A., Tebabi, P., Dieu, M., Raes, M., Moestrup, S. K., Pays, E. (2008): A haptoglobin-hemoglobin receptor conveys innate immunity to *Trypanosoma brucei* in humans. *Science* 320, 677-681.
- Vanhollebeke, B., Lecordier, L., Pérez-Morga, D., Amiguet-Vercher, A., Pays E. (2007): Human serum lyses *Trypanosoma brucei* by triggering uncontrolled swelling of the parasite lysosome. *J Eukaryot Microbiol* 54, 448-451.
- Varga, V., Helenius, J., Tanaka, K., Hyman, A. A., Tanaka, T. U., Howard, J. (2006): Yeast kinesin-8 depolymerizes microtubules in a length-dependent manner. *Nat Cell Biol* 8, 957-962.
- Varma, N., Janic, B., Ali, M., Iskander, A., Arbab, A. (2011): Lentiviral based gene transduction and promoter studies in human hematopoietic stem cells (hHSCs). *J Stem Cells Regen Med* 7, 41-53.
- Vassella, E., Reuner, B., Yutzy, B., Boshart, M. (1997): Differentiation of African trypanosomes is controlled by a density sensing mechanism which signals cell cycle arrest via the cAMP pathway. *J Cell Sci* 110, 2661-2671.
- Vaughan, S., Attwood, T., Navarro, M., Scott, V., McKean, P., Gull, K. (2000): New tubulins in protozoal parasites. *Curr Biol* 10, R258-259.

References

- Vedrenne, C., Giroud, C., Robinson, D. R., Besteiro, S., Bosc, C., Bringaud, F., Baltz, T. (2002): Two related subpellicular cytoskeleton-associated proteins in *Trypanosoma brucei* stabilize microtubules. *Mol Biol Cell* 13, 1058-1070.
- Vickerman, K. (1962): The mechanism of cyclical development in trypanosomes of the *Trypanosoma brucei* sub-group: an hypothesis based on ultrastructural observations. *Trans R Soc Trop Med Hyg* 56, 487-495.
- Vickerman, K. (1969): On the surface coat and flagellar adhesion in trypanosomes. *J Cell Sci* 5, 163-193.
- Vickerman, K. (1994): The evolutionary expansion of the trypanosomatid flagellates. *Int J Parasitol* 24, 1317-1331.
- Vickerman, K., Preston, T. M. (1970): Spindle microtubules in the dividing nuclei of trypanosomes. *J Cell Sci* 6, 365-383.
- Visintin, R., Prinz, S., Amon, A. (1997): CDC20 and CDH1: a family of substrate-specific activators of APC-dependent proteolysis. *Science* 278, 460-463.
- Volkov, O. A., Cosner, C. C., Brockway, A. J., Kramer, M., Booker, M., Zhong, S., Ketcherside, A., Wie, S., Longgood, J., McCoy, M., Richardson, T. E., Wring, S. A., Peel, M., Klinger, J. D., Posner, B. A., De Brabander, J. K., Phillips, M. A. (2017): Identification of *Trypanosoma brucei* AdoMetDC inhibitors using a high-throughput mass spectrometry-based assay. *ACS Infect Dis* 7b00022.
- Wagenbach, M., Domnitz, S., Wordeman, L., Cooper, J. (2008): A kinesin-13 mutant catalytically depolymerizes microtubules in ADP. *J Cell Biol* 183, 617-623.
- Wagner, A. D., Syn, N. L., Moehler, M., Grothe, W., Yong, W. P., Tai, B. C., Ho, J., Unverzagt, S. (2017): Chemotherapy for advanced gastric cancer. *Cochrane Database Syst Rev* 8, CD004064.
- Walczak, C. E., Mitchison, T. J., Desai, A. (1996): XKCM1: a *Xenopus* kinesin-related protein that regulates microtubule dynamics during mitotic spindle assembly. *Cell* 84, 37-47.
- Wang, C. C., Bozdech, Z., Liu, C. L., Shipway, A., Backes, B. J., Harris, J. L., Bogoy, M. (2003): Biochemical analysis of the 20 S proteasome of *Trypanosoma brucei*. *J Biol Chem* 278, 15800-15808.
- Wang, W., Jiang, Q., Argentini, M., Cornu, D., Gigant, B., Knossow, M., Wang, C. (2012): Kif2C minimal functional domain has unusual nucleotide binding properties that are adapted to microtubule depolymerization. *J Biol Chem* 287, 15143-15153.
- Wang, H. W., Nogales, E. (2005): Nucleotide-dependent bending flexibility of tubulin regulates microtubule assembly. *Nature* 435, 911-915.

References

- Wang, W., Shen, T., Guerois, R., Zhang, F., Kuerban, H., Lv, Y., Gigant, B., Knossow, M., Wang, C. (2015): New insights into the coupling between microtubule depolymerization and ATP hydrolysis by kinesin-13 protein Kif2C. *J Biol Chem* 290, 18721-18731.
- Wani, M. C., Taylor, H. L., Wall, M. E., Coggon, P., McPhail, A. T. (1971): Plant antitumor agents. VI. The isolation and structure of taxol, a novel antileukemic and antitumor agent from *Taxus brevifolia*. *J Am Chem Soc* 93, 2325-2327.
- Welburn, J. P., Cheeseman, I. M. (2012): The microtubule-binding protein Cep170 promotes the targeting of the kinesin-13 depolymerase Kif2b to the mitotic spindle. *Mol Biol Cell* 23, 4786-4795.
- Welburn, J. P., Vleugel, M., Liu, D., Yates, J. R. 3rd, Lampson, M. A., Fukagawa, T., Cheeseman, I. M. (2010): Aurora B phosphorylates spatially distinct targets to differentially regulate the kinetochore-microtubule interface. *Mol Cell* 38, 383-392.
- Werbovetz, K. A., Sackett, D. L., Delfín, D., Bhattacharya, G., Salem, M., Obrzut, T., Rattendi, D., Bacchi, C. (2003): Selective antimicrotubule activity of N1-phenyl-3,5-dinitro-N4,N4-di-n-propylsulfanilamide (GB-II-5) against kinetoplastid parasites. *Mol Pharmacol* 64, 1325-1333.
- Wheatley, S. P., Kandels-Lewis, S. E., Adams, R. R., Ainsztein, A. M., Earnshaw, W. C. (2001): INCENP binds directly to tubulin and requires dynamic microtubules to target to the cleavage furrow. *Exp Cell Res* 262, 122-127.
- Wickstead, B., Carrington, J. T., Gluenz, E., Gull, K. (2010a): The expanded Kinesin-13 repertoire of trypanosomes contains only one mitotic Kinesin indicating multiple extra-nuclear roles. *PLoS One* 5, e15020.
- Wickstead, B., Ersfeld, K., Gull, K. (2004): The small chromosomes of *Trypanosoma brucei* involved in antigenic variation are constructed around repetitive palindromes. *Genome Res* 14, 1014-1024.
- Wickstead, B., Gull, K. (2006): A "holistic" kinesin phylogeny reveals new kinesin families and predicts protein functions. *Mol Biol Cell* 17, 1734-1743.
- Wickstead, B., Gull, K. (2007): Dyneins across eukaryotes: a comparative genomic analysis. *Traffic* 8, 1708-1721.
- Wickstead, B., Gull, K., Richards, T. A. (2010b): Patterns of kinesin evolution reveal a complex ancestral eukaryote with a multifunctional cytoskeleton. *BMC Evol Biol* 10: 110.
- Widener, J., Nielsen, M. J., Shiflett, A., Moestrup, S. K., Hajduk, S. (2007): Hemoglobin is a co-factor of human trypanosome lytic factor. *PLoS Pathog* 3, 1250-1261.
- Woehlke, G., Ruby, A. K., Hart, C. L., Ly, B., Hom-Booher, N., Vale, R. D. (1997): Microtubule interaction site of the kinesin motor. *Cell* 90, 207-216.

References

- Wood, K. W., Lad, L., Luo, L., Qian, X., Knight, S. D., Nevins, N., Brejc, K., Sutton, D., Gilmartin, A. G., Chua, P. R., Desai, R., Schauer, S. P., McNulty, D. E., Annan, R. S., Belmont, L. D., Garcia, C., Lee, Y., Diamond, M. A., Faucette, L. F., Giardiniere, M., Zhang, S., Sun, C. M., Vidal, J. D., Lichtsteiner, S., Cornwell, W. D., Greshock, J. D., Wooster, R. F., Finer, J. T., Copeland, R. A., Huang, P. S., Morgans, D. J. Jr, Dhanak, D., Bergnes, G., Sakowicz, R., Jackson, J. R. (2010): Antitumor activity of an allosteric inhibitor of centromere-associated protein-E. *Proc Natl Acad Sci* 107, 5839-5844.
- Woods, A., Baines, A. J., Gull, K. (1992): A high molecular mass phosphoprotein defined by a novel monoclonal antibody is closely associated with the intermicrotubule cross bridges in the *Trypanosoma brucei* cytoskeleton. *J Cell Sci*, 103, 665-675.
- Woods, A., Sherwin, T., Sasse, R., MacRae, T. H., Baines, A. J., Gull, K. (1989): Definition of individual components within the cytoskeleton of *Trypanosoma brucei* by a library of monoclonal antibodies. *J Cell Sci* 93, 491-500.
- Woodward, R., Gull, K. (1990): Timing of nuclear and kinetoplast DNA replication and early morphological events in the cell cycle of *Trypanosoma brucei*. *J Cell Sci* 95, 49-57.
- Wordeman, L., Mitchison, T. J. (1995): Identification and partial characterization of mitotic centromere-associated kinesin, a kinesin-related protein that associates with centromeres during mitosis. *J Cell Biol* 128, 95-104.
- Wordeman, L., Wagenbach, M., Maney, T. (1999): Mutations in the ATP-binding domain affect the subcellular distribution of mitotic centromere-associated kinesin (MCAK). *Cell Biol Int* 23, 275-286.
- Wordeman, L., Wagenbach, M., von Dassow, G. (2007): MCAK facilitates chromosome movement by promoting kinetochore microtubule turnover. *J Cell Biol* 179, 869-879.
- Xong, H. V., Vanhamme, L., Chamekh, M., Chimfwembe, C. E., van den Abbeele, J., Pays, A., van Meirvenne, N., Hamers, R., De Baetselier, P., Pays, E. (1998): A VSG expression site-associated gene confers resistance to human serum in *Trypanosoma rhodesiense*. *Cell* 95, 839-846.
- Xu, D., Farmer, A., Collett, G., Grishin, N. V., Chook, Y. M. (2012): Sequence and structural analyses of nuclear export signals in the NESdb database. *Mol Biol Cell* 23, 3677-3693.
- Xu, C., Zhang, J., Zhang, W., Liu, H., Fang, J., Xie, H. (2013): An improved workflow for identifying ubiquitin/ubiquitin-like protein conjugation sites from tandem mass spectra. *Proteomics* 13, 2579-2584.
- Yahya, M. F. Z. R., Yusof, F. Z. M., Hamid, U. M. A. (2012): Investigation on nuclear transport of *Trypanosoma brucei*: An in silico approach. In Pérez-Sánchez, H. (editor, 2012): *Bioinformatics*. InTech Open Access Publisher, 31-54.

References

- Yang, H., Ganguly, A., Cabral, F. (2010): Inhibition of cell migration and cell division correlates with distinct effects of microtubule inhibiting drugs. *J Biol Chem* 285, 32242-32250.
- Yasui, Y., Urano, T., Kawajiri, A., Nagata, K., Tatsuka, M., Saya, H., Furukawa, K., Takahashi, T., Izawa, I., Inagaki, M. (2004): Autophosphorylation of a newly identified site of Aurora-B is indispensable for cytokinesis. *J Biol Chem* 279, 12997-13003.
- Yen, T. J., Compton, D. A., Wise, D., Zinkowski, R. P., Brinkley, B. R., Earnshaw, W. C., Cleveland, D. W. (1991): CENP-E, a novel human centromere-associated protein required for progression from metaphase to anaphase. *EMBO J* 10, 1245-1254.
- Yun, M., Zhang, X., Park, C. G., Park, H. W., Endow, S. A. (2001): A structural pathway for activation of the kinesin motor ATPase. *EMBO J* 20, 2611-2618.
- Zhang, X., Ems-McClung, S. C., Walczak, C. E. (2008): Aurora A phosphorylates MCAK to control ran-dependent spindle bipolarity. *Mol Biol Cell* 19, 2752-2765.
- Zhang, X., Lan, W., Ems-McClung, S. C., Stukenberg, P. T., Walczak, C. E. (2007): Aurora B phosphorylates multiple sites on mitotic centromere-associated kinesin to spatially and temporally regulate its function. *Mol Biol Cell* 18, 3264-3276.
- Zhang, L., Shao, H., Huang, Y., Yan, F., Chu, Y., Hou, H., Zhu, M., Fu, C., Aikhionbare, F., Fang, G., Ding, X., Yao, X. (2011): PLK1 phosphorylates mitotic centromere-associated kinesin and promotes its depolymerase activity. *J Biol Chem* 286, 3033-3046.
- Zhang, C., Zhu, C., Chen, H., Li, L., Guo, L., Jiang, W., Lu, S. H. (2010): Kif18A is involved in human breast carcinogenesis. *Carcinogenesis* 31, 1676-1684.
- Zhou, Q., Gu, J., Lun, Z. R., Ayala, F. J., Li, Z. (2016): Two distinct cytokinesis pathways drive trypanosome cell division initiation from opposite cell ends. *PNAS* 113, 3287-3292.
- Zhou, Q., Hu, H., Li, Z. (2014): New insights into the molecular mechanisms of mitosis and cytokinesis in trypanosomes. *Int Rev Cell Mol Biol* 308, 127-166.
- Zimmermann, S., Hall, L., Riley, S., Sørensen, J., Amaro, R. E., Schnauffer, A. (2016): A novel high-throughput activity assay for the *Trypanosoma brucei* editosome enzyme REL1 and other RNA ligases. *Nucleic Acids Res* 44, e24.
- Zong, H., Carnes, S. K., Moe, C., Walczak, C. E., Ems-McClung, S. C. (2016): The far C-terminus of MCAK regulates its conformation and spindle pole focusing. *Mol Biol Cell* 27, 1451-1464.

References

Sources from internet

arm.biocuckoo.org (25.09.2017)

dndi.org (25.09.2017)

<http://emboss.bioinformatics.nl/cgi-bin/emboss/epestfind> (25.09.2017)

smart.embl-heidelberg.de (25.09.2017)

7. Supplementary figures

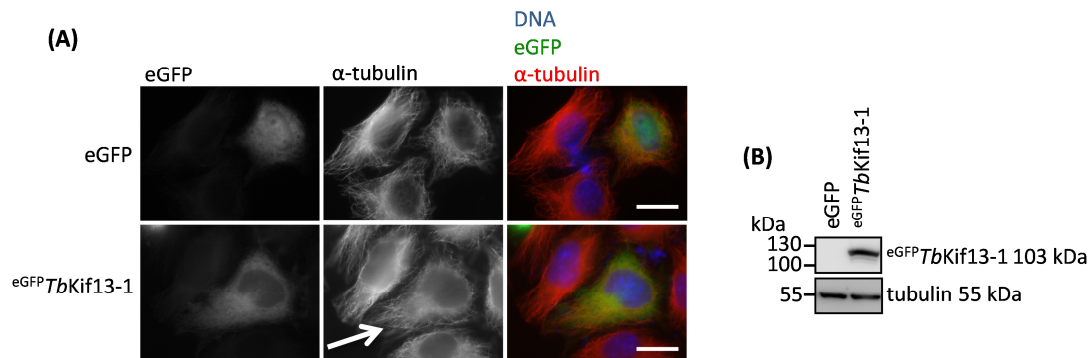


Figure S 1: No Microtubule cytoskeleton depolymerisation of HeLa L cells transiently transfected with pCS2-^{eGFP}TbKif13-1. (A) HeLa L cells transiently transfected with pCS2-^{eGFP}TbKif13-1 that overexpressed ^{eGFP}TbKif13-1 (green, autofluorescence) showed no reduced microtubule cytoskeleton (red, α-tubulin antibody TAT) 24 h after transfection; white arrow: cell that overexpressed ^{eGFP}TbKif13-1, but showed no reduced cytoskeleton. The nucleus was DAPI (blue) stained. Cells were harvested 24 h after transfection and fixed with methanol. Non transfected cells and HeLa L cells transfected with the vector pCS2-eGFP served as control. Overexpression of eGFP did not result in cytoskeleton depolymerisation 24 h after transfection. Scale bar 20 μm. (B) Westernblot of pCS2-^{eGFP}TbKif13-1 transfected HeLa L cells to verify the overexpression of ^{eGFP}TbKif13-1 after transfection. As control served cells transfected with pCS2-eGFP, expressing eGFP. ^{eGFP}TbKif13-1 was detected using α-GFP, tubulin was detected using α-tubulin antibody TAT.

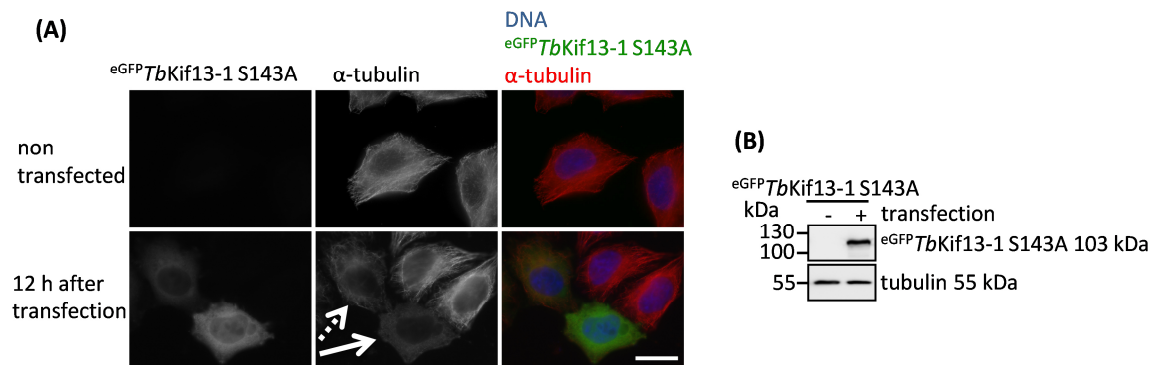


Figure S 2: Microtubule cytoskeleton depolymerisation of HeLa L cells transiently transfected with pCS2-^{eGFP}TbKif13-1 S143A. (A) HeLa L cells transiently transfected with pCS2-^{eGFP}TbKif13-1 S143A that overexpressed ^{eGFP}TbKif13-1 S143A (green, autofluorescence) showed a reduced microtubule cytoskeleton (red, α-tubulin antibody TAT) already 12 h after transfection; white arrow: cell with reduced cytoskeleton; dashed arrow: cell with less reduced cytoskeleton probably due to lower ^{eGFP}TbKif13-1 S143A expression rate. The nucleus was DAPI (blue) stained. Cells were harvested 12 h after transfection and fixed with methanol. Non transfected cells served as control. Scale bar 20 μm. (B) Westernblot of pCS2-^{eGFP}TbKif13-1 S143A transfected HeLa L cells to verify the overexpression of ^{eGFP}TbKif13-1 S143A after transfection. ^{eGFP}TbKif13-1 S143A was detected using α-GFP, tubulin was detected using α-tubulin antibody TAT.

Supplementary figures

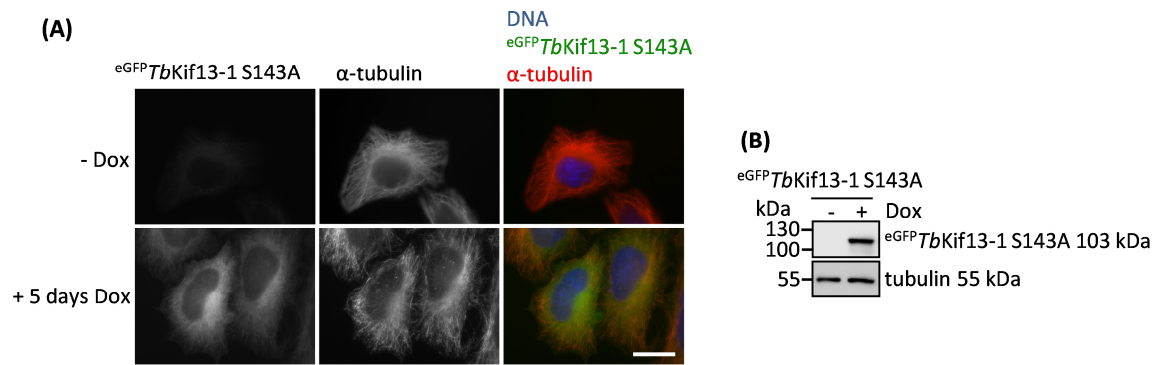


Figure S 3: No microtubule cytoskeleton depolymerisation of double stable HeLa Flp-In cells transfected with *pcDNA5/FRT/TO-eGFP TbKif13-1 S143A* and *pcDNA3.1-eGFP TbKif13-1 S143A* 5 days after induction. (A) Double stable HeLa Flp-In cells transfected with *pcDNA5/FRT/TO-eGFP TbKif13-1 S143A* and *pcDNA3.1-eGFP TbKif13-1 S143A* showed 5 days after induction of eGFP*TbKif13-1 S143A* overexpression (green, autofluorescence) no reduced microtubule cytoskeleton (red, α-tubulin antibody TAT). The nucleus was DAPI (blue) stained. Cells were harvested 5 days after induction and fixed with methanol. Non induced cells served as control. Scale bar 20 μm. (B) Westernblot of *pcDNA5/FRT/TO-eGFP TbKif13-1 S143A* and *pcDNA3.1-eGFP TbKif13-1 S143A* stable transfected HeLa Flp-In cells to verify the expression of eGFP*TbKif13-1 S143A* after induction. eGFP*TbKif13-1 S143A* was detected using α-GFP, tubulin was detected using α-tubulin antibody TAT.

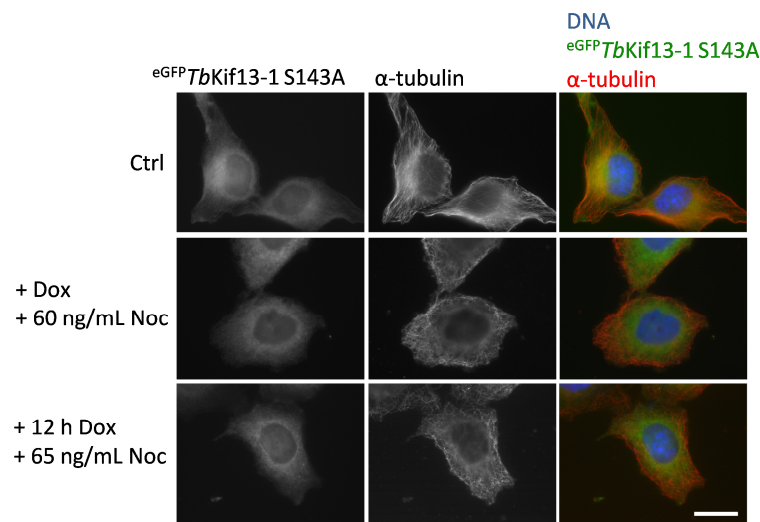


Figure S 4: No microtubule cytoskeleton depolymerisation of single stable HeLa Flp-In cells after eGFP*TbKif13-1 S143A* overexpression and addition of nocodazole. To single stable HeLa Flp-In cells, transfected with *pcDNA5/FRT/TO-eGFP TbKif13-1 S143A*, 60 ng/mL and 65 ng/mL, respectively, nocodazole were added in order to favour microtubule cytoskeleton depolymerisation by overexpressed eGFP*TbKif13-1 S143A* by weakening microtubules. Overexpression of eGFP*TbKif13-1 S143A* occurred simultaneously (+ Dox + 60 ng/mL Noc; middle panel line) or 12 h prior (+ 12 h Dox + 65 ng/mL Noc; lower panel line) to nocodazole addition. Cells were harvested 24 h post induction and fixed with methanol. Control cells were not supplied with nocodazole, but overexpression of eGFP*TbKif13-1 S143A* was induced. eGFP*TbKif13-1 S143A* overexpression: green, autofluorescence; microtubule cytoskeleton: red, α-tubulin antibody TAT; nucleus: blue; DAPI. Scale bar 20 μm.

Supplementary figures

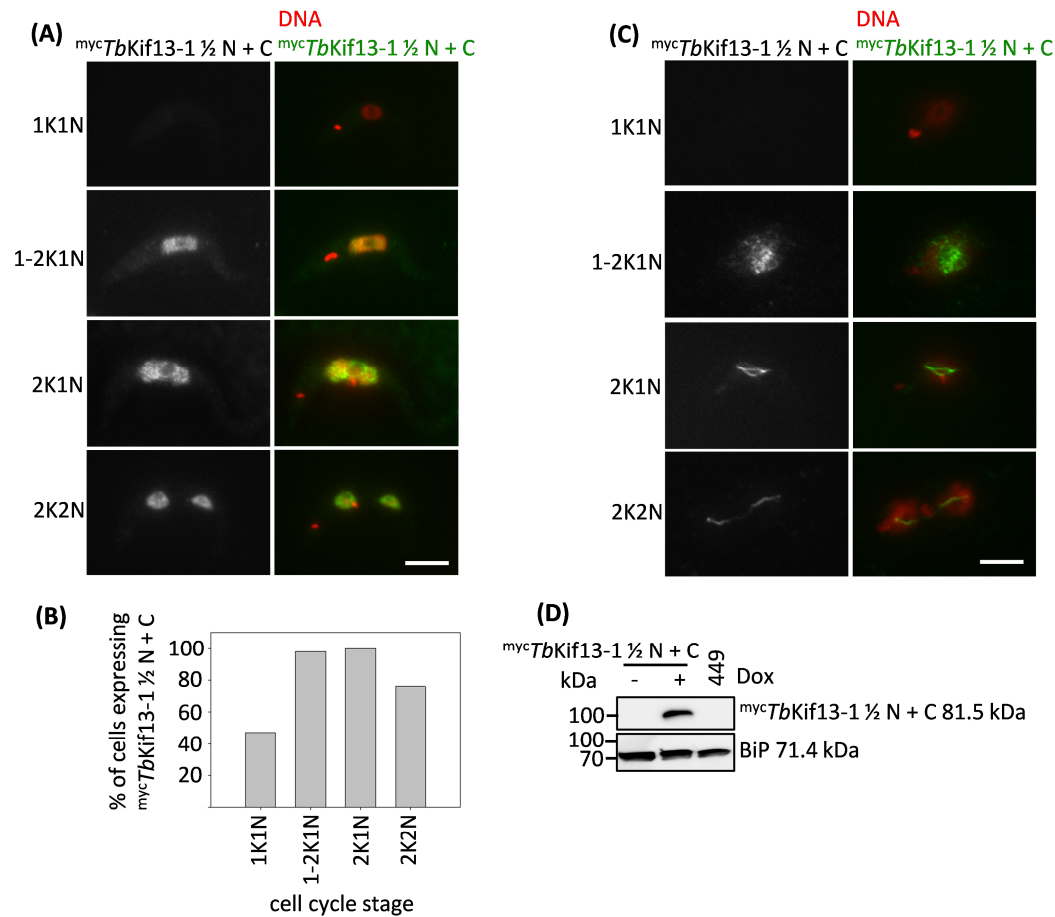


Figure S 5: Nuclear localisation of *mycTbKif13-1 ½ N + C* in *T. brucei* from 1-2K1N to 2K2N cell stages. **(A)** Whole cell samples of transgenic 449 cells ectopically expressing *mycTbKif13-1 ½ N + C*. DNA was DAPI (red) stained, *mycTbKif13-1 ½ N + C* (green) was visualised using α -myc antibody. Scale bar 5 μ m. **(B)** Diagram shows percentage of cells with visual detectable ectopically expressed *mycTbKif13-1 ½ N + C* within each cell cycle stage, detected according to kinetoplast and nucleus postioning. **(C)** Cytoskeleton samples of transgenic 449 cells ectopically expressing *mycTbKif13-1 ½ N + C*. Staining and scale bar according to subfigure (A). **(D)** Westernblot analysis verifying doxycycline (Dox) inducible ectopic expression of *mycTbKif13-1 ½ N + C* in transgenic 449 cells with α -myc antibody. 449 cells were used as negative control, BiP staining was used as loading control.

Supplementary figures

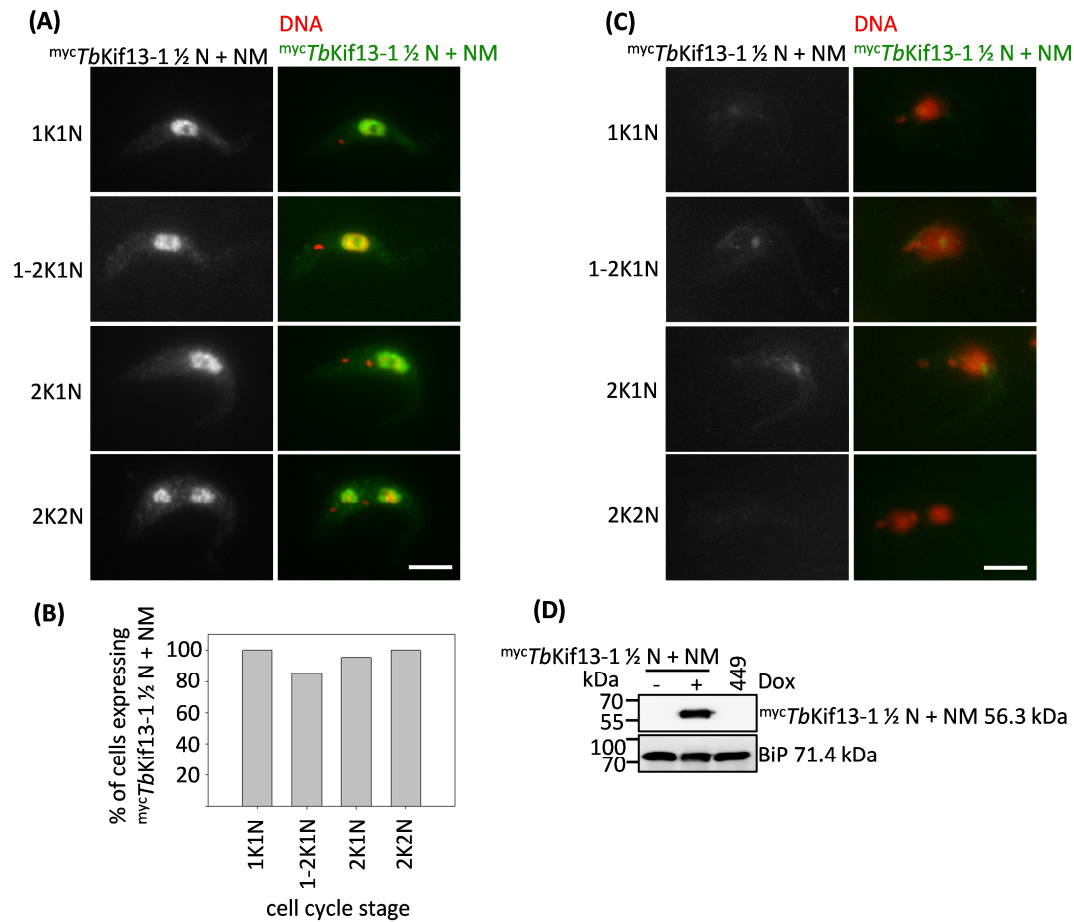


Figure S 6: Nuclear and slight cytoplasmic localisation of *mycTbKif13-1 1/2 N + NM* in *T. brucei* throughout the cell cycle. (A) Whole cell samples of transgenic 449 cells ectopically expressing *mycTbKif13-1 1/2 N + NM*. DNA was DAPI (red) stained, *mycTbKif13-1 1/2 N + NM* (green) was visualised using α -myc antibody. Scale bar 5 μ m. **(B)** Diagram shows percentage of cells with visual detectable ectopically expressed *mycTbKif13-1 1/2 N + NM* within each cell cycle stage, detected according to kinetoplast and nucleus positioning. **(C)** Cytoskeleton samples of transgenic 449 cells ectopically expressing *mycTbKif13-1 1/2 N + NM*. Staining and scale bar according to subfigure (A). **(D)** Westernblot analysis verifying doxycycline (Dox) inducible ectopic expression of *mycTbKif13-1 1/2 N + NM* in transgenic 449 cells with α -myc antibody. 449 cells were used as negative control, BiP staining was used as loading control.

Supplementary figures

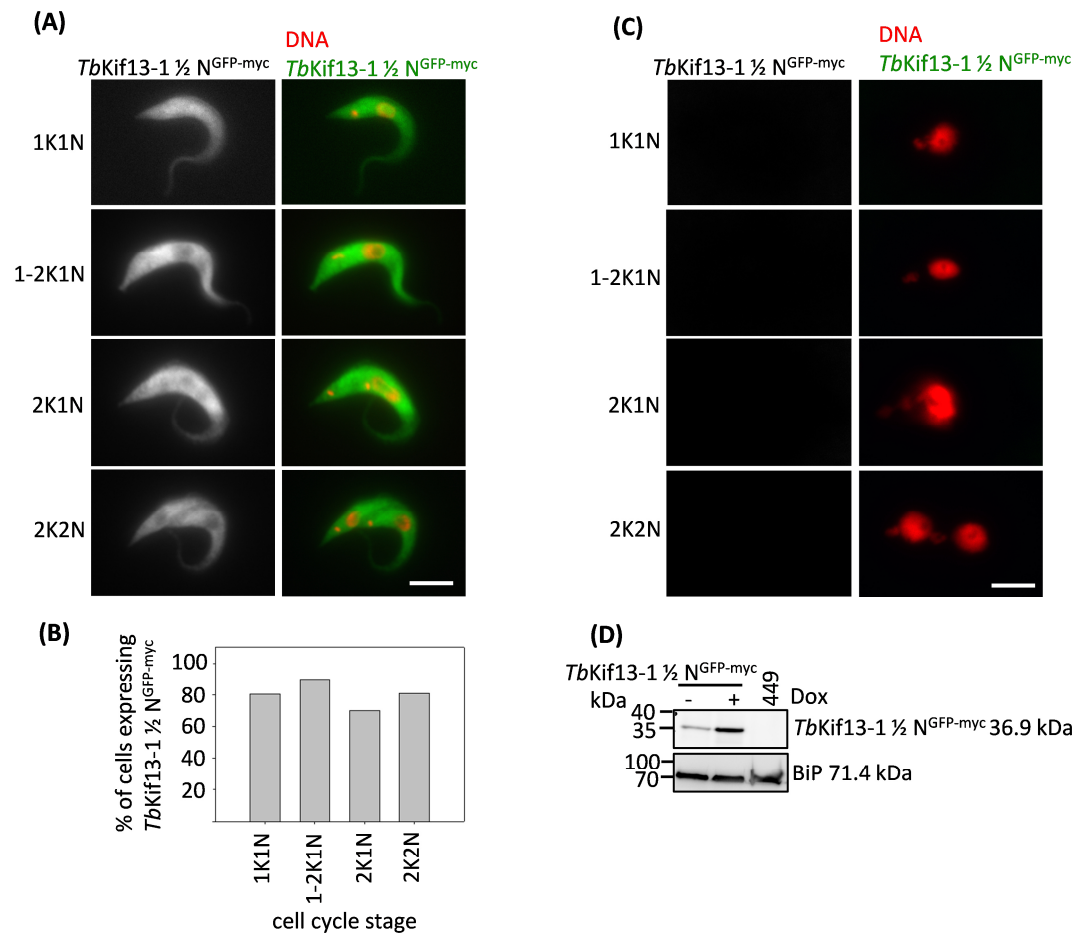


Figure S 7: Cytoplasmic localisation of *TbKif13-1 1/2 N^{GFP-myc}* in *T. brucei* throughout the cell cycle. (A) Whole cell samples of transgenic 449 cells ectopically expressing *TbKif13-1 1/2 N^{GFP-myc}*. DNA was DAPI (red) stained, *TbKif13-1 1/2 N^{GFP-myc}* (green) was visualised using α -myc antibody. Scale bar 5 μ m. **(B)** Diagram shows percentage of cells with visual detectable ectopically expressed *TbKif13-1 1/2 N^{GFP-myc}* within each cell cycle stage, detected according to kinetoplast and nucleus positioning. **(C)** Cytoskeleton samples of transgenic 449 cells ectopically expressing *TbKif13-1 1/2 N^{GFP-myc}*. Staining and scale bar according to subfigure (A). **(D)** Westernblot analysis verifying doxycycline (Dox) inducible ectopic expression of *TbKif13-1 1/2 N^{GFP-myc}* in transgenic 449 cells with α -myc antibody. 449 cells were used as negative control, BiP staining was used as loading control.

Supplementary figures

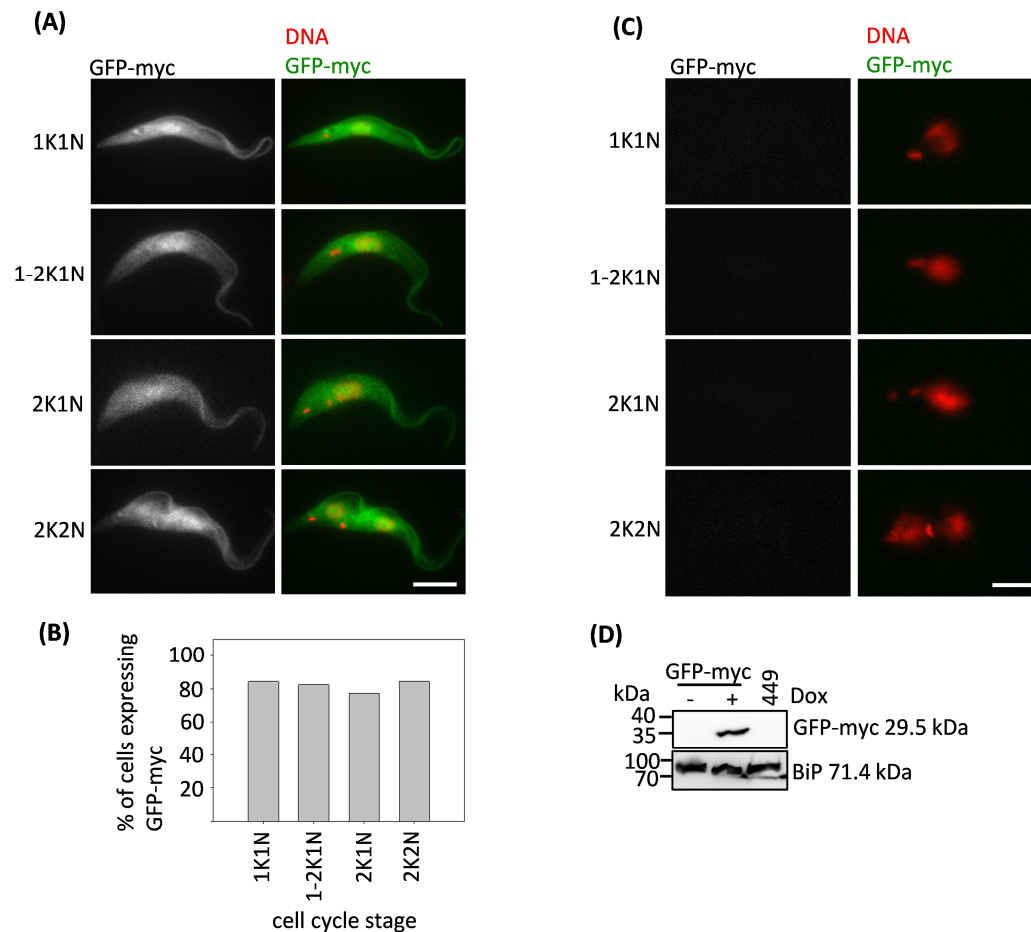


Figure S 8: Nuclear and cytoplasmic localisation of GFP-myc in *T. brucei* throughout the cell cycle. **(A)** Whole cell samples of transgenic 449 cells ectopically expressing GFP-myc. DNA was DAPI (red) stained, GFP-myc (green) was visualised using α -myc antibody. Scale bar 5 μ m. **(B)** Diagram shows percentage of cells with visual detectable ectopically expressed GFP-myc within each cell cycle stage, detected according to kinetoplast and nucleus positioning. **(C)** Cytoskeleton samples of transgenic 449 cells ectopically expressing GFP-myc. Staining and scale bar according to subfigure (A). **(D)** Westernblot analysis verifying doxycycline (Dox) inducible ectopic expression of GFP-myc in transgenic 449 cells with α -myc antibody. 449 cells were used as negative control, BiP staining was used as loading control.

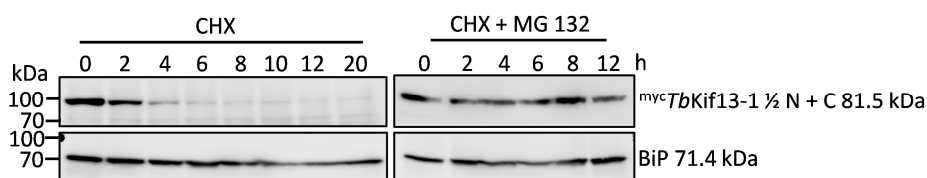


Figure S 9: Proteasome-dependent degradation of $^{myc}TbKif13-1 \frac{1}{2} N + C$. In transgenic 449 cells ectopic expression of $^{myc}TbKif13-1 \frac{1}{2} N + C$ was induced for four hours. Then cycloheximide (CHX) was added for translational inhibition (left Westernblot); in addition to CHX also MG 132 for proteasome inhibition was added (right Westernblot). Westernblot samples were kept every two hours. Time point 0 is when CHX or in addition MG 132 were added to the cell culture. For detection of $^{myc}TbKif13-1 \frac{1}{2} N + C$ α -myc antibody was used; α -BiP served as loading control.

Supplementary figures

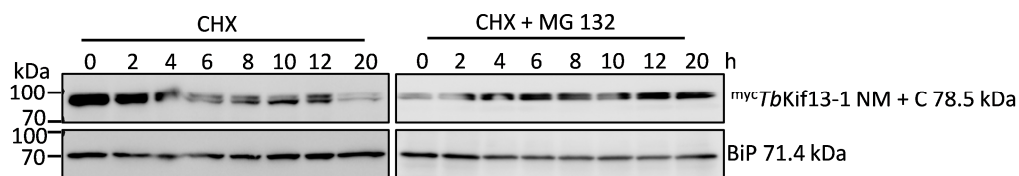


Figure S 10: No degradation of *mycTbKif13-1 NM + C*. In transgenic 449 cells ectopic expression of *mycTbKif13-1 NM + C* was induced for four hours. Then cycloheximide (CHX) was added for translational inhibition (left Westernblot); in addition to CHX also MG 132 for proteasome inhibition was added (right Westernblot). Western blot samples were kept every two hours. Time point 0 is when CHX or in addition MG 132 were added to the cell culture. For detection of *mycTbKif13-1 NM + C* α -myc antibody was used; α -BiP served as loading control.

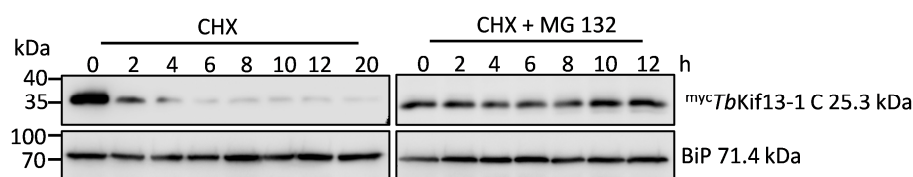


Figure S 11: Proteasome-dependent degradation of *mycTbKif13-1 C*. In transgenic 449 cells ectopic expression of *mycTbKif13-1 C* was induced for four hours. Then cycloheximide (CHX) was added for translational inhibition (left Westernblot); in addition to CHX also MG 132 for proteasome inhibition was added (right Westernblot). Western blot samples were kept every two hours. Time point 0 is when CHX or in addition MG 132 were added to the cell culture. For detection of *mycTbKif13-1 C* α -myc antibody was used; α -BiP served as loading control.

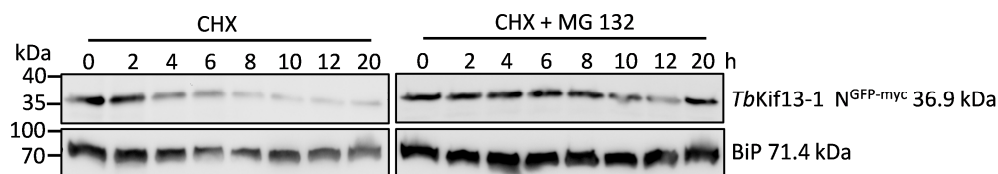


Figure S 12: Proteasome-dependent degradation of *TbKif13-1 N^{GFP-myc}*. In transgenic 449 cells ectopic expression of *TbKif13-1 N^{GFP-myc}* was induced for four hours. Then cycloheximide (CHX) was added for translational inhibition (left Westernblot); in addition to CHX also MG 132 for proteasome inhibition was added (right Westernblot). Western blot samples were kept every two hours. Time point 0 is when CHX or in addition MG 132 were added to the cell culture. For detection of *TbKif13-1 N^{GFP-myc}* α -myc antibody was used; α -BiP served as loading control.

Supplementary figures

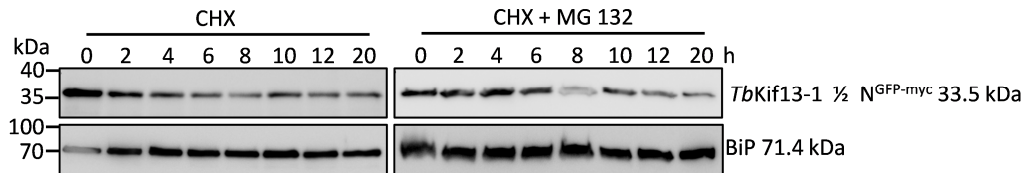


Figure S 13: Proteasome dependent degradation of *TbKif13-1 1/2 N^{GFP-myc}*. In transgenic 449 cells ectopic expression of *TbKif13-1 1/2 N^{GFP-myc}* was induced for four hours. Then cycloheximide (CHX) was added for translational inhibition (left Westernblot); in addition to CHX also MG 132 for proteasome inhibition was added (right Westernblot). Westernblot samples were kept every two hours. Time point 0 is when CHX or in addition MG 132 were added to the cell culture. For detection of *TbKif13-1 1/2 N^{GFP-myc}* α -myc antibody was used; α -BiP served as loading control.

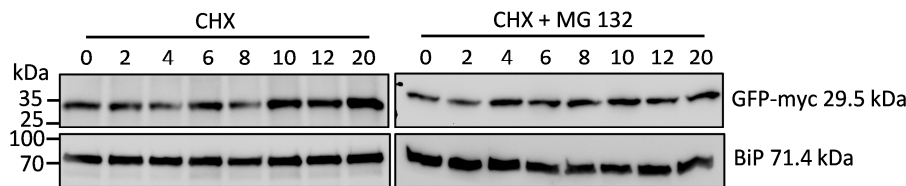


Figure S 14: No degradation of GFP-myc. In transgenic 449 cells ectopic expression of GFP-myc was induced for four hours. Then cycloheximide (CHX) was added for translational inhibition (left Westernblot); in addition to CHX also MG 132 for proteasome inhibition was added (right Westernblot). Westernblot samples were kept every two hours. Time point 0 is when CHX or in addition MG 132 were added to the cell culture. For detection of GFP-myc α -myc antibody was used; α -BiP served as loading control.

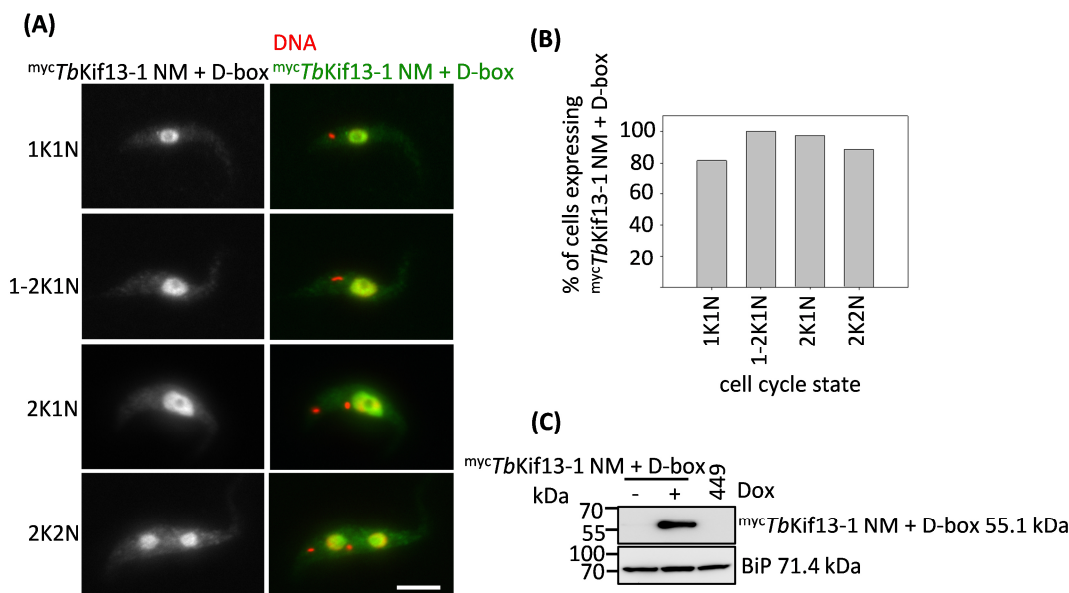


Figure S 15: Nuclear localisation of *mycTbKif13-1 NM + D-box* in *T. brucei* throughout the cell cycle. (A) Whole cell samples of transgenic 449 cells ectopically expressing *mycTbKif13-1 NM + D-box*. DNA was DAPI (red) stained, *mycTbKif13-1 NM + D-box* (green) was visualised using α -myc antibody. Scale bar 5 μ m. (B) Diagram shows percentage of cells of each cell cycle stage ectopically expressing *mycTbKif13-1 NM + D-box*, detected according to kinetoplast and nucleus postioning. (C) Westernblot verifying inducible ectopic expression of *mycTbKif13-1 NM + D-box* in transgenic 449 cells with α -myc antibody. 449 cells were used as negative control, BiP staining was used as loading control.

Supplementary figures

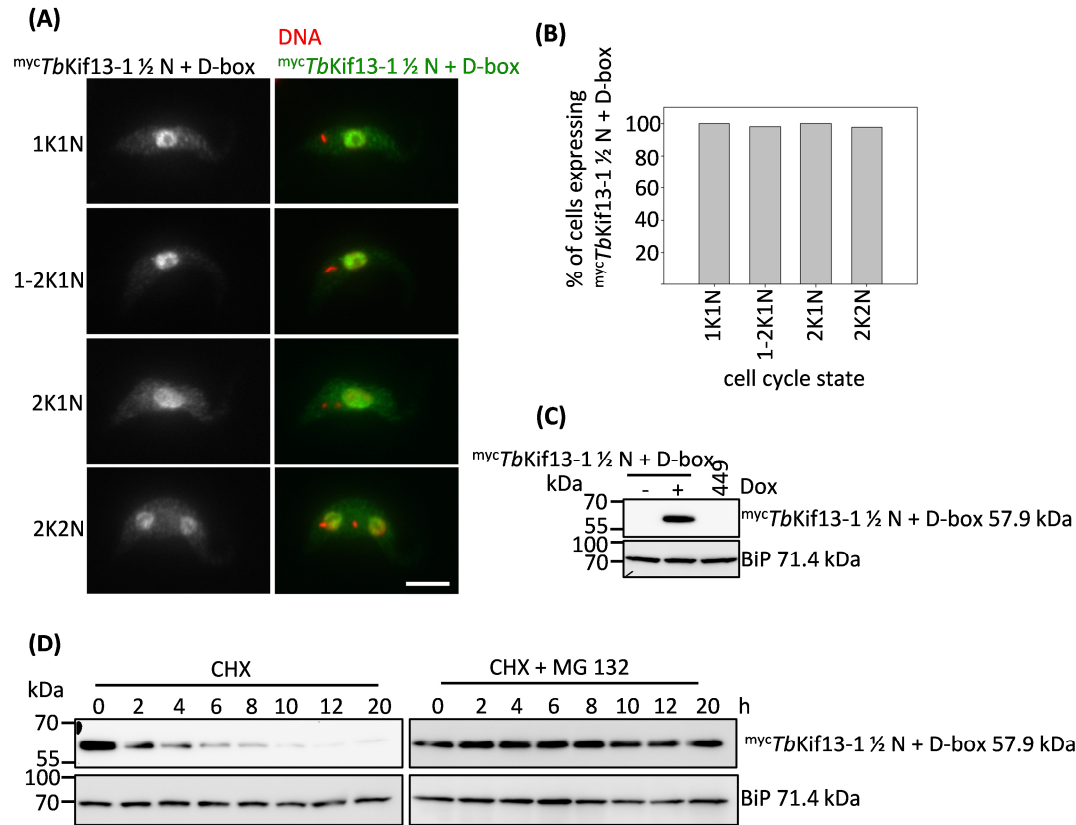


Figure S 16: Nuclear localisation of *mycTbKif13-1 1/2 N + D-box* in *T. brucei* throughout the cell cycle and proteasome dependent degradation of *mycTbKif13-1 1/2 N + D-box*. **(A)** Whole cell samples of transgenic 449 cells ectopically expressing *mycTbKif13-1 1/2 N + D-box*. DNA was DAPI (red) stained, *mycTbKif13-1 1/2 N + D-box* (green) was visualised using α -myc antibody. Scale bar 5 μ m. **(B)** Diagram shows percentage of cells with visual detectable ectopically expressed *mycTbKif13-1 1/2 N + D-box* within each cell cycle stage, detected according to kinetoplast and nucleus positioning. **(C)** Westernblot analysis verifying doxycycline (Dox) inducible ectopic expression of *mycTbKif13-1 1/2 N + D-box* in transgenic 449 cells with α -myc antibody. 449 cells were used as negative control, BiP staining was used as loading control. **(D)** In transgenic 449 cells ectopic expression of *mycTbKif13-1 1/2 N + D-box* was induced for four hours. Then cycloheximide (CHX) was added for translational inhibition (left Westernblot, CHX); in addition to CHX also MG 132 for proteasome inhibition was added (right Westernblot, CHX + MG 132). Westernblot samples were taken every two hours. Time point 0 marks when CHX or in addition MG 132 were added to the cell culture. For detection of *mycTbKif13-1 1/2 N + D-box* α -myc antibody was used; α -BiP served as loading control.

Supplementary figures

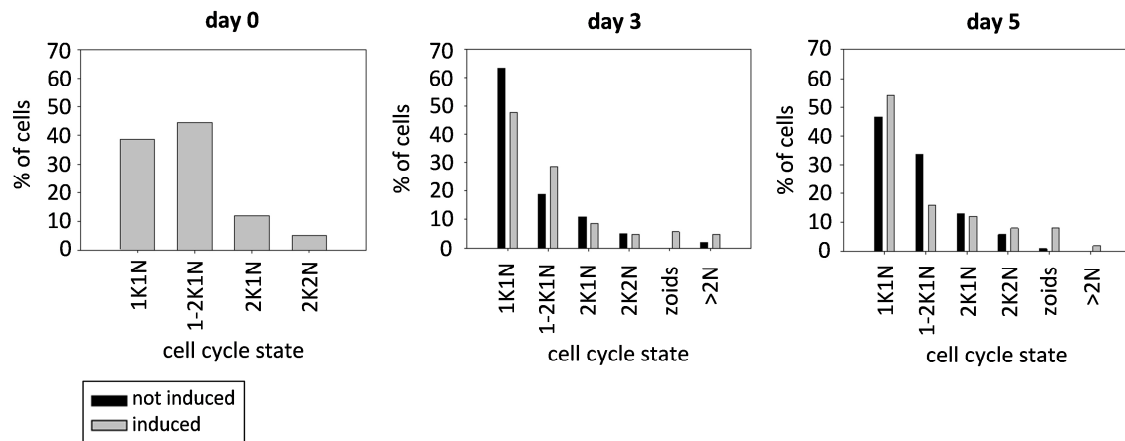


Figure S 17: Immunfluorescence microscopy evaluation of flow cytometry analysis of the cell line ectopically expressing ^{myc}TbKif13-1 FL. 100 cells were determined for their cell cycle stage at the given time points. grey: induced transgenic 449 cell line for ectopic expression of ^{myc}TbKif13-1 FL; black: non induced cell line.

Supplementary figures

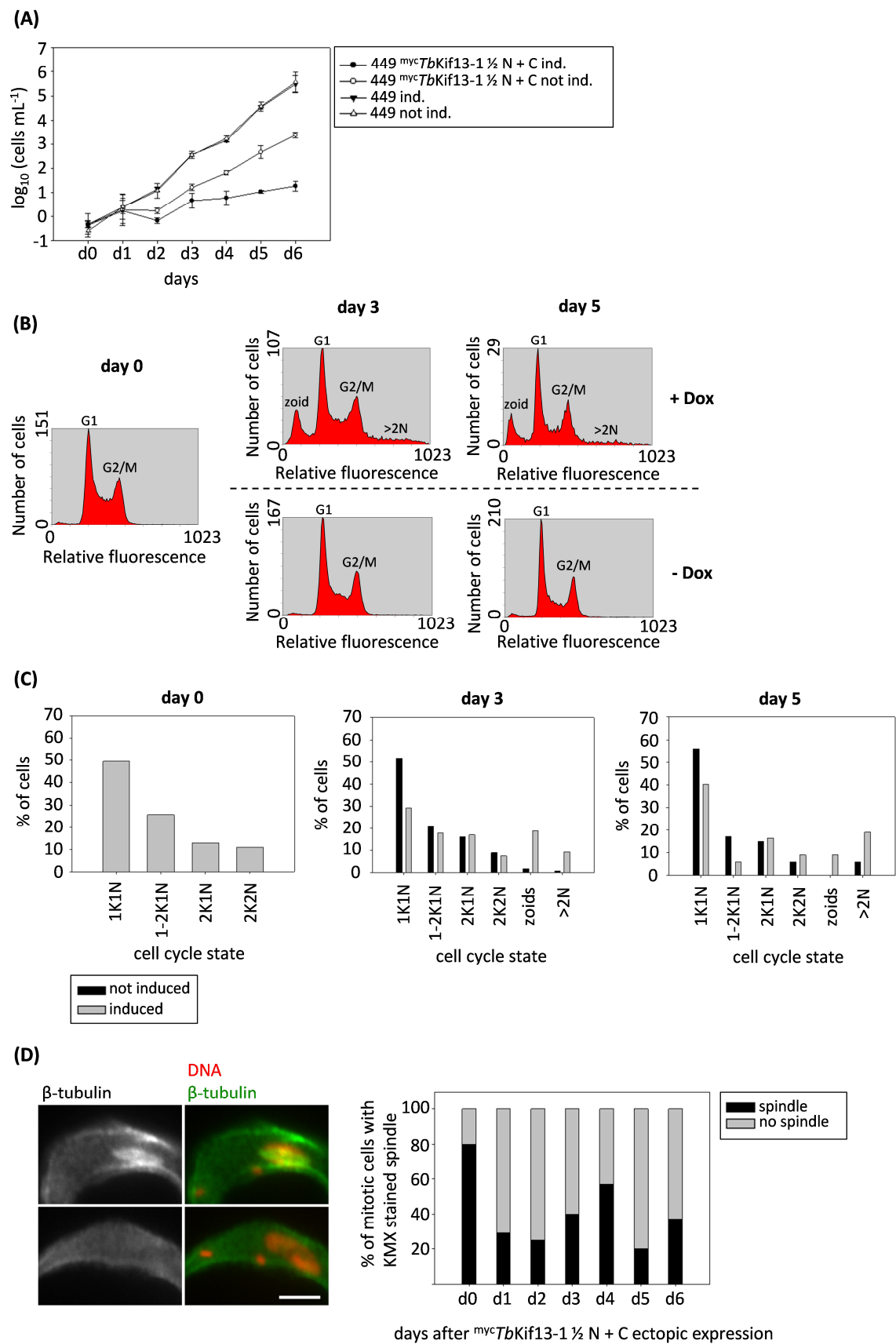


Figure S 18: Reduced growth and increase of zoids and cells >2N in the cell line ectopically expressing *mycTbKif13-1* 1/2 N + C. (A) Growth curve of the transgenic 449 cell line ectopically expressing *mycTbKif13-1* 1/2 N + C; control cells: non induced and non transfected 449 cells. (B) Flow cytometry analysis of the transgenic 449 cell line ectopically expressing *mycTbKif13-1* 1/2 N + C (+ Dox,

Supplementary figures

upper panels), control cells: non induced (- Dox, lower panels). **(C)** Immunfluorescence microscopy evaluation of flow cytometry analysis of the cell line ectopically expressing ^{myc}TbKif13-1 ½ N + C. 100 cells were determined for their cell cycle stage at the given time points. grey: induced transgenic 449 cell line for ectopic expression of ^{myc}TbKif13-1 ½ N + C; black: non induced cell line. **(D)** Immunfluorescence analysis of mitotic 2K1N cells after ectopic expression of ^{myc}TbKif13-1 ½ N + C, depicting a cell with spindle formation (upper panel) and one without detectable spindle (lower panel). KMX antibody was used for β-tubulin staining (green), DNA was stained with DAPI (red). Scale bar 3 μm. Diagram shows evaluation of spindle formation in mitotic 2K1N cells ectopically expressing ^{myc}TbKif13-1 ½ N + C from day 0 to day 6; black: spindle formation; grey: no spindle formation.

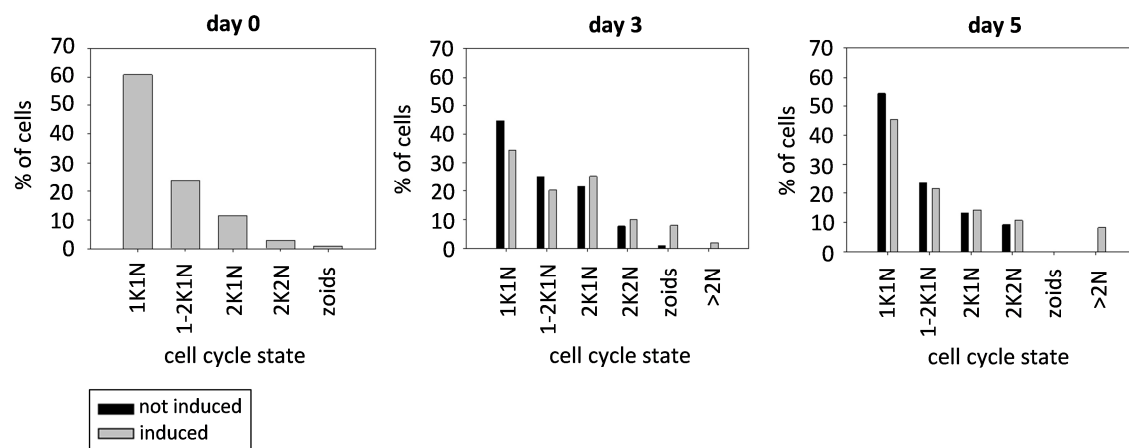


Figure S 19: Immunfluorescence microscopy evaluation of flow cytometry analysis of the cell line ectopically expressing ^{myc}TbKif13-1 NM + C. 100 cells were determined for their cell cycle stage at the given time points. grey: induced transgenic 449 cell line for ectopic expression of ^{myc}TbKif13-1 NM + C; black: non induced cell line.

Supplementary figures

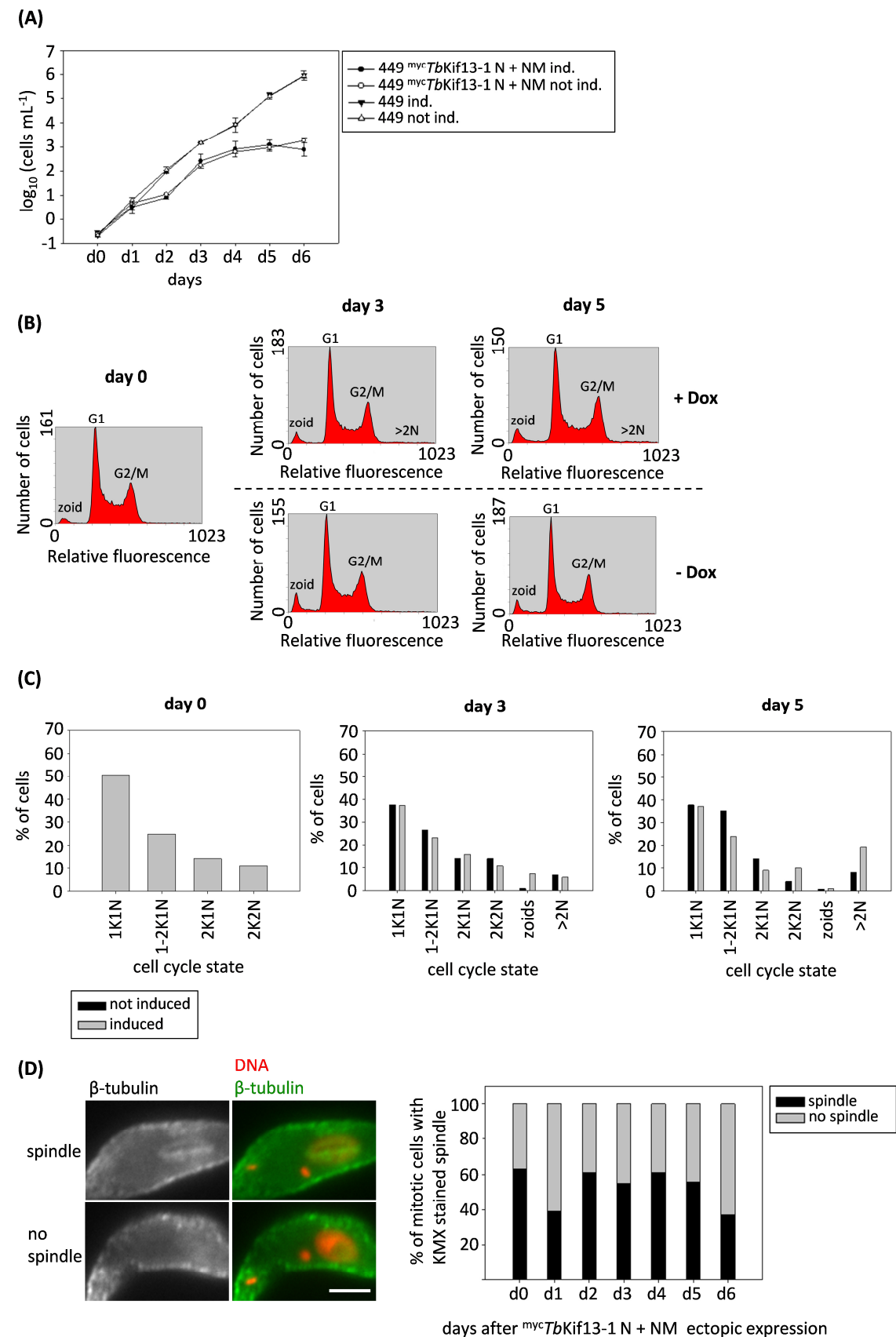


Figure S 20: No reduced growth of the cell line ectopically expressing *mycTbKif13-1* N + NM compared to non induced cells. (A) Growth curve of the transgenic 449 cell line ectopically expressing *mycTbKif13-1* N + NM; control cells: non induced and non transfected 449 cells. **(B)** Flow cytometry analysis of the transgenic 449 cell line ectopically expressing *mycTbKif13-1* N + NM (+ Dox,

Supplementary figures

upper panels), control cells: non induced (- Dox, lower panels). **(C)** Immunfluorescence microscopy evaluation of flow cytometry analysis of the cell line ectopically expressing *myc*^{TbKif13-1} N + NM. 100 cells were determined for their cell cycle stage at the given time points. grey: induced cell line for ectopic expression of *myc*^{TbKif13-1} N + NM; black: non induced cell line. **(D)** Immunfluorescence analysis of mitotic 2K1N cells after ectopic expression of *myc*^{TbKif13-1} N + NM, depicting a cell with spindle formation (upper panel) and one without detectable spindle (lower panel). KMX antibody was used for β -tubulin staining (green), DNA was stained with DAPI (red). Scale bar 3 μ m. Diagram shows evaluation of spindle formation in mitotic 2K1N cells ectopically expressing *myc*^{TbKif13-1} N + NM from day 0 to day 6; black: spindle formation; grey: no spindle formation.

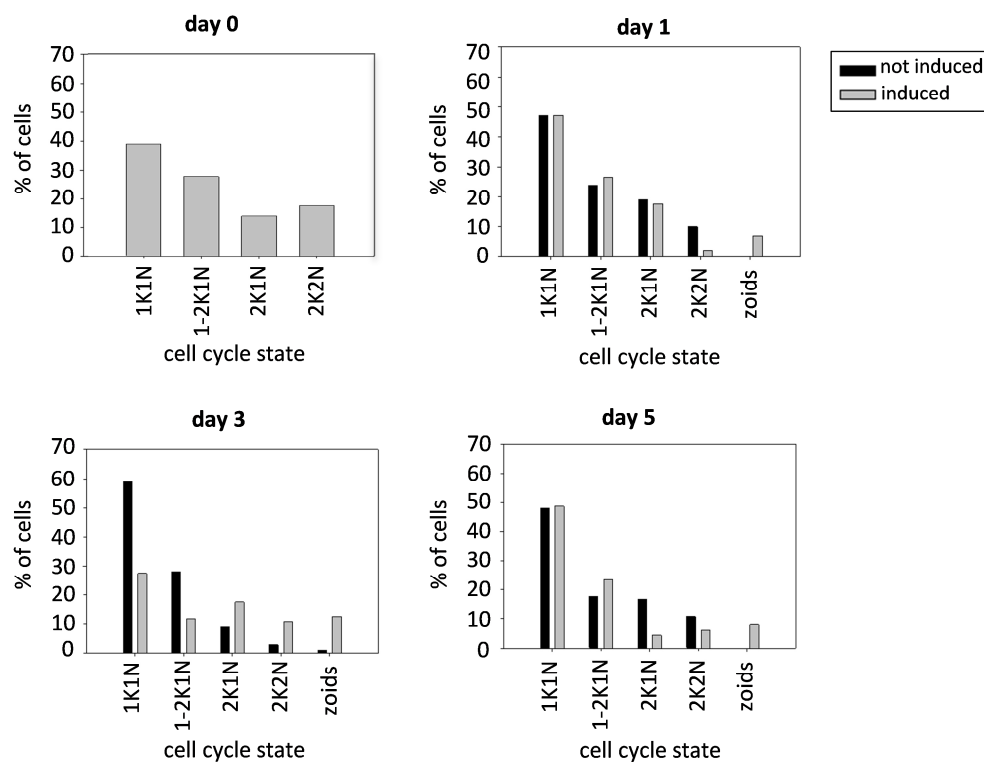


Figure S 21: Immunfluorescence microscopy evaluation of flow cytometry analysis of the cell line ectopically expressing *myc*^{TbKif13-1} ½ N + NM. 100 cells were determined for their cell cycle stage at the given time points. grey: induced cell line for ectopic expression of *myc*^{TbKif13-1} ½ N + NM; black: non induced cell line.

Supplementary figures

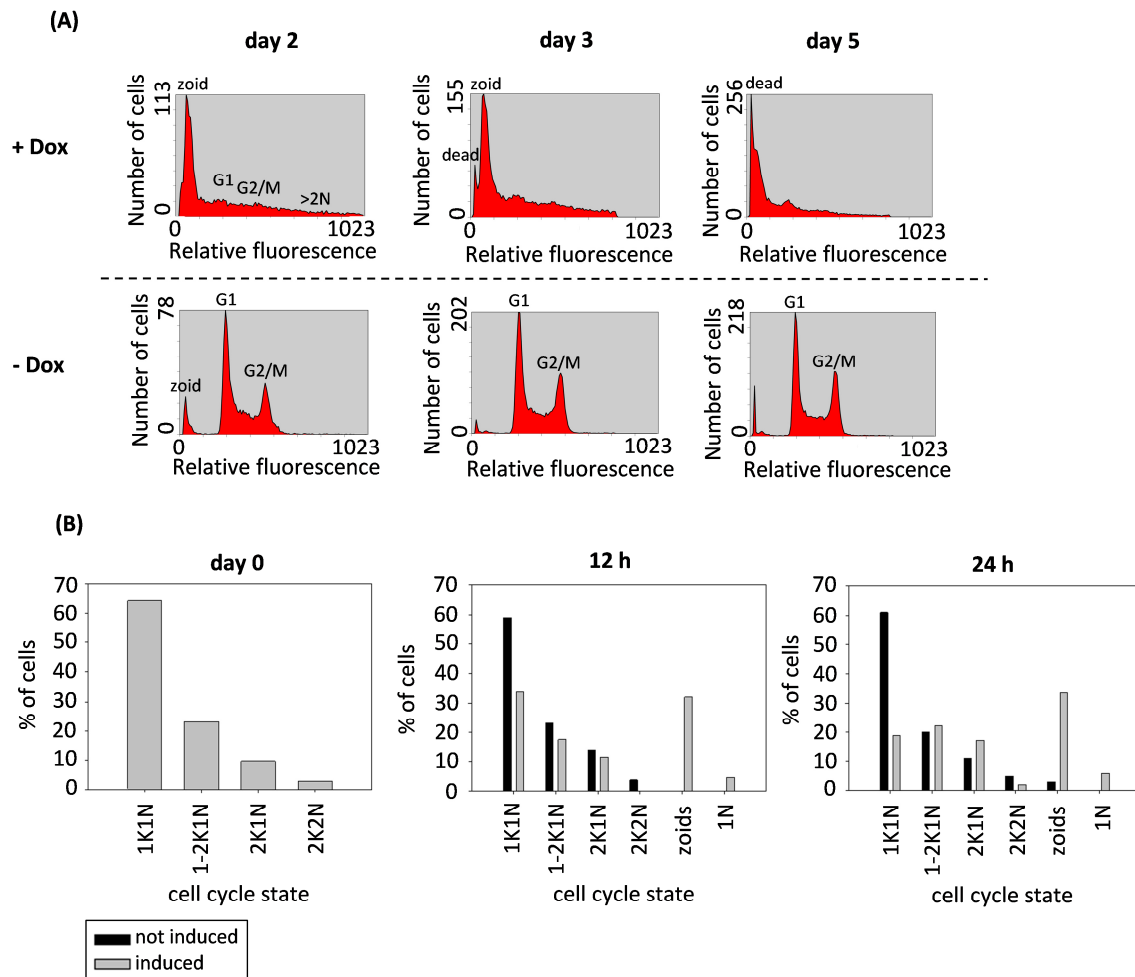


Figure S 22: Flow cytometry analysis of the transgenic 449 cell line ectopically expressing ^{myc}TbKif13-1 NM at day 2, 3 and 5 after induction. (A) Flow cytometry analysis of the transgenic 449 cell line ectopically expressing ^{myc}TbKif13-1 NM (+ Dox, upper panels) at day 2, day 3 and day 5 after induction, control cells: non induced (- Dox, lower panels). **(B)** Immunofluorescence microscopy evaluation of flow cytometry analysis of the transgenic 449 cell line ectopically expressing ^{myc}TbKif13-1 NM. 100 cells were determined for their cell cycle stage at the given time points. grey: induced cell line for ectopic expression of ^{myc}TbKif13-1 NM; black: non induced cell line.

Supplementary figures

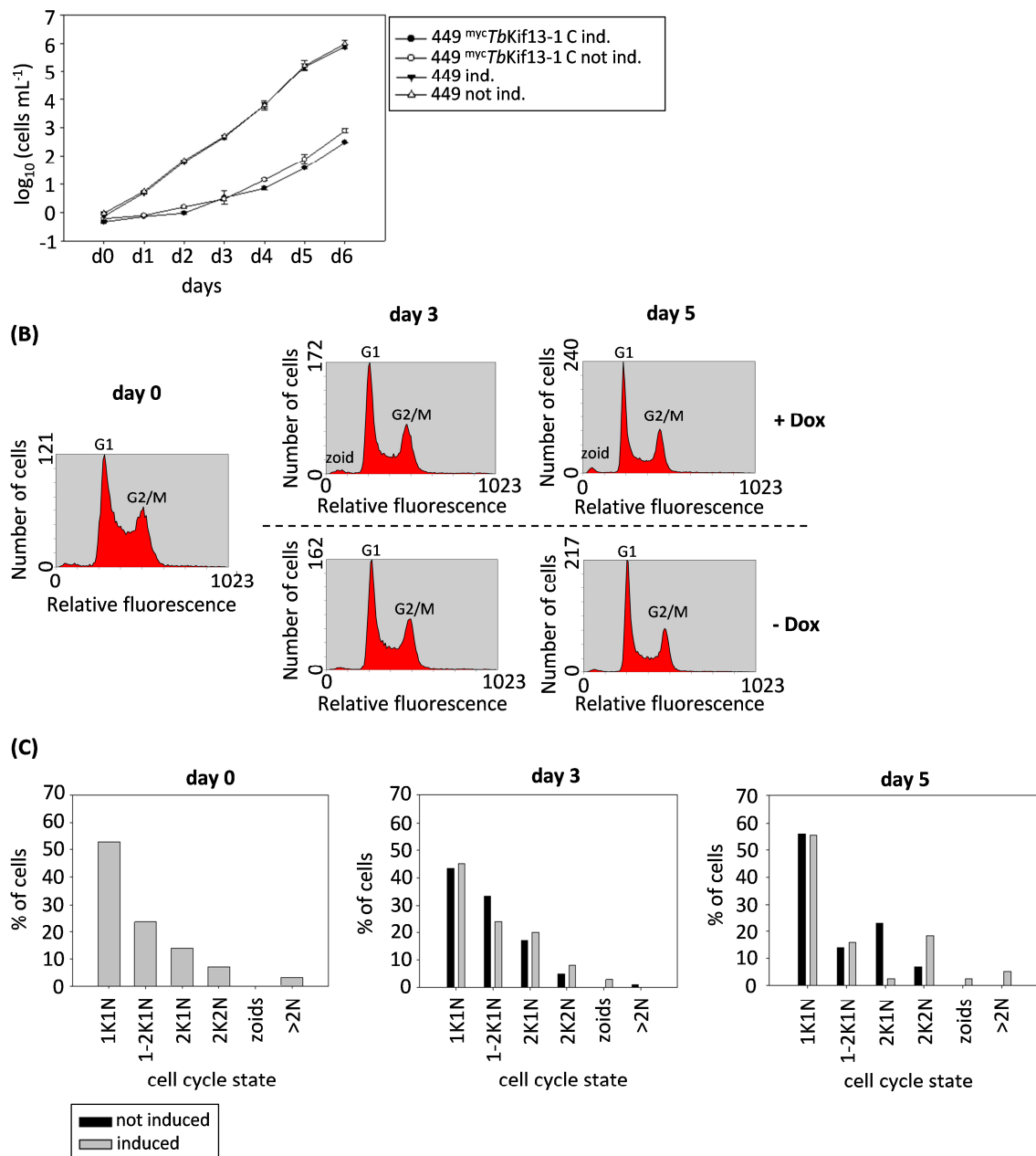


Figure S 23: No reduced growth of the cell line ectopically expressing *mycTbKif13-1* C compared to non induced cells. (A) Growth curve of the transgenic 449 cell line ectopically expressing *mycTbKif13-1* C; control cells: non induced and non transfected 449 cells. (B) Flow cytometry analysis of the transgenic 449 cell line ectopically expressing *mycTbKif13-1* C (+ Dox, upper panels), control cells: non induced (- Dox, lower panels). (C) Immunofluorescence microscopy evaluation of flow cytometry analysis of the transgenic 449 cell line ectopically expressing *mycTbKif13-1* C. 100 cells were determined for their cell cycle stage at the given time points. grey: induced cell line for ectopic expression of *mycTbKif13-1* C; black: non induced cell line.

Supplementary figures

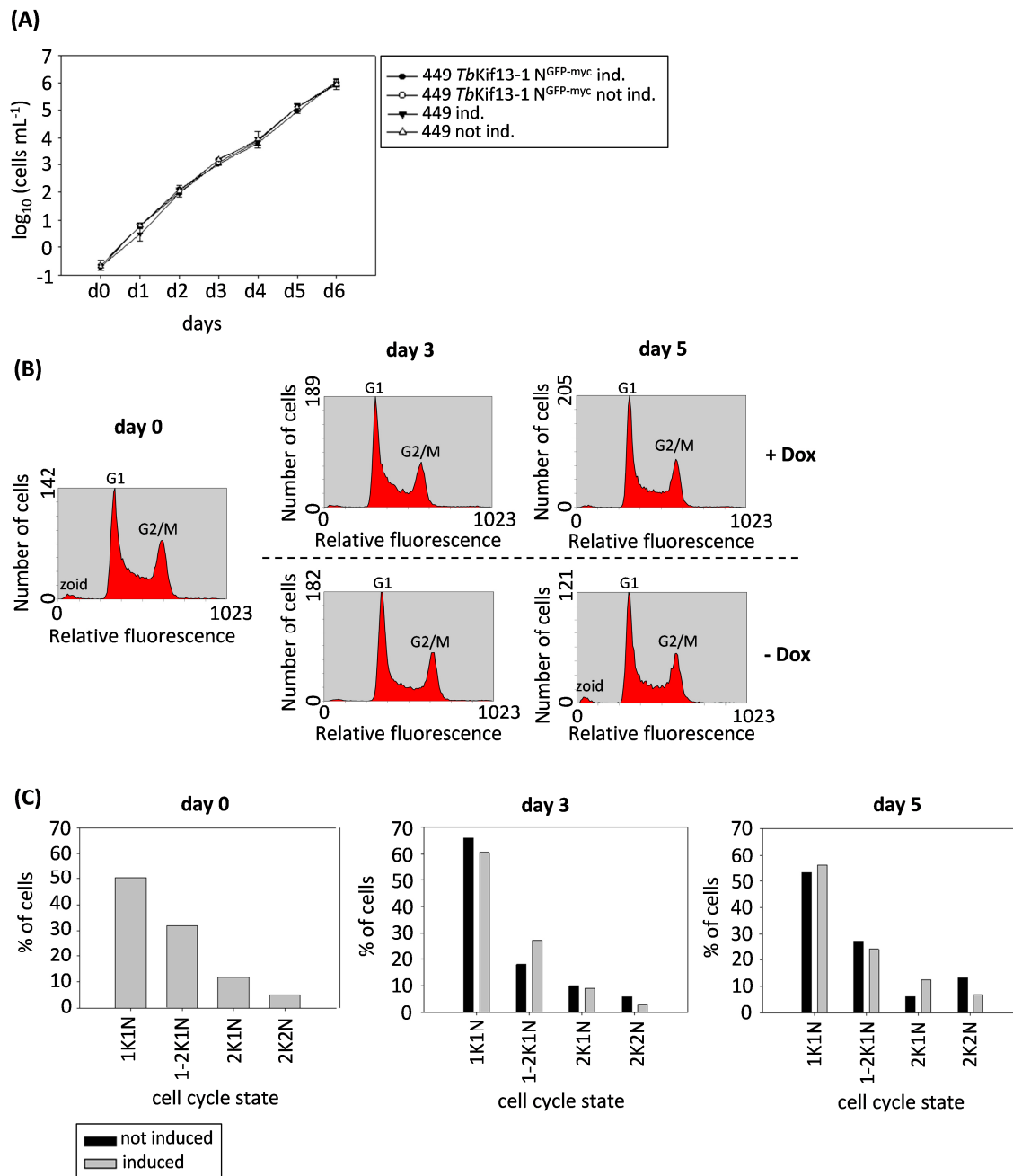


Figure S 24: No reduced growth of the cell line ectopically expressing *TbKif13-1* N^{GFP-myc}. **(A)** Growth curve of the transgenic 449 cell line ectopically expressing *TbKif13-1* N^{GFP-myc}; control cells: non induced and non transfected 449 cells. **(B)** Flow cytometry analysis of the transgenic 449 cell line ectopically expressing *TbKif13-1* N^{GFP-myc} (+ Dox, upper panels), control cells: non induced (- Dox, lower panels). **(C)** Immunofluorescence microscopy evaluation of flow cytometry analysis of the transgenic 449 cell line ectopically expressing *TbKif13-1* N^{GFP-myc}. 100 cells were determined for their cell cycle stage at the given time points. grey: induced cell line for ectopic expression of *TbKif13-1* N^{GFP-myc}; black: non induced cell line.

Supplementary figures

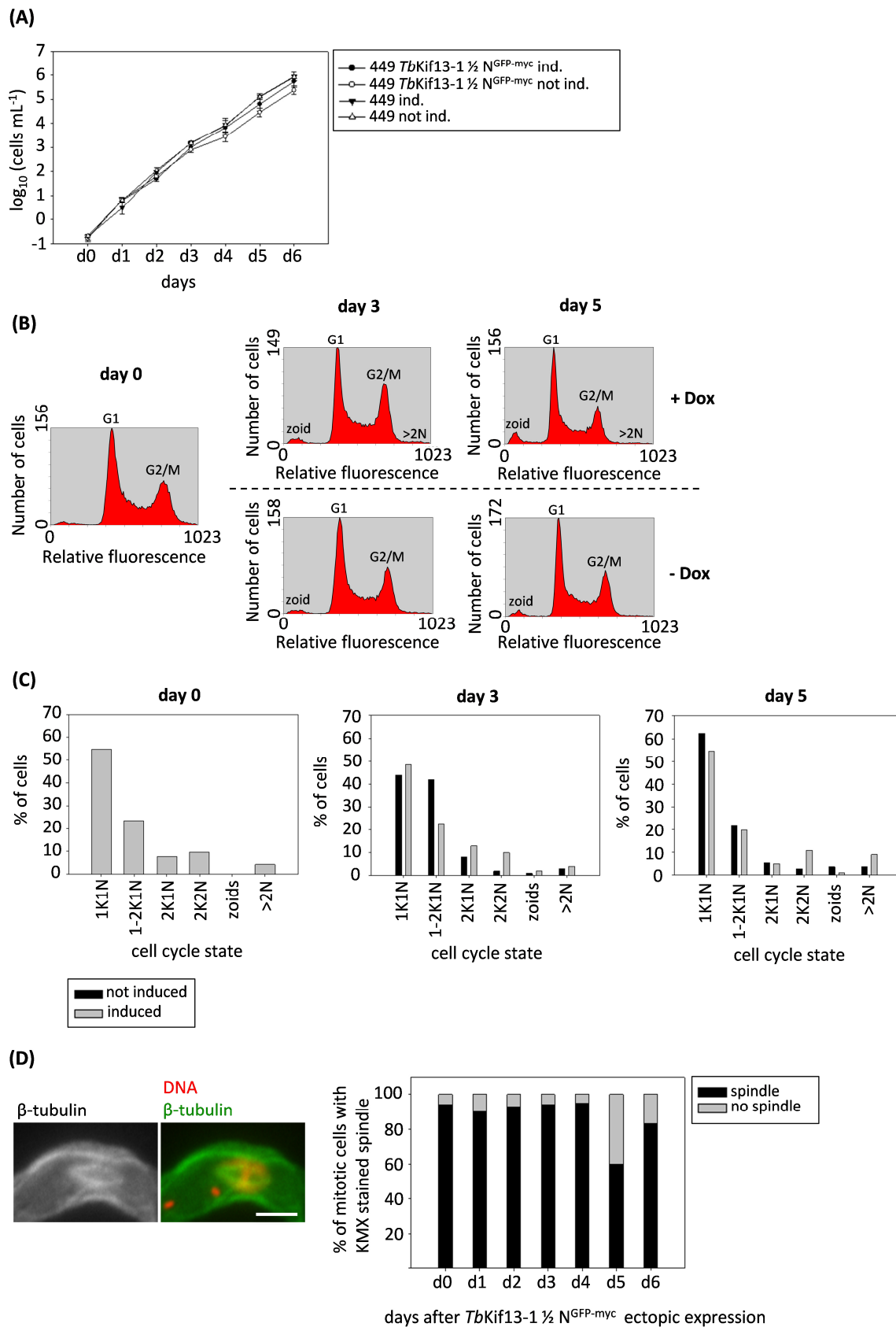


Figure S 25: No reduced growth of the cell line ectopically expressing *TbKif13-1* ½ $N^{GFP-myc}$. (A) Growth curve of the transgenic 449 cell line ectopically expressing *TbKif13-1* ½ $N^{GFP-myc}$; control cells: non induced and non transfected 449 cells. (B) Flow cytometry analysis of the transgenic 449 cell line ectopically expressing *TbKif13-1* ½ $N^{GFP-myc}$ (+ Dox, upper panels), control cells: non induced (- Dox,

Supplementary figures

lower panels). **(C)** Immunofluorescence microscopy evaluation of flow cytometry analysis of the transgenic 449 cell line ectopically expressing *TbKif13-1* ½ N^{GFP-myc}. 100 cells were determined for their cell cycle stage at the given time points. grey: induced cell line for ectopic expression of *TbKif13-1* ½ N^{GFP-myc}; black: non induced cell line. **(D)** Immunofluorescence analysis of spindle formation in mitotic 2K1N cells after ectopic expression of *TbKif13-1* ½ N^{GFP-myc}; KMX antibody was used for staining β-tubulin (green), DNA was stained with DAPI (red). Scale bar 3 μm. Diagram shows evaluation of spindle formation in mitotic 2K1N cells ectopically expressing ^{myc}*TbKif13-1* ½ N^{GFP-myc} from day 0 to day 6; black: spindle formation; grey: no spindle formation.

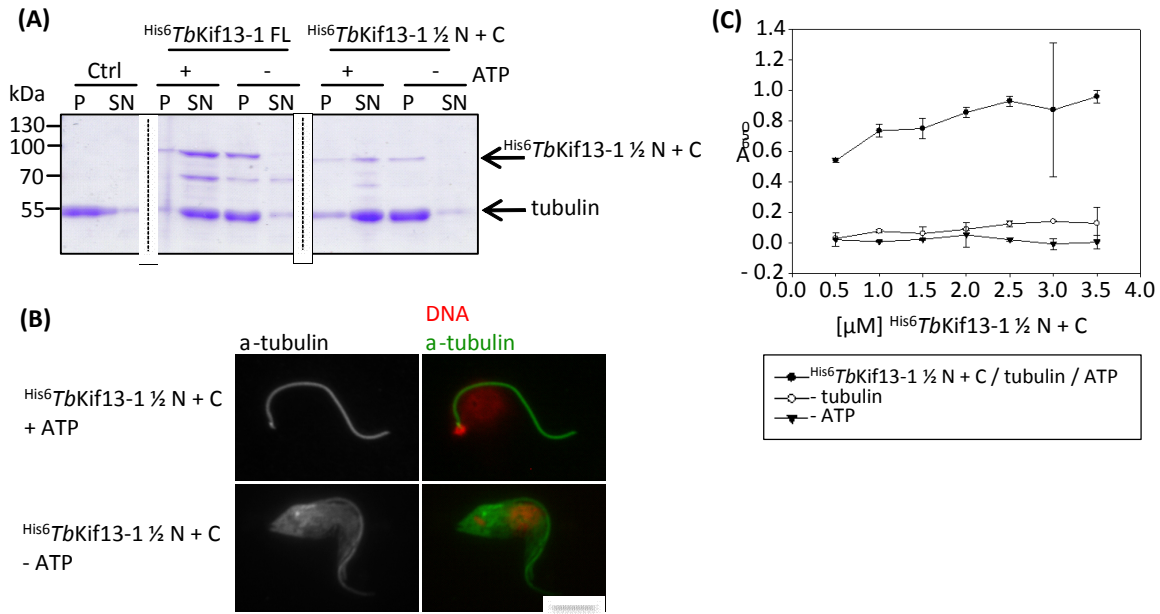


Figure S 26: ^{His6}*TbKif13-1* ½ N + C is a microtubule depolymeriser. **(A)** Tubulin sedimentation assay. 0.75 μM ^{His6}*TbKif13-1* ½ N + C were used. 1.5 μM ^{His6}*TbKif13-1* FL were used as positive control. Substrate were 3 μM taxol-stabilised microtubules. Control (Ctrl) sample was not treated with recombinantly purified ^{His6}*TbKif13-1* ½ N + C. P: pellet; SN: supernatant; SDS-PAGE analysis. **(B)** Cytoskeleton depolymerisation assay. 0.5 μM ^{His6}*TbKif13-1* ½ N + C were used. Cytoskeleton tubulin (green) was stained with α-tubulin antibody. DNA was DAPI (red) stained. Scale bar 5 μm. **(C)** Malachite green assay for ^{His6}*TbKif13-1* ½ N + C. ATPase activity of ^{His6}*TbKif13-1* ½ N + C increased with increasing ^{His6}*TbKif13-1* ½ N + C concentration. Approaches without tubulin or ATP served as control.

Supplementary figures

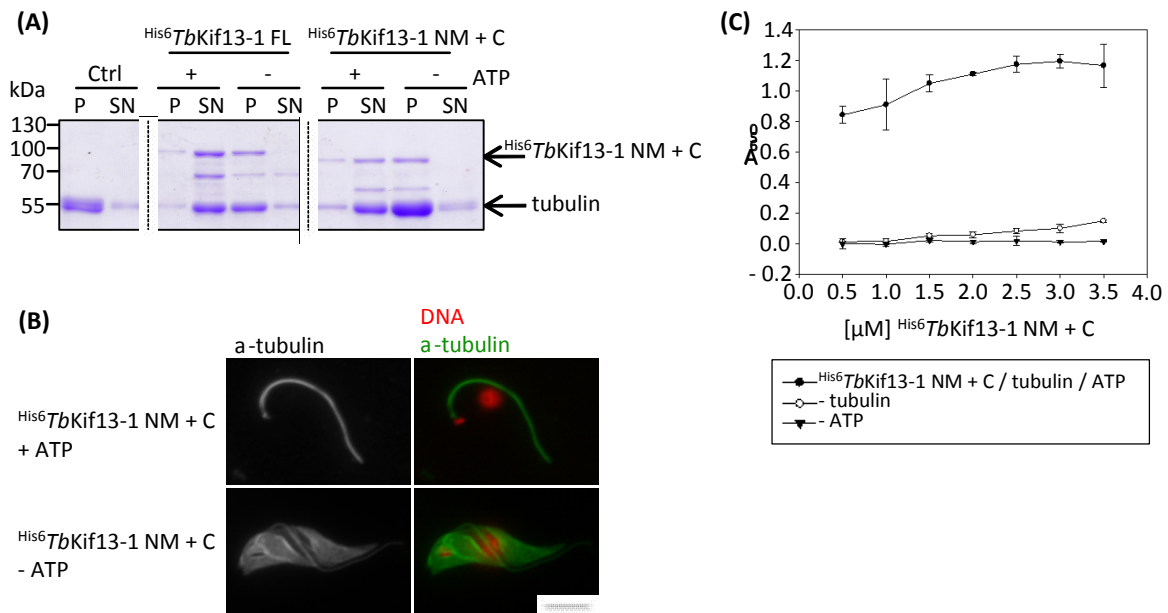


Figure S 27: $\text{His6TbKif13-1 NM + C}$ is a microtubule depolymeriser. (A) Tubulin sedimentation assay. 1 μM $\text{His6TbKif13-1 NM + C}$ was used. 1.5 μM His6TbKif13-1 FL were used as positive control. Substrate were 3 μM taxol-stabilised microtubules. Control (Ctrl) sample was not treated with recombinantly purified $\text{His6TbKif13-1 NM + C}$. P: pellet; SN: supernatant; SDS-PAGE analysis. **(B)** Cytoskeleton depolymerisation assay. 0.5 μM $\text{His6TbKif13-1 NM + C}$ were used. Cytoskeleton tubulin (green) was stained with α -tubulin antibody. DNA was DAPI (red) stained. Scale bar 5 μm . **(C)** Malachite green assay for $\text{His6TbKif13-1 NM + C}$. ATPase activity of $\text{His6TbKif13-1 NM + C}$ increased with increasing $\text{His6TbKif13-1 NM + C}$ concentration. Approaches without tubulin or ATP served as control.

Supplementary figures

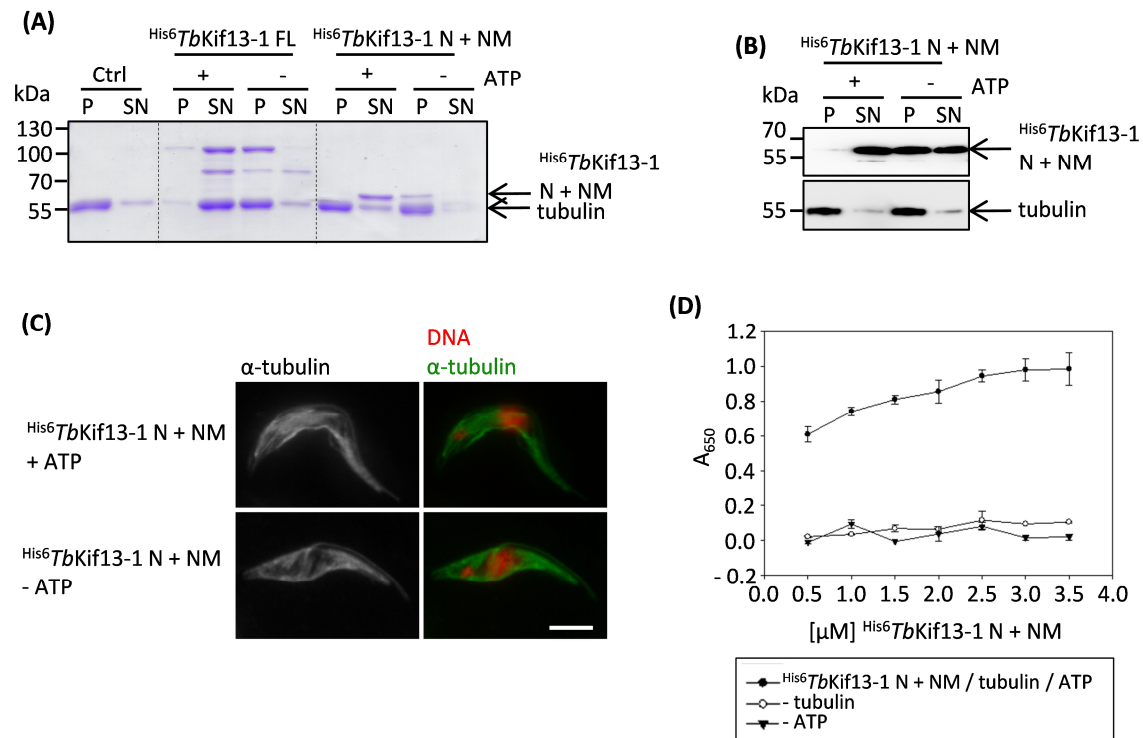


Figure S 28: His6TbKif13-1 N + NM is no microtubule depolymeriser but retains ATPase activity. (A) Tubulin sedimentation assay. 1 μM His6TbKif13-1 N + NM was used. 1.5 μM His6TbKif13-1 FL were used as positive control. Substrate were 3 μM taxol-stabilised microtubules. Control (Ctrl) sample was not treated with recombinantly purified His6TbKif13-1 N + NM. P: pellet; SN: supernatant; SDS-PAGE analysis. **(B)** Western blot analysis of the tubulin sedimentation assay samples. His6TbKif13-1 N + NM was detected using α-His antibody; tubulin was detected using α-tubulin antibody. **(C)** Cytoskeleton depolymerisation assay. 1 μM His6TbKif13-1 N + NM was used. Cytoskeleton tubulin (green) was stained with α-tubulin antibody. DNA was DAPI (red) stained. Scale bar 5 μm. **(D)** Malachite green assay for His6TbKif13-1 N + M. ATPase activity of His6TbKif13-1 N + M increased with increasing His6TbKif13-1 N + M concentration. Approaches without tubulin or ATP served as control.

Supplementary figures

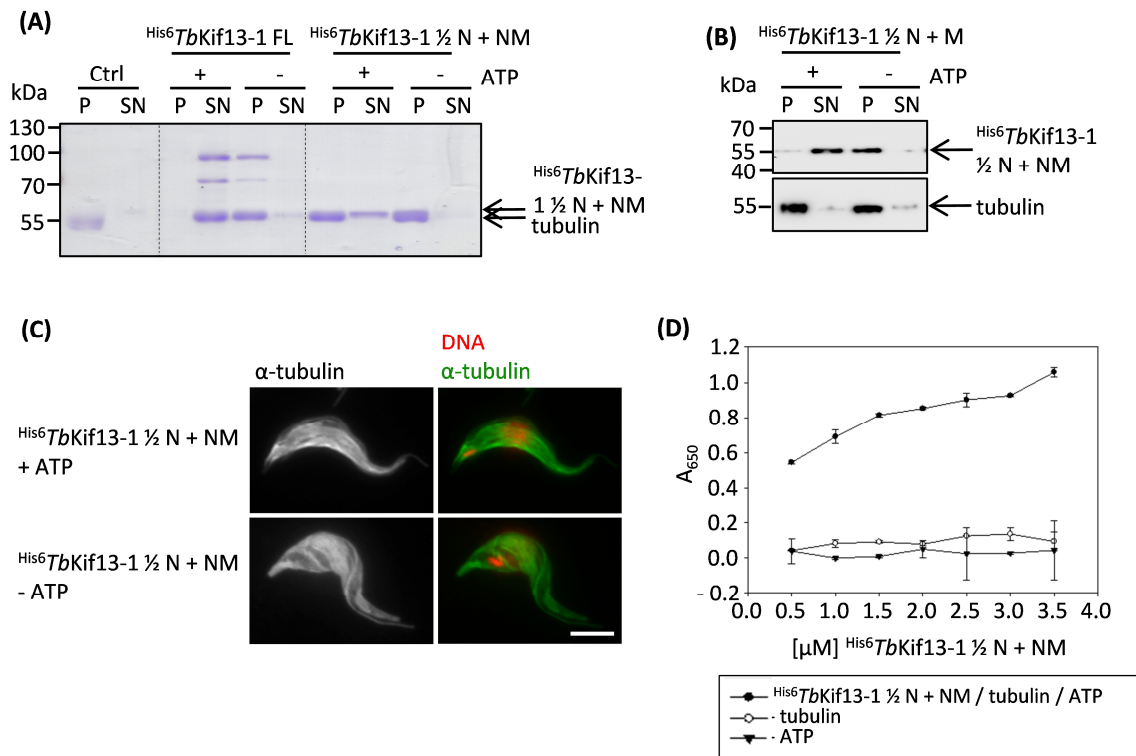


Figure S 29: $\text{His}_6\text{TbKif13-1 } \frac{1}{2} \text{ N + NM}$ is no microtubule depolymeriser but retains ATPase activity. (A) Tubulin sedimentation assay. 1.5 μM $\text{His}_6\text{TbKif13-1 } \frac{1}{2} \text{ N + M}$ were used. 1.5 μM $\text{His}_6\text{TbKif13-1 FL}$ were used as positive control. Substrate were 3 μM taxol-stabilised microtubules. Control (Ctrl) sample was not treated with recombinantly purified $\text{His}_6\text{TbKif13-1 } \frac{1}{2} \text{ N + NM}$. P: pellet; SN: supernatant; SDS-PAGE analysis. (B) Westernblot analysis of the tubulin sedimentation assay samples. $\text{His}_6\text{TbKif13-1 } \frac{1}{2} \text{ N + NM}$ was detected using $\alpha\text{-His}$ antibody; tubulin was detected using $\alpha\text{-tubulin}$ antibody. (C) Cytoskeleton depolymerisation assay. 1 μM $\text{His}_6\text{TbKif13-1 } \frac{1}{2} \text{ N + NM}$ was used. Cytoskeleton tubulin (green) was stained with $\alpha\text{-tubulin}$ antibody. DNA was DAPI (red) stained. Scale bar 5 μm . (D) Malachite green assay for $\text{His}_6\text{TbKif13-1 } \frac{1}{2} \text{ N + NM}$. ATPase activity of $\text{His}_6\text{TbKif13-1 } \frac{1}{2} \text{ N + NM}$ increased with increasing $\text{His}_6\text{TbKif13-1 } \frac{1}{2} \text{ N + NM}$ concentration. Approaches without tubulin or ATP served as control.

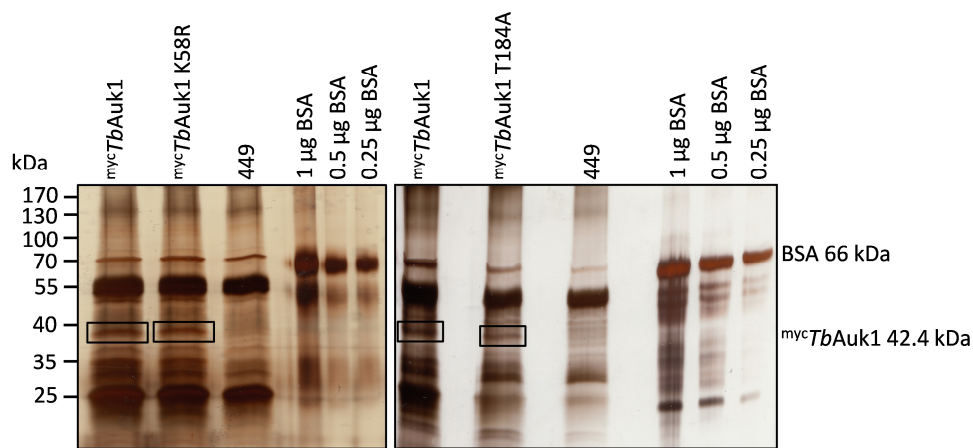


Figure S 30: Silver staining of immunoprecipitation products from 449 *mycTbAuk1*, *mycTbAuk1* K58R and *mycTbAuk1* T184A cell lysates. 10 µL of each immunoprecipitation product was loaded. BSA (bovine serum albumin) served as standard for concentration determination. *mycTbAuk1*, *mycTbAuk1* K58R and *mycTbAuk1* T184A were highlighted with boxes.

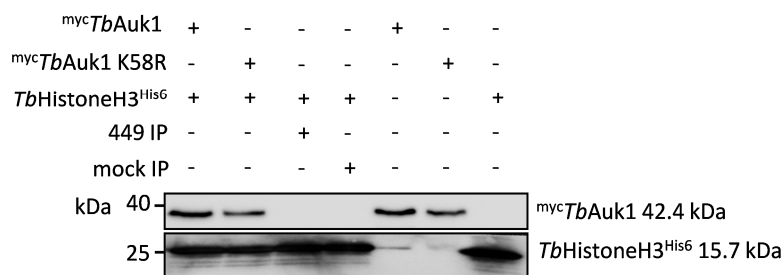


Figure S 31: Westerblot analysis confirming addition of *mycTbAuk1*, *mycTbAuk1* K58R and *TbHistoneH3*^{His6}. Samples from the radioactive ³³P γATP phosphorylation assay were used. *mycTbAuk1* and *mycTbAuk1* K58R were detected using α-myc, *TbHistoneH3*^{His6} was detected using α-His.

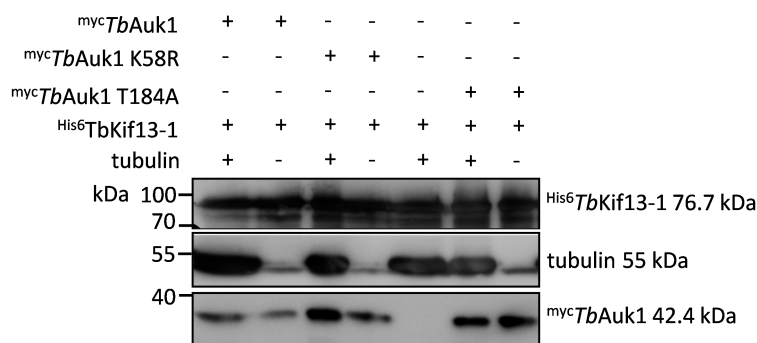


Figure S 32: Westerblot analysis confirming addition of *His6TbKif13-1*, *mycTbAuk1*, *mycTbAuk1* K58R, *mycTbAuk1* T184A and tubulin. Samples from radioactive ³³P γATP phosphorylation assay were used. *mycTbAuk1*, *mycTbAuk1* K58R and *mycTbAuk1* T184A were detected using α-myc, *His6TbKif13-1* was detected using α-His, tubulin was detected using TAT antibody.

Supplementary figures

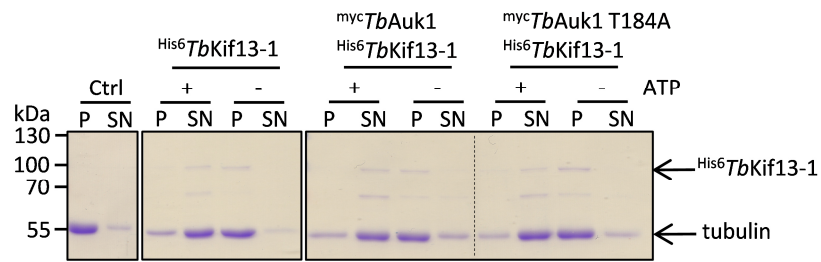


Figure S 33: No inhibition of $^{His6}TbKif13-1$'s depolymerisation activity by $^{myc}TbAuk1$. A depolymerisation assay with addition of immunoprecipitated $^{myc}TbAuk1$ or $^{myc}TbAuk1$ T184A, respectively, was conducted. 1 μ M $^{His6}TbKif13-1$ was used. The components were pre-incubated 1 h at RT before addition of 3 μ M taxol stabilised microtubules. Control (Ctrl) sample was not treated with recombinant purified $^{His6}TbKif13-1$. P: pellet; SN: supernatant.

8. Danksagung

Prof. Dr. Klaus Ersfeld danke ich für die gewissenhafte Betreuung, die anregenden Diskussionen, das stets offene Ohr und den guten Humor während meiner Doktorandenzeit in seinem Labor.

PD Dr. Stefan Heidmann und Prof. Dr. Benedikt Westermann durfte ich in meinem Mentorat willkommen heißen und ich bin dankbar für ihr Interesse an meiner Arbeit und die konstruktive Diskussion.

Prof. Dr. Olaf Stemmann sage ich Dank für die Nutzung der Geräte am Lehrstuhl für Genetik, sowie das Interesse an meiner Forschung während der Seminarvorträge.

Den Doktoranden am Lehrstuhl Genetik danke ich für die gute Zusammenarbeit und die gemeinsame Zeit – Michaela Meyerholz, Brigitte Neumann, Kristina Seel, Philip Kahlen, Dr. Peter Wolf, Dr. Juliane Karich, Dr. Lisa Mohr, Dr. Johannes Buheitel und Susanne Hellmuth. Danke auch an Markus Hermann, der mir bei technischen Fragen zur Protein- und Antikörperaufreinigung zur Seite stand, ebenso an Petra Helies und Heike Haase, die dafür sorgten, dass immer genügend saubere Pipetten zur Verfügung standen. Ein Dank geht auch an Karin Angermann für die technische Assistenz und an Petra Seidler für die Hilfestellung bei organisatorischen Dingen. Danke auch an Jutta Hübner und Brigitte Jaunich.

Bei den Doktoranden aus dem Nachbarlabor für Zellbiologie bedanke ich mich für die Kollegialität und Freundschaft – Dr. Dirk Scholz, Nadine Hock, Dr. Stefan Böckler, Maria Stenger, Xenia Chelius und Christine Leibiger.

Ein besonderer Dank geht an die Studenten, die während ihrer Bachelor- oder Masterarbeit ihre Zeit im Labor mit mir geteilt haben und mir zu Freunden geworden sind – Stefan Lenz, Ann-Kathrin Sommer, Maria Helgert, Dr. Bianca Kakoschky, Ines Böhm, Markus Spindler, Julia Bittmann, Julia Lockhauserbäumer, Kathrin Starz und Dorothea Zimon.

Michaela Meyerholz, Brigitte Neumann und Johannes Selig danke ich für die Korrektur der Arbeit. Ich weiß es sehr zu schätzen, dass sie mir ihre freie Zeit dafür geschenkt haben.

Ein großer Dank geht an meine Familie, ohne deren Unterstützung ich diesen Weg nicht hätte gehen können.

(Eidesstattliche) Versicherung und Erklärungen

(§ 9 Satz 2 Nr. 3 PromO BayNAT)

Hiermit versichere ich eidesstattlich, dass ich die Arbeit selbständig verfasst und keine anderen als die von mir angegebenen Quellen und Hilfsmittel benutzt habe (vgl. Art. 64 Abs 1 Satz 6 BayHSchG).

(§ 9 Satz 2 Nr. 3 PromO BayNAT)

Hiermit erkläre ich, dass ich die Dissertation nicht bereits zur Erlangung eines akademischen Grades eingereicht habe und dass ich nicht bereits diese oder eine gleichartige Doktorprüfung endgültig nicht bestanden habe.

(§ 9 Satz 2 Nr. 4 PromO BayNAT)

Hiermit erkläre ich, dass ich Hilfe von gewerblichen Promotionsberatern bzw. -vermittlern oder ähnlichen Dienstleistern weder bisher in Anspruch genommen habe noch künftig in Anspruch nehmen werde.

(§ 9 Satz 2 Nr. 7 PromO BayNAT)

Hiermit erkläre ich mein Einverständnis, dass die elektronische Fassung meiner Dissertation unter Wahrung meiner Urheberrechte und des Datenschutzes einer gesonderten Überprüfung unterzogen werden kann.

(§ 9 Satz 2 Nr. 8 PromO BayNAT)

Hiermit erkläre ich mein Einverständnis, dass bei Verdacht wissenschaftlichen Fehlverhaltens Ermittlungen durch universitätsinterne Organe der wissenschaftlichen Selbstkontrolle stattfinden können.